

Diss. ETH No. 19387

U-SERIES CONSTRAINTS ON MANTLE MELTING AND MAGMA EVOLUTION

A dissertation submitted to the

ETH ZÜRICH

For the degree of
Doctor of Sciences

Presented by

Janne Marij Koornneef

MSc. Vrije Universiteit Amsterdam

Date of birth: 02.01.1979

Citizen of The Netherlands

Accepted on the recommendation of:

Prof. Dr. Bernard Bourdon

Prof. Dr. Andreas Stracke

Prof. Dr. Max Schmidt

Prof. Dr. Tim Elliott

Dr. John MacLennan

Zürich, 2011

Contents

Summary	1
Zusammenfassung	3
Chapter 1. Introduction and overview	7
1. Mantle melting and source heterogeneity	8
2. Tracers of source heterogeneity, mantle melting and melt mixing	9
3. U-series geochemistry in high temperature environments	10
3.1 Basic principles	10
3.2 U-series melting models	12
4. Iceland: dynamic mantle melting and source heterogeneity.	14
5. Iceland: Aims and outline.	15
6. In situ analyses of U-Th disequilibria in accessory minerals	16
References	16
Chapter 2. Melting of a two-component source beneath Iceland	23
Abstract	24
1. Introduction	25
2. Geology and sample collection	27
3. Analytical techniques	29
4. Results	30
4.1 Major elements	30
4.2 Trace elements	31

4.3 Hf and Nd isotopes	42
5. Discussion	44
5.1 Influence of shallow level processes on lava composition	44
5.2 Distinguishing between source heterogeneity and fractional melting	45
5.3 Partial melting of a heterogeneous source and melt mixing	52
5.3.1 The nature and location of melt mixing	52
5.3.2 Modelling melting and mixing of a heterogeneous source	52
5.3.3 Model results and implications	59
6. Conclusions	64
References	65

Chapter 3. A new method for U-Th-Pa-Ra separation and accurate measurement of ^{234}U - ^{230}Th - ^{231}Pa - ^{226}Ra disequilibria in volcanic rocks by MC-ICPMS **73**

Abstract	74
1. Introduction	74
2. Experimental	76
2.1 Reagents and materials	76
2.2 Spike preparation and calibration	77
2.3 Sample preparation and chemical separation	79
2.3.1 Sample preparation	79
2.3.2 Chemical separation	80
2.4 Mass spectrometric procedures and data reduction	85
2.4.1 Instrumentation	85
2.4.2 General procedures and MC-ICPMS settings	85
2.4.3 Data reduction	87
2.5 Characterisation of SEM dead time and nonlinearity	90
3. Results	94
4. Discussion	97
4.1 Uranium	97
4.2 Thorium	97
4.3 Protactinium	99
4.4 Radium	100
5. Comparison with previous methods	100

6. Conclusions	103
Acknowledgements	103
References	104
Appendix.	110

Chapter 4. Disentangling processes recorded by U-Th-Pa-Ra disequilibria in post-glacial tholeiites from Iceland **111**

Abstract	112
1. Introduction	113
2. Sample preparation and analytical techniques	115
3. Results	117
3.1 ^{238}U - ^{234}U - ^{230}Th disequilibria	117
3.2 ^{231}Pa - ^{235}U disequilibria	119
3.3 ^{226}Ra - ^{230}Th disequilibria	119
3.4. Comparison of Theistareykir data with previous U-series data	122
4. Discussion	123
4.1 A role for crustal processes?	125
4.2 Interpreting U series data using dynamic melting	128
4.3 U-series nuclide partitioning	129
4.4 Melt productivity	130
4.5 Mantle upwelling velocity	134
4.6 Mantle porosity	136
4.7 The influence of source heterogeneity	137
4.7.1 Evidence for variable melting behaviour?	138
4.7.2 Relations between U-series and Hf and Nd isotopes	142
4.7.3 Mixing melts from a two-component source	142
4.7.4 Incomplete random mixing	146
5. Conclusions	148
References	149

Chapter 5. In situ analysis of U-Th disequilibria in titanite by femto second laser-ablation multi-collector ICP-MS **157**

1. Introduction	158
---------------------------	-----

1.1 U-series constraints on time scales of magma differentiation	158
1.2 In-situ analyses of U-series disequilibria	159
2. Analytical methods	160
2.1 System set-up	160
2.1.1 Mass spectrometry	160
2.1.2 Laser ablation	161
2.2 Reference materials and samples	162
2.2.1 LA reference materials	165
2.2.2 Solution mode reference standards	165
2.2.3 Laacher See samples	165
2.3 Analytical methods and data reduction	166
2.3.1 Analyses routines	166
2.3.2 Data reduction	168
3. Results and discussion	169
3.1 NIR mode analyses	169
3.1.1 Standard data by NIR-fs-MC-ICPMS	169
3.1.2 Samples by NIR-fs-MC-ICPMS	172
3.2 UV-mode analyses	178
3.2.1 Standard data for UV-fs-MC-ICPMS	178
3.2.2 Samples by UV-fs-MC-ICPMS	180
4. Conclusions	184
References	186

Chapter 6. Conclusions and perspectives **191**

Acknowledgements **195**

Curriculum Vitae **199**

Summary

The main part of this thesis investigates mantle melting beneath Iceland based on the geochemistry of postglacial lavas collected across the Iceland hotspot. The use of a wide variety of geochemical tracers allows constraining the relative influence of physical source parameters and dynamic melting processes. Particularly U-series isotopes, which inform us on rates of mantle melting are a sensitive tool to map the lateral expression of the temperature anomaly and to resolve variability in melt productivity as a result of source heterogeneity.

The first part of the thesis presents major- and trace element data, and Hf and Nd isotope compositions of lavas erupted along Iceland's main rift zones (Chapter 2). Relationships between trace element ratios that involve a moderately incompatible element (i.e. La/Yb) and Hf and Nd isotope compositions demonstrate that the melting processes and sampling of source heterogeneity beneath Iceland are closely related. Variability in the degree of melting on a local scale (a few square km) suggests that the depth from which melts are extracted is variable, which has a dominant control on the geochemistry of the lavas. This effect overwhelms the effect of lateral variation in excess mantle temperature (ΔT) across the Iceland plume on the trace element and isotope ratios that involve a moderately incompatible element. Highly incompatible elements are not influenced by the degree of melting, which leads to a decoupling from trace element ratios involving a moderately incompatible element and from Hf and Nd isotope compositions. Variable enrichments in ratios of highly incompatible trace elements such as Nb/U, Nb/La and U/La in different zones rift zones suggests that the enriched component, which has characteristics similar to a recycled E-MORB crust, is heterogeneously distributed in the mantle beneath Iceland. The importance of melt mixing during progressive melting is emphasised in Chapter 2 by a polybaric mixing model, which applies different styles of melt mixing during melt extraction. The majority of combined trace element and Nd-Hf-Sr-Pb isotope systematics of Icelandic basalts can be explained by a scenario in which melts from a recycled E-MORB crust and the depleted mantle are randomly and incompletely mixed and extracted from variable depths.

The results of Chapter 2 serve as the framework for the application of U-series systematics in the basalts presented in Chapter 4. A new method to separate U, Th, Pa and Ra from a single sample aliquot, and the mass spectrometric techniques to determine concentrations and isotope ratios by MC-ICPMS are presented in Chapter 3. This new method is applied to investigate the U-series systematics of the postglacial Icelandic lavas in Chapter 4.

The variability in U-series disequilibria measured on samples from Iceland's main rift zones reveals the influence of both ΔT and source heterogeneity (Chapter 4). A general decrease in the ^{230}Th and ^{231}Pa excesses towards the centre of Iceland is consistent with a model of increasing upwelling velocity and complies with the presence of a buoyant thermal plume beneath Iceland. However, local variability in the ^{230}Th - ^{238}U and ^{231}Pa - ^{235}U disequilibria for the samples that are also characterised by variable Nb/U, Nb/La and U/Th demonstrates that source heterogeneity induces variability in melting rates on a local scale. Low ^{230}Th - and ^{231}Pa -excesses for the most enriched samples indicate that the enriched source component is characterised by higher melt productivity, consistent with predictions from experimental studies. The results therefore highlight the importance of lithological heterogeneities to the physical mantle melting process and the final chemistry of MORB and OIB lavas.

In the final part of this thesis (Chapter 5) the potential to measure in situ U-Th disequilibria in titanite and apatite by femto second LA-MC-ICPMS is investigated. The study aimed to spatially resolve variability in U-series disequilibria in accessory minerals from Laacher See Volcano, Germany to constrain timescales of magma evolution within the crust. Accurate data obtained on an in-house standard titanite mineral (SM) bracketed by an in-house titanite glass (TG) are promising and show the great potential of this time efficient analysis technique. Two aspects are, however, found to limit the accuracy and precision of data for Laacher See titanite minerals: (1) Variable elemental fractionation between standards and samples and (2) Low signal intensities. This prevented using the collected data to infer timescales of crystal growth for the Laacher See samples. Further analytical developments to be preformed in near future experiments are required to improve both analytical precision and accuracy.

Zusammenfassung

Der Schwerpunkt dieser Arbeit liegt auf der Untersuchung von Erdmantelschmelzen aus Island, basierend auf der Geochemie von postglazialen Laven, welche entlang des Island-Hotspots beprobt wurden. Die Verwendung diverser geochemischer Tracer erlaubt es, Rückschlüsse auf das Zusammenspiel von physikalischen Parametern der Magmenquelle und dynamischen Schmelzprozessen zu ziehen. Hervorzuheben sind Uran-Serien-Isotope, über welche sich Aufschmelzraten des Erdmantels bestimmen lassen. Darüber hinaus lassen sich laterale Temperaturanomalien auskartieren, sowie Veränderungen in der Magmenproduktionsrate aufgrund von Heterogenitäten in der Quellregion feststellen.

Im ersten Teil der Arbeit werden Haupt- und Spurenelementzusammensetzungen, sowie Hf- und Nd-Isotopendaten von Laven aus der Haupt-Riftzone Islands präsentiert (Kapitel 2). Anhand von Spurenelementverhältnissen, welche ein moderat inkompatibles Element beinhalten (z.B. La/Yb), und den Hf- und Nd-Isotopenzusammensetzungen wird eine Korrelation von Aufschmelzprozessen mit Quellheterogenitäten deutlich. Unterschiedliche Aufschmelzgrade deuten auf variable Quelltiefen hin, und bestimmen dadurch die lokale (wenige Quadratkilometer) chemische Zusammensetzung der Laven. Somit ist der Einfluss lateraler Unterschiede in überschüssiger Mantelwärme (ΔT) entlang des Island-Plumes auf die Isotopen- und Spurenelementverhältnisse mit moderat inkompatiblen Elementen sekundär. Hochinkompatible Elemente werden nicht vom Aufschmelzgrad beeinflusst und sind somit von den Hf und Nd Isotopenzusammensetzungen, sowie den Spurenelementverhältnissen, welche ein moderat inkompatibles Element beinhalten, entkoppelt. Entlang der Riftzone sind unterschiedlich starke Anreicherungen von hochinkompatiblen Spurenelementen in unter anderem Nb/U-, Nb/La- und U/La-Verhältnissen sichtbar. Dies deutet darauf hin, dass eine angereicherte Komponente, ähnlich zu rezykliertem E-MORB, heterogen im Erdmantel unter Island verteilt ist. Der Einfluss von Magmenmischung während des Aufschmelzprozesses wird in Kapitel 2 mit einem polybaren Mischungsmodell verdeutlicht. Das Modell verwendet dabei unterschiedliche Mischungsarten während der Schmelzextraktion. Der Grossteil der Spurenelement- und Nd-Hf-Sr-Pb Systematik wird dadurch erklärt, dass Schmelzen eines

rezyklierten E-MORB und verarmten Mantels regellos und unvollständig gemischt und aus unterschiedlichen Tiefen angezapft werden.

Die Ergebnisse aus Kapitel 2 werden als Grundlage für die U-Serien-Systematik der Basalte in Kapitel 4 genommen. In Kapitel 3 werden eine neuartige Methode zur Separation von U, Th, Pa und Ra von ein und derselben Probe, sowie die massenspektrometrischen Techniken zur Ermittlung ihrer Konzentrationen und Isotopenverhältnisse mittels MC-ICPMS präsentiert. Die neu entwickelte Technik wurde angewandt, um die U-Serien-Systematik der postglazialen isländischen Laven in Kapitel 4 zu untersuchen.

Die variablen U-Serien-Ungleichgewichte der Proben aus der isländischen Riftzone demonstrieren den Einfluss von ΔT und der Heterogenität der Magmenquelle (Kapitel 4). Allgemein abnehmende ^{230}Th - und ^{231}Pa -Überschüsse in Richtung Zentralislands sind im Einklang mit der Annahme eines heißen Plumes unter Island und einem Modell mit zunehmenden Auftriebsraten. Die neben den Nb/U-, Nb/La-, U/Th-Verhältnissen ebenfalls variablen ^{230}Th - ^{238}U - und ^{231}Pa - ^{235}U -Ungleichgewichte zeigen jedoch auf, dass Aufschmelzraten lokal durch die Heterogenitäten in der Magmenquelle beeinflusst werden. Geringe ^{230}Th - und ^{231}Pa -Überschüsse in den am stärksten angereicherten Proben zeigen, dass eine höhere Magmenproduktivität für die angereicherte Mantelkomponente typisch ist, was im Einklang mit experimentellen Beobachtungen steht. Die Ergebnisse verdeutlichen daher den Einfluss von lithologischen Heterogenitäten im Erdmantel auf Aufschmelzprozesse und die geochemische Zusammensetzung von MORB und OIB Laven.

Das abschliessende Kapitel 5 untersucht das Potenzial U-Th Ungleichgewichte in Titanit und Apatit mittels Femtosekunden-LA-MC-ICPMS zu quantifizieren. Ziel der Studie war es, eine räumliche Auflösung der U-Serien-Ungleichgewichte in akzessorischen Mineralen vom Laacher See Vulkan (Deutschland) zu erhalten, um Zeitskalen der Magmenentwicklung in der Erdkruste zu ermitteln. Sorgfältige Messungen eines hauseigenen Titanitminerals relativ zu einem hauseigenen Titanitglas-Standard sind vielversprechend und deuten auf ein grosses Potenzial dieser zeitsparenden Technik hin. Die Genauigkeit und Präzision der Daten für die Laacher See Titanite wird jedoch durch folgende Punkte beschränkt: (1) Unbeständige Elementfraktionierung zwischen Standards und Proben, sowie (2) niedrige Intensitäten. Als Folge dessen war es nicht möglich anhand der gesammelten Daten Zeitskalen von

Kristallwachstum an den Proben vom Laacher See zu bestimmen. Die Verbesserung der Präzision und Genauigkeit der Analysen ist zeitnah geplant.

Chapter 1

Introduction and overview

Introduction and overview

This thesis consists of two parts. The first part investigates the relative importance of plume influenced melting and source heterogeneity on the major- and trace element, Hf and Nd isotope, and U-series systematics in Holocene basalts from Iceland's main rift zones (Chapters 2, 3, and 4). In the second part of the thesis, the potential of an in-situ technique for dating magmatic processes by measuring U-Th disequilibria in accessory minerals (titanite and apatite) by LA-MC-ICPMS (Chapter 5) is evaluated.

1. Mantle melting and source heterogeneity

The geochemistry of basalts from Mid Ocean Ridges (MORB) and Ocean Islands (OIB) provides a window into the Earth's mantle, which is otherwise not directly accessible for sampling. The magmas produced beneath MORs and OIs record not only the mantle's chemical composition but also the physical melting conditions. Whereas MORB is thought to result from melting the passively upwelling mantle at relatively shallow depths (e.g. Klein and Langmuir, 1987), OIB lavas are thought to result from melting hot actively upwelling mantle that rises from deep boundary layers (e.g., Morgan, 1971). Both MORB and OIB have highly variable chemical and isotopic compositions showing that their mantle sources are heterogeneous. While mantle heterogeneity is often attributed to the presence of recycled oceanic crust (Chase, 1981; Chauvel et al., 1992; Hofmann and White, 1982; Willbold and Stracke, 2006; Zindler and Hart, 1986b) the physical properties, scale and distribution of the recycled crust are poorly constrained (Hart, 1984; Ito and Mahoney, 2005b; Kellogg et al., 2002; Phipps Morgan and Morgan, 1999; Sobolev et al., 2005; Staudigel et al., 1991; Wood et al., 1979; Zindler et al., 1984). Recently, it has been demonstrated that mafic lithologies have significantly different melting behaviour (Pertermann and Hirschmann, 2003) supporting former inferences that heterogeneities in the source melt preferentially (Hirschmann and Stolper, 1996; Phipps Morgan and Morgan, 1999; Phipps Morgan et al., 1995; Yaxley and Green, 1998). The combination of chemical enrichment and different physical behaviour of the mafic entities entrained in ambient depleted mantle potentially results in a disproportionate influence of only small quantities of these heterogeneities to the geochemistry of erupted lavas (e.g. Hirschmann and Stolper, 1996). The relative importance of these mantle heterogeneities to the overall physical mantle melting process and the final chemistry of the lavas remains controversial.

2. Tracers of source heterogeneity, mantle melting and melt mixing

A vast quantity of major element, trace element and isotope studies on oceanic basalts were designed to understand melt generation and source heterogeneity. The earliest recognition that enrichments in OIB could represent old recycled crustal material was based on Nd, Sr and Pb isotopic compositions that required lower Sm/Nd and Rb/Sr but elevated U/Pb compared to MORB (e.g. Armstrong, 1968; Chase, 1981; Hart et al., 1973; Hofmann and White, 1982; Zindler and Hart, 1986a). Numerous subsequent studies have used isotopic data from MORB and OIB to infer a large range of mantle end-member reservoirs including the depleted mantle (DM), the Focal Zone (FOZO), high μ (HIMU) and enriched mantle (EM1 and EM2). The enrichment of the depleted mantle is generally ascribed to the recycling of crustal material either by subduction or by delamination (e.g., Hanan et al., 2004; McKenzie and O'Nions, 1983; Stracke et al., 2003a; White and Hofmann, 1982; Zindler and Hart, 1986a).

These large scale isotope studies assume that the isotopic compositions of erupted lavas are negligibly influenced by the melting process and thus directly translate into the composition of the source. Theoretical models that consider fractional melting of a compositionally heterogeneous mantle predict, however, that the isotopic composition of an eruption product is different from that of the bulk mantle due to mixing of partial melts during melt extraction (Ito and Mahoney, 2005a; Phipps Morgan, 1999; Stracke and Bourdon, 2009). The importance of melt mixing also became apparent from the substantial variability in isotopic composition of melt inclusions in oceanic basalts which by far exceed that recorded by their hosts (MacLennan, 2008a; MacLennan, 2008b; Saal et al., 1998; Saal et al., 2005; Slater et al., 2001).

Major element and moderately incompatible trace element systematics in MORB and OIB were shown to be fundamental in investigations of mantle melting processes as they allow estimating the average degree and pressure of melting (e.g. Klein and Langmuir, 1987). Both major and trace elements of primitive OIBs were also used as tracers for mantle heterogeneity considering relations observed between these components and isotope compositions (Dasgupta et al., 2010; Hemond et al., 1994; Jackson and Dasgupta, 2008; Prytulak and Elliott, 2007; Sobolev et al., 2007; Sobolev et al., 2005; Willbold and Stracke, 2006). The combination of trace element ratios of elements with different compatibilities and isotopic data allows a qualitative evaluation of the respective influence of the melting process and source heterogeneity (Stracke and

Bourdon, 2009). Note, however, that quantifications of melting and source related processes based on trace element systematics require assumptions on the melting and partitioning behaviour of mantle minerals and estimates of the initial elemental abundances in the source region.

The use of U-series as tracers for mantle melting processes (e.g., McKenzie, 1985b; Spiegelman and Elliott, 1993a; Williams and Gill, 1989) circumvents the need to know the composition of the source as the short half-lives of the U-series nuclides are in secular equilibrium in a mantle that was undisturbed for longer than ~ 6 times the half-life of the longest-lived intermediate nuclide (see section 1.3). U-series disequilibria measured in OIB and MORB depend on physical and dynamical parameters during melting, such as residual mantle porosity, bulk solid-melt partition coefficients and mantle melting rate (e.g., Sims et al., 1999). The mantle melting rate, in turn, directly relates to mantle upwelling velocity and therefore mantle temperature (Bourdon et al., 2006a; Stracke et al., 2006b), but is also controlled by the melt productivity of the source (e.g. Prytulak et al., 2009, Pertermann and Hirschmann 2003). Consequently, U-series provide a unique link between geochemical and geophysical processes that occur in the mantle. Furthermore, because it was recently demonstrated that melt productivities for mafic lithologies are much higher than for peridotitic mantle, U-series are another tracer for mantle heterogeneity.

3. U-series geochemistry in high temperature environments

3.1 Basic principles

The fundamentals of U-series geochemistry lie in the fractionation between the elements within the ^{238}U and ^{235}U decay chains due to their different chemical properties and thus behaviour during geological processes (Bourdon et al., 2003). The variable half-lives of the radioactive nuclides within the decay chains allow constraining time-scales at which the fractionation processes occur. The long-lived parent isotopes of uranium, ^{238}U and ^{235}U , ultimately decay to the stable isotopes of lead, ^{206}Pb and ^{207}Pb , respectively via a series of intermediate unstable nuclides with half-lives ranging from 250 kyr to microseconds (Fig. 1). In a closed system, such a decay series evolves to a state of secular equilibrium where the activity ($a_i = \lambda_i C_i$) of each intermediate nuclide equals its production rate due to the decay of its respective parent element. Therefore, in secular equilibrium the ratio of activities of any two nuclides in the chain is unity. If the

system is disturbed by a process that fractionates parent and daughter elements (e.g. melting) disequilibrium is induced causing so called excesses or deficits (activity ratios greater or less than 1, respectively) that will decay toward unity on a time scale on the order of the half life of the daughter nuclide (Spiegelman and Elliott, 1993a). The Earth's mantle has likely been undisturbed for many millions of years before melting and is therefore assumed to be in secular equilibrium. Since at secular equilibrium, atomic ratios of the intermediate nuclides are simply the ratio of their half-lives, the abundance ratio of the intermediate nuclides in the source prior to melting is constrained (Elliott, 1997).

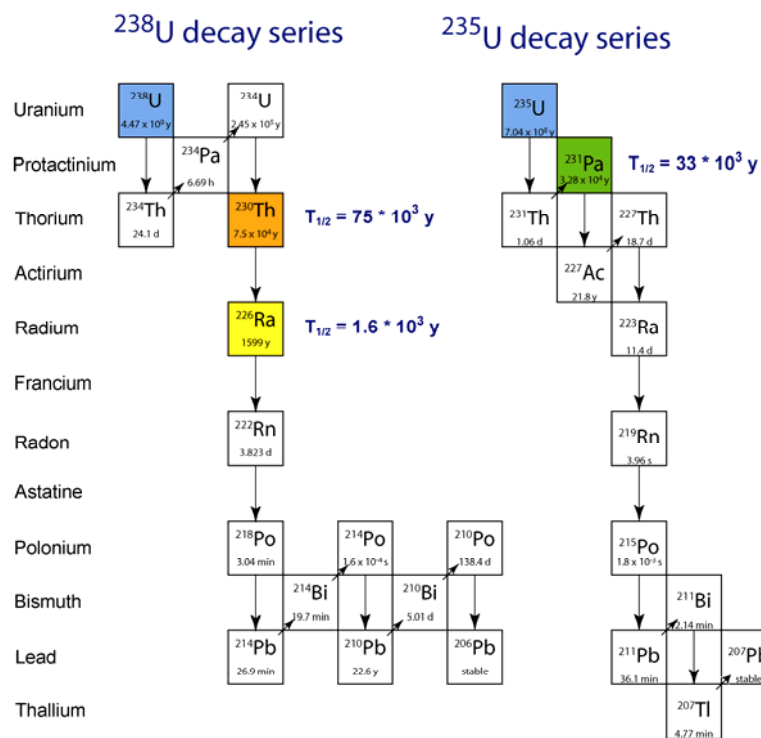


Figure 1. Decay scheme for the ^{238}U and ^{235}U decay chains highlighting the nuclides of interest to this study and their half-lives.

The intermediate U series nuclides that are of interest to the work in this thesis are ^{230}Th ($t_{1/2} \sim 75$ kyr) and ^{226}Ra ($t_{1/2} \sim 1.6$ kyr) in the ^{238}U chain, and ^{231}Pa ($t_{1/2} \sim 33$ kyr) in the ^{235}U chain (Fig. 1) as their relatively long half-lives are appropriate for studying melting processes that occur over a similar time-scale (Bourdon et al., 2003). The fractionation between the U-series nuclides at small degrees of melting is controlled by their relative compatibilities. Knowledge of the partitioning behaviour of the elements in the source is

therefore fundamental in understanding the U-series disequilibria recorded by volcanic samples. An overview on U-series elemental partitioning obtained from theoretical considerations and experimental determination is given in Chapter 4.

3.2 U-series melting models

Studies of U-series disequilibria in MORB and OIB reveal systematic differences that imply different melting processes to be important for each tectonic setting (see Peate and Hawkesworth, 2005, for an overview). In order to explain the observations in MORB and OIB previous workers have proposed a range of models based on the concept of ‘ingrowth’ of daughter nuclides from parent nuclides travelling at different speeds in the melt column. These time-dependent models range from assuming complete melt-solid equilibrium during melt transport (Spiegelman and Elliott, 1993b) to assuming disequilibrium (McKenzie, 1985a) to models that argue for different degrees of equilibrium at different depths in the mantle (Jull et al., 2002; Lundstrom, 2001; Lundstrom et al., 2000). Based on the lack of evidence for equilibration between uprising melt and material through which it passes (i.e. melts retain correlations between isotopes, trace elements and major elements) and the high rates of melt transport indicated by OIB lavas, many recent OIB studies used the disequilibrium ‘dynamic’ melting model to interpret the U-series data (Bourdon et al., 2006b; Bourdon et al., 2005; Kokfelt et al., 2003; Prytulak and Elliott, 2009; Stracke et al., 2006a; Stracke et al., 2003b).

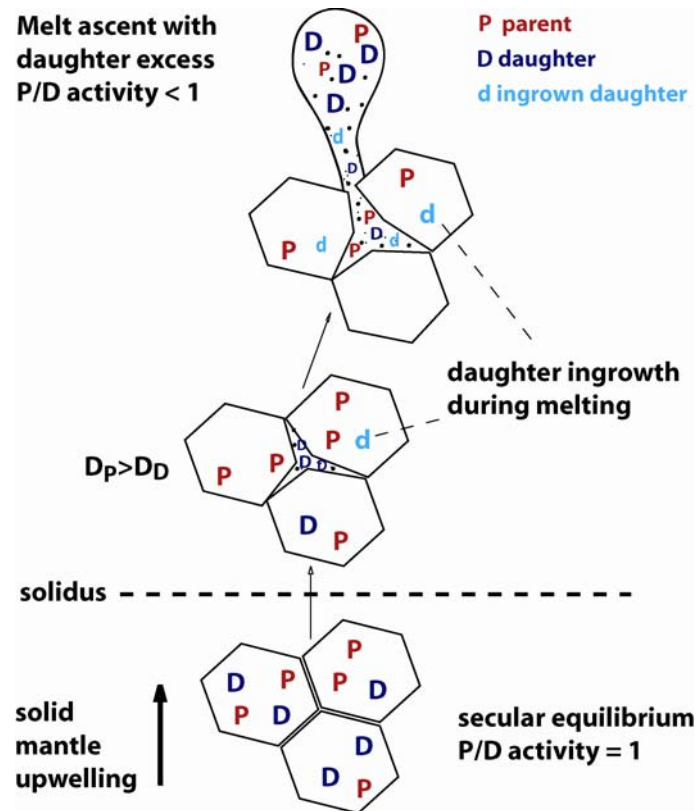


Figure 2. Schematic representation of dynamic melting model in which parent (P) or daughter (D) excesses in melts result from ‘ingrowth’ by decay of the parent during melting. Modified from (Lundstrom et al., 1995).

In the dynamic melting model the more buoyant melt moves faster relative to the solid and the excesses are produced by the ingrowth of daughter nuclides in the residue during melting (Fig. 2. e.g. (Lundstrom et al., 1995; McKenzie, 1985b; Williams and Gill, 1989). The model is typically a one-dimensional steady-state formulation in which the melt (in equilibrium with the solid) is extracted from the solid after it reaches a threshold porosity. Because the U-series nuclides are highly incompatible they are effectively stripped from the solid residue after a few percent of melting (Spiegelman and Elliott, 1993a). Therefore, the initial stages of melting dominate the U-series disequilibria. The first dynamic melting models assumed infinite melt extraction (McKenzie, 1985b; Williams and Gill, 1989), but subsequent models (Stracke et al., 2006) allow for variation of the melt extraction velocity. In Chapter 4, I apply the dynamic melting model to derive information on melting rates and to distinguish

between the importance of variability in mantle upwelling velocity and melt source productivity.

4. Iceland: dynamic mantle melting and source heterogeneity

Iceland, located on the Mid Atlantic Ridge (MAR), forms the ideal location to study plume influenced melting processes and the effect of source heterogeneity as interaction of the passive MOR and actively upwelling hot Iceland plume results in continuous melt production along the main rift zones (Bijwaard and Spakman, 1999; Montelli et al., 2004; Schilling, 1973; Shen et al., 1998; Wolfe, 1997). As a result, young primitive lavas are relatively easily accessible along the subaerially continuing MAR across Iceland.

The presence of source heterogeneities beneath Iceland has been established based on major element, trace element, and isotope evidence (Fitton et al., 1997; Hanan et al., 2000; Hanan and Schilling, 1997; Hémond et al., 1993; Kempton et al., 2000; MacLennan, 2008a; MacLennan et al., 2003a; MacLennan et al., 2003b; Sigmarsson et al., 1992; Slater et al., 2001; Thirlwall et al., 2004) and correlation between long lived isotope ratios and trace elements suggest that progressive melting and sampling of at least two mantle components is systematic (Elliott et al., 1991; Kokfelt et al., 2006; Stracke and Bourdon, 2009; Stracke et al., 2003c). It was suggested that the erupting lavas represent incomplete mixtures of small degree melts from variable depths in the melting region and that the heterogeneities in the mantle source are of small scale (~1km)(Elliott et al., 1991; Kokfelt et al., 2006; MacLennan et al., 2003b; Slater et al., 2001).

Additionally, Iceland is characterised by lower ($^{230}\text{Th}/^{238}\text{U}$) compared to global MORB, which was ascribed to faster mantle upwelling beneath Iceland (Bourdon et al., 1996). A radial increase in the Th-excesses in postglacial lavas with distance from the plume centre was inferred to reflect a decrease in the mantle potential temperature and upwelling velocity further away from the plume centre (Kokfelt et al., 2003). ($^{231}\text{Pa}/^{235}\text{U}$) disequilibria which are more sensitive to the melting process due to the shorter half life of ^{231}Pa compared to ^{230}Th (see section 1.4), are reported as part of this study.

5. Iceland: Aims and outline

The aim for the first part of this thesis (Chapter 2, 3 and 4) was to re-assess the relative importance of melting and source heterogeneity on the geochemistry of basalts erupted along Iceland's main rift zones. The ultimate aim was to use U-series data as a high-resolution tool to constrain the lateral expression of the mantle plume and to resolve variability in melt productivity of the mantle source beneath Iceland. In combination with other geochemical tracers (e.g. trace elements and long-lived isotopes) we aimed to map the geophysical anomaly and long-lived geochemical mantle heterogeneities (Bourdon et al., 2006a; Stracke et al., 2006b; Stracke et al., 1999). Key questions that are considered in the next three chapters are therefore: Can we resolve the Icelandic mantle plume from systematic changes in geochemistry with distance from the plume centre? Is the melting process obscured by source heterogeneity? What is the composition of the enriched source component(s)? How does mixing of melts from a heterogeneous source and melt extraction influence the geochemistry of erupted basalts? Can we distinguish variability in melting behaviour (i.e. melt productivity) across Iceland?

In Chapter 2, I present combined trace element and Hf-Nd isotope data on postglacial tholeiites from the main-rift and off-rift zones with the goal to distinguish between melting effects and source heterogeneity effects. Especially highly incompatible trace element ratios reveal more pronounced contributions of an enriched source component in the South Western Rift Zones of Iceland compared to in the Northern Rift Zone. The influence of melt mixing during melt extraction is evaluated by applying a model that considers different mixing scenarios of a two-component mantle source. Chapter 3 describes a new method to separate U, Th, Ra and Pa from a single basaltic aliquot and MC-ICPMS techniques for accurate measurements of elemental concentrations and isotope ratios. Chapter 4 reports the obtained ^{230}Th - ^{238}U , ^{231}Pa - ^{235}U and ^{226}Ra - ^{230}Th disequilibria data on 25 Icelandic samples. A detailed evaluation of the U-series data in combination with major- and trace element and Hf and Nd isotopes highlights the importance of lithological heterogeneities to the melting behaviour on a local scale beneath Iceland.

6. In situ analyses of U-Th disequilibria in accessory minerals to investigate timescales of magma differentiation

Other than using U-series as tracers for primary mantle melting processes as shown in Chapter 4, in the second part of this thesis (Chapter 5) I aimed to use the U-Th disequilibria to constrain time scales of magma evolution in reservoirs within the crust. Our target location is the Laacher See Volcano, Germany, which has been extensively studied by Tait and Wörner and co-workers (Tait, 1988; Tait et al., 1989; Wörner et al., 1985; Wörner and Wright, 1984). Crystals in cumulate nodules from the Laacher See phonolites are zoned (Bourdon et al., 1994) and these were suggested to record a protracted growth history. To measure in-situ U-series isotopes in accessory minerals demanded development of an in situ Laser Ablation MC-ICP-MS method, which was initially explored by (Stirling et al., 2000). In this study I focus on accessory phases that are rich in U and Th (titanite and apatite) as the efficiency of transfer of the laser ablation aerosol and ionization of U and Th in the plasma is limited. The analytical development was done in collaboration with D. Günther, at the Laboratory of Inorganic Chemistry, ETH Zurich. The main challenge was to achieve good sensitivity while keeping the elemental fractionation low. The results are presented in Chapter 5.

References

- Armstrong, R.I., 1968. A Model for Evolution of Strontium and Lead Isotopes in a Dynamic Earth. *Reviews of Geophysics*, 6, 175-&.
- Bijwaard, H. and Spakman, W., 1999. Tomographic evidence for a narrow whole mantle plume below Iceland. *Earth and Planetary Science Letters*, 166, 121-126.
- Bourdon, B., Langmuir, C.H. and Zindler, A., 1996. Ridge-hotspot interaction along the Mid-Atlantic Ridge between 37[degree sign]30' and 40[degree sign]30'N: the U-Th disequilibrium evidence. *Earth and Planetary Science Letters*, 142, 175-189.
- Bourdon, B., Ribe, N.M., Stracke, A., Saal, A.E. and Turner, S.P., 2006a. Dynamics of mantle plumes : insights from U-series geochemistry. in preparation.
- Bourdon, B., Ribe, N.M., Stracke, A., Saal, A.E. and Turner, S.P., 2006b. Insights into the dynamics of mantle plumes from uranium-series geochemistry. *Nature*, 444, 713-717.

- Bourdon, B., Turner, S., Henderson, G.M. and Lundstrom, C.C., 2003. Introduction to U-series geochemistry. In: Uranium-Series Geochemistry, Reviews in Mineralogy and Geochemistry 52. B. Bourdon, G.M. Henderson, C.C. Lundstrom and S.P. Turner (Editors), pp. 1-21.
- Bourdon, B., Turner, S.P. and Ribe, N.M., 2005. Partial melting and upwelling rates beneath the Azores from a U-series isotope perspective. *Earth and Planetary Science Letters*, 239, 42-56.
- Chase, C.G., 1981. Oceanic Island Pb - 2-Stage Histories and Mantle Evolution. *Earth and Planetary Science Letters*, 52, 277-284.
- Chauvel, C., Hofmann, A.W. and Vidal, P., 1992. Himu Em - the French-Polynesian Connection. *Earth and Planetary Science Letters*, 110, 99-119.
- Dasgupta, R., Jackson, M.G. and Lee, C.T.A., 2010. Major element chemistry of ocean island basalts - Conditions of mantle melting and heterogeneity of mantle source. *Earth and Planetary Science Letters*, 289, 377-392.
- Elliott, T., 1997. Fractionation of U and Th during mantle melting: a reprise. *Chemical Geology*, 139, 165-183.
- Elliott, T.R., Hawkesworth, C.J. and Gronvold, K., 1991. Dynamic Melting of the Iceland Plume. *Nature*, 351, 201-206.
- Fitton, J.G., Saunders, A.D., Norry, M.J., Hardarson, B.S. and Taylor, R.N., 1997. Thermal and chemical structure of the Iceland plume. *Earth and Planetary Science Letters*, 153, 197-208.
- Hanan, B.B., Blichert-Toft, J., Kingsley, R. and Schilling, J.G., 2000. Depleted Iceland mantle plume geochemical signature: Artifact of multicomponent mixing? *Geochem. Geophys. Geosyst.*, 1.
- Hanan, B.B., Blichert-Toft, J., Pyle, D.G. and Christie, D.M., 2004. Contrasting origins of the upper mantle revealed by hafnium and lead isotopes from the Southeast Indian Ridge. *Nature*, 432, 91-94.
- Hanan, B.B. and Schilling, J.G., 1997. The dynamic evolution of the Iceland mantle plume: the lead isotope perspective. *Earth and Planetary Science Letters*, 151, 43-60.
- Hart, S.R., 1984. A Large-Scale Isotope Anomaly in the Southern-Hemisphere Mantle. *Nature*, 309, 753-757.
- Hart, S.R., Schilling, J.G. and Powell, J.L., 1973. Basalts from Iceland and Along Reykjanes Ridge - Sr Isotope Geochemistry. *Nature-Physical Science*, 246, 104-107.
- Hémond, C. et al., 1993. The Heterogeneous Iceland Plume - Nd-Sr-O Isotopes and Trace-Element Constraints. *Journal of Geophysical Research-Solid Earth*, 98, 15833-15850.
- Hémond, C., Devey, C.W. and Chauvel, C., 1994. Source Compositions and Melting Processes in the Society and Austral Plumes (South-Pacific Ocean) - Element and Isotope (Sr, Nd, Pb, Th) Geochemistry. *Chemical Geology*, 115, 7-45.

- Hirschmann, M.M. and Stolper, E.M., 1996. A possible role for garnet pyroxenite in the origin of the "garnet signature" in MORB. *Contributions to Mineralogy and Petrology*, 124, 185-208.
- Hofmann, A.W. and White, W.M., 1982. Mantle Plumes from Ancient Oceanic-Crust. *Earth and Planetary Science Letters*, 57, 421-436.
- Ito, G. and Mahoney, J.J., 2005a. Flow and melting of a heterogeneous mantle: 1. Method and importance to the geochemistry of ocean island and mid-ocean ridge basalts. *Earth and Planetary Science Letters*, 230, 29-46.
- Ito, G. and Mahoney, J.J., 2005b. Flow and melting of a heterogeneous mantle: 2. Implications for a chemically nonlayered mantle. *Earth and Planetary Science Letters*, 230, 47-63.
- Jackson, M.G. and Dasgupta, R., 2008. Compositions of HIMU, EM1, and EM2 from global trends between radiogenic isotopes and major elements in ocean island basalts. *Earth and Planetary Science Letters*, 276, 175-186.
- Jull, M., Kelemen, P. and Sims, K.W.W., 2002. Consequences of diffuse and channelled porous melt migration on uranium series disequilibria. *Geochimica et Cosmochimica Acta*, 66, 4133-4148.
- Kellogg, J.B., Jacobsen, S.B. and O'Connell, R.J., 2002. Modeling the distribution of isotopic ratios in geochemical reservoirs. *Earth and Planetary Science Letters*, 204, 183-202.
- Kempton, P.D. et al., 2000. The Iceland plume in space and time: a Sr-Nd-Pb-Hf study of the North Atlantic rifted margin. *Earth and Planetary Science Letters*, 177, 255-271.
- Klein, E.M. and Langmuir, C.H., 1987. Global Correlations of Ocean Ridge Basalt Chemistry with Axial Depth and Crustal Thickness. *Journal of Geophysical Research-Solid Earth and Planets*, 92, 8089-8115.
- Kokfelt, T.F., Hoernle, K. and Hauff, F., 2003. Upwelling and melting of the Iceland plume from radial variation of ^{238}U - ^{230}Th disequilibria in postglacial volcanic rocks. *Earth and Planetary Science Letters*, 214, 167-186.
- Kokfelt, T.F. et al., 2006. Combined traced element and Pb-Nd-Sr-O isotope evidence for recycled oceanic crust (upper and lower) in the Iceland mantle plume. *Journal of Petrology*, 47, 1705-1749.
- Lundstrom, C., 2001. Models of U-series disequilibria generation in MORB: the effects of two scales of melt porosity. *Physics of the Earth and Planetary Interiors*, 121, 189-204.
- Lundstrom, C.C., Gill, J. and Williams, Q., 2000. A geochemically consistent hypothesis for MORB generation. *Chemical Geology*, 162, 105-126.
- Lundstrom, C.C., Gill, J., Williams, Q. and Perfit, M.R., 1995. Mantle Melting and Basalt Extraction by Equilibrium Porous Flow. *Science*, 270, 1958-1961.

- MacLennan, J., 2008a. Concurrent Mixing and Cooling of Melts under Iceland. *Journal of Petrology*, 49, 1931-1953.
- MacLennan, J., 2008b. Lead isotope variability in olivine-hosted melt inclusions from Iceland. *Geochimica Et Cosmochimica Acta*, 72, 4159-4176.
- MacLennan, J. et al., 2003a. Melt mixing and crystallization under Theistareykir, northeast Iceland. *Geochemistry Geophysics Geosystems*, 4.
- MacLennan, J., McKenzie, D., Hilton, F., Gronvold, K. and Shimizu, N., 2003b. Geochemical variability in a single flow from northern Iceland. *Journal of Geophysical Research-Solid Earth*, 108.
- McKenzie, D., 1985a. ^{230}Th - ^{238}U disequilibrium and the melting processes beneath ridge axes. *Earth and Planetary Science Letters*, 72, 149-157.
- McKenzie, D., 1985b. ^{230}Th - ^{238}U disequilibrium and the melting processes beneath ridge axes. *Earth and Planetary Science Letters*, 72, 149-157.
- McKenzie, D. and O'Nions, R.K., 1983. Mantle reservoirs and ocean island basalts. *Nature*, 301, 229-231.
- Montelli, R., Nolet, G., Masters, G., Dahlen, F.A. and Hung, S.H., 2004. Global P and PP traveltimes tomography: rays versus waves. *Geophysical Journal International*, 158, 637-654.
- Morgan, W.J., 1971. Convection Plumes in Lower Mantle. *Nature*, 230, 42-&.
- Peate, D.W. and Hawkesworth, C.J., 2005. U series disequilibria: Insights into mantle melting and the timescales of magma differentiation,. *Rev. Geophys*, 43.
- Pertermann, M. and Hirschmann, M.M., 2003. Partial melting experiments on a MORB-like pyroxenite between 2 and 3 GPa: Constraints on the presence of pyroxenite in basalt source regions from solidus location and melting rate. *Journal of Geophysical Research-Solid Earth*, 108.
- Phipps Morgan, J., 1999. Isotope topology of individual hotspot basalt arrays: Mixing curves or melt extraction trajectories? *Geochem. Geophys. Geosyst.*, 1.
- Phipps Morgan, J. and Morgan, W.J., 1999. Two-stage melting and the geochemical evolution of the mantle: a recipe for mantle plum-pudding. *Earth and Planetary Science Letters*, 170, 215-239.
- Phipps Morgan, J., Morgan, W.J. and Price, E., 1995. Hotspot Melting Generates Both Hotspot Volcanism and a Hotspot Swell. *Journal of Geophysical Research-Solid Earth*, 100, 8045-8062.
- Prytulak, J. and Elliott, T., 2007. TiO_2 enrichment in ocean island basalts. *Earth and Planetary Science Letters*, 263, 388-403.

- Prytulak, J. and Elliott, T., 2009. Determining melt productivity of mantle sources from ^{238}U - ^{230}Th - and ^{235}U - ^{231}Pa disequilibria; an example from Pico Island, Azores. *Geochimica Et Cosmochimica Acta*, 73, 2103-2122.
- Saal, A.E., Hart, S.R., Shimizu, N., Hauri, E.H. and Layne, G.D., 1998. Pb isotopic variability in melt inclusions from oceanic island basalts, Polynesia. *Science*, 282, 1481-1484.
- Saal, A.E. et al., 2005. Pb isotopic variability in melt inclusions from the EMI-EMII-HIMU mantle end-members and the role of the oceanic lithosphere. *Earth and Planetary Science Letters*, 240, 605-620.
- Schilling, J., 1973. Iceland Mantle Plume - Geochemical Study of Reykjanes Ridge. *Nature*, 242, 565-571.
- Shen, Y., Solomon, S.C., Bjarnason, I.T. and Wolfe, C.J., 1998. Seismic evidence for a lower-mantle origin of the Iceland plume. *Nature*, 395, 62-65.
- Sigmarsson, O., Condomines, M. and Fourcade, S., 1992. Mantle and crustal contribution in the genesis of Recent basalts from off-rift zones in Iceland: Constraints from Th, Sr and O isotopes. *Earth and Planetary Science Letters*, 110, 149-162.
- Sims, K.W.W. et al., 1999. Porosity of the melting zone and variations in the solid mantle upwelling rate beneath Hawaii: inferences from ^{238}U - ^{230}Th - ^{226}Ra and ^{235}U - ^{231}Pa disequilibria. *Geochimica et Cosmochimica Acta*, 63, 4119-4138.
- Slater, L., McKenzie, D.A.N., Gronvold, K. and Shimizu, N., 2001. Melt Generation and Movement beneath Theistareykir, NE Iceland, pp. 321-354.
- Sobolev, A.V. et al., 2007. The amount of recycled crust in sources of mantle-derived melts. *Science*, 316, 412-417.
- Sobolev, A.V., Hofmann, A.W., Sobolev, S.V. and Nikogosian, I.K., 2005. An olivine-free mantle source of Hawaiian shield basalts. *Nature*, 434, 590-597.
- Spiegelman, M. and Elliott, T., 1993a. Consequences of melt transport for uranium series disequilibrium in young lavas. *Earth and Planetary Science Letters*, 118, 1-20.
- Spiegelman, M. and Elliott, T., 1993b. Consequences of melt transport for uranium series disequilibrium in young lavas. *Earth Plan. Sci. Lett.*, 118, 1-20.
- Staudigel, H. et al., 1991. The Longevity of the South-Pacific Isotopic and Thermal Anomaly. *Earth and Planetary Science Letters*, 102, 24-44.
- Stirling, C.H., Lee, D.-C., Christensen, J.N. and Halliday, A.N., 2000. High-precision in situ ^{238}U - ^{234}U - ^{230}Th isotopic analysis using laser ablation multiple-collector ICP-MS. *Geochimica et Cosmochimica Acta*, 64, 3737-3750.
- Stracke, A., Bizimis, M. and Salters, V.J.M., 2003a. Recycling oceanic crust: Quantitative constraints. *Geochemistry Geophysics Geosystems*, 4, 33.

- Stracke, A. and Bourdon, B., 2009. The importance of melt extraction for tracing mantle heterogeneity. *Geochimica Et Cosmochimica Acta*, 73, 218-238.
- Stracke, A., Bourdon, B. and McKenzie, D., 2006a. Melt extraction in the Earth's mantle: Constraints from U-Th-Pa-Ra studies in oceanic basalts. *Earth and Planetary Science Letters*, 244, 97-112.
- Stracke, A., Bourdon, B. and McKenzie, D., 2006b. Melt extraction in the Earth's mantle: Constraints from U-Th-Pa-Ra studies in oceanic basalts. *Earth and Planetary Science Letters*, in press.
- Stracke, A., Salters, V.J.M. and Sims, K.W.W., 1999. Assessing the presence of garnet-pyroxenite in the mantle sources of basalts through combined hafnium-neodymium-thorium isotope systematics. *Geochemistry, Geophysics, Geosystems*, 1, Paper number 1999GC000013, pp. 13.
- Stracke, A., Zindler, A., Salters, V.J.M., McKenzie, D. and Grönvold, K., 2003b. The dynamics of melting beneath Theistareykir, northern Iceland. *Geochem. Geophys. Geosyst.*, 4, 8513. doi: 10.1029/2002GC000347.
- Stracke, A. et al., 2003c. Theistareykir revisited. *Geochemistry Geophysics Geosystems*, 4, 8507. doi: 10.1029/2001GC000201.
- Tait, S.R., 1988. Samples from the crystallizing boundary layer of a zoned magma chamber. *Contributions to Mineralogy and Petrology*, 100, 470-483.
- Tait, S.R., Wörner, G., Bogaard, P. and Schmincke, H.-U., 1989. Cumulate nodules as evidence for convective fractionation in a phonolite magma chamber. *Earth and Planetary Science Letters*, 92, 107-123.
- Thirlwall, M.F., Gee, M.A.M., Taylor, R.N. and Murton, B.J., 2004. Mantle components in Iceland and adjacent ridges investigated using double-spike Pb isotope ratios. *Geochimica Et Cosmochimica Acta*, 68, 361-386.
- White, W.M. and Hofmann, A.W., 1982. Sr and Nd Isotope Geochemistry of Oceanic Basalts and Mantle Evolution. *Nature*, 296, 821-825.
- Willbold, M. and Stracke, A., 2006. Trace element composition of mantle end-members: Implications for recycling of oceanic and upper and lower continental crust. *Geochemistry Geophysics Geosystems*, 7, 30.
- Williams, R.W. and Gill, J.B., 1989. Effects of partial melting on the uranium decay series. *Geochimica et Cosmochimica Acta*, 53, 1607-1619.
- Wolfe, C.J., Bjarnason, I.Th., Vandecar, C.J., Solomon, S.C., 1997. Seismic structure of the Iceland mantle plume. *Nature*, 385, 245-247.

-
- Wood, D.A., Joron, J.L., Treuil, M., Norry, M. and Tarney, J., 1979. Elemental and Sr Isotope Variations in Basic Lavas from Iceland and the Surrounding Ocean-Floor - Nature of Mantle Source Inhomogeneities. *Contributions to Mineralogy and Petrology*, 70, 319-339.
- Wörner, G., Staudigel, H. and Zindler, A., 1985. Isotopic Constraints On Open System Evolution of the Laacher- See Magma Chamber (Eifel, West-Germany). *Earth and Planetary Science Letters*, 75, 37-49.
- Wörner, G. and Wright, T.L., 1984. Evidence for magma mixing within the Laacher See magma chamber (East Eifel, Germany). *Journal of Volcanology and Geothermal Research*, 22, 301-307.
- Yaxley, G.M. and Green, D.H., 1998. Reactions between eclogite and peridotite: Mantle refertilisation by subduction of oceanic crust. *Schweizerische Mineralogische Und Petrographische Mitteilungen*, 78, 243-255.
- Zindler, A. and Hart, S., 1986a. *Chemical Geodynamics*, pp. 493-571.
- Zindler, A. and Hart, S., 1986b. Helium - Problematic Primordial Signals. *Earth and Planetary Science Letters*, 79, 1-8.
- Zindler, A., Staudigel, H. and Batiza, R., 1984. Isotope and Trace-Element Geochemistry of Young Pacific Seamounts - Implications for the Scale of Upper Mantle Heterogeneity. *Earth and Planetary Science Letters*, 70, 175-195.

Chapter 2

Melting of a two-component source beneath Iceland

This chapter is submitted to *Journal of Petrology* as: Koornneef, J.M., Stracke, A., Meier, M.A., Bourdon, B., Jochum, K.P., Stoll, B., Grönvold, K. Melting of a two-component source beneath Iceland

Abstract

New trace element and Hf-Nd isotope data on postglacial basalts from Iceland are used in combination with existing trace element and isotope data to evaluate the relative importance of source heterogeneity and the melting process for the final composition of lavas erupted along Iceland's main rift zones. Good correlations between Hf and Nd isotope compositions and trace element ratios sensitive to the degree of melting indicate that at least two source components are sampled systematically as a function of the degree and pressure of melting beneath Iceland. Strong depletion in Rb, Ba, U and Th and enrichment in Nb and Ta compared to La in the most enriched samples from the Reykjanes Peninsula and Western Rift Zone suggests mixing with an enriched component similar to a recycled E-MORB crust. Large variability in highly incompatible trace element ratios such as Nb/La and Nb/U and Pb isotope composition for these samples compared to samples from the Northern Rift Zone suggests that the abundance of the enriched component in the source is variable across Iceland or that the enriched component is intrinsically heterogeneous. The composition of Iceland lavas was modelled with a one-dimensional polybaric melt mixing model that mixes accumulated melts from a depleted MORB mantle and a recycled E-MORB. Using this model we evaluate the potential effect of mixing melts from two components during melt extraction. We simulate two styles of melt mixing; (1) complete mixing of melts from a source with variable proportions of the enriched and depleted component; (2) incomplete mixing of melts from a source with a constant abundance of the enriched component. Calculated pressure-dependent compositional changes using these simple two-component models can explain trends in trace element ratio and isotope ratio diagrams for Icelandic basalts where simple binary mixing models would require multiple source components. The compositional variability predicted from incomplete mixing of partially accumulated mixtures is particularly consistent with the trace element and isotopic data for Icelandic postglacial basalts. The example of Iceland demonstrates that mixing during melt extraction is a key process controlling the trace element and isotope variability observed in basaltic lavas. It is therefore stressed that polybaric mixing and melting needs to be considered in the interpretation of global MORB and OIB data before the presence of multiple source components can be inferred.

1. Introduction

Iceland, as part of the Mid-Atlantic Ridge (MAR), is characterised by a geophysical anomaly (gravity, thermal and topography) that results from buoyant upwelling of hot mantle material (Bijwaard & Spakman, 1999, Montelli *et al.*, 2004, Schilling, 1973, Shen *et al.*, 1998, Wolfe, 1997). Icelandic basalts are compositionally much more variable than mid-ocean ridge basalt from the adjacent MAR (Blichert-Toft *et al.*, 2005, Chauvel & Hémond, 2000, Elliott *et al.*, 1991, Fitton *et al.*, 1997, Hart *et al.*, 1973, Jakobsson, 1972, Kempton *et al.*, 2000, Kokfelt *et al.*, 2006, Schilling, 1973, Sigmarsson *et al.*, 1992b, Stracke *et al.*, 2003c, Thirlwall *et al.*, 2004) and melt inclusions in Icelandic basalts show even larger variability than their host rocks (Gurenko & Chaussidon, 1995, MacLennan, 2008a, MacLennan *et al.*, 2003a, MacLennan *et al.*, 2003b, Slater *et al.*, 2001).

In principle, the trace element composition of Icelandic basalts is variable for two main reasons. (1) The fractional melting process (i.e. the pressure and degree of melting), induces considerable compositional variability (2) The source composition entering the melting region is variable. Combined trace element and isotope data in Icelandic basalts indicate that these processes are interrelated and it has been shown that the erupted melts represent incomplete mixtures of small degree melts from a heterogeneous source extracted from different depths in the melting region. (Elliott *et al.*, 1991, Kokfelt *et al.*, 2006, MacLennan *et al.*, 2003a, MacLennan *et al.*, 2003b, Stracke *et al.*, 2003c, Wood, 1981). The relative importance of the source heterogeneity and the melting and mixing process for the observed compositional variability, however, has proven difficult to disentangle (MacLennan, 2008a, MacLennan *et al.*, 2003b, McKenzie *et al.*, 2004, Slater *et al.*, 2001, Stracke *et al.*, 2003c, Wood *et al.*, 1979).

The variable Sr-Nd-Pb isotopic compositions of Icelandic lavas are generally explained by mixing between different enriched and depleted mantle source components (e.g. Chauvel & Hémond, 2000, Hanan *et al.*, 2000, Hanan & Schilling, 1997, Kitagawa *et al.*, 2008, Kokfelt *et al.*, 2006, Peate *et al.*, 2009, Stracke *et al.*, 2003c, Thirlwall *et al.*, 2004). These studies often assume solid state mixing of mantle sources and therefore exclusively relate the observed isotopic variability in the lavas to variations in the bulk source composition. Hanan and Schilling (1997) and Hanan *et al.*, (2000), for

example, suggested the presence of three components in the Icelandic source based on Pb isotope compositions of Tertiary basalts. The Pb isotope variability was explained by mixing between a depleted N-MORB component (d), and two different enriched components, an EM1 (e) and an enriched plume component (p) that is similar to the common 'C' or 'FOZO' component (Hanan & Graham, 1996, Hart *et al.*, 1992, Stracke *et al.*, 2005). Similarly, Thirlwall *et al.* (2004) advocated the presence of four major source components based on combined Sr-Nd-Pb data. These major end-members (ID1, ID2, IE1, IE2, Fig. 9g) were thought to contribute in local rift areas to intermediate end-member compositions that display near binary mixing relations. Kokfelt *et al.* (2006) proposed that three main end-members represented different components from a recycled oceanic slab; the altered upper basaltic crust, the recycled lower gabbroic crust and recycled sediments. Recently, Peate *et al.*, (2010), confirmed that post-glacial lavas from the Northern and Eastern Volcanic Zone define separate sub-parallel linear trends on a $^{206}\text{Pb}/^{204}\text{Pb}$ versus $^{208}\text{Pb}/^{204}\text{Pb}$ plot and propose the presence of at least four mantle components. Details to the nature of the different components are not discussed.

In addition to solid-state mixing of mantle sources, mixing of melts from different source components during partial melting was shown to play a fundamental role for how source heterogeneity is transferred from source to lava (Ito & Mahoney, 2005, Phipps Morgan, 1999, Stracke & Bourdon, 2009). Mixing the melts during melting and melt extraction from variable depths has the effect that the isotopic compositions of erupted lavas can differ significantly from the bulk mantle source. This observation is in stark contrast to "solid state" mixing models that inherently assume that source heterogeneity is conveyed unmodified from source to melt. Phipps Morgan, (1999) and Ito and Mahoney, (2005), for example, demonstrated that progressive melting and mixing of a heterogeneous source can account for the elongated arrays in isotope space for OIB and MORB data. For Iceland, the correlations observed between trace elements and isotopes suggest that different source components are tapped systematically as a function of the degree and pressure of melting (Stracke *et al.*, 2003). Stracke *et al.*, (1999, 2003) and Stracke and Bourdon (2009) showed that factors such as different solidus temperatures for the source components, the extent, style and depth range of melt aggregation and melt extraction all have an important effect on the relationships between trace element and isotope ratios in Icelandic basalts, and MORB and OIB in general.

Here, new trace element and Hf and Nd isotope data on young tholeiitic basalts collected along Iceland's main rift are presented to evaluate the relative importance of source heterogeneity, and variable partial melting and melt mixing processes on the chemical composition of Icelandic basalts. We focus on postglacial (<10 ka) main-rift lavas to minimize complications by temporal changes in both the melting style and the composition of the mantle entering the melting region (Gee *et al.*, 1998a, Jull & McKenzie, 1996, Kempton *et al.*, 2000, Kitagawa *et al.*, 2008, MacLennan *et al.*, 2002, Slater *et al.*, 2001). Our new data is used in combination with existing data on young main-rift lavas to improve sample coverage and spatial resolution. We demonstrate that polybaric melting and mixing melts from only two source components can account for the majority of combined trace element and Nd-Hf-Sr-Pb isotope systematics of Icelandic basalts if melt mixing occurs during melt extraction.

2. Geology and sample collection

In Iceland, the Mid-Atlantic Ridge emerges in four 40-50 km wide rift zones (Reykjanes, South Western, South Eastern and North Eastern) defined by en-echelon fissure swarms and central volcanoes (Sigmundsson, 2006). The submarine Reykjanes Ridge in the Southwest progresses into the subaerial Reykjanes Rift Zone (RRZ) and the Western Rift Zone (WRZ, Fig. 1). The Eastern rift Zone (ERZ) is connected to the Western Rift Zone via the Southwestern Seismic Zone and continues northwards of the Vatnajökull Icecap as the Northern Rift Zone (NRZ). In the North, the NRZ connects to the submarine Kolbeinsey ridge via the Tjörnes Fracture Zone. Off-rift volcanic activity occurs in several localities, for example the Snæfellsnes Peninsula and the Eastern- and Southern flank zones. Crustal thickness varies from about 40 km in the centre of Iceland (underneath the Vatnajökull Icecap) to approximately 15 km under the Southwestern part of the Reykjanes Peninsula and 18 km in the Northeast underneath the Theistareykir area (Darbyshire *et al.*, 2000, Kaban *et al.*, 2002).

Fifty-one post glacial basalts from Iceland's rift and off-rift zones, which are generally less than 3000 year old have been collected for this study (Fig. 1, Table 1). Sampling focussed on collecting fresh and least differentiated samples to minimize the influence of crustal processes. We distinguish five different sample groups: samples from the Reykjanes Peninsula (RP), the Western, Eastern and Northern Volcanics (WV, EV and NV, respectively) and the off-rift basalts from the Snæfellsnes Peninsula (SP). The majority of the samples ($n = 42$) are tholeiitic rift-basalts but also include alkalic basalts from the off-rift Snæfellsnes Peninsula ($n = 7$) and the Eastern Volcanic Zone ($n = 2$). Tholeiites range from aphyric to porphyritic rocks containing phenocrysts of plagioclase (2-10 mm) and lesser amounts of olivine (0.5-5 mm) and accessory magnetite (<1mm). Total amounts of phenocrysts are below 10%. The alkali basalts typically contain a larger amount of olivine (0.5-5 mm), clinopyroxene (0.5-10 mm) and plagioclase (0.5-7 mm) phenocrysts with totals between 5 and 20%.

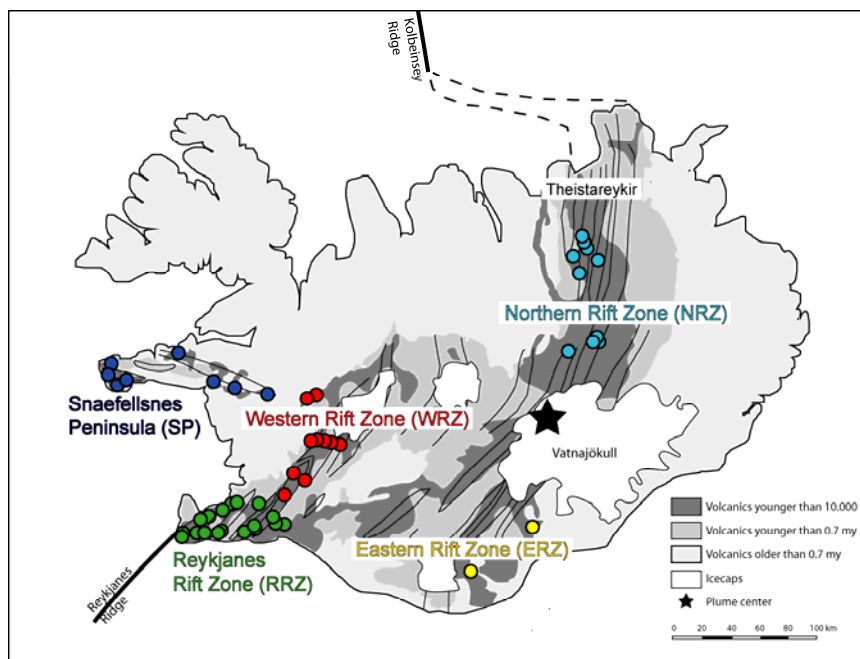


Figure 1. Simplified geological map of Iceland showing the sampling localities of all 51 lavas in coloured circles (Modified after geological map published on www.tephrabase.org). Green: Reykjanes Peninsula (RP); red: Western Volcanics (WV); light blue: Northern Volcanics (NV); dark blue: Snæfellsnes Peninsula (SP); yellow: Eastern Volcanics (EV). All samples are younger than 10 kyr.

3. Analytical techniques

Hand specimens free of weathered surfaces were cut and crushed using a diamond saw, a hydraulic press and an agate mill to produce a homogeneous rock powder. Major elements were analysed by XRF at ETH Zürich on glass beads produced using dilithium tetraborate as a flux agent. Trace elements were analysed by LA-ICPMS at the Max-Planck Institute for Chemistry, Mainz using a solid-state 213 nm Nd:YAG laser connected to a Thermo Element 2. The LA-ICPMS analyses were carried out on glasses produced from 40 mg sample powders using an automated Iridium Strip heater (Stoll *et al.*, 2008). The fused glass beads were analysed nine times (100 µm spots) to account for possible heterogeneities. ^{43}Ca (calculated from CaO wt% obtained by XRF) was used as an internal standard and all analyses were calibrated with reference glasses KL-2G and GSD-G that were interspersed after every third sample. Replicate analyses of BHVO-2 (n=3) indicate an external reproducibility (2 S.D.) of less than 3% for all measured elements except Ni, Rb, Ba, Eu, Ta, U, and Th which reproduced to 3-5%, and Cs with an external reproducibility of ~8% (2 S.D.). Pb concentrations cannot be measured precisely (2 S.D. = 50%) using this technique due to its volatile behaviour during the glass fusion process (Stoll *et al.*, 2008). The BHVO-2 concentrations are within 3% of the preferred values (<http://georem.mpch-mainz.gwdg.de>) for Co, Rb, Sr, Nb, Ba, La, Ce, Pr, Nd, Sm, Eu, Ta and U; between 3 and 6 % for V, Ni, Cu, Y, Cs, Gd, Tb, Dy, Ho, Er, Tm, Th; and better than 9% for Zr, Lu, Hf and Yb.

For Hf and Nd isotope analyses approximately 100 mg of sample powder was dissolved in a mixture of HF and HNO₃. After dissolution samples were converted to a chloride form and at this stage boric acid was added to complex any remaining fluorides. Hf was separated from the matrix with EichromTM LN-spec resin (100-150 mesh) using the technique described in detail in (Münker *et al.*, 2001). The fraction from the first Hf column was used for separation of bulk REE on a 0.5 ml TRU-spec column (50-100 mesh). Nd was purified using a 1.5 ml LN spec column (50-100 mesh) adapted from Pin and Zalduegui (1997) (Pin & Zalduegui, 1997). Hf isotope analyses were performed on a Nu Plasma Instruments MC-ICPMS at ETH Zürich in static mode using $^{179}\text{Hf}/^{177}\text{Hf} = 0.7325$ as a reference for exponential mass bias correction. ^{172}Yb and ^{175}Lu were monitored and used to correct isobaric interferences on ^{176}Hf . The contribution of ^{176}Yb to the ^{176}Hf signal never exceeded 0.012 % during analysis and is therefore within the

reported analytical error. Repeated measurements of JMC-475 during the analysis period yielded a mean of $^{176}\text{Hf}/^{177}\text{Hf}$ of 0.282194 ± 16 (2 S.D., $n = 15$). The measured Hf isotope values were corrected by sample-standard-bracketing using JMC-475 $^{176}\text{Hf}/^{177}\text{Hf} = 0.282160$ (Blichert-Toft & Albarède, 1997). Accuracy and precision of the full analytical procedure was monitored by repeated measurements of USGS rock reference material BCR-2 and BHVO-2 over an 8 month period. $^{176}\text{Hf}/^{177}\text{Hf}$ ratios of 0.282861 ± 25 (2 S.D., $n = 7$) for BCR-2 and 0.283107 ± 16 (2 S.D., $n = 5$) for BHVO-2 are in excellent agreement with reported literature values (Table 1, e.g. Bizzarro *et al.*, 2003, Chu *et al.*, 2002, Weis *et al.*, 2007).

Nd isotopic compositions were determined by thermal ionization mass spectrometry (TIMS) on a Thermo Triton at ETH Zürich. Instrumental mass fractionation was corrected using $^{146}\text{Nd}/^{144}\text{Nd} = 0.7219$. The La Jolla Nd standard yielded an average $^{143}\text{Nd}/^{144}\text{Nd}$ of 0.511855 ± 15 ($n=21$) over the measurement period. Blanks are ~ 380 pg for Hf and ~ 225 pg for Nd and are insignificant compared to the analysed amount of sample.

4. Results

4.1 Major elements

Major and trace element concentrations for the 51 samples are reported in Table 1. The main rift lavas are olivine tholeiites with MgO between 4.7 and 9.3 wt. %. The dominant phases in equilibrium with primitive Icelandic rift-zone basalts are olivine, clinopyroxene (cpx) and plagioclase (plag) with chromium spinel and magnetite as accessory phases (Carmichael, 1964, Gurenko & Sobolev, 2006, Jakobsson, 1972, Maclennan *et al.*, 2003a). Fractional crystallisation of primitive lavas results in consecutive lowering of the MgO (olivine), CaO (cpx, plag), Al_2O_3 (plag) and, to a lesser extent, Na_2O (plag). Our samples define trends of olivine (ol), plagioclase (plag) and clinopyroxene (cpx) fractionation with the different sample groups (RP, WV, NV, EV and SP) showing both differences in the mineral proportion of the fractionating assemblage and in the absolute degree of crystal fractionation (Fig. 2).

The Northern and Eastern Volcanics generally have lower MgO compared to the Western Volcanics (MgO 4.7 – 7.8 wt. % compared to 7.4 – 9.3 wt. %) and exhibit a positive correlation on diagrams of MgO versus $\text{CaO}/\text{Al}_2\text{O}_3$ and $\text{Al}_2\text{O}_3/\text{TiO}_2$ (Fig. 2e-f).

These characteristics indicate higher degrees of olivine, plagioclase and clinopyroxene ($\text{CaO}/\text{Al}_2\text{O}_3$ and $\text{Al}_2\text{O}_3/\text{TiO}_2$ decrease with decreasing MgO) crystallisation for the NV and EV samples compared to the WV samples. The two samples from the Eastern Volcanic field have relatively high TiO_2 (2.7 and 4.3 wt. % respectively) and therefore low $\text{Al}_2\text{O}_3/\text{TiO}_2$. The WV samples define a trend of combined olivine and plagioclase fractionation ($\text{CaO}/\text{Al}_2\text{O}_3$ increases but $\text{Al}_2\text{O}_3/\text{TiO}_2$ decreases with decreasing MgO) and are not significantly affected by cpx fractionation. Samples from the Reykjanes Peninsula have intermediate MgO (6.8 – 8.4 wt. %), $\text{CaO}/\text{Al}_2\text{O}_3$ and $\text{Al}_2\text{O}_3/\text{TiO}_2$ similar to the least differentiated NV samples. The more alkalic Snæfellsnes Peninsula samples have the highest MgO ranging from 9.3 to 14.5 wt. %. On a MgO versus $\text{CaO}/\text{Al}_2\text{O}_3$ diagram the SP samples lie on a positive trend implying fractionation dominated by cpx and olivine at higher pressures relative to main rift lavas. Negative correlations on diagrams of MgO versus K_2O , Na_2O and TiO_2 defined by NV and EV samples reflect the incompatibility of these elements during fractional crystallisation (Fig. 2a-d).

4.2 Trace elements

Primitive mantle normalised multi-element patterns are shown in Figure 3, with the samples grouped by geographic area. Overall, the Iceland samples display a large to moderate degree of enrichment in light rare earth element (LREE) and highly incompatible element (Cs, Ba, Rb, U, Th, Nb, Ta) (Fig. 3a). Compared to neighbouring elements, all lavas display positive anomalies in Ba, Nb and Ta and negative anomalies in Th, U and K. Relative fractionation between Nb, Ta and neighbouring elements such as U, Th and La are largest for samples from the Reykjanes Peninsula and the Western Volcanic Zone (Fig. 3b-c).

Samples from the Western Volcanics are the least LREE enriched compared to samples from other areas. For the majority of the WV samples La_N ranges from 7.5 to 10.5 and $(\text{La}/\text{Sm})_N = 1.2$ to 1.5 (where subscript N denotes primitive mantle normalised values, (McDonough & Sun, 1995). Two WV lavas from Hallmundarhraun (WV30 and WV31), however, have significantly less enriched trace element contents with $\text{La}_N = 4.5$, and relatively flat patterns with $(\text{La}/\text{Yb})_N = 1.2$ and $(\text{La}/\text{Sm})_N = 1.1$ (Fig. 3c, Table 1). Basalts from the Reykjanes Peninsula (RP) and the Northern Volcanic zone (NV) have similar REE contents with La_N ranging from 9 to 14. Samples from Askja volcano, in the Northern Volcanic zone (NV51 - NV53) are exceptional among this group as they

have more enriched ($La_N = \sim 26$ versus 12) and more fractionated ($La/Yb_N = 2.4$ versus 1.9) patterns with pronounced negative Sr anomalies, indicating a higher relative amount of plagioclase fractionation (Fig. 3e). SP alkali lavas have highly enriched and fractionated trace element patterns with La_N ranging from 16 to 40 and fractionated HREE patterns with $(Sm/Yb)_N$ from 1.7 to 3.2 (Fig. 3d). HREE patterns for RP, WV and NV samples, on the other hand, are flat with $(Sm/Yb)_N = 1.3$ to 1.6. Incompatible trace element concentrations (e.g. La, V, Y, U, Rb) and ratios (e.g. La/Sm, Sm/Yb, Lu/Hf, Y/Nb) are generally correlated with major element concentrations and ratios (e.g. MgO, K₂O, TiO₂, K₂O/TiO₂, CaO/Na₂O, Al₂O₃/TiO₂) (Fig. 4), suggesting a strong relation between the pressure (P) and degree (F) of melting (see also Elliott *et al.*, 1991, Stracke *et al.*, 2003c). Fe₂O₃ and Lu/Hf increase and SiO₂/FeO decreases with increasing pressure of melting whereas incompatible element contents (e.g. K₂O) or ratios such as La/Yb, and La/Sm decrease with increasing degree of melting (Table 1 and Fig 4). Data on main rift lavas from this study fit into the general correlations observed for Iceland (Fig. 5, Kitagawa *et al.*, 2008, Kokfelt *et al.*, 2006, Peate *et al.*, 2009, Peate *et al.*, 2010, Stracke *et al.*, 2003c). There is no systematic relation between the observed variations and the different geographic areas (i.e. RP, WV, NV), and thus distance to the plume centre. Samples from Theistareykir in the Northern Volcanic Zone (Fig. 1) represent the high-F, low-P melts and the Eastern Volcanic Zone lavas the low-F high-P melts. The off-rift SP samples have highly variable trace element contents and ratios at a given major element concentration.

Compared to the main rift lavas, their much more variable and higher La/Sm, La/Yb ratios (Fig. 4) suggest that they are smaller degree melts, whereas their overlapping Fe₂O₃, Lu/Hf and Al₂O₃/TiO₂ imply similar average pressures of melting compared to main rift lavas.

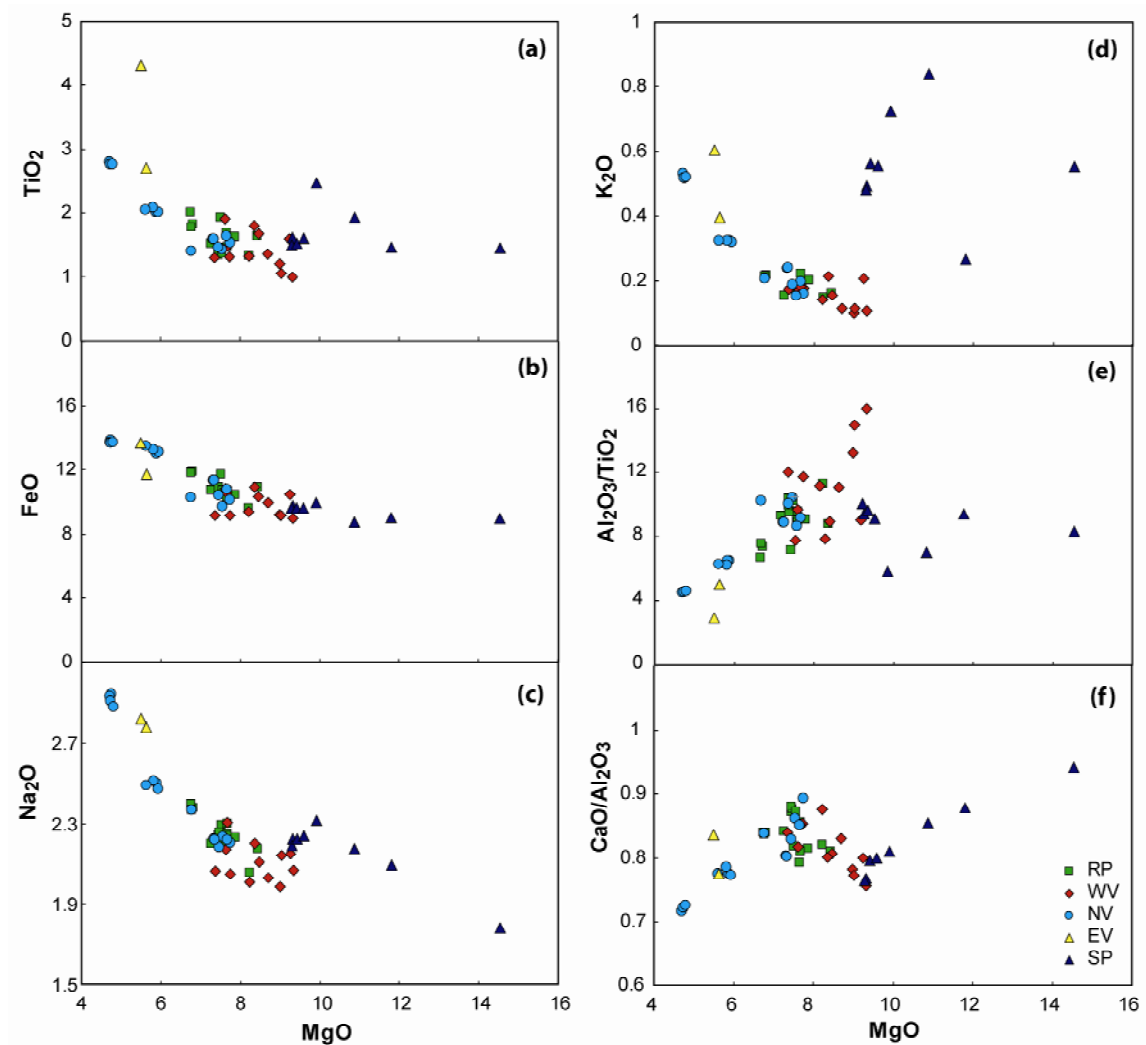


Figure 2. Whole rock major element variation in Iceland basalts per geographical area against MgO. (a) TiO_2 , (b) Fe_2O_3 , (c) Na_2O , (d) K_2O , (e) $\text{Al}_2\text{O}_3/\text{TiO}_2$, (f) $\text{CaO}/\text{Al}_2\text{O}_3$. Fractional crystallisation trends are defined by consecutive lowering of the MgO (olivine), CaO (cpx, plag), Al_2O_3 (plag) and, to a lesser extent, Na_2O (plag). Samples from the different areas show both differences in the mineral proportion of the fractionating assemblage and in the absolute degree of crystal fractionation. WV samples lie on trends of combined olivine and plagioclase fractionation whereas RP and NV samples lie on trends indicating progressive simultaneous fractionation of plagioclase and clinopyroxene. Especially NV samples with low MgO (4.7 - 6 wt. %) are characterised by significant fractionation of clinopyroxene and plagioclase.

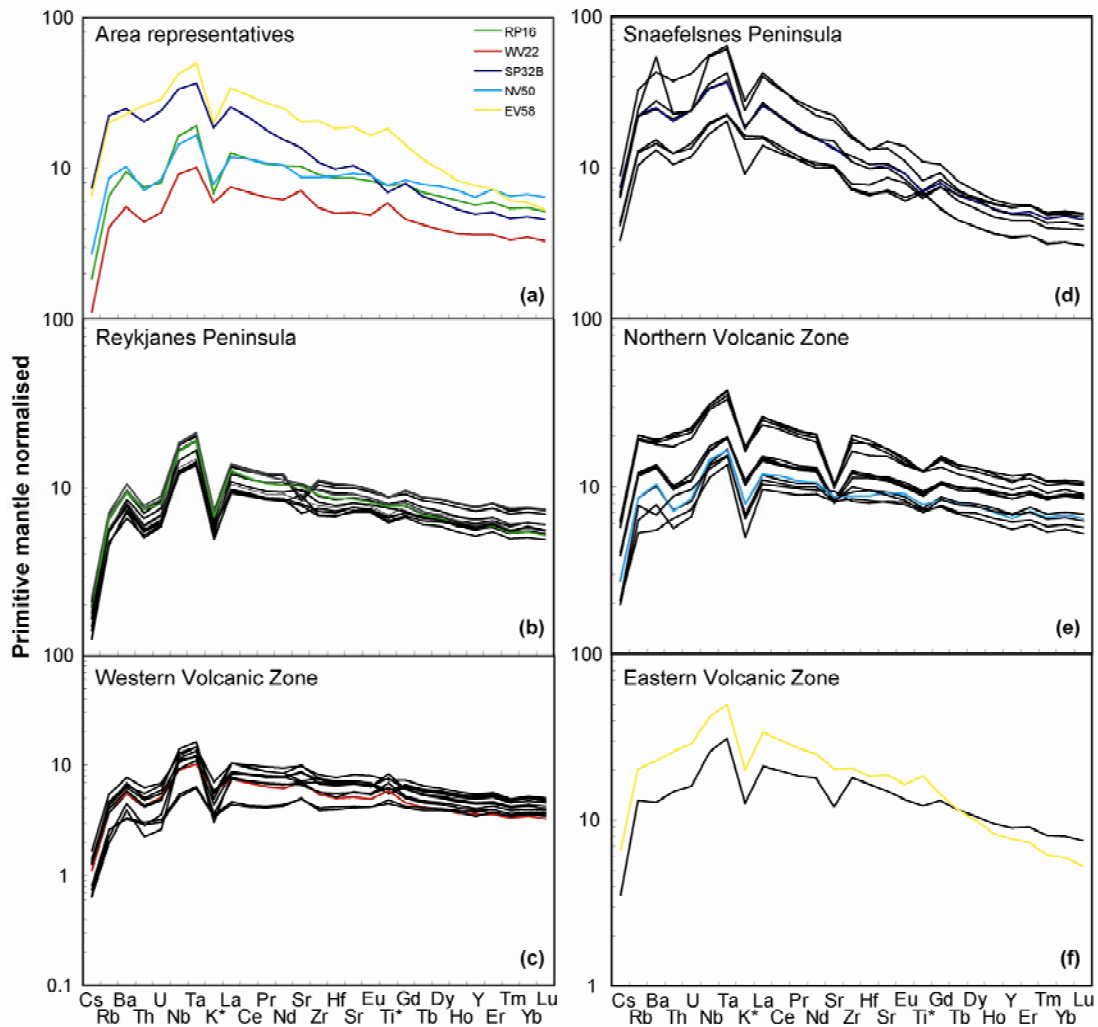


Figure 3. Primitive mantle normalised extended trace element patterns for area representatives (a showing RP16, WV22, SP35, NV50, EV58) and for all samples per geographical area (b, c, d, e, f). Coloured patterns in panels b, c, d, e, and f are group representatives shown in a. Primitive mantle values are from (McDonough & Sun, 1995)

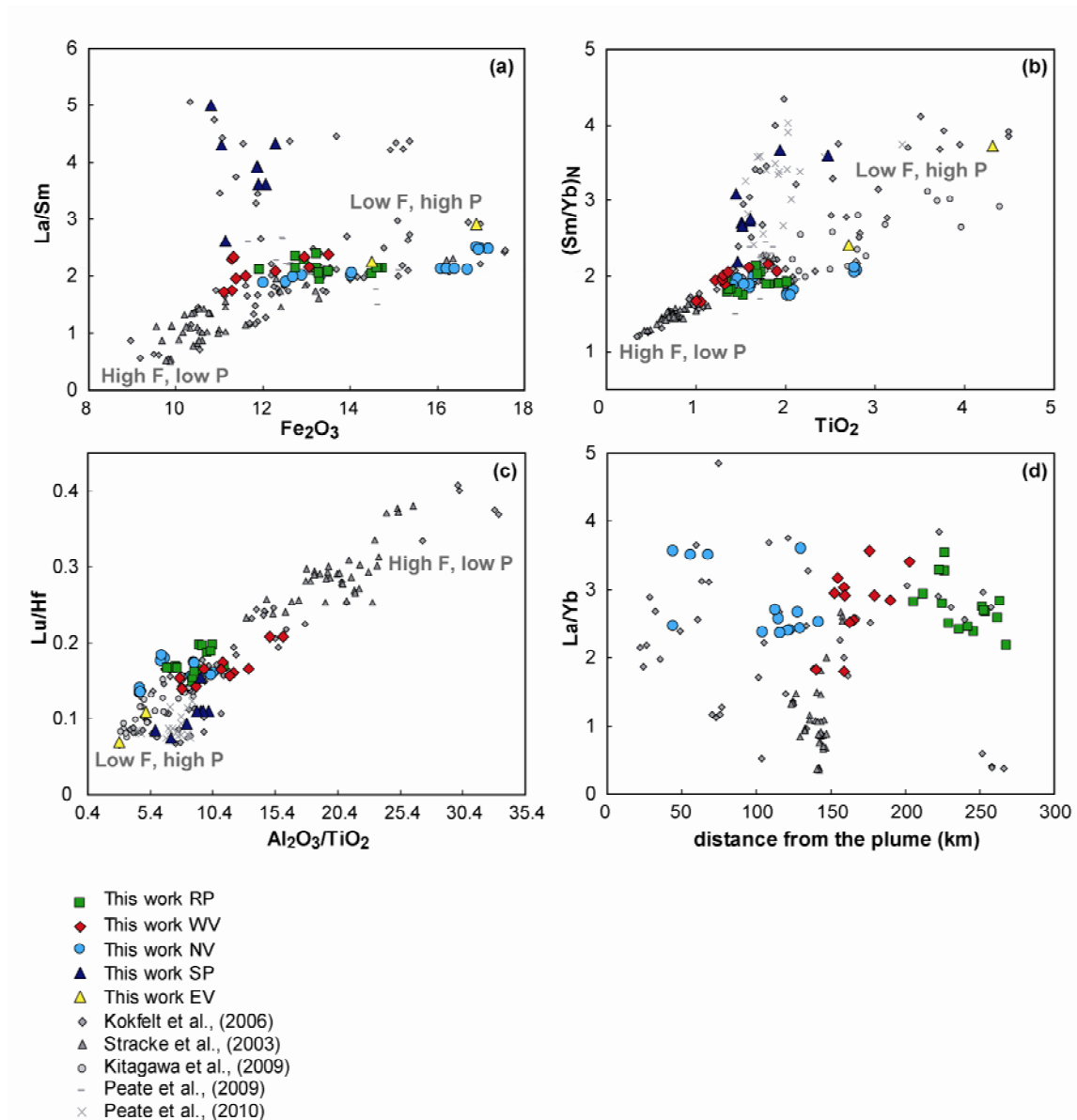


Figure 4. Correlations between major element and trace element concentrations and ratios for Icelandic samples (a-c) and La/Yb variability with distance from the inferred plume center (d). Main rift lavas show correlations indicating a relation between the pressure (P) and the degree (F) of melting. FeO, Lu/Hf increase and Al₂O₃/TiO₂ decreases with increasing pressure of melting whereas incompatible element contents and ratios such as K₂O, La/Yb and La/Sm decrease with increasing degree of melting. Variability of La/Yb on a local scale is as large as the overall variability across Iceland, indicating that the melting behaviour is not primarily controlled by the temperature anomaly across the Iceland plume ($\Delta T \sim 100$ °C).

Table 1. Major, trace and Hf-Nd isotope compositions of Icelandic post-glacial lavas.

Sample	RP1	RP2	RP 3	RP5	RP6	RP7	RP8	RP9	RP10
Flow name	Illahraun	Afstaparhraun	Arnarseturshraun	Stamparhraun	Eldvarpahraun	Eldvarpahraun	Arnarseturshraun	Arnarseturshraun	Ögmundarhraun
Age ¹	1211-1240	1325 AD	1211-1240 AD	1211-1240 AD	1211-1240 AD	1211-1240 AD	1211-1240 AD	1211-1240 AD	1151-1188 AD
Longitude	21.991	22.173	22.425	22.709	22.600	22.558	22.420	22.426	22.233
Latitude	64.054	64.016	63.928	63.830	63.822	63.819	63.909	63.890	63.854
Distance from plume	226.4	236.1	254.0	268.0	263.5	261.7	251.6	252.7	245.6
Major elements (wt%) ^a									
SiO ₂	47.84	48.87	48.74	49.22	47.77	48.28	48.57	48.46	48.84
TiO ₂	1.72	1.35	1.82	1.52	1.64	1.93	2.01	1.78	1.46
Al ₂ O ₃	15.02	13.99	13.50	14.18	14.44	13.89	13.52	13.52	13.94
Fe ₂ O _{3total}	12.74	13.24	14.73	13.30	13.49	14.49	14.64	14.60	13.31
FeO	10.31	10.72	11.93	10.77	10.92	11.73	11.85	11.82	10.78
MgO	7.93	7.45	6.80	7.26	8.43	7.52	6.76	6.77	7.46
MnO	0.19	0.21	0.22	0.21	0.20	0.22	0.22	0.22	0.21
CaO	12.14	12.21	11.33	11.93	11.70	11.37	11.34	11.31	12.23
Na ₂ O	2.18	2.24	2.38	2.20	2.18	2.30	2.40	2.37	2.25
K ₂ O	0.20	0.18	0.22	0.16	0.16	0.19	0.21	0.21	0.18
P ₂ O ₅	0.17	0.13	0.20	0.15	0.19	0.20	0.20	0.20	0.13
Cr ₂ O ₃	0.05	0.02	0.02	0.03	0.05	0.04	0.03	0.02	0.02
NiO	0.02	0.01	0.01	0.01	0.02	0.01	0.01	0.01	0.01
Sum	99.5	99.2	99.1	99.4	99.5	99.6	99.1	99.1	99.2
Trace elements (ppm) ^b									
V	327	379	451	391	357	409	444	428	385
Co	54	52	55	53	57	55	55	52	53
Ni	119	83	92	93	156	117	88	81	86
Cu	149	158	172	161	149	161	181	187	176
Rb	3.87	3.39	4.11	2.83	2.72	3.34	3.98	4.09	3.52
Sr	205	156	172	141	188	172	168	173	159
Y	26	24	33	26	28	33	31	33	26
Zr	98	72	114	79	103	115	109	117	77
Nb	11.3	8.3	12.6	8.3	11.4	12.3	12.3	12.5	8.5
Cs	0.04	0.04	0.04	0.03	0.03	0.04	0.04	0.05	0.04
Ba	61	53	64	44	49	56	62	64	54
La	8.3	6.2	9.0	6.0	7.8	8.6	8.8	9.0	6.5
Ce	19	15	22	15	19	21	22	21	16
Pr	2.75	2.15	3.11	2.18	2.75	3.03	3.06	3.08	2.23
Nd	13.2	10.4	15.1	10.6	13.4	14.8	14.7	15.0	10.9
Sm	3.53	2.97	4.21	3.08	3.74	4.20	4.07	4.20	3.13
Eu	1.29	1.12	1.50	1.14	1.35	1.48	1.45	1.48	1.17
Gd	4.28	3.72	5.19	3.92	4.58	5.25	5.01	5.27	4.00
Tb	0.70	0.63	0.87	0.66	0.75	0.87	0.84	0.88	0.68
Dy	4.52	4.24	5.76	4.48	4.89	5.75	5.50	5.80	4.56
Ho	0.93	0.89	1.20	0.94	1.01	1.19	1.13	1.21	0.96
Er	2.69	2.61	3.51	2.77	2.91	3.50	3.30	3.56	2.82
Tm	0.38	0.37	0.50	0.40	0.41	0.49	0.47	0.51	0.40
Yb	2.53	2.55	3.36	2.74	2.73	3.32	3.18	3.34	2.72
Lu	0.37	0.38	0.49	0.41	0.41	0.49	0.47	0.50	0.41
Hf	2.46	1.92	2.92	2.06	2.63	2.98	2.82	3.01	2.06
Ta	0.72	0.51	0.79	0.51	0.71	0.77	0.75	0.79	0.53
Pb	0.43	0.31	0.53	0.46	0.48	0.50	0.54	0.57	0.51
Th	0.57	0.45	0.59	0.41	0.43	0.52	0.56	0.60	0.48
U	0.16	0.13	0.17	0.12	0.13	0.15	0.17	0.17	0.14
Hf-Nd isotope composition ^c									
¹⁷⁶ Hf/ ¹⁷⁷ Hf	0.283167	0.283199		0.283197	0.283175	0.283186	0.283189	0.283195	0.283195
2σ SE ±	12	7		8	7	7	8	6	11
¹⁴³ Nd/ ¹⁴⁴ Nd	0.513036	0.513057		0.513051	0.513033	0.513051	0.513050	0.513050	0.513032
2s SE ±	6	8		8	5	6	9	7	7

¹ Ages are from Peate et al., 2009 and Sinton et al., 2005^a Major element compositions were determined by XRF at ETH Zürich. FeO is calculated using Fe²⁺/Fe³⁺ of 0.9.^b Trace element concentrations were measured by LA-ICPMS at MaxPlanck Institut für Chemie, Mainz.^c Hf and Nd isotope compositions were measured by MC-ICPMS and Triton-TIMS at ETH, Zürich. 2s SE are internal error at the last significant digit

Table 1. Continued

Sample flow name age	RP11 Herðisarvík post glacial	RP12 Grindaskörð post glacial	RP 13 Hlíðarvatn post glacial	RP15 Nesjahraun ~1800 BP	RP17 Hólmshraun post glacial	RP55 Straumsvík post glacial	RP56 Ögmundarhraun 1151-1188 AD	WV16 Svinahraunsbruni ~1000 AD	WV18 Skjaldbreiður I post glacial
Longitude	21.786	21.741	21.740	21.445	21.701	22.027	22.155	21.452	20.920
Latitude	63.870	63.876	63.875	63.956	64.081	64.043	63.859	64.028	64.437
distance from plume	224.9	222.6	226.5	205.8	212.1	229.0	241.9	202.9	165.3
Major elements (wt%)									
SiO ₂	47.84	47.91	47.88	48.28	47.78	48.83	48.87	47.41	47.68
TiO ₂	1.34	1.63	1.67	1.48	1.69	1.39	1.37	1.59	1.21
Al ₂ O ₃	15.15	14.81	15.12	14.25	15.04	13.88	14.01	14.42	16.02
Fe ₂ O _{3total}	11.92	12.94	13.21	13.21	12.74	13.50	13.28	12.94	11.37
FeO	9.65	10.48	10.70	10.70	10.32	10.94	10.75	10.48	9.21
MgO	8.22	7.87	7.66	7.68	7.67	7.46	7.56	9.25	8.99
MnO	0.18	0.20	0.20	0.20	0.19	0.21	0.21	0.20	0.17
CaO	12.43	12.07	11.99	12.20	12.18	12.23	12.23	11.54	12.53
Na ₂ O	2.06	2.23	2.25	2.30	2.24	2.26	2.21	2.15	1.99
K ₂ O	0.15	0.20	0.22	0.19	0.18	0.18	0.17	0.21	0.10
P ₂ O ₅	0.13	0.17	0.18	0.15	0.16	0.14	0.14	0.17	0.13
Cr ₂ O ₃	0.05	0.04	0.04	0.02	0.04	0.02	0.02	0.06	0.06
NiO	0.02	0.02	0.02	0.01	0.01	0.01	0.01	0.02	0.02
Sum	99.1	99.3	99.8	99.2	99.2	99.3	99.6	99.2	99.7
Trace elements (ppm)									
V	331	354	364	357	368	388	381	338	287
Co	52	53	53	52	51	53	55	56	57
Ni	159	118	121	90	108	84	95	188	192
Cu	148	167	153	177	161	168	193	140	144
Rb	2.77	3.90	4.23	3.55	3.31	3.45	3.27	3.94	1.33
Sr	181	208	212	202	193	167	160	204	169
Y	22	25	26	25	25	27	25	25	21
Zr	73	94	101	86	86	82	76	95	78
Nb	8.6	11.3	12.7	9.2	10.0	9.1	8.6	11.3	7.5
Cs	0.03	0.04	0.05	0.04	0.03	0.04	0.04	0.04	0.01
Ba	47	62	69	55	54	54	51	62	30
La	6.2	8.1	9.0	7.1	7.1	6.8	6.4	8.2	5.4
Ce	15	19	21	17	17	16	15	19	14
Pr	2.15	2.71	2.97	2.42	2.43	2.33	2.22	2.72	2.03
Nd	10.5	13.0	14.0	11.7	11.8	11.4	10.8	13.0	9.9
Sm	2.92	3.53	3.74	3.28	3.30	3.24	3.08	3.51	2.76
Eu	1.11	1.29	1.34	1.19	1.22	1.20	1.14	1.26	1.03
Gd	3.61	4.27	4.44	4.08	3.97	4.15	3.83	4.25	3.43
Tb	0.60	0.70	0.72	0.68	0.66	0.70	0.65	0.68	0.57
Dy	3.95	4.48	4.61	4.42	4.32	4.72	4.33	4.44	3.74
Ho	0.82	0.92	0.94	0.92	0.88	0.99	0.90	0.90	0.77
Er	2.39	2.66	2.74	2.67	2.54	2.89	2.64	2.61	2.23
Tm	0.34	0.37	0.38	0.38	0.36	0.41	0.37	0.37	0.31
Yb	2.21	2.46	2.53	2.51	2.41	2.71	2.59	2.41	2.12
Lu	0.33	0.36	0.37	0.37	0.36	0.40	0.38	0.35	0.31
Hf	1.94	2.42	2.56	2.25	2.20	2.16	2.01	2.45	1.87
Ta	0.52	0.70	0.79	0.58	0.62	0.55	0.53	0.71	0.44
Pb	0.41	0.54	0.54	0.48	0.47	0.51	0.47	0.38	0.34
Th	0.40	0.56	0.62	0.50	0.47	0.46	0.45	0.59	0.22
U	0.12	0.17	0.18	0.14	0.14	0.14	0.13	0.16	0.07
Hf-Nd isotope composition									
¹⁷⁶ Hf/ ¹⁷⁷ Hf	0.283180	0.283169		0.283198	0.283170		0.283218	0.283163	0.283199
2σ SE ±	6	15		8	8		17	5	6
¹⁴³ Nd/ ¹⁴⁴ Nd	0.513044	0.513017		0.513043	0.513042		0.513036	0.513033	0.513062
2σ SE ±	6	6		7	8		4	7	6

Table 1. Continued

Sample flow name age	WV19 Skjaldbreiður II post glacial	WV20 Skjaldbreiður II post glacial	WV21 Sköflungur 5300 BP 2	WV 21 B Sköflungur 5300 BP 2	WV22 Skjaldbreiður II post glacial	WV25 Thjófahraun 3360 BP 2	WV26 Thingvallhraun 10,200 BP 2	WV27 Nesjahraun ~1800 BP 2	WV30 Iallmundarhraun 1050 AD 2
Longitude	20.866	20.783	20.650	20.650	20.694	21.051	21.028	21.247	20.924
Latitude	64.439	64.444	64.447	64.447	64.446	64.263	64.145	64.124	64.728
distance from plume	162.7	158.7	152.3	159.5	154.4	175.9	179.0	189.8	140.0
Major elements (wt%)									
SiO ₂	48.29	48.20	47.54	47.78	48.31	47.52	47.51	48.04	48.32
TiO ₂	1.32	1.30	1.67	1.91	1.31	1.80	1.36	1.48	1.06
Al ₂ O ₃	14.83	15.64	14.97	14.79	15.36	14.23	15.08	14.27	15.80
Fe ₂ O _{3total}	11.59	11.28	12.73	13.39	11.32	13.50	12.27	13.05	11.29
FeO	9.39	9.14	10.31	10.84	9.16	10.93	9.94	10.57	9.14
MgO	8.22	7.36	8.47	7.63	7.74	8.36	8.70	7.67	9.03
MnO	0.18	0.18	0.19	0.20	0.18	0.20	0.19	0.20	0.18
CaO	12.99	13.12	12.07	12.09	13.11	11.40	12.53	12.17	12.21
Na ₂ O	2.01	2.06	2.11	2.17	2.05	2.20	2.03	2.30	2.14
K ₂ O	0.14	0.17	0.16	0.17	0.18	0.21	0.11	0.18	0.11
P ₂ O ₅	0.12	0.13	0.16	0.19	0.13	0.19	0.17	0.14	0.11
Cr ₂ O ₃	0.05	0.04	0.05	0.04	0.05	0.05	0.05	0.02	0.02
NiO	0.01	0.01	0.02	0.01	0.01	0.02	0.02	0.01	0.02
Sum	99.3	99.0	99.5	99.8	99.2	98.9	99.4	98.9	99.6
Trace elements (ppm)									
V	333	323	336	276	230	257	219	264	199
Co	50	48	54	39	35	41	39	40	40
Ni	112	90	144	84	76	113	111	71	121
Cu	157	145	159	132	109	117	103	121	106
Rb	2.59	3.25	2.62	2.19	2.43	2.82	1.18	2.43	1.56
Sr	174	199	195	137	141	142	133	141	99
Y	22	22	23	20	16	19	17	17	16
Zr	72	80	86	74	57	80	60	59	43
Nb	7.3	8.5	9.7	8.1	6.2	9.0	7.6	6.4	3.7
Cs	0.03	0.04	0.03	0.02	0.02	0.03	0.01	0.03	0.02
Ba	42	51	46	37	37	43	26	39	22
La	5.6	6.7	6.8	5.7	4.9	6.7	4.8	5.0	3.0
Ce	14	16	17	14	12	16	12	12	7
Pr	1.97	2.23	2.45	2.02	1.63	2.26	1.76	1.74	1.09
Nd	9.6	10.7	11.9	9.9	7.7	10.7	8.5	8.4	5.6
Sm	2.77	2.92	3.30	2.74	2.08	2.82	2.31	2.31	1.72
Eu	1.03	1.07	1.24	1.00	0.76	1.00	0.84	0.86	0.65
Gd	3.48	3.62	3.98	3.30	2.51	3.29	2.74	2.84	2.31
Tb	0.58	0.60	0.64	0.54	0.42	0.53	0.45	0.47	0.40
Dy	3.82	3.93	4.21	3.50	2.67	3.42	2.96	3.10	2.73
Ho	0.80	0.81	0.86	0.72	0.55	0.70	0.61	0.65	0.58
Er	2.30	2.38	2.46	2.06	1.58	1.99	1.75	1.88	1.74
Tm	0.32	0.33	0.34	0.29	0.23	0.28	0.24	0.27	0.25
Yb	2.21	2.22	2.30	1.95	1.53	1.89	1.65	1.75	1.65
Lu	0.32	0.33	0.34	0.29	0.22	0.27	0.24	0.26	0.25
Hf	1.86	2.04	2.18	1.86	1.42	1.96	1.46	1.56	1.18
Ta	0.46	0.54	0.60	0.50	0.38	0.55	0.45	0.41	0.24
Pb	0.40	0.48	0.43	0.38	0.29	0.45	0.24	0.33	0.21
Th	0.38	0.50	0.40	0.33	0.35	0.44	0.18	0.35	0.24
U	0.11	0.14	0.12	0.10	0.10	0.13	0.05	0.10	0.07
Hf-Nd isotope composition									
¹⁷⁶ Hf/ ¹⁷⁷ Hf	0.283204	0.283188	0.283199		0.283173	0.283164	0.283191	0.283184	
2σ SE ±	7	6	7		10	6	5	5	
¹⁴³ Nd/ ¹⁴⁴ Nd	0.513068	0.513037	0.513050		0.513055	0.513034	0.513051	0.513041	
2σ SE ±	8	7	7		8	6	8	5	

Table 1. Continued

Sample flow name age	WV31 Íallmundarhraun 1050 AD 2	SP 28 Gábrókarhraun 1, post glacial	SP29 Gábrókarhraun post glacial	SP 32 A Rauðhálsahraun historic	SP 32 B Rauðhálsahraun historic	SP 33 Miðhraun <4000 BP	SP 34 Porserkjähraun <4000 BP	SP 35 Porserkjähraun <4000 BP	SP36 Prestahraun <4000 BP
Longitude	20.842	21.578	21.578	22.291	22.291	22.661	22.931	22.946	23.959
Latitude	64.745	64.747	64.747	64.834	64.834	64.860	64.973	64.971	64.881
distance from plume	158.9	203.0	193.8	237.0	237.0	259.0	268.0	271.5	306.7
Major elements (wt%)									
SiO ₂	48.21	47.35	47.14	47.47	47.50	46.67	46.53	47.07	45.72
TiO ₂	1.00	1.61	1.50	1.52	1.60	1.47	1.45	1.94	2.47
Al ₂ O ₃	16.00	15.20	15.16	14.65	14.63	13.83	12.07	13.64	14.38
Fe ₂ O _{3total}	11.11	12.05	11.90	11.88	11.86	11.13	11.05	10.81	12.28
FeO	8.99	9.76	9.64	9.62	9.61	9.02	8.95	8.76	9.94
MgO	9.33	9.32	9.30	9.43	9.60	11.81	14.54	10.88	9.92
MnO	0.18	0.19	0.19	0.19	0.19	0.18	0.18	0.18	0.19
CaO	12.10	11.67	11.59	11.65	11.69	12.14	11.36	11.67	11.65
Na ₂ O	2.07	2.23	2.19	2.23	2.24	2.09	1.78	2.18	2.32
K ₂ O	0.11	0.49	0.48	0.56	0.56	0.27	0.55	0.84	0.72
P ₂ O ₅	0.10	0.19	0.19	0.21	0.21	0.18	0.22	0.31	0.50
Cr ₂ O ₃	0.02	0.04	0.04	0.07	0.07	0.13	0.24	0.13	0.08
NiO	0.02	0.02	0.02	0.02	0.02	0.04	0.05	0.03	0.02
Sum	99.6	99.8	99.2	99.3	99.6	99.3	99.4	99.1	99.6
Trace elements (ppm)									
V	196	235	229	317	305	291	280	294	336
Co	39	41	40	56	55	59	64	51	51
Ni	121	105	107	190	185	284	417	220	174
Cu	100	74	73	110	110	72	88	80	60
Rb	1.55	7.75	7.52	13.19	13.44	6.28	12.96	19.61	14.52
Sr	101	205	199	264	272	207	301	408	447
Y	15	15	15	24	21	23	19	21	25
Zr	41	75	77	125	116	82	115	164	171
Nb	3.5	13.6	13.1	23.0	22.8	11.6	24.6	38.4	37.1
Cs	0.02	0.09	0.09	0.14	0.16	0.07	0.13	0.19	0.14
Ba	22	101	96	159	163	86	184	283	356
La	2.9	10.5	10.2	17.0	16.5	9.1	17.5	27.4	26.1
Ce	7	23	22	37	36	21	36	56	55
Pr	1.05	3.02	2.87	4.65	4.56	2.88	4.49	6.79	7.01
Nd	5.4	13.0	12.6	19.9	19.4	13.5	19.3	27.8	30.1
Sm	1.67	2.89	2.82	4.33	4.21	3.48	4.06	5.46	6.02
Eu	0.64	0.99	0.93	1.41	1.39	1.22	1.30	1.70	2.14
Gd	2.24	2.92	2.94	4.55	4.30	4.05	4.08	5.01	5.73
Tb	0.39	0.44	0.44	0.69	0.65	0.65	0.60	0.71	0.81
Dy	2.63	2.76	2.76	4.29	4.02	4.21	3.60	4.16	4.72
Ho	0.56	0.55	0.55	0.86	0.80	0.86	0.71	0.79	0.91
Er	1.65	1.55	1.56	2.43	2.25	2.46	1.95	2.13	2.49
Tm	0.24	0.22	0.21	0.34	0.31	0.34	0.27	0.29	0.33
Yb	1.59	1.42	1.42	2.22	2.10	2.28	1.74	1.92	2.16
Lu	0.23	0.21	0.21	0.33	0.31	0.34	0.26	0.28	0.32
Hf	1.13	1.85	1.91	2.99	2.78	2.19	2.79	3.75	3.73
Ta	0.23	0.84	0.82	1.39	1.36	0.75	1.56	2.35	2.26
Pb	0.21	0.70	0.65	1.10	1.01	0.57	0.90	0.92	0.93
Th	0.23	0.99	0.99	1.68	1.62	0.84	1.84	2.97	1.79
U	0.06	0.29	0.28	0.48	0.49	0.24	0.48	0.84	0.48
Hf-Nd isotope composition									
¹⁷⁶ Hf/ ¹⁷⁷ Hf	0.283224		0.283135						0.283128
2σ SE ±	16		5						5
¹⁴³ Nd/ ¹⁴⁴ Nd	0.513069		0.512941						0.512960
2σ SE ±	6		5						4

Table 1. Continued

Sample flow name age	NV41 Prengslaborgir ~3000 BP 2	NV42 Elda 1729 AD 2	NV43 Nyarhraun 1875 AD	NV44 Bürfellshraun ~3000 BP	NV45 Krafla 1729 AD	NV47 Krafla 1984 AD	NV48 Daleldar 3000 BP	NV49 Krafla 1984 AD	NV50 Krafla 1984 AD
Longitude	16.948	16.945	16.390	16.752	16.784	16.791	16.793	16.841	16.841
Latitude	65.575	65.656	65.651	65.649	65.718	65.716	65.664	65.795	65.795
distance from plume	104.2	129.1	130.0	113.0	121.5	141.5	115.7	129.1	114.6
Major elements (wt%)									
SiO ₂	48.94	49.37	50.15	48.80	49.78	49.79	49.60	49.04	49.20
TiO ₂	1.54	2.02	2.78	1.64	2.02	2.09	2.05	1.60	1.60
Al ₂ O ₃	14.16	13.20	12.64	14.23	13.22	13.07	12.91	14.19	14.21
Fe ₂ O _{3total}	12.53	16.08	17.17	13.32	16.21	16.40	16.70	14.01	14.04
FeO	10.15	13.02	13.90	10.78	13.12	13.28	13.52	11.34	11.37
MgO	7.75	5.88	4.75	7.66	5.94	5.82	5.62	7.32	7.34
MnO	0.20	0.24	0.26	0.21	0.24	0.24	0.25	0.21	0.21
CaO	12.66	10.24	9.11	12.11	10.22	10.27	10.00	11.38	11.40
Na ₂ O	2.20	2.50	2.95	2.22	2.47	2.51	2.49	2.22	2.22
K ₂ O	0.16	0.32	0.52	0.20	0.32	0.32	0.32	0.24	0.24
P ₂ O ₅	0.14	0.21	0.31	0.16	0.21	0.21	0.20	0.17	0.17
Cr ₂ O ₃	0.02	0.02	0.01	0.02	0.02	0.02	0.01	0.04	0.04
NiO	0.01	0.01	0.01	0.01	0.01	0.01	0.01	0.01	0.01
Sum	99.6	99.1	99.5	99.8	99.5	99.5	99.1	99.5	99.7
Trace elements (ppm)									
V	342	476	528	336	481	493	472	381	393
Co	53	55	50	51	53	54	54	50	53
Ni	91	74	38	89	66	62	56	109	117
Cu	169	153	125	169	151	161	157	146	148
Rb	3.17	7.12	11.26	3.77	6.90	7.25	7.09	5.15	5.15
Sr	162	160	197	186	164	165	158	171	173
Y	26	38	41	24	38	37	36	29	28
Zr	89	130	170	85	128	125	118	97	92
Nb	7.7	11.3	19.8	9.1	11.1	11.9	11.3	9.4	9.8
Cs	0.04	0.08	0.12	0.04	0.08	0.08	0.08	0.06	0.06
Ba	36	87	117	51	85	89	85	66	68
La	6.2	9.7	15.2	6.7	9.5	9.8	9.3	7.5	7.7
Ce	16	23	36	17	23	24	22	18	19
Pr	2.26	3.28	5.02	2.45	3.22	3.41	3.19	2.65	2.74
Nd	11.3	16.0	23.2	11.8	15.7	16.4	15.4	13.0	13.3
Sm	3.27	4.55	6.10	3.32	4.45	4.60	4.38	3.72	3.74
Eu	1.19	1.56	2.06	1.24	1.55	1.63	1.52	1.34	1.38
Gd	4.18	5.81	7.14	4.07	5.79	5.72	5.59	4.69	4.57
Tb	0.70	0.98	1.17	0.68	0.98	0.97	0.94	0.79	0.77
Dy	4.66	6.57	7.49	4.36	6.58	6.43	6.32	5.32	5.11
Ho	0.96	1.38	1.52	0.89	1.39	1.35	1.33	1.11	1.05
Er	2.76	4.06	4.47	2.60	4.09	3.96	3.96	3.28	3.14
Tm	0.39	0.59	0.62	0.36	0.59	0.57	0.57	0.46	0.44
Yb	2.61	3.99	4.20	2.47	3.95	3.87	3.91	3.09	2.98
Lu	0.38	0.60	0.61	0.36	0.60	0.57	0.59	0.46	0.43
Hf	2.33	3.32	4.32	2.26	3.33	3.24	3.19	2.66	2.49
Ta	0.50	0.72	1.23	0.57	0.71	0.73	0.73	0.61	0.61
Pb	0.46	0.77	1.11	0.41	0.80	0.85	0.79	0.59	0.62
Th	0.51	0.79	1.37	0.45	0.81	0.80	0.76	0.57	0.56
U	0.15	0.22	0.39	0.13	0.22	0.24	0.22	0.17	0.17
Hf-Nd isotope composition									
¹⁷⁶ Hf/ ¹⁷⁷ Hf	0.283204	0.283201		0.283192	0.283198		0.283194	0.283188	0.283191
2σ SE ±	5	11		4	8		5	7	6
¹⁴³ Nd/ ¹⁴⁴ Nd	0.513078	0.513040		0.513048	0.513034		0.513053	0.513044	0.513029
2σ SE ±	6	6		6	6		7	6	5

Table 1. Continued

Sample flow name age	NV51 Askja 1961 AD	NV52 Askja ~1920 AD	NV53 Askja 1961 AD an	NV54 Frambruni n/skaftafellhraun 1362 ashlayer	EV57 1783 AD	EV58 Hólmsbraun 934 AD	USGS BHVO reference material Average (n = 3)
Longitude	16.638	16.721	16.770	17.075	17.739	18.541	
Latitude	65.057	65.044	64.914	65.017	63.891	63.629	
distance from pl	67.5	55.7	44.2	43.8	72.5	110.0	
Major elements (wt%)							
SiO ₂	50.15	50.03	50.43	49.74	49.31	45.89	
TiO ₂	2.80	2.77	2.76	1.41	2.71	4.31	
Al ₂ O ₃	12.64	12.63	12.74	14.49	13.61	12.68	
Fe ₂ O ₃	16.97	16.90	16.94	12.68	14.50	16.90	
FeO	13.74	13.68	13.72	10.27	11.74	13.68	
MgO	4.71	4.73	4.80	6.77	5.64	5.50	
MnO	0.25	0.25	0.25	0.20	0.21	0.21	
CaO	9.06	9.12	9.25	12.14	10.54	10.60	
Na ₂ O	2.93	2.91	2.88	2.37	2.78	2.82	
K ₂ O	0.53	0.52	0.52	0.21	0.40	0.60	
P ₂ O ₅	0.31	0.31	0.31	0.15	0.29	0.41	
Cr ₂ O ₃	0.00	0.01	0.01	0.02	0.01	0.01	
NiO	0.01	0.00	0.01	0.01	0.01	0.01	
Trace elements (ppm)							
V	533	541	513	349	410	558	329
Co	50	51	48	51	48	56	44.9
Ni	30	33	36	68	46	64	124
Cu	124	128	121	145	104	153	132
Rb	12.15	11.63	12.24	4.60	7.86	12.26	9.19
Sr	198	195	204	163	241	404	390
Y	50	47	46	29	39	33	27.7
Zr	214	201	191	104	188	219	188
Nb	21.1	20.5	21.2	8.7	17.7	28.8	17.8
Cs	0.13	0.12	0.13	0.04	0.07	0.14	0.09
Ba	123	120	127	44.8	84.7	151	130
La	17.0	16.2	16.8	7.1	13.7	22.2	15.5
Ce	39.2	38.0	39.8	17.6	33.4	51.2	37.2
Pr	5.41	5.21	5.47	2.53	4.69	6.90	5.24
Nd	25.6	24.5	25.6	12.4	22.4	31.6	24.7
Sm	6.81	6.46	6.84	3.60	6.07	7.62	6.12
Eu	2.19	2.11	2.26	1.28	2.05	2.53	2.03
Gd	8.22	7.82	8.07	4.54	7.12	7.84	6.49
Tb	1.34	1.27	1.32	0.77	1.13	1.15	0.96
Dy	8.73	8.24	8.63	5.10	7.12	6.67	5.57
Ho	1.80	1.70	1.76	1.06	1.42	1.23	1.02
Er	5.19	4.88	5.16	3.08	3.97	3.22	2.67
Tm	0.74	0.69	0.73	0.43	0.55	0.42	0.34
Yb	4.83	4.61	4.72	2.89	3.53	2.63	2.13
Lu	0.72	0.69	0.69	0.42	0.51	0.36	0.29
Hf	5.37	5.05	5.10	2.67	4.64	5.25	4.67
Ta	1.36	1.29	1.39	0.56	1.14	1.87	1.15
Pb	1.31	1.26	1.22	0.54	0.86	1.47	1.64
Th	1.66	1.57	1.60	0.70	1.19	2.11	1.28
U	0.45	0.43	0.45	0.19	0.32	0.60	0.40
Hf-Nd isotope composition							
¹⁷⁶ Hf/ ¹⁷⁷ Hf		0.283185	0.283180	0.283197			
eHf		14.610185	14.441236	15.038684			
¹⁴³ Nd/ ¹⁴⁴ Nd		0.513028	0.513047	0.513032			
eNd		7.612981	7.975877	7.679439			

4.3 Hf and Nd isotopes

Hf and Nd isotope data are reported in Table 1 and compared to literature Nd-Hf data for Iceland and the Mid-Atlantic Ridge (MAR) to the North and South, in Figure 5 (Blichert-Toft *et al.*, 2005, Hanan *et al.*, 2000, Kempton *et al.*, 2000, Kitagawa *et al.*, 2008, Kokfelt *et al.*, 2006, Salters & White, 1996, Stracke *et al.*, 2003c). The rift-zone tholeiites have a restricted range in $^{176}\text{Hf}/^{177}\text{Hf} = 0.28313\text{-}0.28322$ and $^{143}\text{Nd}/^{144}\text{Nd} = 0.51294\text{-}0.51308$. Samples from Snæfellsnes Peninsula have the lowest Hf and Nd isotope ratios whereas those from Theistareykir have the highest ratios. MAR samples generally have higher Hf and Nd isotope composition compared to the main-rift lavas analysed here and are similarly or more depleted compared to those from Theistareykir. Our new data are consistent with other data for main rift lavas (Fig. 4). There are no systematic distinctions in Hf and Nd isotope compositions between samples from the three main rift areas (RP, WV, NV). $^{143}\text{Nd}/^{144}\text{Nd}$ and $^{176}\text{Hf}/^{177}\text{Hf}$ do not correlate with MgO or other fractionation indices (not shown), but generally show good correlations with trace element ratios involving a moderately and a highly incompatible element (e.g. La/Sm, La/Yb, Lu/Hf and Sm/Nd; Fig. 6). Correlations between Hf and Nd isotopes and trace element ratios of two highly incompatible elements, however, are less well defined (e.g. Th/La, U/Nb, Fig. 6c). While the NV and Theistareykir samples form broad trends on diagrams of $^{143}\text{Nd}/^{144}\text{Nd}$ or $^{176}\text{Hf}/^{177}\text{Hf}$ versus highly incompatible element ratios, especially the RP and WV samples show a large variability in these elements for a narrow range in $^{143}\text{Nd}/^{144}\text{Nd}$ and $^{176}\text{Hf}/^{177}\text{Hf}$.

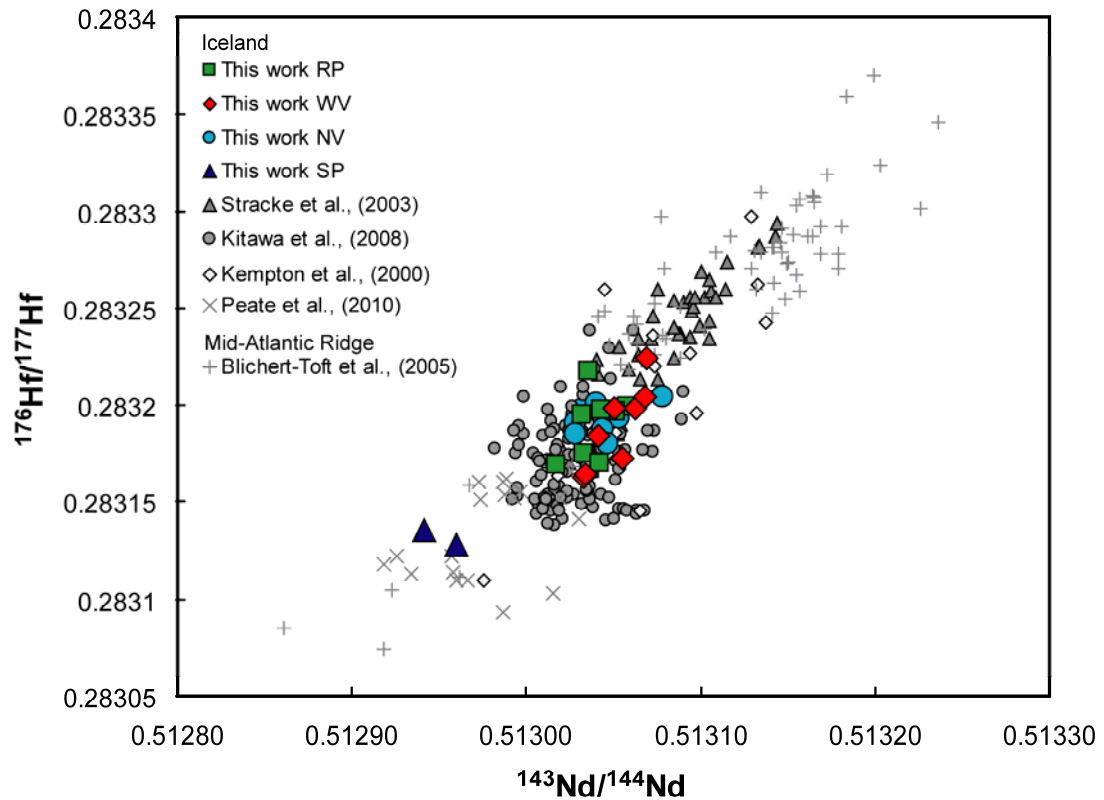


Figure 5. $^{143}\text{Nd}/^{144}\text{Nd}$ versus $^{176}\text{Hf}/^{177}\text{Hf}$ for Icelandic samples from this work Off-rift area samples (e.g. SP) form the most enriched samples and Theistareykir lavas form the most depleted Icelandic samples. Plusses represent samples from the MAR to the north and the south of Iceland (Blichert-Toft et al., 2005) that are similar and more depleted than the most depleted Icelandic samples.

5. Discussion

5.1 Influence of shallow level processes on lava composition

The extent of crystal fractionation and its potential effect on the trace element budget of the magmas is estimated with a least squares approach using a primitive parent magma composition (Theistareykir sample 9394, (Stracke *et al.*, 2003b), constant mineral compositions (ol, cpx, plag), and constant mineral-melt partition coefficients (plag: Aigner-Torres *et al.*, 2007, ol: Beattie, 1994, cpx: Hart & Dunn, 1993). The estimated effect on the trace element composition is significant for elements that are compatible in plagioclase (e.g. Cs, Sr, Eu) if plagioclase fractionation exceeds 5%, which affects approximately 90% of the samples. The Sr concentrations, for example, can change by up to 10% and therefore care needs to be taken in the interpretation of trace elements compatible in plagioclase. For the other incompatible elements (e.g. Rb, U, Th, Nb, Ta, REE) the effect of fractional crystallisation is relatively small (1-3%) and trace element ratios such as La/Sm, La/Yb and Lu/Hf are only affected by a maximum of 4%, 7.5% and 3.5%, respectively, which is comparable to the reproducibility of the trace element analyses (2 S.D. ~ 3 to 8%), but small compared to the observed overall variability (70%, 370% and 220%, respectively). Using a different parent magma composition to calculate the proportions of minerals crystallised does not significantly change the outcome of the least squares calculations.

Assimilation of the thick altered crust may also affect the geochemical and isotope composition of Icelandic lavas (e.g. Eiler *et al.*, 2000, Gee *et al.*, 1998b, Hémond *et al.*, 1993, Nicholson *et al.*, 1991, Oskarsson *et al.*, 1985, Sigmarsson *et al.*, 1992a, Sigmarsson *et al.*, 1992b). This process is difficult to resolve owing to the small compositional difference between the young basaltic Icelandic crust and the recent erupted lavas. The oxygen isotope composition of Icelandic lavas has been used as the main tracer for assimilation, because meteoric water at the latitude of Iceland has low $\delta^{18}\text{O}$ (down to -11‰ (Gautason & Muehlenbachs, 1998, and references therein). Low $\delta^{18}\text{O}$ in combination with enrichments in K_2O and fluid-mobile trace elements such as, Rb, U in differentiated samples from the Northern Volcanic Zone (Eiler *et al.*, 2000, Nicholson *et al.*, 1991) and Eastern Volcanic zone (Bindeman *et al.*, 2008) suggest that interaction with the altered Icelandic crust is potentially important for the more evolved lavas. Other studies have, however, argued that assimilation of altered crust is

insignificant and rather attribute the observed $\delta^{18}\text{O}$ heterogeneity to mantle source heterogeneity (Chauvel & Hémond, 2000, Gautason & Muehlenbachs, 1998, Kokfelt *et al.*, 2006, MacLennan *et al.*, 2003a, Stracke *et al.*, 2003c). Dredged submarine samples from the Reykjanes Ridge between 63 and 60°N do not travel through thick subaerially altered crust as in Iceland. These submarine lavas also have low $\delta^{18}\text{O}$ ratios (4.5 - 5.2 ‰, (Thirlwall *et al.*, 2006) indicating that the low oxygen isotope compositions of Icelandic lavas are indeed a mantle source feature. Moreover, studies that considered Sr isotope data and trace element ratios of fluid mobile highly incompatible elements (e.g. Cs/Rb, K/Rb or Ba/Th) in Icelandic lavas with low $\delta^{18}\text{O}$ signatures found that these lack expected signatures for hydrothermal alteration and conclude that crustal assimilation does not significantly influence the geochemistry of Icelandic lavas (Chauvel & Hémond, 2000, Kokfelt *et al.*, 2003, Kokfelt *et al.*, 2006, MacLennan *et al.*, 2003a, Skovgaard *et al.*, 2001, Stracke *et al.*, 2003c). None of our samples here have anomalous Cs/Rb, K/Rb, indicating no significant interaction with crustal fluids and/or the hydrothermally altered Icelandic crust. The more evolved ($\text{MgO} < 6$) and the more incompatible element enriched samples from the large central Askja and Krafla volcanoes in the NRZ and the two ERZ samples possibly experienced crustal assimilation but this is not expected to significantly affect the Nd and Hf isotope compositions.

5.2 Distinguishing between source heterogeneity and fractional melting

Qualitatively, the importance of source heterogeneity relative to parameters sensitive to the melting process can be assessed using a combination of isotope ratios and trace element ratios that vary with the depth and degree of partial melting. Trace element ratios most sensitive to the extent of partial melting are ratios of two elements with a large difference in compatibility such as La/Sm or La/Yb. The large variations in these ratios in Icelandic lavas (Fig. 4, 6a, b) suggest that melts are extracted from different depths in the melting region and that melt mixing only homogenise the compositional variability to a certain extent (Elliott *et al.*, 1991, MacLennan, 2008a, MacLennan, 2008b, MacLennan *et al.*, 2003a, Slater *et al.*, 2001, Stracke *et al.*, 2003c, Wood, 1981, Wood *et al.*, 1979). Note that regional variations in trace element ratios for the main rift lavas are of similar magnitude to the variations at a local scale for a single eruptive

centre (e.g. Skjaldbreiður in Western Rift, Fig. 4d, Table 1, and Theistareykir in Northern Volcanic Zone). This suggests that variability induced by the local melting and melt extraction process overwhelms regional changes in the melting behaviour expected from the temperature anomaly across the Iceland plume, i.e. higher degree of melting and depth of melt initiation towards the plume centre. As a consequence the effect of the variation in excess mantle temperature (~ 100 °C, Bourdon *et al.*, 2006, Putirka, 2005, Ribe *et al.*, 1995) across Iceland cannot be resolved using the trace element composition of the aggregated melts.

The systematic relationship between trace element ratios sensitive to the degree of melting and Hf-Nd isotopic composition, both on a regional and local scale (Fig. 6a, b), can be explained by sampling of two components as a function of the extent and pressure of melting (Elliott *et al.*, 1991; Kokfelt *et al.*, 2006; Stracke and Bourdon, 2009; Stracke *et al.*, 2003b). Lavas produced by high degrees of melting (low La/Sm, La/Yb, K₂O) have more depleted isotope signatures (high $^{143}\text{Nd}/^{144}\text{Nd}$ and $^{176}\text{Hf}/^{177}\text{Hf}$) whereas samples resulting from low degrees of melting (high La/Sm, La/Yb, K₂O) have enriched isotope signatures (low $^{143}\text{Nd}/^{144}\text{Nd}$ and $^{176}\text{Hf}/^{177}\text{Hf}$). This observation indicates that with increasing extent of melting the enriched component becomes progressively diluted and that the abundance of the enriched component is relatively small (a few % of the mantle source, Stracke *et al.*, 2003). Picritic lavas from Theistareykir represent the most depleted samples and alkalic off-rift Snæfellsnes Peninsula lavas represent the most enriched samples. The main-rift lavas from all three rift areas (RRZ, WRZ and NRZ) have intermediate compositions and do not show systematic variations between the different groups.

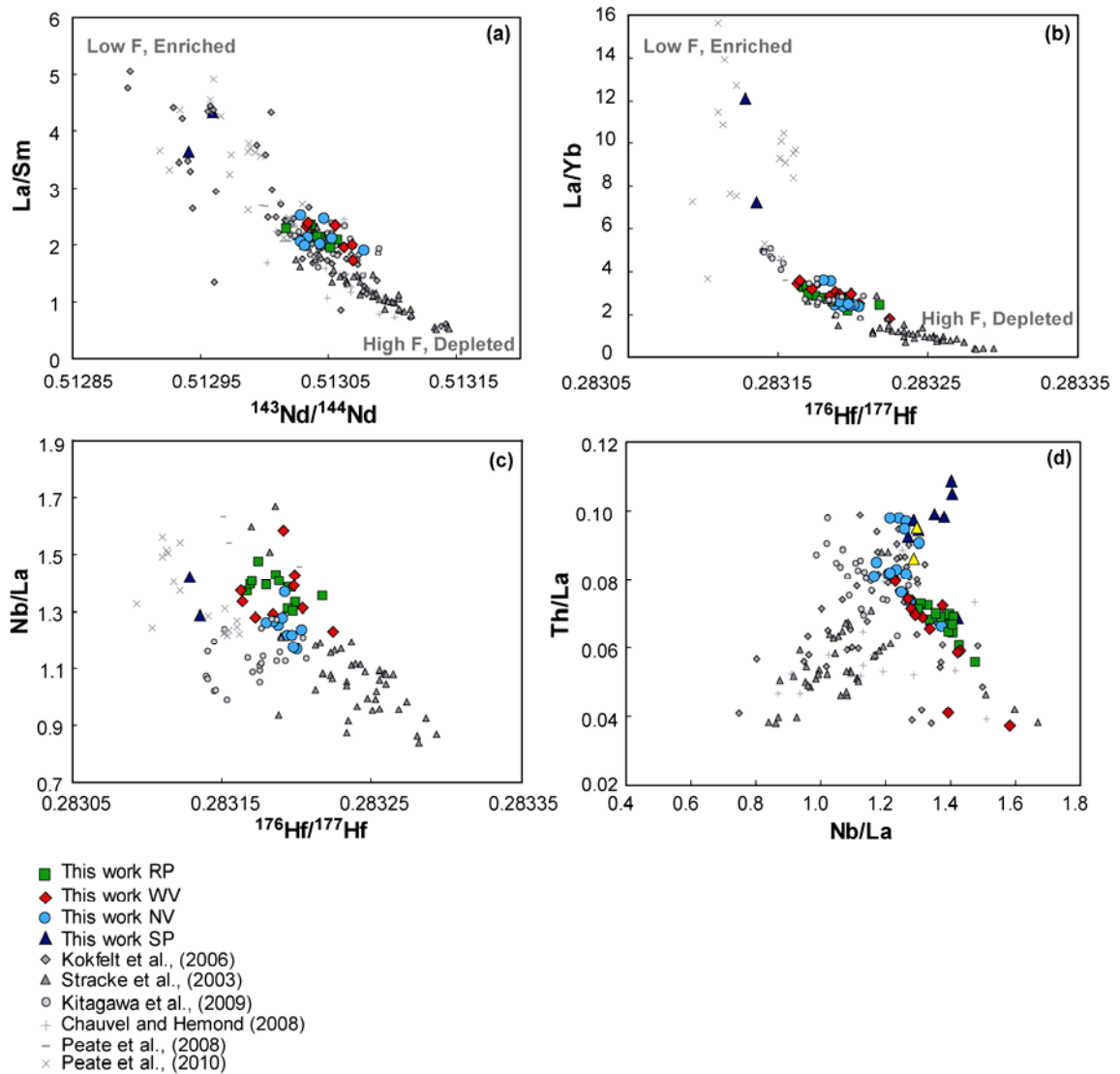


Figure 6. Relations between Nd and Hf isotope composition and trace element ratios. Hf and Nd isotope composition correlate well with trace element ratios involving a moderately incompatible element (a, b), whereas correlations between Hf and Nd isotope compositions and trace element ratios involving two highly incompatible trace elements trends (c) are less well defined. RP and WV samples show significant variability in highly incompatible element ratios at a range of $^{143}\text{Nd}/^{144}\text{Nd}$ and $^{176}\text{Hf}/^{177}\text{Hf}$. The samples from the South Western rift Zones require mixing with increased proportions of a source that has low Ba-Rb-U-Th/La but high Nb-Ta/La.

In contrast to trace element ratios that involve a moderately (e.g. Sm, Hf, Yb, Lu) and a highly incompatible element, trace element ratios of two highly incompatible

elements (i.e. Th, U, Rb, Ba, Nb, Ta, La) approach the source composition at very small extents of melting and melt mixing. Highly incompatible element ratios in erupted melts from a multi-component source thus should represent the weighted average of the compositions of the respective source components. As opposed to the good correlations between La/Yb or La/Sm and isotope ratios suggesting simple binary mixing, relations involving highly incompatible elements suggest that more than two components are required (Fig. 6, 7). For example, in diagrams of Nb/La versus Th/La or U/La., two striking orthogonal trends are seen for samples from the Northern Volcanic Zone, Theistareykir and the Snæfellsnes Peninsula on the one hand and samples from the Western Volcanics and Reykjanes Peninsula on the other (Fig 6d). The trend defined by the WV and RP zone lavas require mixing with melts from a source that has high Nb/La and low Th/La. If simple binary mixing of accumulated melts in a magma chamber is considered the perpendicular trends in Figure 6d require mixing of melts from at least three components. Note that mixing between three components would require that two of the components had very similar La/Yb, La/Sm and $^{143}\text{Nd}/^{144}\text{Nd}$ and $^{176}\text{Hf}/^{177}\text{Hf}$ ratios to explain the apparent binary relations in Figures 6a and b.

In a Yb/La versus Nb/U diagram (e.g. Fig 7a) the NV, Theistareykir and SP data form trends with decreasing Nb/U ratios for increasing Yb/La, i.e. increasing F. SP samples represent the small degree melts with low Yb/La (0.07 - 0.25) whereas Theistareykir samples represent the large degree melts with highly variable but generally larger Yb/La (0.35 - 2.85). In contrast, RP and WV samples have highly variable Nb/U ratios for a relatively narrow range of Yb/La (0.27 - 0.55). The variability in highly incompatible elements for the Western Rift Zone and Reykjanes Rift Zone of Iceland compared to the Northern Rift Zone (Table 1) suggests mixing with melts of an enriched component with low (Rb, U, Th)/La but high (Nb, Ta)/La and Nb/U ratios. The most enriched samples (WV26, WV18 and RP6) have Nb/U ranging between 91 and 143, significantly larger than the estimate of 42 ± 1 for Atlantic MORB by (Sun *et al.*, 2008). Similar, but less extreme enrichments were reported for samples from the RRZ and WRZ of Iceland by Kokfelt *et al.*, (2006) and were ascribed to mixing with a recycled crust component. Note that despite the large variability in highly incompatible trace element ratios for WV and RP samples their Yb/La is relatively constant (Fig 7a) suggesting a constant degree of melting. Whereas the variability in ratios Nb/U or

Nb/La indicates variability in the source composition, the restricted range in Yb/La requires similar melting conditions. The variability in the source composition can be explained in two ways (1) the abundance of the enriched component in the source is variable or (2) the enriched component is intrinsically heterogeneous. Whichever of these scenarios is correct, the degree of melting must be not affected.

Pb isotope data in combination with Hf, Nd and Sr data from previous studies on young basalts from Iceland's axial rift zone (Chauvel & Hémond, 2000, Hanan *et al.*, 2000, Hanan & Schilling, 1997, Kempton *et al.*, 2000, Kitagawa *et al.*, 2008, Kokfelt *et al.*, 2006, Peate *et al.*, 2009, Peate *et al.*, 2010, Thirlwall *et al.*, 2004) reveal differences in isotope compositions between rift areas similar to the variability in Nb/U presented in this study. For example, samples from the WRZ and RRZ have more enriched $^{206}\text{Pb}/^{204}\text{Pb}$ ratios at slightly lower Hf, Nd but higher Sr isotope compositions compared to samples from the NRZ (Fig. 7g). Samples from off-rift areas (SP and ERZ) are more enriched compared to the axial-rift lavas. The isotopic variability of lavas is generally interpreted using simple mixing of solids and therefore multiple components are required to explain the full range of data for Iceland (see introduction and Fig. 7g). Similarly to the variability in highly incompatible trace element ratios the variability in $^{206}\text{Pb}/^{204}\text{Pb}$ ratios within the RP and WV sample groups could arise from mixing with variable proportions of an enriched component or, alternatively, with a component that is intrinsically heterogeneous. As the relationships between the Hf and Nd isotopic compositions and La/Yb or La/Sm are consistent with melting and mixing two source components, we investigate in the following whether the full trace element variability combined with Pb-Hf-Nd-Sr isotope data for Iceland can be reproduced using a two-component polybaric melting and melt mixing model. We will test two different mixing scenarios; complete mixing using variable proportions of the enriched and depleted components and incomplete random mixing using a constant source component proportion.

Figure 7. Part 1

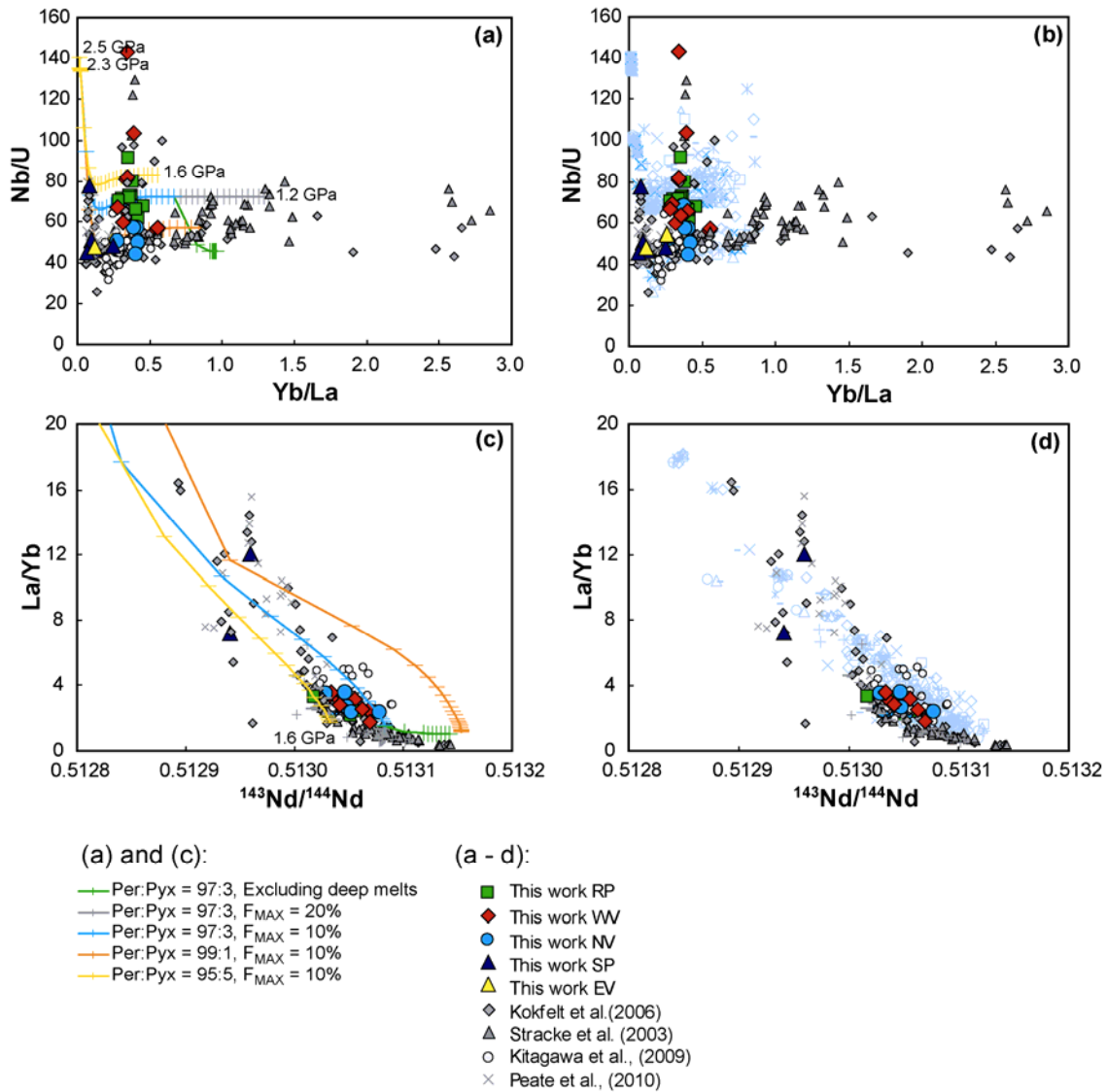


Figure 7. Comparison of model calculations with data from Iceland. See text and Figure 9 for model descriptions. Left panels show calculated trends for complete mixing of melts extracted from variable pressures using variable proportions of the enriched component; Right panels show model calculations for incomplete and random mixing and extraction of these mixtures from variable depths. Orange trends represent melting a mixture with a peridotite-pyroxenite ratio of 99:1; blue trends represent melting a mixture with a ratio of 97:3; yellow trends are calculated for a ratio of 95:5. Tick marks represent pressures of melt extraction (~ 0.03 GPa = 1km). The model trends represent accumulation over 27 km and a total F of 10% for the peridotite consistent with the main rift lavas, whereas the grey trend represents accumulation over 40 km with $F = 20\%$, consistent with the Theistareykir data.

Figure 7 Continued

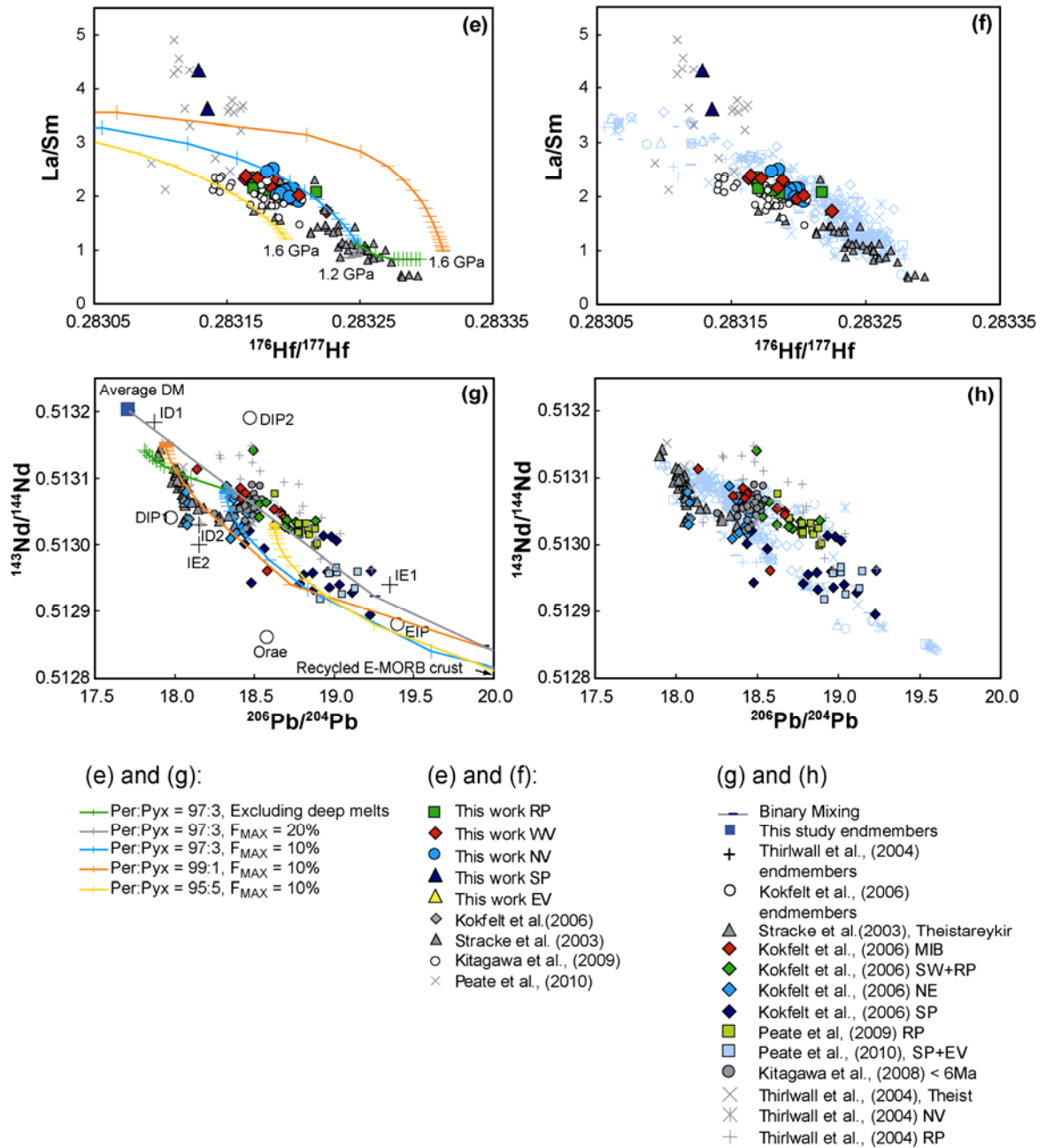


Figure 7 Continued. The green trend represents scenario B in Fig 9a for an initial peridotite-pyroxenite ratio of 97:3. Extraction of these melts is always from 1.6 GPa. For details on model input parameters see section 5.3.2. All 20 calculations shown in the right panels are for an initial peridotite-pyroxenite proportion of 97:3. Panels (g) and (h) display compiled Icelandic $^{206}\text{Pb}/^{204}\text{Pb}$ versus $^{143}\text{Nd}/^{144}\text{Nd}$ isotope data. Note that when binary mixing between our two inferred end-members is considered (grey trend with blue tick marks representing 10% mixing steps) more source components are required. Source components in the Icelandic mantle as suggested by Thirlwall et al., (2004) and Kokfelt et al., (2006) are shown for comparison.

5.3 Partial melting of a heterogeneous source and melt mixing

5.3.1 The nature and location of melt mixing

The large variability in trace element ratios in Icelandic basalts and especially in melt inclusions in olivine suggests that the melts are not efficiently mixed before eruption (MacLennan, 2008a, MacLennan, 2008b, MacLennan *et al.*, 2003b, Slater *et al.*, 2001). However, trace element compositions of predicted instantaneous melts formed near the base of the melting region are much more extreme than the main rift lavas (MacLennan, 2008a, Slater *et al.*, 2001) indicating that a relatively large extent of mixing of these fractional melts with melts formed at lower pressures is required. Channelled flow during melt extraction is in addition required for Iceland to explain the compositional variability observed in melt inclusions ((Gurenko & Chaussidon, 1995, MacLennan, 2008a, MacLennan, 2008b, MacLennan *et al.*, 2003a, Slater *et al.*, 2001) and the preserved U-series disequilibria in basalts (Kokfelt *et al.*, 2003, Stracke *et al.*, 2006, Stracke *et al.*, 2003b). A large part of melt mixing likely occurs in these melt channels, but some of the mixing also takes place in magma chambers during fractional crystallisation and cooling (MacLennan, 2008b, MacLennan *et al.*, 2003a). Because of the apparent greater role of melt mixing during extraction, compared to mixing in magma chambers, we focus here on mixing within the high porosity channels.

5.3.2 Modelling melting and mixing of a heterogeneous source

During fractional melting of a heterogeneous mantle source, the final trace element and isotopic composition of the erupted melt depends on: (1) the composition of the source components involved, (2) the difference in melting and partitioning behaviour of the different source components, (3) the relative mass fractions of the source components, and (4) the style of melt mixing during partial melting and melt extraction. Partial melting of a compositionally heterogeneous mantle is approximated here by a polybaric melting model that systematically samples and mixes melts from two source components with progressive melting (see also Stracke & Bourdon, 2009). Compositions of instantaneous and accumulated melts in a one-dimensional melting column are calculated for an enriched (recycled oceanic crust) and a depleted component (depleted MORB mantle) separately, and mixed at any given depth according to their relative mass proportions. The model differs from conventional mixing models in that it mixes accumulated melts from two sources during the

extraction process (see also Ito & Mahoney, 2005, Phipps Morgan, 1999) rather than mixing final melt batches that are integrated over the entire melting column or ‘solid’ source end-member compositions (e.g. Chauvel & Hémond, 2000, Hanan *et al.*, 2000, Kitagawa *et al.*, 2008, Kokfelt *et al.*, 2006, MacLennan, 2008b, Thirlwall *et al.*, 2004).

Input composition of source components

The enriched pyroxenite component used in the model calculations is a 2Ga old recycled crust modified during the subduction process by dehydration (Stracke *et al.*, 2003a). Such a component (often referred to as the HIMU-component) has repeatedly been inferred to be the enriched component in the Icelandic source (e.g., Chauvel & Hémond, 2000, Kokfelt *et al.*, 2006, Stracke *et al.*, 2003c) and has several characteristics typical for the enriched component in Icelandic lavas, i.e. it is depleted in Ba, Rb, U, and Th but enriched in Nb and Ta compared to La. The strong enrichment in Nb and Ta relative to the neighbouring highly incompatible elements in our most enriched samples (i.e. RP6 has Nb/La of 1.5) suggests that the enriched component represents recycled enriched MORB (E-MORB as suggested by McKenzie *et al.* (2004) (McKenzie *et al.*, 2004). In general, E-MORB and seamount samples are characterised by strong fractionations between Nb and Ta and the neighbouring elements (La, U, Th, Fig. 8, Niu & Batiza, 1997, Regelous *et al.*, 2003, Sun *et al.*, 2008, Zindler *et al.*, 1984). However, the absolute fractionation between the highly incompatible elements in E-MORB and seamount basalts is still less pronounced compared to our most enriched RP and WV lavas (e.g. U/Nb ~ 50, in E-MORB versus U/Nb ~130 in WV 26, Regelous *et al.*, 2003). Applying a dehydration model (for parameters see Beier *et al.*, 2007, Stracke *et al.*, 2003b, Willbold *et al.*, 2009, Willbold & Stracke, 2006) to a crust consisting of 50% E-MORB (sample 1312-47, Sun *et al.*, 2008) and 50% gabbros (Hart *et al.*, 1999), decreases the Rb, U, Th and La compared to Nb and Ta yields a recycled component with similar Rb/La, U/La, Nb/La, and U/Nb to our most enriched samples (Fig. 7). Isotope compositions for the 2 Ga recycled E-MORB component are calculated following the approach from Stracke *et al.* (2003a) and are $^{143}\text{Nd}/^{144}\text{Nd} = 0.51275$, $^{176}\text{Hf}/^{177}\text{Hf} = 0.282706$, $^{86}\text{Sr}/^{87}\text{Sr} = 0.703652$ and $^{206}\text{Pb}/^{204}\text{Pb} = 21.177$. The depleted component in the model represents average depleted mantle with $^{143}\text{Nd}/^{144}\text{Nd} = 0.5132$,

$^{176}\text{Hf}/^{177}\text{Hf} = 0.28335$, $^{86}\text{Sr}/^{87}\text{Sr} = 0.7027$ and $^{206}\text{Pb}/^{204}\text{Pb} = 17.72$ (Salters & Stracke, 2004, Stracke *et al.*, 2003a, Workman & Hart, 2005).

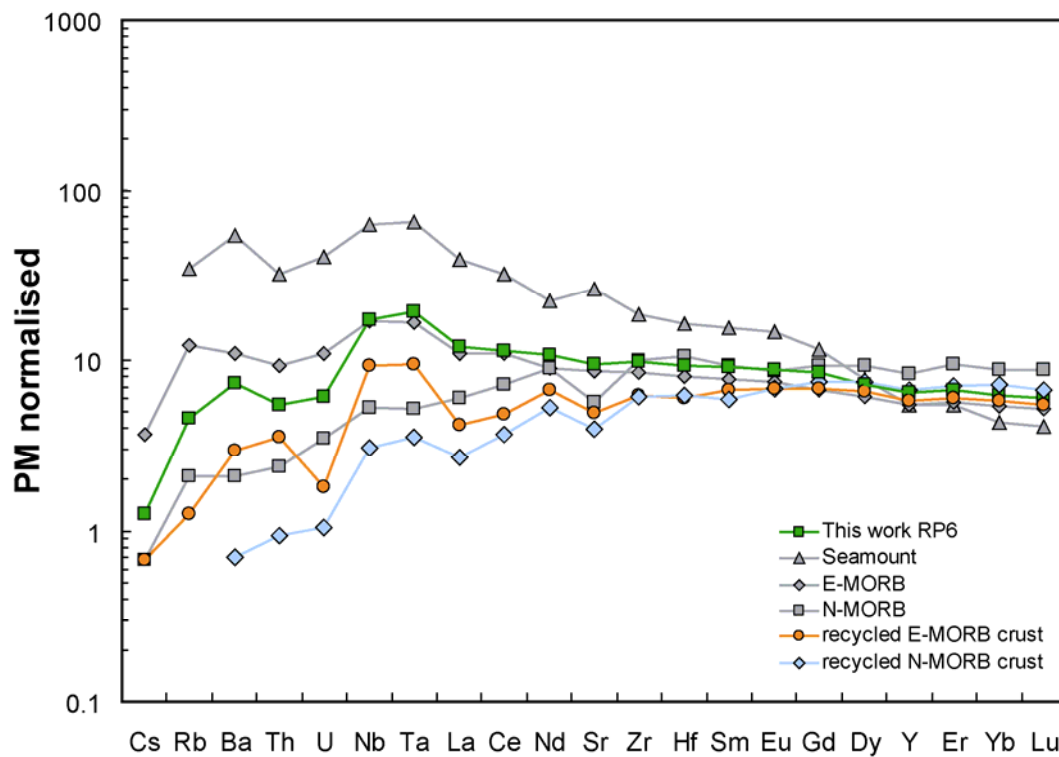


Figure 8. PM normalized trace element patterns of possible enriched source components. The trace element pattern of the enriched Reykjanes Peninsula sample RP6 is shown for comparison. E-MORB (unlike N-MORB) shows similar enrichment in Nb and Ta relative to the neighbouring elements (Th, U and La) as seen in the most enriched samples. Dehydration by subduction enhances the fractionation between U-Th-Rb-Nb-Ta and La. The geometry of the PM normalised patterns of a recycled E-MORB crust (50% E-MORB - 50% gabbro) is very similar to the geometry of patterns that show evidence for mixing with an enriched component except for Th that is significantly higher compared to U. To have similar Th/U (and Th/La and Th/Nb) ratios for the recycled crust to our enriched samples a larger fraction of the Th (50% instead of 38) has to be removed during dehydration or the initial Th concentration of the crust has to be lower. Note that the absolute effect of the modification during the subduction process is only constrained to a limited degree e.g. (Ayers *et al.*, 1997, Hermann *et al.*, 2006, Johnson & Plank, 1999, Klimm *et al.*, 2008, Kogiso *et al.*, 1997, Melekhova *et al.*, 2007) and that the composition of E-MORB is highly variable. The E-MORB composition represents sample 1312-47 from (Sun *et al.*, 2008); Gabbro in the recycled crust is from (Hart *et al.*, 1999); the seamount is sample Nintoku 55-8 from (Regelous *et al.*, 2003), N-MORB from (Hofmann, 1988). The recycled N-MORB crust represents the enriched component used in the polybaric melting and mixing model in Stracke *et al.*, 2009.

Melting behaviour of source components

Pyroxenite and peridotite have different melting behaviours (e.g., Hirschmann *et al.*, 1999, Pertermann & Hirschmann, 2003). These differences in melting behaviour enhance the variability in melt compositions during melting and mixing of a heterogeneous source. Pyroxenite solidus temperatures were determined to range from being similar to that of peridotite to solidus temperatures that are ~250 °C lower than that of the peridotite at a given pressure (Kogiso *et al.*, 2004, Pertermann & Hirschmann, 2003). Melting of the pyroxenite is therefore expected to start at similar or higher pressures compared to the peridotite. Additionally, the melt productivities of peridotite and pyroxenite lithologies vary differently with pressure, thereby exerting a control on the relative contribution of the melts from the two lithologies. The model used here considers slightly deeper melt initiation for the pyroxenite compared to the peridotite (i.e. 2.5 GPa versus 2.3 GPa) because significantly deeper melt initiation for the pyroxenite component was found to be inconsistent with the large variability in La/Yb and La/Sm (see Stracke and Bourdon *et al.*, 2009). The polybaric melt productivity function of Pertermann and Hirschmann (2003) is implemented for the pyroxenite and the melt productivity function of Asimow (2005) for the peridotite. The relative contributions of the peridotite and the pyroxenite are thus a function of the degree of melting at any given depth (depending on melt productivity) and the abundance of the two components at the onset of melting. Modal compositions, melt reactions and partition coefficients are given in Stracke and Bourdon (2009).

Different styles of melt aggregation and mixing

To model the compositions of melt mixtures covering the full range of highly depleted (Theistareykir) to highly enriched lavas (off-rift) and the variability observed within the different sample groups (WV and RP) we apply two different 'styles' of mixing and melt accumulation (Fig. 9). (1) Complete mixing of all instantaneous melts and extraction of the accumulated melts from various depths in the melting and mixing column (as in Stracke and Bourdon, (2009) (2) Incomplete and random mixing of partially aggregated instantaneous melts and extraction of these mixtures from various depth in the melting region.

Figure 9 Part 1

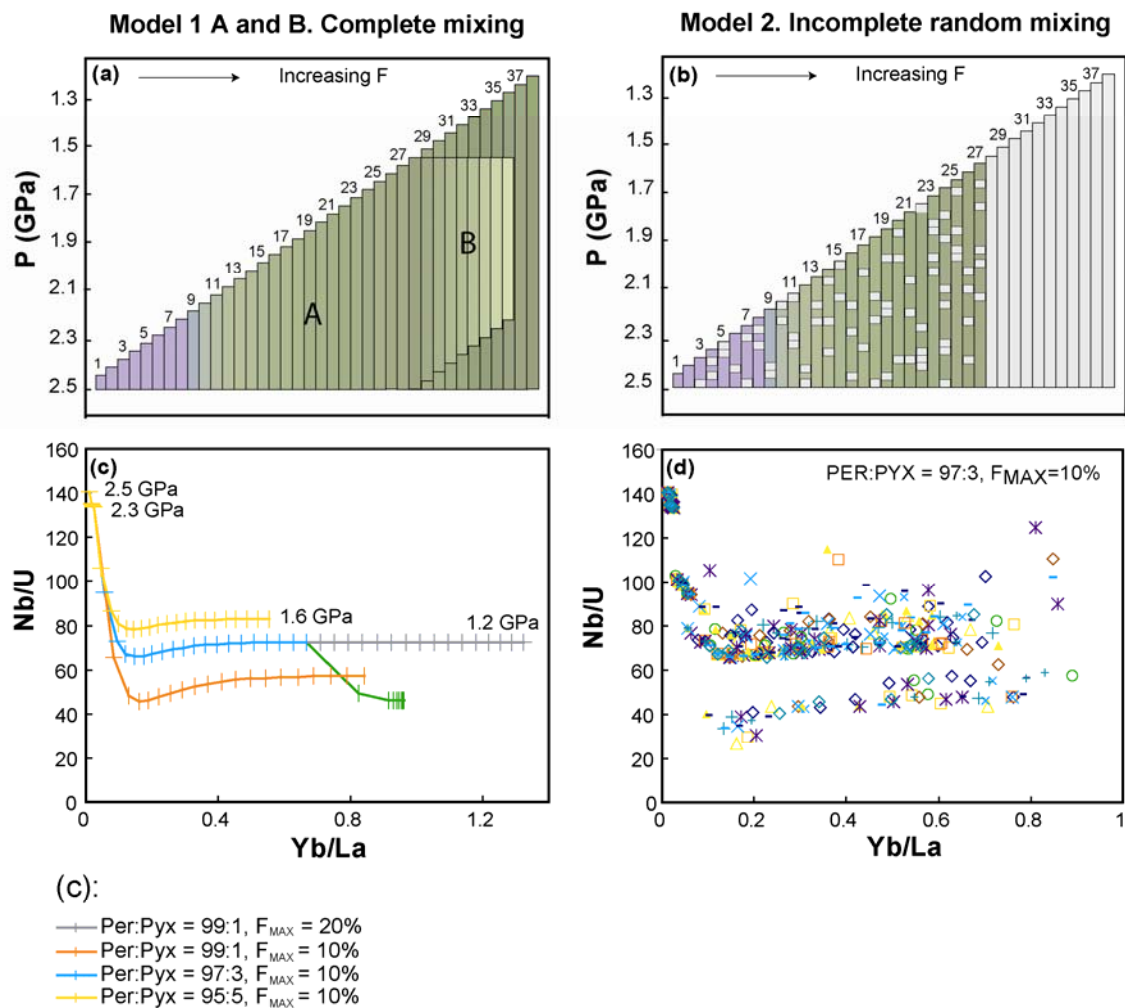


Figure 9. Schematic presentation of the polybaric melt accumulation model and model results in diagrams of Yb/La versus Nb/La (part 1), $^{143}\text{Nd}/^{144}\text{Nd}$ versus La/Yb, and $^{206}\text{Pb}/^{204}\text{Pb}$ versus $^{143}\text{Nd}/^{144}\text{Nd}$ (part 2). The left panels display the complete mixing scenarios A and B and the right panels display the incomplete and random mixing scenario (section 5.2.2). The columns shown in (a) and (b) represent 1-dimensional melt accumulation and mixing columns, where the length is proportional to the depth range of mixed melt accumulation. Purple = pyroxenite, green is peridotite and grey intervals in (b) represent melt packages that do not mix as assigned by our random number generator. (c, e, g) Calculated compositions for fully mixed melts extracted from variable pressures (model A, tick marks are for ~ 0.03 GPa = 1km). Coloured trends are calculated using variable proportions of the peridotite and pyroxenite (see legend on figure). Green trends represent results for model B: extraction of accumulated melts from a constant depth where melts from the bottom of the melting region are progressively excluded. (d, f, h) Compositions of incomplete mixtures of melts accumulated over variable depth ranges for a peridotite pyroxenite ratio of 97:3. Symbol groups represent results from a single batch of randomly assigned mixing numbers. Results for 20 different random calculations are shown.

Figure 9 continued

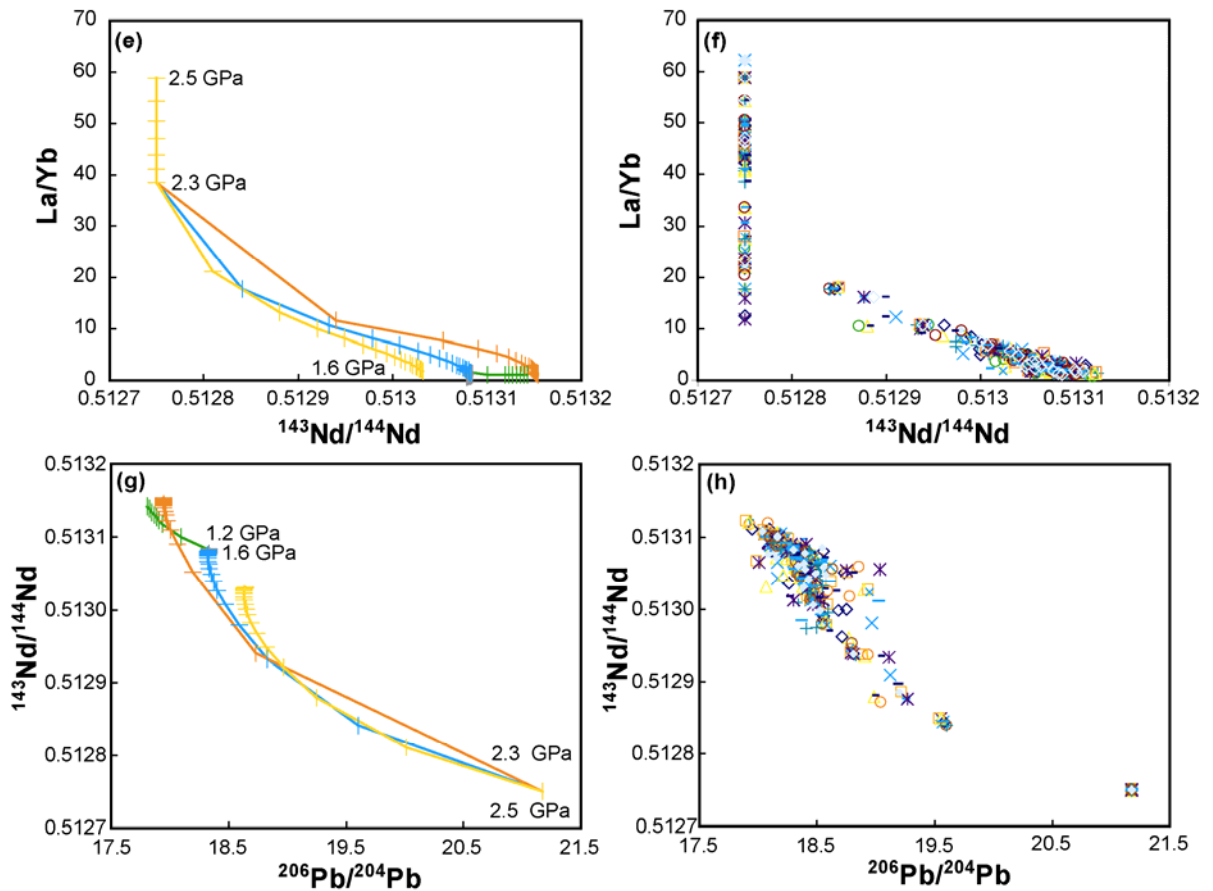


Figure 9. Part 2 (see caption above)

The first style of mixing considers extraction of fully accumulated melts from variable depths, assuming complete mixing of melts from the initial pressure until a given pressure (Fig 9a). The compositions of mixed melts at every depth are calculated by mixing the compositions of separately accumulated peridotite and pyroxenite melts according to their relative proportions. The maximum degree of melting over the full depth interval of 40 km is 20% for the peridotite, whereas it assumed to be 25% for the pyroxenite. The influence of changing the abundance of pyroxenite in the source is investigated by calculating compositions of melt mixtures for three abundance ratios of the depleted and enriched component, 99:1, 97:3 and 95:5%.

In addition to this scenario of melt mixing (model A in Fig 8a) we also tested complete mixing of melts extracted from a constant depth where melts from the base of the melting region are progressively excluded from the aggregated melt (model B in Fig 9a), i.e. rather than truncating the top of the melting region as in melting scenario 1A, the bottom of the melting region is truncated and the final depth of melting is kept constant. Such a scenario was suggested by Elliott et al., (1991) as an alternative model to explain the highly depleted nature of picrites from Theistareykir and the Reykjanes Peninsula. Compositions of accumulated melts excluding the first 1 to 8 km depth intervals of melting were calculated and are shown in the left panels in Fig 7 and 9. Extraction of the partially accumulated melts in this scenario is from a constant pressure (~1.6 GPa).

The second style of melt mixing simulates incomplete mixing of ‘instantaneous’ melts. For the sake of simplicity the instantaneous melts of the peridotite and pyroxenite component are accumulated over 1 km depth intervals (= 0.03 GPa) and mixed according to their relative proportions at that depth. A constant peridotite- pyroxenite ratio of 97 : 3 is assumed. These pre-mixed melt batches are randomly and incompletely mixed over various pressure ranges to simulate extraction of the incompletely aggregated melts from various depths in the melt region (Fig. 9b). To model the incomplete mixing, we used a function based on a random number generator to simulate a variable probability of mixing (p). This function yields the value of the “mixing factor” for every depth, which is equal to 1 if the melt mixes and equal to 0 if the melt does not mix. The probability (p) of mixing for each melt batch is assumed to be 0.8, i.e. the chance that the pre-mixed melt batches mix is 80%. The final composition of the incompletely aggregated melts are calculated using the following equation:

$$\overline{X}_i(z) = \sum_{j=z_0}^z (x_j \times f_j \times b_j)$$

Where X_i is the composition of the final accumulated melt calculated at depth z of melt extraction for element i , z_0 is the initial depth of melt accumulation (81 km), x_j is the composition of the mixed melt package, f_j is the volume fraction of each melt batch and b_j is the mixing factor (i.e., $b_j = 1$ or 0 ; $p(b_j = 1) = p$; $p(b_j = 0) = 1 - p$). The model calculations presented in the right panels of Figure 7 represent 20 calculations for every depth of melt extraction in which the mixing factors b_j are randomly assigned.

5.3.3 Model results and implications

A comparison of the model results with the Iceland data is shown in Fig 7. Generally, the incomplete mixing model predicts trace element and isotopic variability that complies with the observed systematics for Icelandic lavas even if a constant ratio of the enriched and depleted source component (3:97) is assumed. The complete mixing model requires either that the abundance of the enriched component is variable between the rift areas in Iceland or that the enriched source is intrinsically heterogeneous.

Main rift lavas

Accumulation and extraction of fully mixed melts with total degrees of melting of ~10% for the peridotite and 20% for the pyroxenite (i.e. accumulation over 27 km) is consistent with the variability in Yb/La for main rift lavas. The enrichments in highly incompatible elements (i.e. high Nb/U and high Nb/La) for samples from the Reykjanes Rift Zone and Western Rift Zone require the enriched component to have a higher initial source abundance (i.e. 2.5 – 10 %) (Fig 7a) compared to the lavas of the Northern Rift Zone (~1 %).

The enrichments in Nb and Ta compared to La and U in the most enriched RP and WV samples are more extreme than those of our calculated trends assuming complete mixing, even for large (e.g. 50%) initial proportions of the enriched component. This suggests that the composition of the enriched component may be more extreme compared to that assumed in the calculation or that the enriched component is intrinsically heterogeneous, which is not accounted for by the model. Incomplete mixing of instantaneous melts from a source with a constant initial peridotite pyroxenite ratio (97 : 3) results in significant variability in highly incompatible trace elements (Fig 7b). Hence this scenario accounts for a large portion of the scatter observed in the data without having to assume different abundances of the enriched components for the different rift zones.

The extent of mixing with the highly enriched initial pyroxenite melts from the bottom of the melting column is especially crucial to the compositional variability in highly incompatible trace element compositions of the accumulated melts. For example, when the initial melt package formed between 82 and 81 km depth is not included in the accumulated mixture, the composition is significantly more depleted (Fig 7b). Highly

enriched compositions arise from mixing with all of the enriched deep melt packages and lack of mixing with some of the depleted melt packages formed at shallower depths in the melting region. Increasing or decreasing the probability of mixing in the model results in a decrease or increase of the variability in the accumulated melt compositions, respectively. Less efficient mixing of melts as assumed in the model ($p = 0.8$) could therefore explain the larger variability observed in highly incompatible element ratios in some of the WV and RP samples.

In diagrams of $^{143}\text{Nd}/^{144}\text{Nd}$ versus La/Yb or $^{176}\text{Hf}/^{177}\text{Hf}$ versus La/Sm (Fig 7d, f) the variability in the main rift data is better explained by incomplete mixing of instantaneous melts at a constant pyroxenite abundance (3%), than by complete mixing with variable initial proportions of the enriched component. The samples from the RRZ and WRZ that are enriched in highly incompatible elements do not have distinguishable enrichments in Hf and Nd isotope compositions compared to the main-rift lavas from the NRZ. The complete mixing model for larger proportions of the enriched component (5-10 %) predicts larger enrichments in Nd and Hf compared to those observed (Fig 7c, e). This observation either suggests that the Hf and Nd compositions of the end-members used in the modelling are too extreme or that the abundance of the enriched component is actually constant.

Theistareykir lavas

The highly depleted Theistareykir samples with low La/Yb (down to 0.5), and relatively high Nd and Hf isotope compositions require accumulation of melts over a large range of depths (20-40 km) with degrees of melting $>20\%$ for the most depleted picrites (Fig 7a, c). The initial proportion of enriched component required to match the data is small (1 - 2.5 %). The larger variability in trace element and isotope ratios for Theistareykir lavas (Maclennan *et al.*, 2002, Maclennan *et al.*, 2003a, McKenzie *et al.*, 2004, Slater *et al.*, 2001, Stracke *et al.*, 2003c) Fig. 6) compared to other main rift lavas suggests a larger depth interval of melt extraction relative to other areas along the rift. Equally depleted high degree melts are observed for picrites from the Reykjanes Peninsula that similarly to Theistareykir lavas erupted in early Postglacial times (10 000 - 8 000 years, Gee *et al.*, 1998a, Gee *et al.*, 1998b, Maclennan, 2008b). This observation suggests that at that time melting was more extensive at shallow depths compared to subsequent times when the younger main rift lavas were produced. The increased melt

production at relatively shallow depths during early post-glacial times, is thought to be related to the isostatic rebound following unloading of ice sheets (Gee *et al.*, 1998a, Jull & McKenzie, 1996, MacLennan *et al.*, 2002). If the depth range of melt accumulation for the older Theistareykir lavas is assumed to be the same as for the main rift then the peridotite melting rate (dF/dP) for main rift lavas in the model is required to be a factor of 2 lower throughout the entire melting process (e.g. varying from 3 to 30%/GPa instead of 6 to 60%/GPa). Note, however that it is much more likely that the melting rate during early Post-glacial times is higher due to changes in mantle upwelling velocity (decompression) with time rather than that it results from time-dependent changes in dF/dP .

As an alternative to higher degrees of melting owing to increased melt production, Elliott (1991) suggested that the highly depleted nature of the picritic Theistareykir and Reykjanes Peninsula melts could result from lack of mixing with the most enriched melts from the deeper part in the melting column. Model trends that lack the most enriched deep instantaneous melts (Fig. 7a, c, e, and 9c, e, g) show that this process can generate the observed variability in Nd (and Hf) isotopic composition, but that it does not result in the extremely low La/Yb or La/Sm that must be produced from high degrees of melting. Furthermore, the large variability in La/Yb requires extraction of the melts from variable depths rather than from a constant depth as modelled. Instead, the Theistareykir data require incomplete mixing of that were extracted from and accumulated over a large range of depths. The limited variability in highly incompatible trace element ratios (i.e. Nb/U, Fig 7a, b) at a large range of La/Yb compared to main rift lavas suggests a smaller abundance of the enriched component in the source. Alternatively, it can be explained by more efficient mixing for these lavas that erupted in early Postglacial times than is assumed in our model (i.e., $p > 0.8$).

Off-rift lavas

The off-rift samples with variable but generally high incompatible trace element concentrations and ratios (e.g. La = 9 - 27 ppm and La/Yb = 4.0 - 14.3) and low Nd and Hf isotope compositions require mixing of small degree melts (peridotite $F = 1 - 3\%$, pyroxenite $F = 1 - 10\%$) from deep in the melting region and accumulation over a limited depth range (~12 km) compared to samples from the main rifts (La = 2.8 - 17.0

ppm and $\text{La/Yb} = 1.8 - 3.6$) (Fig 7). The generally smaller degree of melting can be explained by the presence of a lithospheric lid that increases in thickness away from the ridge and restricts the final depth of melting to greater depths compared to the main rift lavas (Kokfelt et al., 2006; Peate et al., 2010). Variability of Hf and Nd isotope composition for the off-rift lavas requires variable proportions of the enriched component in the source (~1-5%), but is equally well matched by incomplete mixing of melts and extraction of these partial accumulated melts from variable depths (Fig 7).

The Pb-Sr-Nd variability in Iceland

As for the highly incompatible trace element ratios, combined Pb and Nd data for Iceland's main rift and off rift lavas (Fig. 7g, Chauvel & Hémond, 2000, Hanan et al., 2000, Hanan & Schilling, 1997, Kitagawa et al., 2008, Kokfelt et al., 2006, Peate et al., 2009, Peate et al., 2010, Stracke et al., 2003c, Thirlwall et al., 2004) are reproduced by melting and complete mixing with variable initial abundances of the enriched component. Predicted melting trends assuming a small proportion (1%) of the enriched component in the source are consistent with the data for Theistareykir and the Northern Volcanic zone (low $^{206}\text{Pb}/^{204}\text{Pb}$ and slightly higher $^{143}\text{Nd}/^{144}\text{Nd}$) and the smaller degree off-rift lavas. In contrast, the higher and more variable $^{206}\text{Pb}/^{204}\text{Pb}$ data for Western Rift Zone lavas demand a larger proportion of the enriched component (up to 5%, Fig 7g) similar to what has been observed for the incompatible trace element ratios. Note that simple binary mixing of solid source components would require more than two source components (Fig 7g).

Note that incomplete mixing and accumulation of melts at a fixed abundance ratio results in significant compositional variability of erupted lavas that cover the entire range of the Icelandic data in Fig. 7h. These results demonstrate that concurrent melting and incomplete mixing of mantle melts during melt extraction is also capable of producing significant trace element and isotopic variability in lavas from a two component source. This result suggests that the style of mixing melts from two source components exerts a major control on the isotopic and trace element variability and obviates the need for multiple source components that are required when assuming mixing of solid source components.

Thus the observed enrichments in Nb and Ta compared to U and La and high $^{206}\text{Pb}/^{204}\text{Pb}$ and $^{87}\text{Sr}/^{86}\text{Sr}$ isotope composition for WV and RP samples compared to NV

and Theistareykir samples can be explained by complete mixing of melts from two components with greater abundances of enriched source material beneath the Reykjanes Peninsula and the Western Rift Zone and by incomplete mixing of melts from the two source components with a constant abundance ratio. However, the small range in Hf and Nd isotope compositions for the most enriched WV and RP samples is not consistent with the presence of greater abundances of the enriched component, which makes incomplete mixing with the most depleted melts from a source with a constant peridotite-pyroxenite ratio the more likely scenario.

However, the enriched component could also be intrinsically heterogeneous and be more variable beneath the WRZ and RRZ compared to the NRZ. Assuming that the enriched component represents a recycled oceanic crust, intrinsic heterogeneity in highly incompatible trace elements could result from heterogeneity in the basalts and gabbros that compose the old recycled crust or it could result from non-uniform dehydration during slab subduction. In both cases the solid source heterogeneity would have to be preserved during residence in the convecting mantle.

Intrinsic heterogeneity of the enriched component and Pb isotope variability

Peate et al., (2010), concluded based on a principle component analysis that > 99.5 % of the variance in Pb isotope data in Postglacial Icelandic basalts can be accounted for by mixing between two end members and that the third end member only contributes ~0.5%. Mixing with the third component is suggested to result in the subtle shift from the binary array in a $^{208}\text{Pb}/^{204}\text{Pb}$ versus $^{206}\text{Pb}/^{204}\text{Pb}$ diagram causing a kinked trend for the Icelandic data. Instead of having three components, however, the subtle variability in Pb isotopes could result from the enriched component being intrinsically heterogeneous. The component sampled by lavas in the Eastern Volcanic Zone is more enriched in $^{206}\text{Pb}/^{204}\text{Pb}$ compared to the component present beneath the Northern Volcanic Zone. If the radiogenic Pb component represents recycled oceanic crust, intrinsic heterogeneity in Pb isotopic composition could be explained by initial heterogeneity in Th and/or U concentrations, or it can result from heterogeneity in Pb concentrations. Assuming an age for the recycled crust of 2 Ga, an initial heterogeneity for U contents by 4% would be sufficient to result in an off-set in $^{206}\text{Pb}/^{204}\text{Pb}$ between the Eastern and Northern volcanic zone ($\Delta^{206}\text{Pb}/^{204}\text{Pb} \sim 0.2$) as observed in the

$^{208}\text{Pb}/^{204}\text{Pb}$ versus $^{206}\text{Pb}/^{204}\text{Pb}$ diagram (Fig. 9b in Peate et al., 2010). Variability in Pb concentration of 5% in the enriched component could equally result in the diversity observed in Icelandic and MAR basalts between the ERZ and NRZ. Such variability in Pb or U concentration is small compared to the variability in U in present day MORB (Sun *et al.*, 2008). Thus, if intrinsic heterogeneity in U and Pb in the enriched component is considered, two components suffice to explain the variability in Pb isotopes in Iceland.

6. Conclusions

Combined trace element and isotopic variability observed for Iceland's postglacial basalts can be modelled by polybaric melting and mixing of a depleted source that contains small amounts (1-5%) of an enriched component.

The effect of two styles of mixing melts from two source components was tested with (1) perfect mixing and (2) incomplete mixing of melts during progressive melting and melt extraction. To explain the compositional variability between lavas from the Northern and the Southwestern Rift Zones by complete mixing requires the abundance of the enriched component beneath the Southwest to be larger, or the enriched component to be slightly more enriched below this area. Intrinsic heterogeneity of the enriched component in highly incompatible trace elements could also explain the subtle deviations from two-component mixing trends for Icelandic samples in Pb-Pb isotope diagrams.

Incomplete mixing of instantaneous melts and extraction of these incomplete mixtures from variable depths also results in trace element and isotopic variability that reproduces the observed systematics for Icelandic lavas even if a constant ratio of the enriched and depleted source component (3:97) is assumed. Two components in the mantle source beneath Iceland therefore suffice to explain the full range in compositional variability observed in Post-glacial lavas.

The melt extraction mechanism for a heterogeneous source containing isolated bodies of pyroxenite is still poorly understood but is likely a complex system with melts focussing in multiple channels that converge at various levels within the mantle. The better match of data produced by our incomplete random mixing model with the observed variability for Icelandic basalts implies that mixing and extraction of melts

formed at various depths is stochastic and that separate eruptions therefore likely sample the Icelandic source in a different fashions.

The example of Iceland demonstrates that melt mixing during melting of the heterogeneous source is a key process controlling the trace element and isotopic variability in basaltic lavas. The isotopic compositions of erupted lavas likely do not represent the average composition of the solid upwelling mantle. It is therefore stressed that for the interpretation of data on global MORB or OIB, mixing during melting of a heterogeneous source needs to be taken into account before inferring the presence of multiple source components.

References

- Aigner-Torres, M., Blundy, J., Ulmer, P. & Pettke, T. (2007). Laser Ablation ICPMS study of trace element partitioning between plagioclase and basaltic melts: an experimental approach. *Contributions to Mineralogy and Petrology* 153, 647-667.
- Ayers, J. C., Dittmer, S. K. & Layne, G. D. (1997). Partitioning of elements between peridotite and H₂O at 2.0-3.0 GPa and 900-1100 degrees C, and application to models of subduction zone processes. *Earth and Planetary Science Letters* 150, 381-398.
- Beattie, P. (1994). Systematics and Energetics of Trace-Element Partitioning between Olivine and Silicate Melts - Implications for the Nature of Mineral Melt Partitioning. *Chemical Geology* 117, 57-71.
- Beier, C., Stracke, A. & Haase, K. M. (2007). The peculiar geochemical signatures of São Miguel (Azores) lavas: Metasomatised or recycled mantle sources? *Earth and Planetary Science Letters* 259, 186-199.
- Bijwaard, H. & Spakman, W. (1999). Tomographic evidence for a narrow whole mantle plume below Iceland. *Earth and Planetary Science Letters* 166, 121-126.
- Bindeman, I., Gurenko, A., Sigmarsson, O. & Chaussidon, M. (2008). Oxygen isotope heterogeneity and disequilibria of olivine crystals in large volume Holocene basalts from Iceland: Evidence for magmatic digestion and erosion of Pleistocene hyaloclastites. *Geochimica et Cosmochimica Acta* 72, 4397-4420.
- Bizzarro, M., Baker, J. A. & Ulfbeck, D. (2003). A new digestion and chemical separation technique for rapid and highly reproducible determination of Lu/Hf and Hf isotope ratios in

- geological materials by MC-ICP-MS. *Geostandards Newsletter-the Journal of Geostandards and Geoanalysis* 27, 133-145.
- Blichert-Toft, J., Agraniér, A., Andres, M., Kingsley, R., Schilling, J. G. & Albarede, F. (2005). Geochemical segmentation of the Mid-Atlantic Ridge north of Iceland and ridge-hot spot interaction in the North Atlantic. *Geochemistry Geophysics Geosystems* 6, Q01E19, doi:10.1029/2004gc000788.
- Blichert-Toft, J. & Albarède, F. (1997). The Lu-Hf isotope geochemistry of chondrites and the evolution of the mantle-crust system. *Earth and Planetary Science Letters* 148, 243-258.
- Bourdon, B., Ribe, N. M., Stracke, A., Saal, A. E. & Turner, S. P. (2006). Insights into the dynamics of mantle plumes from uranium-series geochemistry. *Nature* 444, 713-717.
- Carmichael, I. S. E. (1964). The Petrology of Thingmuli, a Tertiary Volcano in Eastern Iceland. *Journal of Petrology* 5, 435-460.
- Chauvel, C. & Hémond, C. (2000). Melting of a complete section of recycled oceanic crust: Trace element and Pb isotopic evidence from Iceland. *Geochem. Geophys. Geosyst.* 1, doi:10.1029/1999GC000002.
- Chu, N. C., Taylor, R. N., Chavagnac, V., Nesbitt, R. W., Boella, R. M., Milton, J. A., German, C. R., Bayon, G. & Burton, K. (2002). Hf isotope ratio analysis using multi-collector inductively coupled plasma mass spectrometry: an evaluation of isobaric interference corrections. *Journal of Analytical Atomic Spectrometry* 17, 1567-1574.
- Darbyshire, F. A., White, R. S. & Priestley, K. F. (2000). Structure of the crust and uppermost mantle of Iceland from a combined seismic and gravity study. *Earth and Planetary Science Letters* 181, 409-428.
- Eiler, J. M., Gronvold, K. & Kitchen, N. (2000). Oxygen isotope evidence for the origin of chemical variations in lavas from Theistareykir volcano in Iceland's northern volcanic zone. *Earth and Planetary Science Letters* 184, 269-286.
- Elliott, T. R., Hawkesworth, C. J. & Gronvold, K. (1991). Dynamic Melting of the Iceland Plume. *Nature* 351, 201-206.
- Fitton, J. G., Saunders, A. D., Norry, M. J., Hardarson, B. S. & Taylor, R. N. (1997). Thermal and chemical structure of the Iceland plume. *Earth and Planetary Science Letters* 153, 197-208.
- Gautason, B. & Muehlenbachs, K. (1998). Oxygen isotopic fluxes associated with high-temperature processes in the rift zones of Iceland. *Chemical Geology* 145, 275-286.
- Gee, M. A. M., Taylor, R. N., Thirlwall, M. F. & Murton, B. J. (1998a). Glacioisostasy controls chemical and isotopic characteristics of tholeiites from the Reykjanes peninsula, SW Iceland. *Earth and Planetary Science Letters* 164, 1-5.

- Gee, M. A. M., Thirlwall, M. F., Taylor, R. N., Lowry, D. & Murton, B. J. (1998b). Crustal processes: Major controls on Reykjanes Peninsula lava chemistry, SW Iceland. *Journal of Petrology* 39, 819-839.
- Gurenko, A. A. & Chaussidon, M. (1995). Enriched and Depleted Primitive Melts Included in Olivine from Icelandic Tholeiites - Origin by Continuous Melting of a Single Mantle Column. *Geochimica et Cosmochimica Acta* 59, 2905-2917.
- Gurenko, A. A. & Sobolev, A. V. (2006). Crust-primitive magma interaction beneath neovolcanic rift zone of Iceland recorded in gabbro xenoliths from Midfell, SW Iceland. *Contributions to Mineralogy and Petrology* 151, 495-520.
- Hanan, B. B., Blichert-Toft, J., Kingsley, R. & Schilling, J. G. (2000). Depleted Iceland mantle plume geochemical signature: Artifact of multicomponent mixing? *Geochem. Geophys. Geosyst.* 1, 1003, doi:10.1029/1999GC000009. .
- Hanan, B. B. & Graham, D. W. (1996). Lead and helium isotope evidence from oceanic basalts for a common deep source of mantle plumes. *Science* 272, 991-995.
- Hanan, B. B. & Schilling, J. G. (1997). The dynamic evolution of the Iceland mantle plume: the lead isotope perspective. *Earth and Planetary Science Letters* 151, 43-60.
- Hart, S. R., Blusztajn, J., Dick, H. J. B., Meyer, P. S. & Muehlenbachs, K. (1999). The fingerprint of seawater circulation in a 500-meter section of ocean crust gabbros. *Geochimica et Cosmochimica Acta* 63, 4059-4080.
- Hart, S. R. & Dunn, T. (1993). Experimental Cpx Melt Partitioning of 24 Trace-Elements. *Contributions to Mineralogy and Petrology* 113, 1-8.
- Hart, S. R., Hauri, E. H., Oschmann, L. A. & Whitehead, J. A. (1992). Mantle Plumes and Entrainment - Isotopic Evidence. *Science* 256, 517-520.
- Hart, S. R., Schilling, J. G. & Powell, J. L. (1973). Basalts from Iceland and Along Reykjanes Ridge - Sr Isotope Geochemistry. *Nature-Physical Science* 246, 104-107.
- Hémond, C., Arndt, N. T., Lichtenstein, U., Hofmann, A. W., Oskarsson, N. & Steinthorsson, S. (1993). The Heterogeneous Iceland Plume - Nd-Sr-O Isotopes and Trace-Element Constraints. *Journal of Geophysical Research-Solid Earth* 98, 15833-15850.
- Hermann, J., Spandler, C., Hack, A. & Korsakov, A. V. (2006). Aqueous fluids and hydrous melts in high-pressure and ultra-high pressure rocks: Implications for element transfer in subduction zones. *Lithos* 92, 399-417.
- Hirschmann, M. M., Asimow, P. D., Ghiorso, M. S. & Stolper, E. M. (1999). Calculation of peridotite partial melting from thermodynamic models of minerals and melts. III. Controls on isobaric melt production and the effect of water on melt production. *Journal of Petrology* 40, 831-851.

- Hofmann, A. W. (1988). Chemical Differentiation of the Earth - the Relationship between Mantle, Continental-Crust, and Oceanic-Crust. *Earth and Planetary Science Letters* 90, 297-314.
- Ito, G. & Mahoney, J. J. (2005). Flow and melting of a heterogeneous mantle: 1. Method and importance to the geochemistry of ocean island and mid-ocean ridge basalts. *Earth and Planetary Science Letters* 230, 29-46.
- Jakobsson, S. P. (1972). Chemistry and distribution pattern of recent basaltic rocks in Iceland. *Lithos* 5, 365-386.
- Johnson, M. C. & Plank, T. (1999). Dehydration and melting experiments constrain the fate of subducted sediments. *Geochem. Geophys. Geosyst.* 1, 1007, doi:10.1029/1999GC000014.
- Jull, M. & McKenzie, D. (1996). The effect of deglaciation on mantle melting beneath Iceland. *Journal of Geophysical Research-Solid Earth* 101, 21815-21828.
- Kaban, M., K., Flóvenz, Ó., G. & Pálmason, G. (2002). Nature of the crust-mantle transition zone and the thermal state of the upper mantle beneath Iceland from gravity modelling. 281-299.
- Kempton, P. D., Fitton, J. G., Saunders, A. D., Nowell, G. M., Taylor, R. N., Hardarson, B. S. & Pearson, G. (2000). The Iceland plume in space and time: a Sr-Nd-Pb-Hf study of the North Atlantic rifted margin. *Earth and Planetary Science Letters* 177, 255-271.
- Kitagawa, H., Kobayashi, K., Makishima, A. & Nakamura, E. (2008). Multiple Pulses of the Mantle Plume: Evidence from Tertiary Icelandic Lavas. *Journal of Petrology* 49, 1365-1396.
- Klimm, K., Blundy, J. D. & Green, T. H. (2008). Trace element partitioning and accessory phase saturation during H₂O-saturated melting of basalt with implications for subduction zone chemical fluxes. *Journal of Petrology* 49, 523-553.
- Kogiso, T., Hirschmann, M. M. & Pertermann, M. (2004). High-pressure partial melting of mafic lithologies in the mantle. *Journal of Petrology* 45, 2407-2422.
- Kogiso, T., Tatsumi, Y. & Nakano, S. (1997). Trace element transport during dehydration processes in the subducted oceanic crust: 1. Experiments and implications for the origin of ocean island basalts. *Earth and Planetary Science Letters* 148, 193-205.
- Kokfelt, T. F., Hoernle, K. & Hauff, F. (2003). Upwelling and melting of the Iceland plume from radial variation of ²³⁸U-²³⁰Th disequilibria in postglacial volcanic rocks. *Earth and Planetary Science Letters* 214, 167-186.
- Kokfelt, T. F., Hoernle, K., Hauff, F., Fiebig, J., Werner, R. & Garbe-Schoenberg, D. (2006). Combined traced element and Pb-Nd-Sr-O isotope evidence for recycled oceanic crust (upper and lower) in the Iceland mantle plume. *Journal of Petrology* 47, 1705-1749.

- MacLennan, J. (2008a). Concurrent Mixing and Cooling of Melts under Iceland. *Journal of Petrology* 49, 1931-1953.
- MacLennan, J. (2008b). Lead isotope variability in olivine-hosted melt inclusions from Iceland. *Geochimica et Cosmochimica Acta* 72, 4159-4176.
- MacLennan, J., Jull, M., McKenzie, D., Slater, L. & Gronvold, K. (2002). The link between volcanism and deglaciation in Iceland. *Geochemistry Geophysics Geosystems* 3, 1062, doi:10.1029/2001GC000282
- MacLennan, J., McKenzie, D., Gronvold, K., Shimizu, N., Eiler, J. M. & Kitchen, N. (2003a). Melt mixing and crystallization under Theistareykir, northeast Iceland. *Geochemistry Geophysics Geosystems* 4, 8624, doi:8610.1029/2003gc000558.
- MacLennan, J., McKenzie, D., Hilton, F., Gronvold, K. & Shimizu, N. (2003b). Geochemical variability in a single flow from northern Iceland. *Journal of Geophysical Research-Solid Earth* 108.
- McDonough, W. F. & Sun, S. S. (1995). The Composition of the Earth. *Chemical Geology* 120, 223-253.
- McKenzie, D., Stracke, A., Blichert-Toft, J., Albarede, F., Gronvold, K. & O'Nions, R. K. (2004). Source enrichment processes responsible for isotopic anomalies in oceanic island basalts. *Geochimica et Cosmochimica Acta* 68, 2699-2724.
- Melekhova, E., Schmidt, M. W., Ulmer, P. & Pettke, T. (2007). The composition of liquids coexisting with dense hydrous magnesium silicates at 11-13.5 GPa and the endpoints of the solidi in the MgO-SiO₂-H₂O system. *Geochimica et Cosmochimica Acta* 71, 3348-3360.
- Montelli, R., Nolet, G., Masters, G., Dahlen, F. A. & Hung, S. H. (2004). Global P and PP traveltimes tomography: rays versus waves. *Geophysical Journal International* 158, 637-654.
- Münker, C., Weyer, S., Scherer, E. & Mezger, K. (2001). Separation of high field strength elements (Nb, Ta, Zr, Hf) and Lu from rock samples for MC-ICPMS measurements. *Geochemistry Geophysics Geosystems* 2, 1064, doi:10.1029/2001GC000183. .
- Nicholson, H., Condomines, M., Fitton, J. G., Fallick, A. E., Gronvold, K. & Rogers, G. (1991). Geochemical and Isotopic Evidence for Crustal Assimilation beneath Krafla, Iceland. *Journal of Petrology* 32, 1005-1020.
- Niu, Y. L. & Batiza, R. (1997). Trace element evidence from seamounts for recycled oceanic crust in the eastern Pacific mantle. *Earth and Planetary Science Letters* 148, 471-483.
- Oskarsson, N., Steinthorsson, S. & Sigvaldason, G. E. (1985). Iceland Geochemical Anomaly - Origin, Volcanotectonics, Chemical Fractionation and Isotope Evolution of the Crust. *Journal of Geophysical Research-Solid Earth and Planets* 90, 11-25.

- Peate, D., Baker, J., Jakobsson, S., Waight, T., Kent, A., Grassineau, N. & Skovgaard, A. (2009). Historic magmatism on the Reykjanes Peninsula, Iceland: a snap-shot of melt generation at a ridge segment. *Contributions to Mineralogy and Petrology* 157, 359-382.
- Peate, D. W., Breddam, K., Baker, J. A., Kurz, M. D., Barker, A. K., Prestvik, T., Grassineau, N. & Skovgaard, A. C. (2010). Compositional Characteristics and Spatial Distribution of Enriched Icelandic Mantle Components. *Journal of Petrology*, egq025.
- Pertermann, M. & Hirschmann, M. M. (2003). Partial melting experiments on a MORB-like pyroxenite between 2 and 3 GPa: Constraints on the presence of pyroxenite in basalt source regions from solidus location and melting rate. *Journal of Geophysical Research-Solid Earth* 108.
- Phipps Morgan, J. (1999). Isotope topology of individual hotspot basalt arrays: Mixing curves or melt extraction trajectories? *Geochem. Geophys. Geosyst.* 1, 1003, doi:10.1029/1999GC000004. .
- Pin, C. & Zalduegui, J. F. S. (1997). Sequential separation of light rare-earth elements, thorium and uranium by miniaturized extraction chromatography: Application to isotopic analyses of silicate rocks. *Analytica Chimica Acta* 339, 79-89.
- Putirka, K. D. (2005). Mantle potential temperatures at Hawaii, Iceland, and the mid-ocean ridge system, as inferred from olivine phenocrysts: Evidence for thermally driven mantle plumes. *Geochemistry Geophysics Geosystems* 6, Q05108, doi:10.1029/2005gc000915.
- Regelous, M., Hofmann, A. W., Abouchami, W. & Galer, S. J. G. (2003). Geochemistry of lavas from the Emperor Seamounts, and the geochemical evolution of Hawaiian magmatism from 85 to 42 Ma. *Journal of Petrology* 44, 113-140.
- Ribe, N. M., Christensen, U. R. & Theissing, J. (1995). The Dynamics of Plume-Ridge Interaction .1. Ridge-Centered Plumes. *Earth and Planetary Science Letters* 134, 155-168.
- Salters, V. J. M. & Stracke, A. (2004). Composition of the depleted mantle. *Geochem. Geophys. Geosyst.* 5, Q05004, doi:05010.01029/02003GC000597.
- Salters, V. J. M. & White, W. M. (1996). Hf isotope constraints on mantle evolution. *Workshop on Geochemical Earth Reference Model*. Lyon, France: Elsevier Science Bv, 447-460.
- Schilling, J. (1973). Iceland Mantle Plume - Geochemical Study of Reykjanes Ridge. *Nature* 242, 565-571.
- Shen, Y., Solomon, S. C., Bjarnason, I. T. & Wolfe, C. J. (1998). Seismic evidence for a lower-mantle origin of the Iceland plume. *Nature* 395, 62-65.
- Sigmarrsson, O., Condomines, M. & Fourcade, S. (1992a). A Detailed Th, Sr and O Isotope Study of Hekla - Differentiation Processes in an Icelandic Volcano. *Contributions to Mineralogy and Petrology* 112, 20-34.

- Sigmarrsson, O., Condomines, M. & Fourcade, S. (1992b). Mantle and crustal contribution in the genesis of Recent basalts from off-rift zones in Iceland: Constraints from Th, Sr and O isotopes. *Earth and Planetary Science Letters* 110, 149-162.
- Sigmundsson, F. (2006). *Iceland geodynamics, crustal deformation and divergent plate tectonics*: Springer-Praxis.
- Skovgaard, A. C., Storey, M., Baker, J., Blusztajn, J. & Hart, S. R. (2001). Osmium-oxygen isotopic evidence for a recycled and strongly depleted component in the Iceland mantle plume. *Earth and Planetary Science Letters* 194, 259-275.
- Slater, L., McKenzie, D. A. N., Gronvold, K. & Shimizu, N. (2001). Melt Generation and Movement beneath Theistareykir, NE Iceland. 321-354.
- Stoll, B., Jochum, K. P., Herwig, K., Amini, M., Flanz, M., Kreuzburg, B., Kuzmin, D., Willbold, M. & Enzweiler, J. (2008). An automated iridium-strip heater for LA-ICP-MS bulk analysis of geological samples. *Geostandards and Geoanalytical Research* 32, 5-26.
- Stracke, A., Bizimis, M. & Salters, V. J. M. (2003a). Recycling oceanic crust: Quantitative constraints. *Geochemistry Geophysics Geosystems* 4, 8003, doi:8010.1029/2001GC000223. .
- Stracke, A. & Bourdon, B. (2009). The importance of melt extraction for tracing mantle heterogeneity. *Geochimica et Cosmochimica Acta* 73, 218-238.
- Stracke, A., Bourdon, B. & McKenzie, D. (2006). Melt extraction in the Earth's mantle: Constraints from U-Th-Pa-Ra studies in oceanic basalts. *Earth and Planetary Science Letters* 244, 97-112.
- Stracke, A., Hofmann, A. W. & Hart, S. R. (2005). FOZO, HIMU, and the rest of the mantle zoo. *Geochemistry Geophysics Geosystems* 6, Q05007, doi:05010.01029/02004gc000824.
- Stracke, A., Zindler, A. , Salters, V. J. M., McKenzie, D. & Grönvold, K. (2003b). The dynamics of melting beneath Theistareykir, northern Iceland. *Geochem. Geophys. Geosyst.* 4, 8513, doi: 8510.1029/2002GC000347.
- Stracke, A., Zindler, A., Salters, V. J. M., McKenzie, D., Blichert-Toft, J., Albarede, F. & Gronvold, K. (2003c). Theistareykir revisited. *Geochemistry Geophysics Geosystems* 4, 8507, doi: 8510.1029/2001GC000201.
- Sun, W., Hu, Y., Kamenetsky, V. S., Eggins, S. M., Chen, M. & Arculus, R. J. (2008). Constancy of Nb/U in the mantle revisited. *Geochimica et Cosmochimica Acta* 72, 3542-3549.
- Thirlwall, M. F., Gee, M. A. M., Lowry, D., Matthey, D. P., Murton, B. J. & Taylor, R. N. (2006). Low delta O-18 in the Icelandic mantle and its origins: Evidence from Reyjanes Ridge and Icelandic lavas. *Geochimica et Cosmochimica Acta* 70, 993-1019.

- Thirlwall, M. F., Gee, M. A. M., Taylor, R. N. & Murton, B. J. (2004). Mantle components in Iceland and adjacent ridges investigated using double-spike Pb isotope ratios. *Geochimica et Cosmochimica Acta* 68, 361-386.
- Weis, D., Kieffer, B., Hanano, D., Silva, I. N., Barling, J., Pretorius, W., Maerschalk, C. & Mattielli, N. (2007). Hf isotope compositions of US Geological Survey reference materials. *Geochemistry Geophysics Geosystems* 8, Q06006, doi:06010.01029/02006gc001473.
- Willbold, M., Hegner, E., Stracke, A. & Rocholl, A. (2009). Continental geochemical signatures in dacites from Iceland and implications for models of early Archaean crust formation. *Earth and Planetary Science Letters* 279, 44-52.
- Willbold, M. & Stracke, A. (2006). Trace element composition of mantle end-members: Implications for recycling of oceanic and upper and lower continental crust. *Geochemistry Geophysics Geosystems* 7, Q04004, 04010.01029/02005gc001005.
- Wolfe, C. J., Bjanason, I.Th., Vandecar, C.J., Solomon, S.C. (1997). Seismic structure of the Iceland mantle plume. *Nature* 385, 245-247.
- Wood, D. A. (1981). Partial Melting Models for the Petrogenesis of Reykjanes Peninsula Basalts, Iceland - Implications for the Use of Trace-Elements and Strontium and Neodymium Isotope Ratios to Record Inhomogeneities in the Upper Mantle. *Earth and Planetary Science Letters* 52, 183-190.
- Wood, D. A., Joron, J. L., Treuil, M., Norry, M. & Tarney, J. (1979). Elemental and Sr Isotope Variations in Basic Lavas from Iceland and the Surrounding Ocean-Floor - Nature of Mantle Source Inhomogeneities. *Contributions to Mineralogy and Petrology* 70, 319-339.
- Workman, R. K. & Hart, S. R. (2005). Major and trace element composition of the depleted MORB mantle (DMM). *Earth and Planetary Science Letters* 231, 53-72.
- Zindler, A., Staudigel, H. & Batiza, R. (1984). Isotope and Trace-Element Geochemistry of Young Pacific Seamounts - Implications for the Scale of Upper Mantle Heterogeneity. *Earth and Planetary Science Letters* 70, 175-195.

Chapter 3

A new method for U-Th-Pa-Ra separation and accurate measurement of ^{234}U - ^{230}Th - ^{231}Pa - ^{226}Ra disequilibria in volcanic rocks by MC-ICPMS

This chapter is published in *Chemical Geology* as: Koornneef, J.M., Stracke, A., Aciego, S., Reubi, O., Bourdon, B. A new method for U-Th-Pa-Ra separation and accurate measurement of ^{234}U - ^{230}Th - ^{231}Pa - ^{226}Ra disequilibria in volcanic rocks by MC-ICPMS

Abstract

A new method for the chemical separation and MC-ICPMS measurements of U-Th-Pa-Ra disequilibria in volcanic samples from a single sample aliquot is presented. The accuracy and precision of our techniques is assessed by replicate analyses of the synthetic U and Th isotope standards IRMM-184 and IRMM-35, and the secular equilibrium rock standards BCR-2, W-2a and TML. A measure of true sample reproducibility including the errors related to sample processing and the chemical separation is obtained from analysis of multiple digestions of the rock standards. ($^{234}\text{U}/^{238}\text{U}$), ($^{230}\text{Th}/^{238}\text{U}$), ($^{231}\text{Pa}/^{235}\text{U}$) and ($^{226}\text{Ra}/^{230}\text{Th}$) activity ratios on ten separate dissolutions of USGS rock standard BCR-2, for example, reproduce to 0.4%, 1.4%, 1.1% and 2.4% (2 SD), respectively. All elements (U-Th-Pa-Ra) are separated from a single spiked sample aliquot and the elemental concentrations are measured on the same solutions as the isotopic compositions. Analytical artefacts from determination of elemental and isotopic concentrations on different sample aliquots due to sample heterogeneity are therefore avoided. In addition, our new chemical separation protocol is time-efficient and allows for rapid processing of volcanic samples with less than 10 fg of Pa and Ra.

1. Introduction

U-series disequilibria provide important constraints on the time scales and rates of a wide range of geological processes and are applied in diverse fields including oceanography, paleoclimatology and volcanology (Bourdon et al., 2003). In volcanic rocks, U-series disequilibria between the long lived parent isotopes ^{238}U and ^{235}U and their short-lived daughter isotopes ^{230}Th , ^{226}Ra and ^{231}Pa have been used to study magma chamber residence or differentiation times (e.g. Allègre and Condomines, 1976; Asmerom et al., 2005; Bourdon et al., 1994; Condomines et al., 2003; Lowenstern et al., 2000; Reid, 2003; Schmitt, 2006; Snyder et al., 2007; Touboul et al., 2007; Volpe and Hammond, 1991; Yokoyama et al., 2006), as well as magma transfer times and mantle melting rates (e.g. Bourdon et al., 2005; Bourdon et al., 1996; Cohen and O'Nions, 1993; Condomines and Sigmarsson, 2000; Elliott, 1997; Goldstein et al., 1989; Lundstrom et al., 1998; McKenzie, 1985; Prytulak and Elliott, 2009; Sims et al., 1999;

Spiegelman and Elliott, 1993; Stracke et al., 2006; Stracke et al., 1999; Stracke et al., 2003; Turner et al., 1997).

Owing to the minute quantities of Ra and Pa in volcanic samples (e.g. typical concentrations of [^{231}Pa] and [^{226}Ra] for Icelandic basalts are less than 100 fg/g), mass spectrometric analyses of U-Th-Pa-Ra disequilibria in volcanic rocks are analytically challenging, and demand clean chemical separation of the elements with high yields. The extreme ratios between the daughter and parent isotopes in volcanic rocks (e.g. $^{232}\text{Th}/^{230}\text{Th} \sim 1\text{-}2 \times 10^5$ or $^{238}\text{U}/^{234}\text{U} \sim 1.8 \times 10^4$) pose further analytical challenges. Measuring these isotope ratios by mass spectrometry requires the use of ion counting systems in conjunction with Faraday cups. This involves: (1) determination of the dead time and (non)linearity of the ion counting systems; (2) the inter-calibration of SEM and Faraday detectors; and (3) a correction for tailing of the high abundance onto the low abundance beams, especially in the case of ^{232}Th and ^{230}Th .

Although numerous studies have previously reported U-series disequilibrium measurements in silicate rocks, a well documented method for the chemical separation and mass spectrometric analysis of U-Th-Pa-Ra on a *single* sample aliquot has not been published. In several previously published methods the Ra and or Pa concentrations were determined on separate sample digestions from the parent Th and U concentrations (Bourdon et al., 1998; Bourdon et al., 1999b; Chabaux and Allègre, 1994; Claude-Ivanaj et al., 1998; Dosseto et al., 2003; Lundstrom et al., 1998; Lundstrom et al., 2003; Sims et al., 1999; Stracke et al., 2006; Turner et al., 2000). The chemical separation of all four elements from a single aliquot is important because sample heterogeneity can contribute significantly to the error of parent-daughter ratios if measured on separate sample splits. In addition, a method using a single aliquot is more time-efficient than previously reported methods.

Here, we present a full description of a new chemical method to separate U, Th, Ra and Pa from a single sample aliquot and MC-ICPMS measurement techniques for accurate elemental concentration and isotope ratio determination. U-series isotope measurements on certified reference materials IRMM-184 and IRMM-35, the secular equilibrium rock sample TML, and international USGS rock standards BCR-2 and W2a, demonstrate the accuracy and precision of our method. The data set represents a true measure of reproducibility on silicate rock samples as it is obtained from multiple

separate digestions of BCR-2, W-2a and TML and therefore includes the errors related to sample preparation and processing, chemical separation and mass spectrometry.

2. Experimental

2.1 Reagents and materials

Reagent grade HCl, HNO₃ and HF used for cleaning and chemical separation procedures were obtained from Merck Chemicals, Germany. The acids used for sample digestion and chemical separation were purified using PicoTrace™ sub-boiling cupola stills. Dilutions were done with 18.2 MΩ purified water from a Milli-Q Element Millipore system. Boric acid, 99.9995%, ascorbic acid, 99%, ammonium-thiocyanate, 98%, and hydrogen peroxide, 29-32%, were purchased from Alfa Aesar, Germany. Sample dissolution and chemical separations were carried out using PFA Teflon vials that were thoroughly cleaned with a multi-step procedure involving initial boiling in a 3% RBS-50 detergent (Carl Roth, Switzerland), followed by fluxing on a hotplate of individual vials with a mixture of ~3 N HF- 3 N HNO₃, and subsequent boiling in 3 N HNO₃, 6 N HCl, and Milli-Q H₂O. In between all these cleaning steps beakers were rinsed with Milli-Q H₂O. Teflon and PP columns, pipette tips and centrifuge tubes were subject to the same cleaning procedure excluding the HF- HNO₃ step.

Resins used for chromatographic separation were EiChrom™ TRU-spec resin (100-150 μm), Sr-spec resin (50-100 μm), Pre-Filter material to remove organics, and Bio-Rad anion- and cation exchange resins, AG 1-X4, AG 1-X8 and AG 50W-X8, 200-400 mesh. EiChrom™ Resins were pre-cleaned with several rinses of Milli-Q H₂O and 1 N HCl, respectively. Bio-Rad resins were pre-cleaned by several successive rinses with 3 N HNO₃, Milli-Q H₂O and 6 N HCl.

Several rock standards and synthetic solution standards were used to evaluate the accuracy and precision of our chemical and analytical method. We have processed and measured rock standard TML (distributed by J. Gill, University of California, Santa Cruz, USA), and USGS rock standards BCR-2 and W-2a. All these rock powders are well characterised for U-series elemental concentration and were shown to be in, or close to, secular equilibrium (Ball et al., 2008; Hoffmann et al., 2007; Sims et al., 2008). The synthetic uranium and thorium reference solutions IRMM-184, IRMM-35 and IRMM-36 were obtained from the Institute for Reference Materials and Measurements,

Geel, Belgium, and used to assess instrumental performance and reproducibility. IRMM-184 and IRMM-35 are especially well suited for this purpose as the $^{234}\text{U}/^{238}\text{U}$ and $^{230}\text{Th}/^{232}\text{Th}$ ratios, 5.314×10^{-5} and 1.137×10^{-5} , respectively, are similar to those of igneous rock (Hoffmann et al., 2007; Richter et al., 2005).

2.2 Spike preparation and calibration

Sample aliquots were spiked with four mono-elemental tracer solutions containing ^{236}U , ^{229}Th , ^{233}Pa and ^{228}Ra prior to dissolution. A careful calibration of individual spike concentration and isotopic composition is essential for the accurate determination of the $^{230}\text{Th}/^{238}\text{U}$, $^{231}\text{Pa}/^{235}\text{U}$ and $^{226}\text{Ra}/^{230}\text{Th}$ ratios.

The ^{236}U spike was calibrated against gravimetric U reference material CRM-145b (New Brunswick Laboratory), which has a certified uncertainty of 0.03‰ (2σ) on the ^{238}U concentration (10.6886 mg/g). The spike concentration was determined gravimetrically using mixtures of diluted CRM145b standard and ^{236}U spike with variable mixing proportions. The propagated error on the spike concentration includes weighing errors involved in dilution of the gravimetric standard as well as weighing of the spike. The spike was determined to have a ^{236}U concentration of 6.783 ± 0.015 ppb and a purity of 99.68%. The ^{229}Th spike (0.1373 ppb) was calibrated using a similar protocol against an in-house gravimetric Th standard, which was prepared by dissolving solid ultrapure (>99.999%) metal Th, to an uncertainty of 0.3%. The ^{233}Pa spike batches were prepared by neutron activation of ^{232}Th using the Swiss Spallation Neutron Source (SINQ) at the Paul Scherrer Institute (PSI), Villigen, Switzerland. ^{233}Th was produced by neutron capture on ^{232}Th , ~1 mg Th as a nitrate salt, in a sealed glass ampoule (Aciego et al., 2009; Bourdon et al., 1999a). The ^{233}Th then decays to ^{233}Pa with a half life of 22.3 min. After decay of the short-lived nuclides formed by the irradiation decay (i.e. ^{24}Na , $T_{1/2} = 15$ h; ^{28}Al , $T_{1/2} = 2.5$ min), the produced ^{233}Pa was dissolved in ~5-10 mL 9 N HCl. Separation of Pa from Th and other impurities by anion exchange was done in two steps, using an 5 mL and a subsequent 0.5 mL anion exchange column (AG1-X8, 200-400 mesh, Bourdon et al., 1999a). The 5 mL column was cleaned with 6 column volumes (cv) 9 N HCl. The Pa fraction was then eluted in 2 cv 9 N HCl + 0.1 N HF, and evaporated to ~1 mL. At this point, saturated boric acid was added to break up PaF_7^{2-} complexes. This solution was loaded on the second column, previously cleaned with 3 cv 9 N HCl. The Pa fraction was then eluted in 3 cv

9 N HCl + 0.1 N HF. The second separation step was repeated until the Pa/Th ratio in the ^{233}Pa spike is greater than 1, which typically required 3 repetitions. Loss of protactinium to beaker walls or wash solutions during the purification procedure was monitored with a gamma-counter equipped with a 44-11 detector, Ludlum Measurements, INC., Texas USA, connected to a ratemeter. The loss of ^{233}Pa during the spike separation procedure was typically less than 10%.

Due to the decay of ^{233}Pa to ^{233}U with a half life of 26.967 days (Usman and MacMahon, 2000) the ^{233}Pa spike batches produced from ^{232}Th have a finite life span of approximately 5 months. Therefore, new batches of spike had to be prepared at PSI several times during this project and subsequently calibrated with the procedure described below. For each aliquot of spike, the initial $^{231}\text{Pa}/^{233}\text{Pa}$ was determined by MC-ICPMS, as described in section 2.4, after chemical purification from ^{233}U using column 2 in our chemical separation procedure described in section 2.3.

The ^{233}Pa spike was calibrated against the Long Valley rhyolite glass LV18 distributed by G. Davies, Free University Amsterdam (Bourdon et al., 1999a). LV18 was dated to have an age of 1.6 ± 0.05 Ma (OL unit in Metz and Mahood, 1985; Metz and Mahood, 1991) and is therefore expected to be in secular equilibrium. Regelous et al., (2004) showed that LV18 is heterogeneous for U and Pa concentrations. For the ^{233}Pa spike calibration, it is therefore critical to measure the U and Pa concentrations on the same digestion. The coarse-grained glassy LV18 was carefully handpicked to avoid alteration and inclusions of accessory phases that may cause the variations in U concentration. The purified fraction was ground in an agate mortar to produce a homogenous powder. Three batches of ~100 mg of LV18 spiked with varying amounts of ^{233}Pa were separated as described in section 2.3 and analysed for uranium and ^{233}Pa spike concentrations for each individual spike calibration. Over a period of 18 months we obtained an average U concentration for LV18 of 15.02 ± 0.09 ppm ($n = 13$), significantly higher than the average of 10.47 ± 0.2 ($n=3$) reported by Regelous et al., (2004). To check the accuracy of the Pa spike calibration, Pa concentrations and $^{235}\text{U}/^{231}\text{Pa}$ activity ratios of international rock standards BCR-2, TML and W-2a were compared to published values (Prytulak et al., 2008); section 3.1). The Pa concentration (and $^{231}\text{Pa}/^{233}\text{Pa}$) of the spike on the day of U-Pa separation must be calculated from its initial calibrated concentration (typically between 2000 and 3000 fg/g) using a correction for radioactive decay. Moreover, it is critical to measure Pa splits within 24

hours after the U-Pa separation as the ingrown ^{233}U interferes with ^{233}Pa during MC-ICPMS analyses.

The ^{228}Ra spike was prepared from a ~50 year old $\text{Th}(\text{NO}_3)_4$ salt by separating the ^{228}Ra from ^{232}Th in nitric acid using cation exchange (Volpe et al., 1991). The spike was calibrated against a gravimetric radium reference solution (SRM-4967) with a certified concentration of 2729 Bq/g (~74.6 ppb) and an overall uncertainty of 1.8 %. The ^{228}Ra spike had an initial ^{228}Ra concentration of 224 fg/g. For the decay of ^{228}Ra to ^{228}Ac ($T_{1/2} = 6.15$ h) and then to ^{228}Th ($T_{1/2} = 5.75$ years) a correction was applied. Accuracy of the Ra measurements was checked on spiked aliquots of TML, BCR-2 and W-2a that are thought to be in U-Th-Ra secular equilibrium (section 3.1, Pietruszka et al., 2002).

2.3 Sample preparation and chemical separation

2.3.1 Sample preparation

Sample powders, typically between 0.5 and 1 g for volcanic rocks with Pa and Ra concentrations of 50 to 200 fg/g, were weighed and spiked with the ^{236}U , ^{229}Th , ^{233}Pa and ^{228}Ra tracer solutions prior to digestion in HF-HNO₃ (see below). Using single non-natural spikes, there is a large range of spike to sample ratios for which error magnification remains close to optimum. Therefore, the amount of added spike was determined by the ability to make precise mass spectrometric and gravimetric measurements. Signal intensities were aimed to be above 500 cps when measured on an ion counter or more than 5 mV when measured on a Faraday cup. Sample weights of more than 0.01 g were aimed for to minimise measurement and weighing errors. For Th analyses, the ^{229}Th spike was added so that the $^{229}\text{Th}/^{230}\text{Th}$ was similar to that in the bracketing ETH-IRMM Th standard ($^{229}\text{Th}/^{230}\text{Th} = 12.4$, see Appendix I for a detailed description of the ETH-IRMM Th standard). Typical spike to sample ratios were less than 1 for uranium, thorium and radium and less than 5 for protactinium.

Sample dissolution and sample-spike equilibration was achieved in a mixture of 1 mL 14 N HNO₃ and 10 mL 27 N HF. Following treatment with ultrasound for a few hours, the samples were placed on a hotplate for a minimum of three days at 120°C. After evaporation to complete dryness, samples were re-dissolved in ~20 mL 6 N HCl. Saturated boric acid was added and allowed to react for a few hours to dissolve insoluble fluorides. The exact amount of boric acid required for complete complexation of all fluorides was calculated using the weight and major element composition of the

sample and is typically around 35% of the sample weight for basaltic samples (Claude-Ivanaj et al., 1998). After drying down and evaporation of the boric acid as HBF_4^- , samples were converted to nitric salts by adding ~20 mL 7.5 N HNO_3 . Re-dissolution in HNO_3 requires ~2 hours on a hotplate at 120°C, after which samples were evaporated to complete dryness and were re-dissolved in 5 mL 2 N HNO_3 . At this stage, ascorbic acid was added to reduce Fe^{3+} , which competes with the rare earth elements (REE) and actinides on the TRU-spec column (Horwitz et al., 1993; Pin and Zalduogui, 1997, see section 2.3.2). The minimum amount of ascorbic acid required was calculated based on the Fe content of the sample. The efficiency of the reaction was tested by adding 20 μL of 0.1 N ammonium thiocyanate, which turns red in the presence of trivalent Fe. Typically, the amount of ascorbic acid required to reduce all iron in basaltic rocks with 9-12 wt % of total FeO was equivalent to about 30% of the sample weight (Caro et al., 2006).

2.3.2 Chemical separation

An overview of the separation method is shown in Fig 1 and Table 1. The first elution step extracts Ra and most other matrix elements (e.g. alkalis, alkali earths, transition metals and heavier lanthanides) following consecutive elution of the Th and U-Pa fractions on a 5 mL TRU spec column (Goldstein and Stirling, 2003). EiChrom Pre-Filter Material, 0.5 mL, was loaded in the bottom of this column to remove organics from the TRU-spec resin (Goldstein and Stirling, 2003; Pietruszka et al., 2002). The TRU-spec resin was pre-cleaned with 5 mL 1 N HF, 2 mL H_2O and 5 mL 2 N HNO_3 , respectively, and conditioned with 2 times 25 mL 2 M HNO_3 , before loading the sample in 5 mL 2 N HNO_3 (+ ascorbic acid and ammonium thiocyanate, see section 2.3.1). Loading this column with 2 N HNO_3 + ascorbic acid instead of using HCl as described by Goldstein and Stirling (2003), reduced the problem of trivalent Fe that has a high distribution coefficient on the TRU-resin in high molar HCl. Ra and most other major and trace elements (e.g. Ca, Na, Fe, Sr, Yb, Lu) were eluted with 25 mL of 2 N HNO_3 , whereas MREE, LREE and the actinides remained on the resin (Fig. 2a). Subsequently, the resin was conditioned with 6 mL of 9 N HCl and the MREE and LREE were eluted with 12 mL of 4 N HCl. Th was then eluted in 30 mL 0.8 N HCl and finally, the U-Pa fraction was eluted in 25 mL 0.1 N HCl + 1 M HF. The TRU-spec resin was discarded

after use and the collected Ra (with most of the matrix), Th and U-Pa fractions were prepared for further purification on subsequent ion exchange columns.

For separation of U from Pa, 5 drops of perchloric acid was added to the U-Pa fraction and evaporated at 180°C to fume off all fluoride ions and to destroy any remaining organics. Condensed perchloric acid on the beaker walls was washed down repeatedly with a jet of Mili-Q water during evaporation. After complete evaporation the sample was dissolved in 0.5 mL 1 N HCl + 0.01 N HF and loaded onto a second 1 mL BioRad AG50-X8 column that separated Pa from U (Burnett and Yeh, 1995). The presence of dilute HF in the solution avoided loss of Pa to the beaker walls. The column was pre-cleaned with 6 N HCl + a few drops of 27 N HF and H₂O and conditioned with 5 mL 0.1 N HCl + 0.01 N HF before loading the U-Pa fraction. Pa eluted readily and was collected together with 4.5 mL 0.1 N HCl + 0.01 N HF and 5 mL of 0.1 N HCl. Uranium was subsequently eluted in 12 mL 2 N HCl. About ~0.4% of the total Th, remained on the resin and was washed off in 6 N HCl and discarded (Fig. 2b). Total column yields for U and Pa were determined by isotope dilution using BCR-2 and were greater than 90%.

The Th fraction from column 1 was partially dried down to ~ 2 mL and loaded on a 0.2 mL Teflon column packed with EiChrom Pre-Filter Material to purify the solution and prevent formation of insoluble precipitates during evaporation. The purified Th fraction was dried down completely, re-dissolved in 0.35 mL 7.5 N HNO₃ and loaded on a 0.2 mL Teflon column packed with AG1-X4 resin to further purify the Th fraction. The Th yield determined by isotope dilution on BCR-2 was greater than 85%.

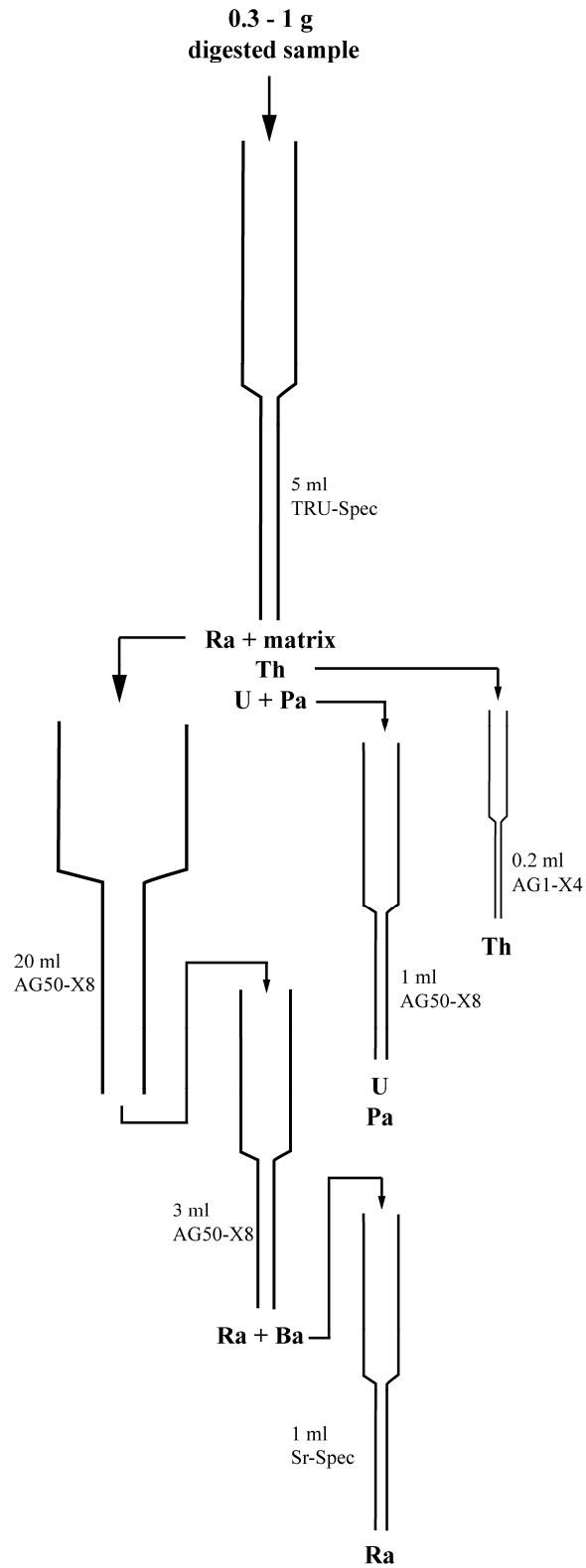


Figure 1. Summary of chemical separation method for U, Th, Pa and Ra from 0.3 to 1 g of volcanic rock powder.

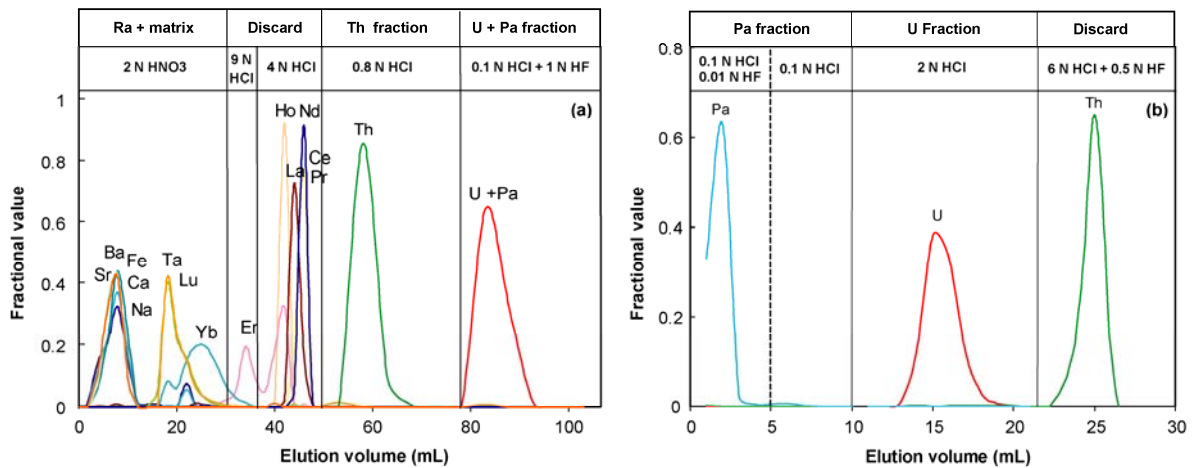


Figure 2. Elution curves for the first two columns (a) 5 mL TRU-Spec to obtain Ra + matrix, Th and U + Pa and (b) 1 mL AG50-X8 to separate the U (and residual Th) from the Pa.

The purification of radium was similar to that described in Chabaux et al., (1994) but modified to reduce the amount of acid used for the column chemistry (Claude-Ivanaj et al., 1998). The method involved two cation columns to separate Ra from the matrix elements, 20 mL and 3 mL AG50-X8, and one Sr-spec column to purify the Ra from Ba and HREE (1 mL). At the bottom of the Sr-spec column 0.1 mL of Eichrom Pre-Filter Material was loaded to remove organics from the Sr-spec resin (Pietruszka et al., 2002). The sample was loaded on the first cation column, which was cleaned and pre-conditioned with 40 mL 6 N HCl. After discarding 55 mL 6 N HCl and 5 mL H₂O, which eluted the main cations (Mg, Ca, Fe etc.), Ba and Ra were eluted in 20 mL 7.5 N HNO₃. The Ra and Ba fraction was evaporated and re-dissolved in 1 mL 6 N HCl, and was loaded onto a second cation column that was cleaned and conditioned with 10 mL 6 N HCl. A further 9 mL 6 N HCl were discarded and the purified Ra-Ba (+ HREE) fraction was eluted in 25 mL 6 N HCl.

The third Sr spec column separated Ra from Ba. The Sr Spec resin was conditioned with 10 mL 3 N HNO₃, the sample was loaded in 0.5 mL 3 N HNO₃, washed with 1 mL 3 N HNO₃ and the pure Ra fraction was eluted in 5 mL 3 N HNO₃. The Sr-resin was discarded after use. Total procedural blanks were ~50 pg for Th, ~25 pg for U whereas for Pa and Ra the blanks were below the limit of detection, i.e. < 4 cps.

Table 1. Summary of chemical separation procedures for U, Th, Pa and Ra

Column 1. Ra + matrix, Th and U + Pa 5 mL TRU-Spec + pre-filter			Column 4. Separate Ra from matrix 20 mL AG50-X8		
procedure	Reagent	volume	procedure	Reagent	volume
Clean	1N HF	5	Clean	6 N HCl + conc. HF	20
	H ₂ O	2		H ₂ O	2
	7.5 N HNO ₃	5		7.5 N HNO ₃	20
	2 N HNO ₃	5		0.25 N HNO ₃	20
Condition	2 N HNO ₃	2 x 25	Condition	6 N HCl	50
Load (collect Ra + matrix)	2 N HNO ₃	5	Load	6 N HCl	40
Wash (collect Ra + matrix)	2 N HNO ₃	25	Wash	6 N HCl	55
	9 N HCl	6		H ₂ O	4
	4 N HCl	12			
Collect Th	0.8 N HCl	30	Collect Ra+ Ba	7.5 N HNO ₃	20
Collect U + Pa	0.1 N HCl + 1 N HF	25			

Column 2. Separate U from Pa 1mL AG50-X8			Column 5. Purify Ra-Ba fraction 3 mL AG50-X8		
procedure	Reagent	volume	procedure	Reagent	volume
Clean	6 N HCl + conc. HF	5	Clean	6 N HCl + conc. HF	3
	H ₂ O	2		H ₂ O	0.3
Condition	0.1 N HCl + 0.01 N HF	5		7.5 N HNO ₃	3
		0.25 N HNO ₃		3	
Load (Collect Pa)	0.1 N HCl + 0.01 N HF	0.5	Condition	6 N HCl	10
Collect Pa	0.1 N HCl + 0.01 N HF	4.5	Load	6 N HCl	1
Collect Pa	0.1 N HCl	5			
Collect U	2 N HCl	12	Wash	6 N HCl	9
				Collect Ra + Ba	6 N HCl

Column 3. Purify Th fraction 0.2 mL AG1-X4			Column 6. Purify Ra fraction 1 mL Sr-Spec + pre-filter			
procedure	Reagent	volume	procedure	Reagent	volume	
Clean	6 N HCl + conc. HF	1.2	Clean	H ₂ O	0.1	
	H ₂ O	0.5		3 N HNO ₃	1	
	7.5 N HNO ₃	0.5				
	0.25 N HNO ₃	1.6				
Condition	7.5 N HNO ₃	0.2	Condition	3 N HNO ₃	10	
Load	7.5 N HNO ₃	0.15	Load	3 N HNO ₃	0.5	
Wash	7.5 N HNO ₃	1.6	Wash	3 N HNO ₃	1	
	0.25 N HNO ₃	0.05				
Collect Th	0.25 N HNO ₃	0.7	Collect Ra	3 N HNO ₃	5	

Volumes are given in mL

2.4 Mass spectrometric procedures and data reduction

2.4.1 Instrumentation

Measurements of U, Th, Pa and Ra isotopes were done on a Nu Plasma MC-ICPMS at ETH Zürich. The instrument is equipped with 12 Faraday cups and two discrete dynode secondary electron multipliers (SEM) operating in pulse counting mode (IC1 and IC2). IC1 is equipped with an energy filter that improves the abundance sensitivity. Samples were introduced using a CetacTM Aridus II desolvator for U, Pa and Ra analyses and an Elemental ScientificTM APEX-HF desolvator for the Th analyses. Both introduction systems are used with a PFA nebuliser with a nominal uptake rate of 100 $\mu\text{l}/\text{min}$.

2.4.2 General procedures and MC-ICPMS settings

U and Th concentrations and isotopic compositions were measured on the same aliquot. The cup configuration used for the U, Th, Pa and Ra measurements is shown in Table 2. Uranium was measured statically, whereas thorium, protactinium and radium were measured by peak-jumping. For the analyses of U and Th, unknowns were bracketed by standards SRM960 (also known as NBL-112a) and IRMM-36, respectively, to derive correction factors for the instrumental mass bias and the relative Faraday to SEM gain. Bracketing Th analyses with U standards introduces significant error in the correction of both the mass bias and Faraday-Ion Counter gain (Hoffmann et al., 2007) hence we used IRMM-36 spiked with ^{229}Th for this purpose. This in-house standard (ETH-IRMM) was analysed first with the ETH Thermo Triton TIMS to determine its $^{229}\text{Th}/^{232}\text{Th}$ ratio (see Appendix I for a description of the method). To minimize potential errors owing to non-linear response of the ion counting system (see detailed discussion in section 2.5), the concentrations of SRM960, IRMM-36 and samples were adjusted to have similar count rates to within a factor of 3 on masses 229 and 230 for standards and unknowns. For the isotope dilution measurements of Pa and Ra concentrations, Ra and Pa solutions were doped with the SRM960 U standard to correct for instrumental mass bias. Even though Pa and Ra likely behave differently compared to U in the plasma source, any difference in the mass bias is insignificant compared to the obtainable precision for count rates of 300-3000 cps.

Table 2. Cup configurations for MC-ICPMS analyses

Cup	cycle	H3	H2	H1	Ax	L1	L2	L3	L4	IC1	L5	IC2
Uranium	1					238		236 ^a	235	234		
Thorium	1							232		230		
	2						232			229		
Protactinium	1		238			235			232	231		
	2				238			235		233	232	231
Radium	1		235							228		226
	2	238				235						228

^a only measured for sample analyses

At the beginning of each analytical session, the relative Faraday cup amplifier gains were determined electronically and corrected for using an on-line correction routine. Tuning of the MC-ICPMS instrument, gas flows, torch position and ion optics, was done to obtain maximum beam intensity. The instrument was allowed to stabilize for at least two hours before measurement initiation. Sensitivity for ²³⁸U was typically between 0.3-0.5 V/ppb for the Aridus, and 0.2-0.3 V/ppb using the APEX at an uptake rate of about 100 µl/min. Peak shapes and coincidence were optimized with the automated Nu Instruments Quad lens routine. The Ion Counting operating voltage or ‘plateau’ voltage of the ion counting system was optimized at the start of each analytical session for each ion counter. Tuning of the IC1 peak shape involved adjusting the ‘Dog Leg IC’ and ‘Dog Leg skew’ lenses located in front of IC1. The retardation filter settings on IC1 were adjusted to attain optimal abundance sensitivity during Th analyses, < 150 ppb at 2 amu. All samples were introduced in a solution of 2 % HCl + 0.2 % HF that was also used as a cleaning solution.

A typical measurement routine involved an automatic peak centre routine, measurement of half mass zeros during 30 s and on-peak measurement of ion beams in 40 cycles of 5 s each. Data outliers were rejected online by a two-sigma outlier test. In between analyses sufficient wash-out time was allowed to achieve negligible background. For effective Th wash-out stronger cleaning solutions of 2 % HCl + 1 % HF and 0.1 N oxalic acid were used in addition to the default rinse with 2 % HCl + 0.2 % HF. On-peak background intensities were monitored carefully and measured on a regular basis to ensure thorough wash-out. Wash out time for U was typically 5-10

minutes, for Th between 10 and 20 minutes and for Ra and Pa 3 minutes. Backgrounds for ^{238}U were <2000 cps, for ^{232}Th $< 20\,000$ cps and for Pa and Ra < 4 cps.

2.4.3 Data reduction

Corrections for background intensities, mass fractionation, relative Faraday-SEM gains, tailing and spike contributions were conducted off-line, as described in more detail below.

Background subtraction

For uranium, protactinium and radium analyses zero beam intensities were measured at half masses above and below the mass of interest. On-peak backgrounds were calculated by linear interpolation and subtracted from the measured intensity. These baseline corrections accounted for both electronic background on Faraday cups (and SEM) as well as for tailing of the large ^{238}U beam onto the smaller masses (i.e. ^{236}U , ^{235}U and ^{234}U).

For the Th isotope analyses in volcanic samples, a precise determination of the contribution of the large ^{232}Th beam to the minor ^{230}Th isotope is required. The contribution of the ^{232}Th tail is determined from a mass scan before the onset of data acquisition for each sample solution (Ball et al., 2008; Hubert et al., 2006). The peak scan covered the mass range from 229.5 to 231 amu in 100 steps of one second acquisitions to achieve a good exponential fit of the ^{232}Th tail on either side of the ^{230}Th peak. The zero on the 230 mass is then calculated from the exponential curve (exponential trend line, Fig. 3) and the centre value of the ^{230}Th peak (see also Ball et al., (2008)). The calculated zero value is subtracted from the measured average ^{230}Th intensity. Zero corrections on the ^{232}Th and ^{229}Th were done by linear interpolation of the half mass beam intensities similar to the procedure employed for the U, Pa and Ra analyses. Even though the tail from the ^{232}Th also contributes slightly to the ^{229}Th mass (abundance sensitivity $^{229}\text{Th}/^{232}\text{Th} < 3 \times 10^{-8}$), an exponential correction similar to the correction applied to the 230 is not required. The effect of using a linear rather than an exponential correction on the final $^{229}\text{Th}/^{232}\text{Th}$ ratio is negligible (1-2%) compared to the error that is derived from the analyses and sample and spike weighing (~5%).

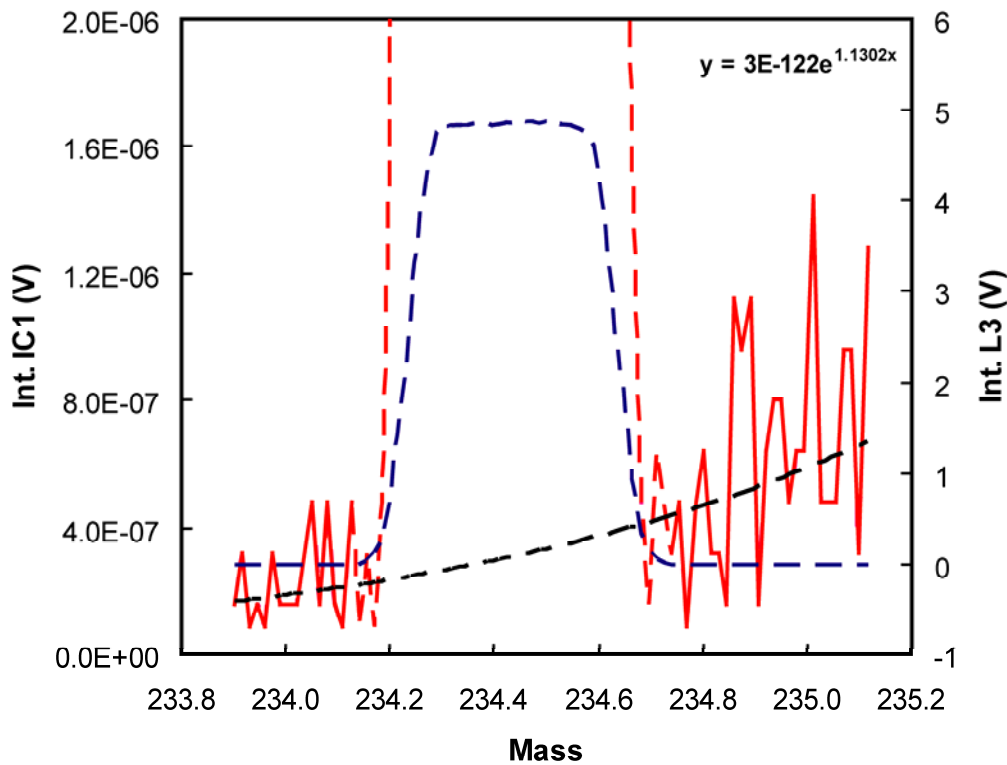


Figure 3. Peak scan over the Th mass range, showing the tail of the ^{232}Th beam that contributes to the ^{230}Th signal. The contribution is calculated from the exponential fit to the tail using the peak centre value. Dashed blue line is the ^{232}Th beam measured in Faraday cup L3 (intensity shown on the secondary y-axis). The pink dashed line is the ^{230}Th beam measured in IC1 (intensity shown on the primary y-axis). The dashed black line is the exponential fit to the ^{232}Th tail (pink line). The parameters for fitting the exponential trend line (shown at upper right corner) are obtained from ExcelTM.

Instrumental mass bias

The $^{238}\text{U}/^{236}\text{U}$, $^{238}\text{U}/^{234}\text{U}$, $^{233}\text{Pa}/^{231}\text{Pa}$ and $^{228}\text{Ra}/^{226}\text{Ra}$ ratios were corrected for instrumental mass fractionation using the exponential law (Russell et al., 1978; Wasserburg et al., 1981). In this procedure a correction factor (β) is derived from:

$$\beta = \frac{\text{Ln} \left(\frac{\left(\frac{^{238}\text{U}}{^{235}\text{U}} \right)_{\text{True}}}{\left(\frac{^{238}\text{U}}{^{235}\text{U}} \right)_{\text{Meas}}} \right)}{\text{Ln} \left(\frac{M^{238}\text{U}}{M^{235}\text{U}} \right)} \quad (1)$$

where $(^{238}\text{U}/^{235}\text{U})_{\text{True}}$ is 137.88 and $M^{238}\text{U}$ and $M^{235}\text{U}$ are the atomic masses.

This value is then used to correct the measured ratios with the follow equation:

$$R_{corrected} = R_{measured} \times \left(\frac{M_1}{M_2} \right)^\beta$$

(2)

where R is the isotope ratio to be corrected and M₁ and M₂ are the atomic masses of the isotopes. The presence of the ²³⁶U spike with a non-natural ²³⁸U/²³⁵U ratio in our uranium sample solutions alters the natural ²³⁸U/²³⁵U ratio of the sample and hence the average mass bias factors of the two bracketing SRM960 standards was used in the mass bias correction for unknowns. For the Pa and Ra analyses the mass bias factor (β) was calculated from the measured ²³⁸U/²³⁵U on the SRM960-doped solutions and used to correct the ²³³Pa/²³¹Pa and ²²⁸Ra/²²⁶Ra ratios.

Relative Faraday-SEM gain

The relative Faraday-SEM gain during uranium analyses was determined on the SRM960 standards using the measured mass fractionation corrected ²³⁴U/²³⁸U ratios and the secular equilibrium ²³⁴U/²³⁸U ratio of Cheng et al., (2000) (²³⁴U/²³⁸U = 5.286 ± 0.003 × 10⁻⁵). The average gain of the SRM960 standard measured before and after each unknown was then used to correct the measured ²³⁴U/²³⁸U of the unknowns. The stability of the Faraday-SEM gain was monitored carefully before and during each analytical session. Over the course of 8 hours, the length of a typical analytical session, the Faraday-SEM gain was stable to within 0.6%.

For thorium analyses, the measured ²³⁰Th/²³²Th and ²²⁹Th/²³²Th ratios of unknowns were corrected for mass bias and for the relative Faraday-SEM gain in a single correction procedure by sample (smpl) standard (std) bracketing. The in-house ETH-IRMM standard was measured before and after each unknown and the corrected ratio was obtained from:

$$(R_i)_{smpl} = (R_i)_{std} \frac{(r_i)_{smpl}}{\sqrt{(r_i)_{std1} \times (r_i)_{std2}}}$$

(3)

where R_i is the true isotope ratio and r_i is the measured isotope ratio (Albarède and Beard, 2004).

Spike correction and error propagation

Finally, the mass bias, Faraday-SEM gain and background corrected U and Th isotope compositions were corrected for spike contributions, and the corrected activity ratios were calculated using the respective half-lives (Cheng et al., 2000; Holden, 1990; Jaffey et al., 1971).

All the uncertainties of variables used in our calculation of concentrations, isotope ratios and activity ratios, i.e. sample and spike weight, measurement errors, errors on the determination of the mass bias factor and relative gain factor, were propagated into the final 2σ standard errors reported in Figure 5. For example, the uncertainty on the $^{230}\text{Th}/^{238}\text{U}$ activity ratio calculated from the $^{230}\text{Th}/^{232}\text{Th}$ and the ^{232}Th and ^{238}U concentrations includes the errors from: (1) $^{230}\text{Th}/^{232}\text{Th}$ measurements on the sample and on the bracketing ETH-IRMM standards, (68% of the propagated error); (2) $^{229}\text{Th}/^{232}\text{Th}$ measurement on the sample and the bracketing standards contributes (23%); (3) $^{236}\text{U}/^{238}\text{U}$ measurement on the sample (1%); (4) $^{235}\text{U}/^{238}\text{U}$ analysis on the bracketing SRM960 standards and (3%); (5) ^{236}U and ^{229}Th spike weighing (1% and 4% of the total respectively). Systematic uncertainties in spike concentrations or the half lives used in activity ratio calculations were not included. As we used different batches of the ^{233}Pa spike, the uncertainty on the Pa spike concentration could not be treated as a systematic error and therefore the uncertainties associated with the spike calibration using LV18 were also propagated in $^{231}\text{Pa}/^{235}\text{U}$ activity ratios. These included the errors on the LV18 U concentration determination, the LV18 sample-spike weighing and the $^{231}\text{Pa}/^{233}\text{Pa}$ measurements.

2.5 Characterisation of SEM dead time and nonlinearity

The operating conditions of the ion counting system are crucial for precise and accurate U-series isotope measurements. Optimisation of these conditions and characterisation of the SEM's dead time and linearity are therefore required. Significant nonlinearity of the SEM has been reported by a number of previous studies (e.g. Goldstein and Stirling, 2003; Hoffmann et al., 2005; Richter et al., 2009; Richter et al., 2001). Nonlinearity is potentially problematic when unknown samples are bracketed by standards to correct for the relative Faraday-SEM gain. If samples and standards have different signal intensities, the differences in signal strength may compromise Faraday-SEM gain measurements if the response of the ion counting system is significantly non-

linear. Nonlinearity may be inherent in the pulse amplification - discrimination circuitry and in the SEM detector itself (Hoffmann et al., 2005; Richter et al., 2009; Richter et al., 2001). A major contribution is the ‘dead time’ (τ) of the ion counting system which is the minimum time required to resolve subsequent pulses. This effect can be accurately corrected for if the dead time is precisely known, independent of count rate and ideally, independent of pulse height distribution. In such a case the relationship between the measured and corrected count rates is given by

$$C_{measured} = C_{corrected} \cdot e^{-C_{corrected} \cdot \tau} \quad (4)$$

where $C_{corrected}$ and $C_{measured}$ are corrected and measured count rates, respectively, and τ is the dead time. This equation applies to so-called paralyzing (extended dead time) ion counting systems such as that installed on the Nu Instruments MC-ICPMS. After being triggered by the pulse from an incoming ion, a paralyzing system remains in a non-active state for a given time interval, τ . Any subsequent pulse arriving before the completion of this interval is not counted and additionally extends the non-active state by another time interval τ , subject to further extension if pulses arrive before completion of the latter (Lampton and Bixler, 1985). The dead time for both our SEM systems was experimentally determined using an oscilloscope that recorded the time span between subsequent pulses collecting >10,000 double pulse events. This yielded an approximate dead time for both our ion counters of 10 ns. Because this dead time is relatively short, the dead time correction has a negligible effect (<150 ppm) for count rates below 1.5×10^4 cps, i.e. the maximum count rates used in our U-series analyses. Up to 3×10^5 cps the correction for such a dead time is below 0.3%, i.e. within the 2 S.E. of a typical $^{234}\text{U}/^{238}\text{U}$ analysis. Thus, for our U-series analysis the uncertainty on the determination of dead time does not contribute significantly to the overall uncertainty.

To evaluate the nonlinearity of our two ion counting systems we performed tests using an off-line dead time correction of 10 ns. For simplicity we use:

$$C_{corrected} = \frac{C_{measured}}{1 - C_{measured} \tau} \quad (5)$$

which applies to non-paralyzing ion counting systems but is a reasonable approximation for count rates applied in our tests. For the maximum possible count rate of 1×10^6 cps, the difference between using this equation and equation 4 is 50 ppm, which is negligible

compared to our analytical errors. We followed the protocols for the determination of the detector nonlinearity outlined in Hoffmann et al., (2005) that involves measuring the U isotope composition of a standard solution with a large range of beam intensities. Uranium standard IRMM-184 was used to measure $^{234}\text{U}/^{238}\text{U}$ and $^{235}\text{U}/^{238}\text{U}$ ratios with ^{234}U and ^{235}U count rates between 1×10^2 cps and 1×10^6 cps. The IRMM-184 analyses were bracketed by SRM960 with a fixed concentration to correct for SEM-Faraday gain. SEM IC1 behaves linearly within 0.5 % up to intensities of 5×10^5 cps (Fig. 4a). For intensities greater than 5×10^5 cps, $R_{\text{measured}}/R_{\text{true}}$ increases slightly indicating modest nonlinear behaviour. SEM IC2 behaves linear up to 3×10^4 (Fig. 4b). For higher count rates SEM2 behaves nonlinearly as shown by a 1.5 % offset of the measured ratios compared to the reference values at 1×10^6 cps (Fig. 4b). However, the observed nonlinearity for either IC1 or IC2 does not significantly compromise our U-series analyses as these only involve count rates below 1.5×10^4 cps where no significant non-linearity effect could be detected.

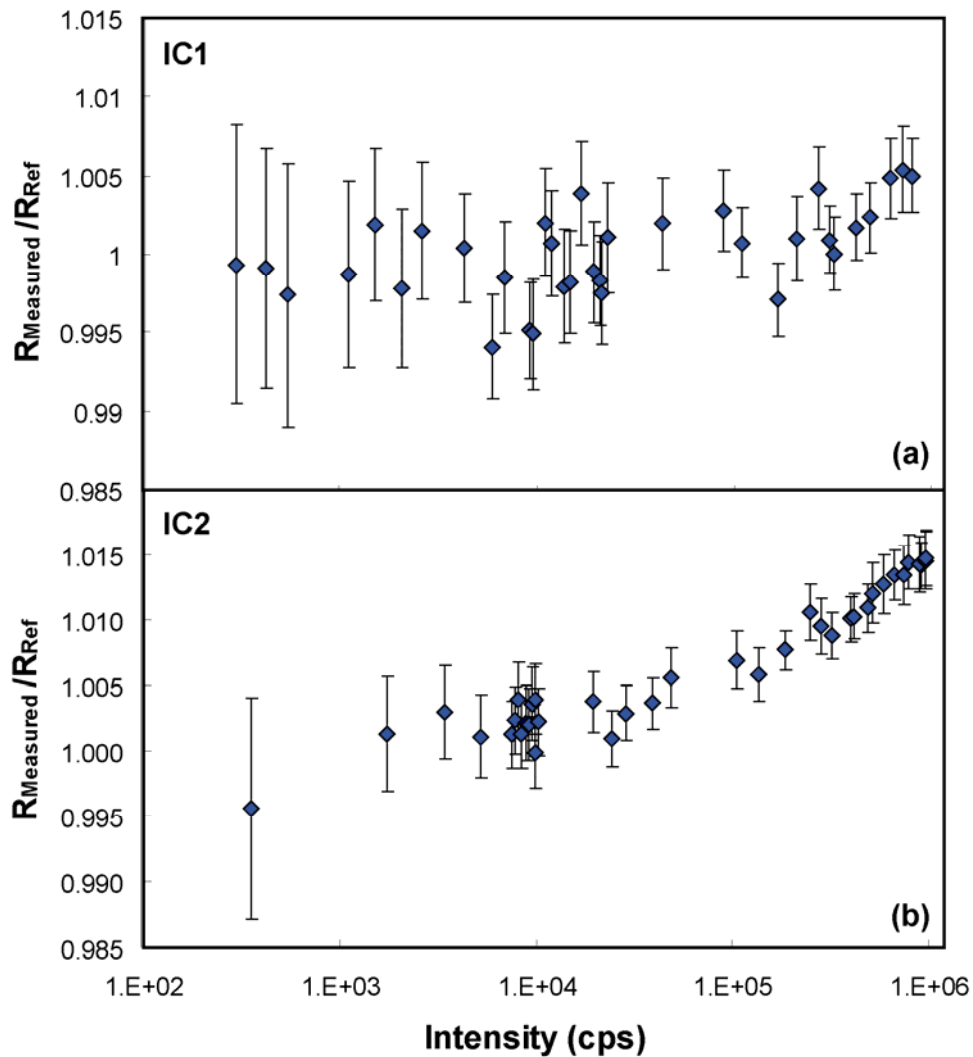


Figure 4. Linearity characterisation for (a) Ion Counter IC1 and (b) Ion Counter IC2. Dead time was corrected off-line (eqn 5). We followed the procedures for SEM linearity characterisation outlined in Hoffman et al., (2005). The measured $^{234}\text{U}/^{238}\text{U}$ and $^{235}\text{U}/^{238}\text{U}$ for IRMM-184 are normalised to the reference values (5.286×10^{-5} and 7.253×10^{-3} , respectively (Cheng et al., 2000)) and plotted against the beam intensity on the ion counter. The $^{234}\text{U}/^{238}\text{U}$ measurements covered an intensity range on the SEM from 1×10^2 to 2.5×10^4 cps, whereas the $^{235}\text{U}/^{238}\text{U}$ measurements covered the range from 1×10^4 to 1×10^6 cps. Error bars represent propagated 2σ standard errors on the measured ratio. IC1 behaves linearly up to intensities of 5×10^5 cps. IC2 behaves linearly up to intensities of 3×10^4 cps. The nonlinearity observed for count rates higher than 3×10^4 cps results in a offset of the measured from the reference ratio of 1.5% at a count rate of 1×10^6 cps. However, the nonlinearity does not affect our U-series analyses as count rates never exceed 1.5×10^4 cps.

3. Results

The accuracy and precision of the U, Th, Pa and Ra isotope analyses were determined by repeated analyses of synthetic isotope standards, U standard IRMM-184 and Th standard IRMM-35, and the secular equilibrium rock standards, BCR-2, W2a and TML, over a period of 15 months. Note that the reproducibility of our measurements for secular equilibrium rock standards includes multiple sample digestions as opposed to replicate analyses of solutions from a single digestion. Our results therefore monitor true accuracy and precision of samples including errors related to sample processing, chemical separation and mass spectrometry (Fig. 5 and Table 3). All errors reported in the following are 2σ standard deviations (2 SD), unless stated otherwise.

The accuracy and precision of the uranium isotope measurements was evaluated by measuring the synthetic solution standard IRMM-184. Typically, the IRMM-184 was run 5 times before starting measurement of unknowns to evaluate instrumental performance. Measurement of this standard over a period of one year ($n=90$) yields a $^{234}\text{U}/^{238}\text{U}$ value of $(5.317 \pm 0.017) \times 10^{-5}$, in excellent agreement with its certified value ($^{234}\text{U}/^{238}\text{U} = 5.314 \pm 0.003 \times 10^{-5}$, Richter et al., 2005). Internal standard errors on $^{234}\text{U}/^{238}\text{U}$ ratios are better than 0.4% (2 SE). Analyses of U concentrations and isotope compositions of different dissolutions of rock standards BCR2, W-2a and TML ($n = 10$, $n = 8$, $n = 4$, respectively) are in good agreement with literature values and confirm secular equilibrium for these rock standards (Table 2, Fig. 5).

The $^{230}\text{Th}/^{232}\text{Th}$ ratio of the synthetic Th standard IRMM-35 averaged $(11.347 \pm 0.130) \times 10^{-6}$, ($n=24$), which is also in excellent agreement with the value reported by Sims et al., (2008) ($^{230}\text{Th}/^{232}\text{Th} = 11.38 \pm 0.096 \times 10^{-6}$). Propagated relative 2σ standard errors on individual $^{230}\text{Th}/^{232}\text{Th}$ measurements are less than 0.9%. The average $^{230}\text{Th}/^{238}\text{U}$ activity ratios on rock standards BCR-2 (1.004 ± 0.014 , $n = 16$, 10 dissolutions), W-2a (1.001 ± 0.014 , $n = 12$, 8 dissolutions), and TML (1.001 ± 0.016 , $n = 10$, 4 dissolutions) confirm that these rock standards are in secular equilibrium with respect to the U and Th nuclides but they have slightly greater errors than the IRMM-35 measurements.

Table 3. Rock standard reproducibility

Standard	BCR-2				W-2a				TML			
	Average	2SD	n	d	Average	2SD	n	d	Average	2SD	n	d
U (mg/g)	1.692	0.006	14	10	0.502	0.006	10	8	10.59	0.32	4	4
Th (mg/g)	5.908	0.061	20	10	2.147	0.023	13	8	30.00	0.55	10	4
Pa (fg/g)	561	8	6	6	166	5	6	6	3542	85	3	3
Ra (fg/g)	580	9	9	9	171	5	8	8	3670	35	4	4
(²³⁴ U/ ²³⁸ U)	1.002	0.004	14	10	1.002	0.006	10	8	0.998	0.003	4	4
(²³⁰ Th/ ²³² Th)	0.875	0.018	20	10	0.712	0.011	13	8	1.067	0.026	10	4
(²³⁰ Th/ ²³⁸ U)	1.004	0.014	16	10	1.004	0.014	8	7	1.001	0.015	4	4
(²³¹ Pa/ ²³⁵ U)	1.006	0.011	6	6	1.005	0.023	6	6	1.013	0.039	3	3
(²²⁶ Ra/ ²³⁰ Th)	0.999	0.025	9	9	0.991	0.027	7	7	1.005	0.024	4	4

n is the total number of measurements, d is the number of dissolutions. Activity ratios, denoted by parentheses are calculated using:
 $\lambda_{234} = 2.8263 \times 10^{-6} \text{ y}^{-1}$, $\lambda_{238} = 1.5513 \times 10^{-10} \text{ y}^{-1}$, $\lambda_{232} = 4.9475 \times 10^{-11} \text{ y}^{-1}$, $\lambda_{230} = 9.1577 \times 10^{-6} \text{ y}^{-1}$, $\lambda_{231} = 2.1158 \times 10^{-5} \text{ y}^{-1}$

Pa measurement accuracy and reproducibility was monitored with rock standards BCR2, TML and W-2a because no synthetic standard is available. The Pa measurements were done over a period of 15 months using three separately produced ²³³Pa spike batches. All measurements are performed on separate dissolutions since solutions were used up after a single analysis. The (²³¹Pa/²³⁵U) of BCR-2, W2 and TML averaged 1.006 ± 0.011 , $n = 6$, 1.005 ± 0.023 , $n = 6$ and 1.013 ± 0.039 , $n = 3$ with ²³¹Pa concentrations of $561 \pm 8 \text{ fg/g}$ ($n = 6$), $166 \pm 5 \text{ fg/g}$ ($n = 6$) and $3542 \pm 85 \text{ fg/g}$ ($n = 3$), respectively. Propagated standard errors (2 SE) on individual ²³¹Pa/²³⁵U analyses are typically 1% (Fig. 5).

Measurements of (²²⁶Ra/²³⁰Th) activity ratios on different dissolutions of BCR-2, W-2a and TML yield averages of 0.999 ± 0.025 ($n = 9$), 0.991 ± 0.027 ($n = 7$), and 1.005 ± 0.024 ($n = 4$), respectively. ²²⁶Ra concentrations were determined to be $580 \pm 9 \text{ fg/g}$ ($n = 9$) for BCR2, 171 ± 5 ($n = 8$) for W-2a and $3670 \pm 35 \text{ fg/g}$ ($n = 4$) for TML. Internal propagated measurement errors (2 SE) on the ²²⁶Ra/²³⁰Th are $< 1\%$.

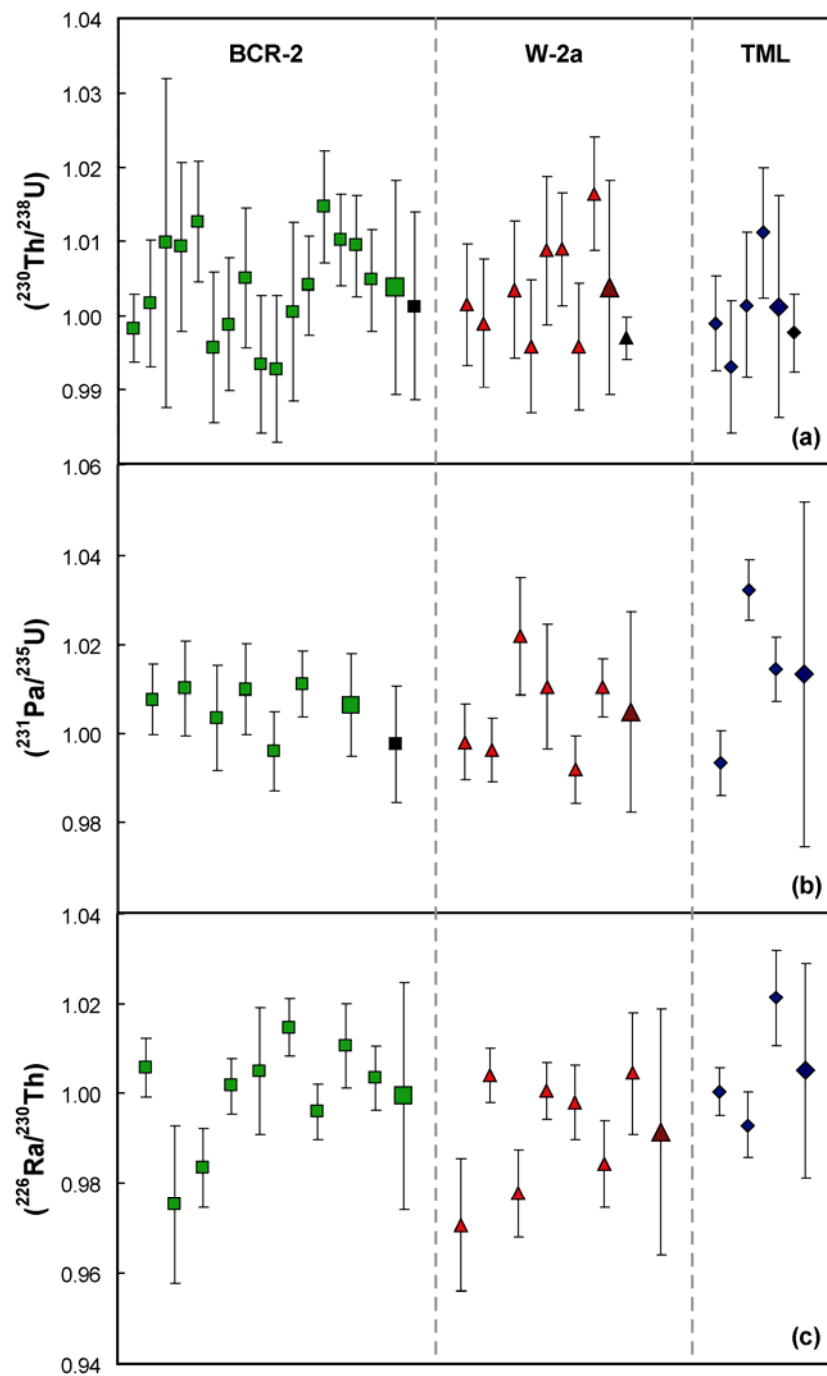


Figure 5. Reproducibility of rock standards BCR-2, W-2a and TML for (a) $(^{230}\text{Th}/^{238}\text{U})$, (b) $(^{231}\text{Pa}/^{235}\text{U})$ and (c) $(^{226}\text{Ra}/^{230}\text{Th})$. Green squares BCR-2; red triangles W-2a; blue diamonds TML. Error bars represent propagated 2σ standard errors except for the larger symbols that represent the average with 2σ standard deviations. Black squares represent literature values with 2 standard deviation; in (a) the value from Sims et al. (2008); in (b) by Prytulak et al. (2008).

4. Discussion

4.1 Uranium

The accuracy and precision of $^{234}\text{U}/^{238}\text{U}$ measurements are mainly influenced by the stability of the relative SEM-Faraday gain determined with the bracketing standards. The average measured uranium isotope ratio for IRMM-184 (n=90) differs by 0.7‰ from the certified value and is well within the 2 SD confidence interval of 0.3%, confirming the accuracy of our $^{234}\text{U}/^{238}\text{U}$ measurement technique. In Table 2, the listed long-term average uranium activity ratios for BCR-2 (n = 14), W2a (n = 10) and TML (n= 4) are within 2‰ of secular equilibrium, which is within the 2 SE of individual analyses and demonstrates that our sample preparation and chemical separation procedures does not significantly increase the error on $^{234}\text{U}/^{238}\text{U}$ measurement. The long-term 2 SD sample reproducibility for the ($^{234}\text{U}/^{238}\text{U}$) ratios determined on multiple digestions of the rock standards is better than 6‰.

4.2 Thorium

High abundance sensitivity and adequate correction for the ^{232}Th tail onto the ^{230}Th signal are essential for Th isotope analyses of silicate samples. Furthermore, the low count rates on the ^{230}Th beam (< 1500 cps) limit precision and reproducibility of $^{230}\text{Th}/^{232}\text{Th}$ analyses.

The average of our replicate $^{230}\text{Th}/^{232}\text{Th}$ analyses of the synthetic IRMM-35 standard ($^{230}\text{Th}/^{232}\text{Th} = 11.347 \pm 0.13 \times 10^{-6}$) is within 3‰ of the consensus value (Sims et al., 2008), i.e. well within the reported inter-laboratory standard deviation of 0.8%. Our average long-term reproducibility of $^{230}\text{Th}/^{232}\text{Th}$ ratios on IRMM-35 and on rock standards BCR-2, W-2a, and TML are slightly worse compared to those reported by other groups (Sims et al., 2008 and references therein). Note that we report reproducibility on multiple sample digestions (n = 10) whereas the reported reproducibilities for $^{230}\text{Th}/^{232}\text{Th}$ data on rock standards in the literature often represent replicate analyses on fewer or even single dissolutions (Hoffmann et al., 2007; Pietruszka et al., 2002; Rubin, 2001; Sims et al., 2008). $^{230}\text{Th}/^{238}\text{U}$ activity ratios on BCR-2, W2a and TML agree to within 4‰ of secular equilibrium, which is within the propagated 2 SE of 8‰. The reproducibility of the $^{230}\text{Th}/^{232}\text{Th}$ analyses on rock standards propagates into our $^{230}\text{Th}/^{238}\text{U}$ activity ratios resulting in 2 sigma SDs for the ($^{230}\text{Th}/^{238}\text{U}$) of up to 1.6% (Table 1). Reproducibility of our multiple sample digestions

is expected to be worse compared to multiple measurements of a single dissolution because (1) the sample preparation (i.e. spiking and weighing), (2) the dissolution procedure (time and effectiveness), and (3) the chemical separation procedure (e.g. resin volume, acid molarity, organics originating from the resin) may all be slightly variable between different chemistry sessions. Our error estimate on ($^{230}\text{Th}/^{238}\text{U}$) for multiple rock standard digestions includes all these additional errors and are therefore slightly larger compared to quoted values in the literature (Sims et al., 2008 and references therein). True sample heterogeneity could in principle also affect the reproducibility and may contribute to the external error. For the rocks standards BCR-2 and W-2a, however, this effect is likely minor compared to the effect of sample preparation and the chemical separation procedure.

It was found that Th beam intensities for samples that were processed through our chemical procedure were initially less stable than for mono-elemental standards (e.g. the 2 SE variability of the ^{232}Th beam in samples was 1.6% versus 0.6% in standards). Larger uncertainties on $^{230}\text{Th}/^{232}\text{Th}$ measurements of rock standards (2 RSD of 1.1 - 2.6 %) compared to those of the synthetic IRMM-35 standard (2 RSD of 1.1 %) are thus attributed to fluctuations in beam intensity. Even though beam instabilities are cancelled out by the simultaneous measurement of all ion beams, they affect the applied tail correction. The tail correction procedure described by Hubert et al., (2006) and Ball et al., (2008) was adopted in this study and involves precise characterisation of the tail by scanning a mass range before analysis of the sample (see section 4.3.2). The recording of this tail is, however, prone to both high frequency (timescale of seconds) and low frequency (timescale of 10-60 s) beam instabilities as these influence the precision of the determination of the exponential curve as well as the shape of the exponential curve, respectively. The instabilities were likely caused by residual organics eluting from the resin, despite the use of a separate 0.2 mL column packed with pre-filter resin to remove the organics from the TRU-spec resin. Treating the samples before the analyses with concentrated aqua regia and HNO_3 significantly reduced the problem of beam instability resulting in the 2 SE of the ^{232}Th beam to be less than 0.7% compared to 2 SE of up to 1.6% without the treatment.

Other than signal instability, the intensity of the ^{230}Th beam and therefore the counting statistics limit reproducibility. In this study, the ^{232}Th beam intensity was typically between 6 and 8 V and the ^{230}Th intensity was between 900 and 1500 cps.

Thus, a measurement of 200 s duration (40 times 5s cycles) could have a maximum of $2\sigma_N = \frac{2}{\sqrt{200 \times 1500}} \times 100 = 0.37\%$, based on counting statistics, whereas twice larger beam intensities could have a $2\sigma_N$ of 0.26%. It is unclear whether the studies that report better reproducibility (Hoffmann et al., 2007; Sims et al., 2008) measured their standards and samples at higher signal intensities on instruments with a greater dynamic range and therefore had better counting statistics.

4.3 Protactinium

The precision of the protactinium analyses is mainly limited by counting statistics due to the small amount of ^{231}Pa available (maximum count rates are 2500 cps). The Pa measurements are, however, also variably affected by the presence of ^{232}Th in the final Pa fraction, which may cause tailing onto the ^{231}Pa and ^{233}Pa masses. Tailing of the ^{232}Th beam on the 231 and 233 masses was corrected for using a linear log interpolation between half mass zeroes measured before each analysis at mass 230.5 and 231.5 for ^{231}Pa and 232.5 and 233.5 for ^{233}Pa . ^{232}Th was monitored in a Faraday cup and was found to vary between 0.2 mV and 55 mV. The maximum amount of Th in the Pa fraction represented $\sim 0.1\%$ of the total Th in the dissolved rock standard (assuming sensitivity for Th of 30V/ppm). The tail contribution was typically about 0.6% of the Pa signal but never exceeded 2%.

Our average $^{231}\text{Pa}/^{235}\text{U}$ activity ratio of BCR-2 of 1.006 ± 0.011 (2 SD) agrees to within 9‰ with the value reported by Prytulak et al. (2008); $^{231}\text{Pa}/^{235}\text{U} = 0.997 \pm 0.013$ (2 SD). The reproducibility on the Pa concentration for this rock standard, using sample sizes of 170 fg Pa, is 1.4% including the uncertainty resulting from the use of 3 distinct spike batches. In addition to BCR-2 (Prytulak et al., 2008), Table 3 and Fig. 5 show that W-2a also provides a suitable secular equilibrium reference rock standard for Pa analyses. W-2a is in U-Pa secular equilibrium with an average $^{231}\text{Pa}/^{235}\text{U}$ of 1.005 ± 0.023 2 SD ($n = 6$), measured using 3 different ^{233}Pa spike batches and typical sample sizes of 120 fg. Similarly to BCR2, W2a is widely available, but has slightly lower U-Th-Pa-Ra concentrations (Table 3) and is therefore analytically more challenging. It is a valuable reference standard for assessing accuracy and reproducibility of rocks with low U-Th-Pa-Ra concentrations. Three analyses of TML yielded an average $^{231}\text{Pa}/^{235}\text{U}$ activity ratio of 1.013 (Table 3), which is inconsistent with ^{234}U - ^{238}U - ^{230}Th secular

equilibrium (this study, Hoffmann et al., 2007; Pietruszka et al., 2002; Sims et al., 1999; Sims et al., 2008; Volpe et al., 1991). The reason for the discrepancy remains unclear as the analyses were carried out using the same spike batches and during the same analytical session as the BCR and W-2a standards.

4.4 Radium

The reproducibility of the ($^{226}\text{Ra}/^{230}\text{Th}$) measurements depends both on the reproducibility of the thorium and Ra analyses (Th and Ra concentration and $^{230}\text{Th}/^{232}\text{Th}$ ratios). The reproducibility of the Ra concentrations is about 1% for BCR-2 ($n = 9$, 2 SD), 3.2% for W2a ($n = 8$), and 1.5 % for TML ($n = 4$). $^{230}\text{Th}/^{232}\text{Th}$ and Th concentrations reproduce to within 2.4 and 1.8%, respectively (Table 3.). Together this leads to measured errors of 2.5, 2.8 and 2.4% for ($^{226}\text{Ra}/^{230}\text{Th}$) activity ratios on the BCR-2, W-2a and TML, which are somewhat inferior to those reported by other laboratories obtained by either TIMS or MC-ICPMS (e.g. 0.32% on TML by Pietruszka et al., 2002). Note again, however, that our reproducibility concerns several single measurements of separate dissolutions, whereas studies that report reproducibility better than 1% report data on multiple measurements of single dissolutions (Chabaux et al., 1994; Claude-Ivanaj et al., 1998; Pietruszka et al., 2002; Turner et al., 2000). Our results for ($^{226}\text{Ra}/^{230}\text{Th}$) ratios and Ra concentrations for TML are in excellent agreement with those reported by (Standish and Sims, 2010). The presented values represent a true measure of sample reproducibility (including instrumental performance and chemical performance) and show that ($^{226}\text{Ra}/^{230}\text{Th}$) on sample sizes of 130 fg can be reproduced at a level of 2.8%.

5. Comparison with previous methods

In our analytical method presented above all U-series elements (U-Th-Pa and Ra) are separated from a single sample dissolution and, in addition, the U and Th isotope ratios and U and Th elemental concentrations are measured on the same solutions. In contrast, several previous studies of U-series disequilibria in volcanic rocks used different sample aliquots to measure the U-Th and Ra and/or Pa concentrations (Bourdon et al., 1998; Bourdon et al., 1999b; Chabaux and Allègre, 1994; Claude-Ivanaj et al., 1998; Dosseto et al., 2003; Sims et al., 1999; Stracke et al., 2006; Turner et al., 2000) or used multiple aliquots of a single digestion to analyse isotope compositions (IC) and elemental

concentrations (ID) separately (Pietruszka et al., 2002; Volpe and Hammond, 1991). As these techniques involve the processing of several sample aliquots and measuring the IC and ID aliquots separately, they are more time consuming than the method described in this study. Additionally, the new U-Pa separation technique described here uses two ion exchange columns compared to three or four required by previously reported methods (Bourdon et al., 1999a; Prytulak et al., 2008; Regelous et al., 2004), reducing the time required for sample separations dramatically. The removal of fluorides prior to loading on the first TRU-spec column is effectively achieved in our method by addition of the exact amount of boric acid required to complex any remaining fluorides after digestion. An initial anionic exchange column conditioned in HF to avoid the problem of loss of Pa to insoluble fluorides as described by Regelous et al., (2004) is therefore not required. To efficiently separate Th from the U and Pa on the second column we use a cation column (AG50-X8), rather than using a second and third TRU-spec column on which the separation between Pa and Th is found to be less effective (Regelous et al., 2004). This second column in the Pa separation scheme (see Fig. 1) is loaded with a dilute HCL-HF solution to circumvent loss of Pa to the beaker walls in between the first and second column passes. Similar Pa yields for our new method compared to the more time consuming method presented by Regelous et al., (2004) confirms similar performance of the two techniques.

Most importantly, however, all four elements are determined on a single sample aliquot. This is essential because sample heterogeneity can contribute significantly to the error of parent-daughter ratios measured on separate sample splits. Especially the determination of Ra or Pa concentration on aliquots different from those used to measure the Th and U concentrations and Th isotope compositions (e.g. Bourdon et al., 1998; Chabaux and Allègre, 1994; Claude-Ivanaj et al., 1998; Dosseto et al., 2003; Stracke et al., 2006; Turner et al., 2000) potentially results in erroneous ($^{231}\text{Pa}/^{235}\text{U}$) and ($^{230}\text{Th}/^{226}\text{Ra}$) data. The potential effect of sample heterogeneity on U-series data is illustrated using reported literature concentration data on TML. This rock standard is known to be heterogeneous in elemental concentrations, but with an age of 10.2 ± 0.1 Ma (Busby et al., 2008) it is expected to be in secular equilibrium (e.g. Hoffmann et al., 2007; Kokfelt et al., 2003; Pietruszka et al., 2002; Reagan et al., 2003; Sims et al., 1999; Sims et al., 2008; Volpe et al., 1991). Elemental Th and U concentrations reported for TML vary from 29.5 to 30.5 ppm and from 10.3 to 10.8 ppm, respectively, whereas the

($^{230}\text{Th}/^{238}\text{U}$) are within error of secular equilibrium (Reagan et al., 2003; Sims et al., 2008). This suggests that the variations result from true sample heterogeneity although analytical biases between different laboratories could also contribute to the variability in the reported concentrations. For clarity, we assume in the following exercise that the observed variability results purely from sample heterogeneity. The source of heterogeneity in Th and U (and Pa and Ra) in TML is likely the heterogeneous distribution of accessory phases in this evolved rock unit.

Based on U-Th-Pa-Ra secular equilibrium of TML the ranges in Pa and Ra concentrations are 3.39 to 3.56 pg/g and 3.51 and 3.68 pg/g, respectively. If the ($^{231}\text{Pa}/^{235}\text{U}$) and ($^{226}\text{Ra}/^{230}\text{Th}$) were to be determined by measuring two separate aliquots having the most extreme difference in concentrations, the activity ratios would be 5% out of secular equilibrium. It should be noted here that additional errors related to sample reproducibility could enhance the bias introduced by sample heterogeneity. Considering the reproducibilities for U, Th, Pa and Ra concentrations and the $^{230}\text{Th}/^{232}\text{Th}$ ratio derived from our multiple dissolutions of homogeneous BCR-2 (i.e. 2RSD's of 0.4%, 1%, 1.4%, 1.5% and 2% respectively; Table 3) maximum deviations from equilibrium of 6.7% for the ($^{231}\text{Pa}/^{235}\text{U}$) ratios and of 9.7% for the ($^{230}\text{Th}/^{226}\text{Ra}$) ratios for TML measured on separate aliquots would become possible. Even though such potential errors would easily be identified when analyzing rock standards such as TML, they would remain unnoticed when measuring unknowns. Hence, the determination of concentrations and isotope compositions on a single sample aliquot that avoids these analytical artefacts is important for obtaining accurate U-series disequilibria data.

6. Conclusions

We describe a new technique to separate uranium, thorium, radium and protactinium from a single sample aliquot, and mass spectrometric techniques to determine concentrations and isotope ratios by MC-ICPMS. The method is significantly less time consuming compared to previous methods as it involves fewer columns in the chemical separation procedure and because the isotope compositions and elemental concentrations are determined on the same aliquots. Separating all U-series elements from a single sample digestion is important because sample heterogeneity can contribute significantly to the error of parent-daughter ratios on separate sample splits. ($^{234}\text{U}/^{238}\text{U}$), ($^{230}\text{Th}/^{238}\text{U}$), ($^{231}\text{Pa}/^{235}\text{U}$) and ($^{226}\text{Ra}/^{230}\text{Th}$) activity ratios in volcanic rocks reproduce to 0.7%, 1.5%, 3.8% and 2.8% accuracy levels, respectively. The dataset presented here represents a true measure of reproducibility on volcanic samples as it is obtained from multiple separate dissolutions of BCR-2, W-2a and TML. The method is established using samples sizes around 1.5 μg Th, 0.5 μg U, and 200 fg Pa and Ra but is suitable for the analyses of volcanic samples with Ra and Pa amounts as small as ~ 25 fg.

Acknowledgements

We would like to thank Felix Oberli for valuable support in the SEM characterisation and for informal reviews of the manuscript. We are grateful to Ed Tipper who always kindly helped out with useful suggestions and improvements in the laboratory. The Paul Scherrer Institute (PSI), Villigen, Switzerland is thanked for producing the ^{233}Pa spike batches. Lastly, we thank the Swiss National Science Foundation for providing funding for this project.

References

- Aciego, S.M., Bourdon, B., Lupker, M. and Rickli, J., 2009. A new procedure for separating and measuring radiogenic isotopes (U, Th, Pa, Ra, Sr, Nd, Hf) in ice cores. *Chemical Geology*, 266, 203-213.
- Albarède, F. and Beard, B., 2004. Analytical Methods for Non-Traditional Isotopes. *Reviews in Mineralogy and Geochemistry* 55, 113-152.
- Allègre, C.J. and Condomines, M., 1976. Fine chronology of volcanic processes using ^{238}U - ^{230}Th systematics. *Earth and Planetary Science Letters*, 28, 395-406.
- Asmerom, Y., DuFrane, S.A., Mukasa, S.B., Cheng, H. and Edwards, R.L., 2005. Time scale of magma differentiation in arcs from protactinium-radium isotopic data. *Geology*, 33, 633-636.
- Ball, L., Sims, K.W.W. and Schwieters, J., 2008. Measurement of $^{234}\text{U}/^{238}\text{U}$ and $^{230}\text{Th}/^{232}\text{Th}$ in volcanic rocks using the Neptune MC-ICP-MS. *Journal of Analytical Atomic Spectrometry*, 23, 173-180.
- Bourdon, B., Joron, J.-L. and Allegre, C.J., 1999a. A method for ^{231}Pa analysis by thermal ionization mass spectrometry in silicate rocks. *Chemical Geology*, 157, 147-151.
- Bourdon, B., Joron, J.-L., Claude-Ivanaj, C. and Allegre, C.J., 1998. U-Th-Pa-Ra systematics for the Grande Comore volcanics: melting processes in an upwelling plume. *Earth and Planetary Science Letters*, 164, 119-133.
- Bourdon, B., Turner, S., All, egrave and gre, C., 1999b. Melting Dynamics Beneath the Tonga-Kermadec Island Arc Inferred from ^{231}Pa - ^{235}U Systematics. *Science*, 286, 2491-2493.
- Bourdon, B., Turner, S., Henderson, G.M. and Lundstrom, C.C., 2003. Introduction to U-series geochemistry. In: *Uranium-Series Geochemistry, Reviews in Mineralogy and Geochemistry* 52. B. Bourdon, G.M. Henderson, C.C. Lundstrom and S.P. Turner (Editors), pp. 1-21.
- Bourdon, B., Turner, S.P. and Ribe, N.M., 2005. Partial melting and upwelling rates beneath the Azores from a U-series isotope perspective. *Earth and Planetary Science Letters*, 239, 42-56.
- Bourdon, B., Zindler, A., Elliott, T. and Langmuir, C.H., 1996. Constraints on mantle melting at mid-ocean ridges from global ^{238}U - ^{230}Th disequilibrium data. *Nature*, 384, 231-235.
- Bourdon, B., Zindler, A. and Worner, G., 1994. Evolution of the Laacher See magma chamber: Evidence from SIMS and TIMS measurements of U-Th disequilibria in minerals and glasses. *Earth and Planetary Science Letters*, 126, 75-90.
- Burnett, W.C. and Yeh, C.C., 1995. Separation of Protactinium from geochemical materials via extraction chromatography. *Radioactivity & Radiochemistry*, 6, 22-32.
- Busby, C.J. et al., 2008. The ancestral Cascades arc: Cenozoic evolution of the central Sierra Nevada (California) and the birth of the new plate boundary. In: *Ophidites, arcs and*

- batholiths J.E. Wright and J.W. Shervais (Editors). Geological Society of America Special Paper, 438, pp. 1-48.
- Caro, G., Bourdon, B., Birck, J.L. and Moorbath, S., 2006. High-precision $^{142}\text{Nd}/^{144}\text{Nd}$ measurements in terrestrial rocks: Constraints on the early differentiation of the Earth's mantle. *Geochimica Et Cosmochimica Acta*, 70, 164-191.
- Chabaux, F. and Allègre, C.J., 1994. ^{238}U - ^{230}Th - ^{226}Ra disequilibria in volcanics: A new insight into melting conditions. *Earth and Planetary Science Letters*, 126, 61-74.
- Chabaux, F., Othman, D.B. and Birck, J.L., 1994. A new Ra-Ba chromatographic separation and its application to Ra mass-spectrometric measurement in volcanic rocks. *Chemical Geology*, 114, 191-197.
- Cheng, H. et al., 2000. The half-lives of uranium-234 and thorium-230. *Chemical Geology*, 169, 17-33.
- Claude-Ivanaj, C., Bourdon, B. and Allègre, C.J., 1998. Ra-Th-Sr isotope systematics in Grande Comore Island: a case study of plume-lithosphere interaction. *Earth and Planetary Science Letters*, 164, 99-117.
- Cohen, A. and O'Nions, S.R.K., 1993. Melting rates beneath Hawaii: Evidence from uranium series isotopes in recent lavas. *Earth and Planetary Science Letters*, 120, 169-175.
- Condomines, M., Gauthier, P.J. and Sigmarsson, G., 2003. Timescales of magma chamber processes and dating of young volcanic rocks. In: *Uranium-Series Geochemistry, Reviews in Mineralogy and Geochemistry 52*. B. Bourdon, G.M. Henderson, C.C. Lundstrom and S.P. Turner (Editors), pp. 125-174.
- Condomines, M. and Sigmarsson, O., 2000. ^{238}U - ^{230}Th disequilibria and mantle melting processes: a discussion. *Chemical Geology*, 162, 95-104.
- Dosseto, A., Bourdon, B., Joron, J.-L. and Dupré, B., 2003. U-Th-Pa-Ra study of the Kamchatka arc: new constraints on the genesis of arc lavas. *Geochimica et Cosmochimica Acta*, 67, 2857-2877.
- Elliott, T., 1997. Fractionation of U and Th during mantle melting: a reprise. *Chemical Geology*, 139, 165-183.
- Goldstein, S. and Stirling, C., 2003. Techniques for measuring uranium-series nuclides: 1992-2002. In: *Uranium-Series Geochemistry, Reviews in Mineralogy and Geochemistry 52*. B. Bourdon, G.M. Henderson, C.C. Lundstrom and S.P. Turner (Editors), pp. 23-57.
- Goldstein, S.J., Murrell, M.T. and Janecky, D.R., 1989. Th and U isotopic systematics of basalts from the Juan de Fuca and Gorda Ridges by mass spectrometry. *Earth and Planetary Science Letters*, 96, 134-146.
- Hoffmann, D.L. et al., 2007. Procedures for accurate U and Th isotope measurements by high precision MC-ICPMS. *International Journal of Mass Spectrometry*, 264, 97-109.

- Hoffmann, D.L. et al., 2005. Characterisation of secondary electron multiplier nonlinearity using MC-ICPMS. *International Journal of Mass Spectrometry*, 244, 97-108.
- Holden, N.E., 1990. Total half-lives for selected nuclides. *Pure Appl. Chem.*, 62, 941-958.
- Horwitz, E.P., Chiarizia, R., Dietz, M.L., Diamond, H. and Nelson, D.M., 1993. Separation and preconcentration of actinides from acidic media by extraction chromatography. *Analytica Chimica Acta*, 281, 361-372.
- Hubert, A., Bourdon, B., Pili, E. and Meynadier, L., 2006. Transport of radionuclides in an unconfined chalk aquifer inferred from U-series disequilibria. *Geochimica et Cosmochimica Acta*, 70, 5437-5454.
- Jaffey, A.H., Flynn, K.F., Glendenin, L.E., Bentley, W.C. and Essling, A.M., 1971. Precision Measurement of Half-Lives and Specific Activities of U-235 and U-238. *Physical Review C*, 4, 1889-1906.
- Kokfelt, T.F., Hoernle, K. and Hauff, F., 2003. Upwelling and melting of the Iceland plume from radial variation of ^{238}U - ^{230}Th disequilibria in postglacial volcanic rocks. *Earth and Planetary Science Letters*, 214, 167-186.
- Lampton, M. and Bixler, J., 1985. Counting efficiency of systems having both paralyzable and nonparalyzable elements. *Review of Scientific Instruments*, 56, 164-165.
- Lowenstern, J.B. et al., 2000. U-Th dating of single zircons from young granitoid xenoliths: new tools for understanding volcanic processes. *Earth and Planetary Science Letters*, 183, 291-302.
- Lundstrom, C.C., Gill, J., Williams, Q. and Hanan, B.B., 1998. Investigating solid mantle upwelling beneath mid-ocean ridges using U-series disequilibria. II. A local study at 33 degrees Mid-Atlantic Ridge. *Earth and Planetary Science Letters*, 157, 167-181.
- Lundstrom, C.C., Hoernle, K. and Gill, J., 2003. U-series disequilibria in volcanic rocks from the Canary Islands: Plume versus lithospheric melting. *Geochimica Et Cosmochimica Acta*, 67, 4153-4177.
- McKenzie, D., 1985. ^{230}Th - ^{238}U disequilibrium and the melting processes beneath ridge axes. *Earth and Planetary Science Letters*, 72, 149-157.
- Metz, J.M. and Mahood, G.A., 1985. Precursors to the Bishop Tuff Eruption - Glass Mountain, Long Valley, California. *Journal of Geophysical Research-Solid Earth and Planets*, 90, 1121-1126.
- Metz, J.M. and Mahood, G.A., 1991. Development of the Long Valley, California, Magma Chamber Recorded in Precaldera Rhyolite Lavas of Glass Mountain. *Contributions to Mineralogy and Petrology*, 106, 379-397.

- Pietruszka, A.J., Carlson, R.W. and Hauri, E.H., 2002. Precise and accurate measurement of ^{226}Ra - ^{230}Th - ^{238}U disequilibria in volcanic rocks using plasma ionization multicollector mass spectrometry. *Chemical Geology*, 188, 171-191.
- Pin, C. and Zalduegui, J.F.S., 1997. Sequential separation of light rare-earth elements, thorium and uranium by miniaturized extraction chromatography: Application to isotopic analyses of silicate rocks. *Analytica Chimica Acta*, 339, 79-89.
- Prytulak, J. and Elliott, T., 2009. Determining melt productivity of mantle sources from ^{238}U - ^{230}Th - and ^{235}U - ^{231}Pa disequilibria; an example from Pico Island, Azores. *Geochimica Et Cosmochimica Acta*, 73, 2103-2122.
- Prytulak, J., Elliott, T., Hoffmann, D.L. and Coath, C.D., 2008. Assessment of USGS BCR-2 as a reference material for silicate rock u-pa disequilibrium measurements. *Geostandards and Geoanalytical Research*, 32, 55-63.
- Reagan, M.K. et al., 2003. Time-scales of differentiation from mafic parents to rhyolite in North American continental arcs. *Journal of Petrology*, 44, 1703-1726.
- Regelous, M., Turner, S.P., Elliott, T.R., Rostami, K. and Hawkesworth, C.J., 2004. Measurement of femtogram quantities of protactinium in silicate rock samples by multicollector inductively coupled plasma mass spectrometry. *Analytical Chemistry*, 76, 3584-3589.
- Reid, M.R., 2003. Timescales of magma transfer and storage in the crust. In: Rudnick, R.L. (ed.) *The Crust*, Vol. 3, Treatise on Geochemistry H. Holland and K. Turekian (Editors). Pergamon, Oxford, pp. 167-193.
- Richter, S. et al., 2009. A new series of uranium isotope reference materials for investigating the linearity of secondary electron multipliers in isotope mass spectrometry. *International Journal of Mass Spectrometry*, 281, 115-125.
- Richter, S. et al., 2005. Re-certification of a series of uranium isotope reference materials: IRMM-183, IRMM-184, IRMM-185, IRMM-186 and IRMM-187. *International Journal of Mass Spectrometry*, 247, 37-39.
- Richter, S., Goldberg, S.A., Mason, P.B., Traina, A.J. and Schwieters, J.B., 2001. Linearity tests for secondary electron multipliers used in isotope ratio mass spectrometry. *International Journal of Mass Spectrometry*, 206, 105-127.
- Rubin, K.H., 2001. Analysis of $^{232}\text{Th}/^{230}\text{Th}$ in volcanic rocks: a comparison of thermal ionization mass spectrometry and other methodologies. *Chemical Geology*, 175, 723-750.
- Russell, W.A., Papanastassiou, D.A. and Tombrello, T.A., 1978. Ca isotope fractionation on the Earth and other solar system materials. *Geochimica et Cosmochimica Acta*, 42, 1075-1090.
- Schmitt, A.K., 2006. Laacher See revisited: High-spatial-resolution zircon dating indicates rapid formation of a zoned magma chamber. *Geology*, 34, 597-600.

- Sims, K.W.W. et al., 1999. Porosity of the melting zone and variations in the solid mantle upwelling rate beneath Hawaii: inferences from ^{238}U - ^{230}Th - ^{226}Ra and ^{235}U - ^{231}Pa disequilibria. *Geochimica et Cosmochimica Acta*, 63, 4119-4138.
- Sims, K.W.W. et al., 2008. An inter-laboratory assessment of the thorium isotopic composition of synthetic and rock reference materials. *Geostandards and Geoanalytical Research*, 32, 65-91.
- Snyder, D.C., Widom, E., Pietruszka, A.J., Carlson, R.W. and Schmincke, H.-U., 2007. Time scales of formation of zoned magma chambers: U-series disequilibria in the Fogo A and 1563 A.D. trachyte deposits, Sao Miguel, Azores. *Chemical Geology*, 239, 138-155.
- Spiegelman, M. and Elliott, T., 1993. Consequences of melt transport for uranium series disequilibrium in young lavas. *Earth and Planetary Science Letters*, 118, 1-20.
- Standish, J.J. and Sims, K.W.W., 2010. Young off-axis volcanism along the ultraslow-spreading Southwest Indian Ridge. *Nature Geosci*, 3, 286-292.
- Stracke, A., Bourdon, B. and McKenzie, D., 2006. Melt extraction in the Earth's mantle: Constraints from U-Th-Pa-Ra studies in oceanic basalts. *Earth and Planetary Science Letters*, 244, 97-112.
- Stracke, A., Salters, V.J.M. and Sims, K.W.W., 1999. Assessing the presence of garnet-pyroxenite in the mantle sources of basalts through combined hafnium-neodymium-thorium isotope systematics. *Geochem. Geophys. Geosyst.*, 1, doi. 10.1029/1999GC000013.
- Stracke, A., Zindler, A., Salters, V.J.M., McKenzie, D. and Grönvold, K., 2003. The dynamics of melting beneath Theistareykir, northern Iceland. *Geochem. Geophys. Geosyst.*, 4, 8513. doi: 10.1029/2002GC000347.
- Touboul, M., Bourdon, B., Villemant, B., Boudon, G. and Joron, J.L., 2007. ^{238}U - ^{230}Th - ^{226}Ra disequilibria in andesitic lavas of the last magmatic eruption of Guadeloupe Soufriere, french Antilles: Processes and timescales of magma differentiation. *Chemical Geology*, 246, 181-206.
- Turner, S., Bourdon, B., Hawkesworth, C. and Evans, P., 2000. ^{226}Ra - ^{230}Th evidence for multiple dehydration events, rapid melt ascent and the time scales of differentiation beneath the Tonga-Kermadec island arc. *Earth and Planetary Science Letters*, 179, 581-593.
- Turner, S., Hawkesworth, C., Rogers, N. and King, P., 1997. U-Th isotope disequilibria and ocean island basalt generation in the Azores. *Chemical Geology*, 139, 145-164.
- Usman, K. and MacMahon, T.D., 2000. Determination of the half-life of ^{233}Pa . *Applied Radiation and Isotopes*, 52, 585-589.
- Volpe, A.M. and Hammond, P.E., 1991. ^{238}U - ^{230}Th - ^{226}Ra disequilibria in young Mount St. Helens rocks: time constraint for magma formation and crystallization. *Earth and Planetary Science Letters*, 107, 475-486.

- Volpe, A.M., Olivares, J.A. and Murrell, M.T., 1991. Determination of radium isotope ratios and abundances in geological samples by thermal ionization mass spectrometry. *Anal. Chem.*, 63, 913-916.
- Wasserburg, G.J., Jacobsen, S.B., DePaolo, D.J., McCulloch, M.T. and Wen, T., 1981. Precise determination of ratios, Sm and Nd isotopic abundances in standard solutions. *Geochimica et Cosmochimica Acta*, 45, 2311-2323.
- Yokoyama, T., Kuritani, T., Kobayashi, K. and Nakamura, E., 2006. Geochemical evolution of a shallow magma plumbing system during the last 500 years, Miyakejima volcano, Japan: Constraints from U-238-Th-230-Ra-226 systematics. *Geochimica Et Cosmochimica Acta*, 70, 2885-2901.

Appendix. Determination of $^{229}\text{Th}/^{232}\text{Th}$ of ETH-IRMM standard solution by Triton TIMS

The isotopic composition of the standard used for bracketing Th analyses was determined by thermal ionization mass spectrometry (TIMS) on a Thermo Triton at ETH Zürich. The Triton is equipped with nine Faraday cups and a single SEM with a RPQ energy filter to improve abundance sensitivity.

The IRMM-36 standard and a ^{229}Th spike were mixed with the aim of yielding a $^{229}\text{Th}/^{230}\text{Th}$ ratio of ~ 10 , similar to the expected ratio in our spiked samples. The ratio was kept deliberately low to avoid memory effects on the ion counter (Hoffmann et al., 2005) of the MC-ICPMS where the ^{229}Th and ^{230}Th are measured consecutively by peak jumping.

For the TIMS measurements the IRMM-36 and ^{229}Th mixture was dried down, dissolved in 7.5 N HNO_3 and loaded (1 μg per filament) on outgassed Re-filaments in double filament configuration. Faraday amplifier gain calibration and determination of SEM dark noise and baselines were performed before the start of an analysis. Filament position and lens voltages were tuned to maximum signal intensity. The relative Faraday-ion counter gain was determined on a ^{232}Th beam of ~ 5 mV by switching between the Faraday and SEM. The filament current was increased slowly to obtain a stable signal of 200 to 500 mV ^{232}Th . Typical currents on the ionisation filament were 5.8 A and 3.2 A on the evaporation filament, which resulted in pyrometer indicated temperatures of $\sim 1700^\circ\text{C}$. The $^{229}\text{Th}/^{232}\text{Th}$ and $^{230}\text{Th}/^{232}\text{Th}$ ratios were measured with a multi-static measurement routine. Instrumental mass fractionation is negligible for the mean isotope ratios when the sample is run to exhaustion. Typically, a run lasted for 8 blocks of 20 cycles of 8s integrations each. The average $^{230}\text{Th}/^{232}\text{Th}$ of our Triton analyses on IRMM-36 doped with ^{229}Th is $(3.053 \pm 0.0245) \times 10^{-6}$ ($n = 12$) in excellent agreement with the IRMM-36 consensus value of $(3.047 \pm 0.049) \times 10^{-6}$ (Sims et al., 2008). The $^{229}\text{Th}/^{232}\text{Th}$ is determined to be $(3.798 \pm 0.046) \times 10^{-5}$ ($n = 12$) and the $^{229}\text{Th}/^{230}\text{Th}$ ratio is 12.442 ± 0.132 ($n=12$).

Chapter 4

Disentangling processes recorded by U-Th-Pa-Ra disequilibria in post- glacial tholeiites from Iceland

To be submitted to *Geochimica and Cosmochimica Acta* as: Koornneef, J.M., Stracke A, Bourdon, B., Grönvold, K. Disentangling processes recorded by U-Th-Pa-Ra disequilibria in post-glacial tholeiites from Iceland.

Abstract

We investigate the relative importance of mantle upwelling velocity and source heterogeneity to melting rates recorded by ^{230}Th - ^{238}U , ^{231}Pa - ^{235}U and ^{226}Ra - ^{230}Th disequilibria in post-glacial tholeiites from Iceland's main rift areas. The measured ($^{230}\text{Th}/^{238}\text{U}$) range from 1.085 to 1.247, the ($^{231}\text{Pa}/^{235}\text{U}$) from 1.333 to 1.925, and the ($^{226}\text{Ra}/^{230}\text{Th}$) from 0.801 to 1.218. A general positive correlation between ^{230}Th and ^{231}Pa excesses and distance from the inferred plume centre is consistent with a model of decreasing mantle upwelling velocity with increasing distance from the plume axis. Significant local variability could partly result from decay during magma storage or slow melt transport, and/or from variations in mantle upwelling velocity in the melting region at a local scale. However, broad correlations between ($^{230}\text{Th}/^{238}\text{U}$) and ($^{231}\text{Pa}/^{235}\text{U}$) and highly incompatible trace element ratios for samples from the Western Volcanic Zone suggest an important effect of source heterogeneity. Low ^{230}Th and ^{231}Pa excesses in the most enriched WV samples (high U/Th, Nb/U and Nb/La) indicate that the enriched component is characterised by high melt productivity. Low ^{230}Th - ^{238}U disequilibria in the most enriched samples furthermore demonstrate that the enriched component must have a low bulk $D_{\text{U}}/D_{\text{Th}}$. The combined U-series and trace element data for Theistareykir, WV and RP data are reproduced by mixing between melts from a garnet peridotite with low melt productivity and a pyroxenite with high melt productivity. Our results also confirm the presence of larger abundances of enriched material in the source beneath the South Western Rift of Iceland, which has been suggested based on relations between highly incompatible elements and Pb isotope composition in Icelandic basalts. The importance of lithological heterogeneity to the melting behaviour in MOR and OIB settings is therefore demonstrated.

1. Introduction

Uranium series disequilibria in young basalts from ocean islands (OIB) have been used to investigate the dynamics of partial melting and melt extraction processes in the upper mantle. Critical parameters for studying these processes are the mantle upwelling velocity and the melt extraction rate, but also intrinsic properties to the source such as porosity, modal mineralogy and melt productivity (Bourdon et al., 1998; Bourdon et al., 2006; Bourdon et al., 2005; Cohen and O'Nions, 1993; Condomines et al., 1981; Kokfelt et al., 2003; Lundstrom et al., 2003; Peate et al., 2001; Pietruszka et al., 2009; Prytulak and Elliott, 2009; Sims et al., 1999; Spiegelman and Elliott, 1993; Stracke et al., 2006; Stracke et al., 1999; Stracke et al., 2003a; Turner et al., 1997).

Melting models explain the observed U-series disequilibria in MORB and OIB by the different residence times between the parent and daughter nuclides in the source. Models range from 'dynamic melting' assuming rapid melt extraction with no further equilibration between the melt and its source (McKenzie, 1985) to 'equilibrium porous-flow' with continuous equilibration of melt and solid (Spiegelman and Elliott, 1993). More complex models call upon dual mechanisms for melt extraction (porous flow and channels) and therefore involve different degrees of equilibrium at different depths in the mantle (Jull et al., 2002; Lundstrom, 2001; Lundstrom et al., 2000). Note that the models generally assume that the source has a homogeneous mineralogical composition and is in secular equilibrium at the onset of melting. These models have been primarily used to constrain the mantle upwelling velocity (which should be directly related to the melting rate) and the residual porosity. However, the presence of mafic lithologies (for example recycled oceanic crust) in OIB mantle sources may drastically change the melting behaviour as these have different mineralogy, trace element partitioning characteristics and melt productivity (Bourdon et al., 1996; Lundstrom et al., 1995; Pertermann and Hirschmann, 2003; Pertermann et al., 2004; Prytulak and Elliott, 2009; Stracke et al., 2006; Stracke et al., 1999).

Unfortunately, the quantitative effect of source heterogeneity on the U-series disequilibria remains difficult to predict a priori as the mineralogy, melting, melt extraction and solid-melt trace element partitioning characteristics of the mantle sources are highly variable (see for example Bourdon and Sims, 2003a). The melt productivity of mafic lithologies is, however, consistently larger compared to those of peridotites (Asimow et al., 1997; Asimow et al., 2001; Hirschmann et al., 1999; Kogiso et al.,

2004; Pertermann and Hirschmann, 2003) and therefore the presence of eclogitic or pyroxenitic components in the source could affect the U-series signatures in the erupted lavas. Recently, Prytulak and Elliott (2009) pointed out that the differences in melt productivity between peridotitic and pyroxenitic mantle components could have a much larger effect on the U-series nuclides in OIB than the mantle upwelling velocity alone. Russo et al. (2009) showed that melting of fertile pyroxenite veins may explain the relationships between trace elements and ^{230}Th and ^{226}Ra excesses in MORB basalts from the South-East Indian Ridge.

In Iceland, the North Atlantic Mid Ocean Ridge (MOR) is impinged by a thermal anomaly due to buoyant upwelling mantle (Bijwaard and Spakman, 1999; Montelli et al., 2004; Schilling, 1973; Shen et al., 1998; Wolfe, 1997). Interaction of the passive Mid-Atlantic ridge and actively upwelling hot Iceland plume leads to increased melt production along Iceland's main rift zones compared to the adjacent Mid Atlantic Ridge. Based on correlations between long lived isotope ratios and trace elements it was shown that melting and sampling of at least two mantle components is required to explain the composition of Icelandic lavas (Elliott et al., 1991; Kokfelt et al., 2006; MacLennan, 2008; MacLennan et al., 2003a; Stracke and Bourdon, 2009; Stracke et al., 2003b; Wood, 1981). A radial increase in ($^{230}\text{Th}/^{238}\text{U}$) activity ratios with increasing distance from the plume centre was related to decreasing mantle potential temperature and upwelling velocity by Kokfelt et al. (2003). The larger variability in melting indicators such as La/Yb or Lu/Hf on a local scale compared to the variability across the Icelandic thermal anomaly led Koornneef et al., (2011) to conclude that melts are extracted from a significant range of depths.

The trace element and isotopic heterogeneity observed in Icelandic lavas shows that the Icelandic mantle source is compositionally heterogeneous and the presence of several different mantle components have been suggested (e.g. Hanan and Schilling, 1997; Hémond et al., 1993; Kokfelt et al., 2006; MacLennan, 2008; MacLennan et al., 2003b; Schilling, 1973; Slater et al., 2001; Stracke et al., 2003b; Zindler et al., 1979). Recently, however, Peate et al. (2010) suggested based on principal component analysis that > 99.5 % of the variance in Pb isotope data in Postglacial Icelandic basalts can be accounted for by mixing between only two end members. Moreover, Koornneef et al., (2011), demonstrated that concurrent melting and incomplete mixing of melts from only two sources matches the combined trace element and Hf-Nd-Sr-Pb data in the

Icelandic lavas suggesting that two source-components suffice to explain the observed compositional variability.

The enriched Icelandic source component has frequently been inferred to represent recycled oceanic crust forming small scale heterogeneities in the sub Icelandic mantle (Kokfelt et al., 2006; Stracke et al., 2003b). Variable enrichments in Nb/La and Nb/U ratios combined with higher $^{206}\text{Pb}/^{204}\text{Pb}$ in samples from the Western Rift Zone and the Reykjanes Peninsula suggests that the abundance of the enriched component could be variable beneath the main rift areas (Koornneef et al., 2011, Hanan et al., 2000). The effect of melting a heterogeneous source beneath Iceland on the ^{230}Th - ^{238}U , ^{231}Pa - ^{235}U and ^{226}Ra - ^{230}Th disequilibria has thus far not extensively been explored.

Here we present new ^{226}Ra - ^{230}Th - ^{238}U and ^{231}Pa - ^{235}U disequilibria data on 25 post glacial tholeiites from Iceland's main rift areas. The samples are well characterised for major- and trace elements and Hf and Nd isotopes (Koornneef et al., 2011). The combination of U-series with high quality trace element data is used to disentangle the relative influence of key parameters and to investigate the potential effect of source variability on U-series systematics. A dynamic melting model including two source components is used to explore the relationships between U-series disequilibria and trace element ratios, Hf and Nd isotopes in the investigated samples.

2. Sample preparation and analytical techniques

U, Th, Pa and Ra concentrations and isotope ratios were determined on 25 post glacial tholeiites from Iceland's main rift areas (Fig.1). These samples were previously analysed for major and trace element and Hf and Nd isotope composition (Koornneef et al., 2011). In addition to the samples from the Reykjanes Peninsula (RP, n= 10), the Western Volcanic Field (WV, n = 7), and the Northern Volcanic Field (NV, n =8) we re-analysed 4 samples from Theistareykir a small area in the Northern Volcanic Field that were previously analysed by Stracke et al., (2003a, 2006). Generally the investigated samples are younger than 3000 years, with the exception of WV21 (~5300 years) and WV25 (~3400 years) and the Theistareykir samples, which are between 3000 and 12 000 years old (Table 1).

A detailed description of the chemical separation procedures and measurement routines is given in (Koornneef et al., 2010; Koornneef et al., 2011). Approximately 1 g of sample powders is spiked with ^{236}U , ^{229}Th , ^{233}Pa and ^{228}Ra tracers and dissolved in a

mixture of HF and HNO₃. After evaporation samples were re-dissolved in HCL and boric acid was used to remove fluorides. After conversion to HNO₃, samples were loaded on the first column in 2 N HNO₃. All elements are separated from this same sample aliquot using a 5 mL TRU-spec column, followed by a 1 mL AG50-X8 and a 0.2 mL AG1-X4 column. The first column yields fractions of Ra + matrix, U + Pa and Th; the second column separates U from Pa; the third column purifies the Th fraction from the first column. The Ra + matrix fraction is further purified using a 20 mL, a 3 mL AG50-x8 column and a 1 mL Sr-Spec column (Chabaux et al., 1994; Claude-Ivanaj et al., 1998). All U, Th, Pa and Ra concentrations and isotope ratios were determined by MC-ICPMS at ETH Zürich. Sample reproducibility was evaluated by measuring multiple dissolutions of USGS rock reference materials BCR-2 and W-2a and on rock standard TML. In Figure 3 the error bars shown for the WV samples represent the 2 σ standard deviations obtained from the multiple analyses of different rock standards digestions. For samples that were analysed multiple times (Table 1) the average is plotted in the figures.

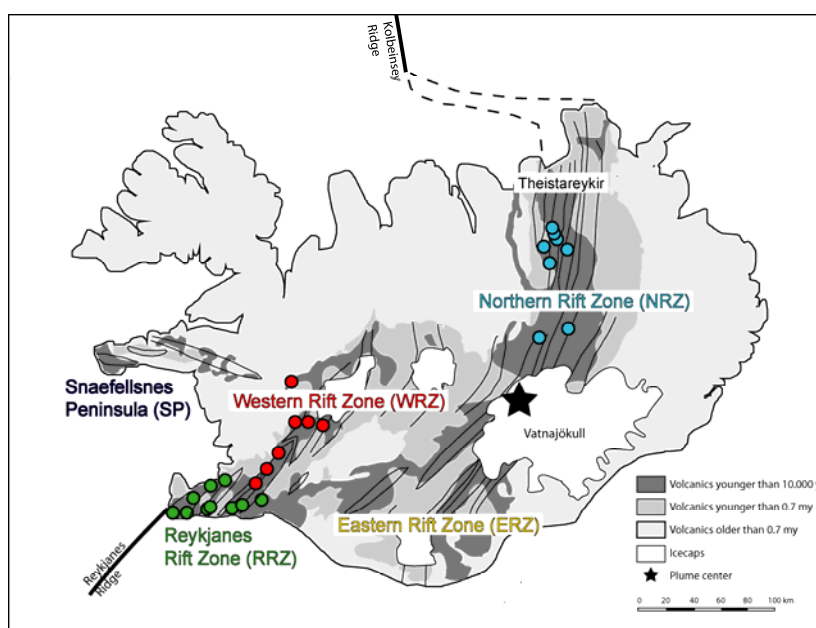


Figure 1. Simplified geological map of Iceland showing the sampling localities of all 25 lavas in coloured circles (Modified after geological map published on www.tephrabase.org). Green: Reykjanes Peninsula (RP); red: Western Volcanics (WV); light blue: Northern Volcanics (NV); All samples are younger than 10 000 yr.

3. Results

U-Th-Pa and Ra concentration and ^{230}Th - ^{238}U , ^{231}Pa - ^{235}U and ^{226}Ra - ^{230}Th disequilibria data are presented in Table 1 and Figures 2 to 4. Data corrected for decay subsequent to eruption of the lavas is also shown (Table 1 and Fig 3), which is mainly important for the Ra-disequilibria. Note that the accuracy of age corrected data is limited by the precision of age estimates for lava flows (Peate et al., 2009; Sinton, 2005).

3.1 ^{238}U - ^{234}U - ^{230}Th disequilibria

Fractionation between ^{234}U and ^{238}U only occurs during low temperature processes and therefore the ($^{234}\text{U}/^{238}\text{U}$) activity ratios serve as an indicator of secondary alteration. All RP, WV and NV samples have ($^{234}\text{U}/^{238}\text{U}$) activity ratios within error of secular equilibrium demonstrating they were not affected by post-eruptive alteration.

All measured samples have ^{230}Th excesses ($(^{230}\text{Th}/^{238}\text{U}) > 1$) in overall agreement with previous studies (Kokfelt et al., 2003; Peate et al., 2001; Stracke et al., 2003a). Western Volcanic (WV) samples show the largest variability with ($^{230}\text{Th}/^{238}\text{U}$) ranging from 1.085 to 1.247, covering the full range of measured values. Northern Volcanic field samples (i.e. NV, excluding Theistareykir) have ($^{230}\text{Th}/^{238}\text{U}$) ratios ranging between 1.130 and 1.174, while Reykjanes Peninsula (RP) samples have ($^{230}\text{Th}/^{238}\text{U}$) between 1.118 and 1.213. In an equiline diagram (Fig. 2) NV and RP samples show a positive correlation semi parallel to the equiline, but the RP samples generally have higher ($^{230}\text{Th}/^{232}\text{Th}$) and ($^{238}\text{U}/^{232}\text{Th}$) ratios. WV samples form a trend perpendicular to that of the NV and RP samples.

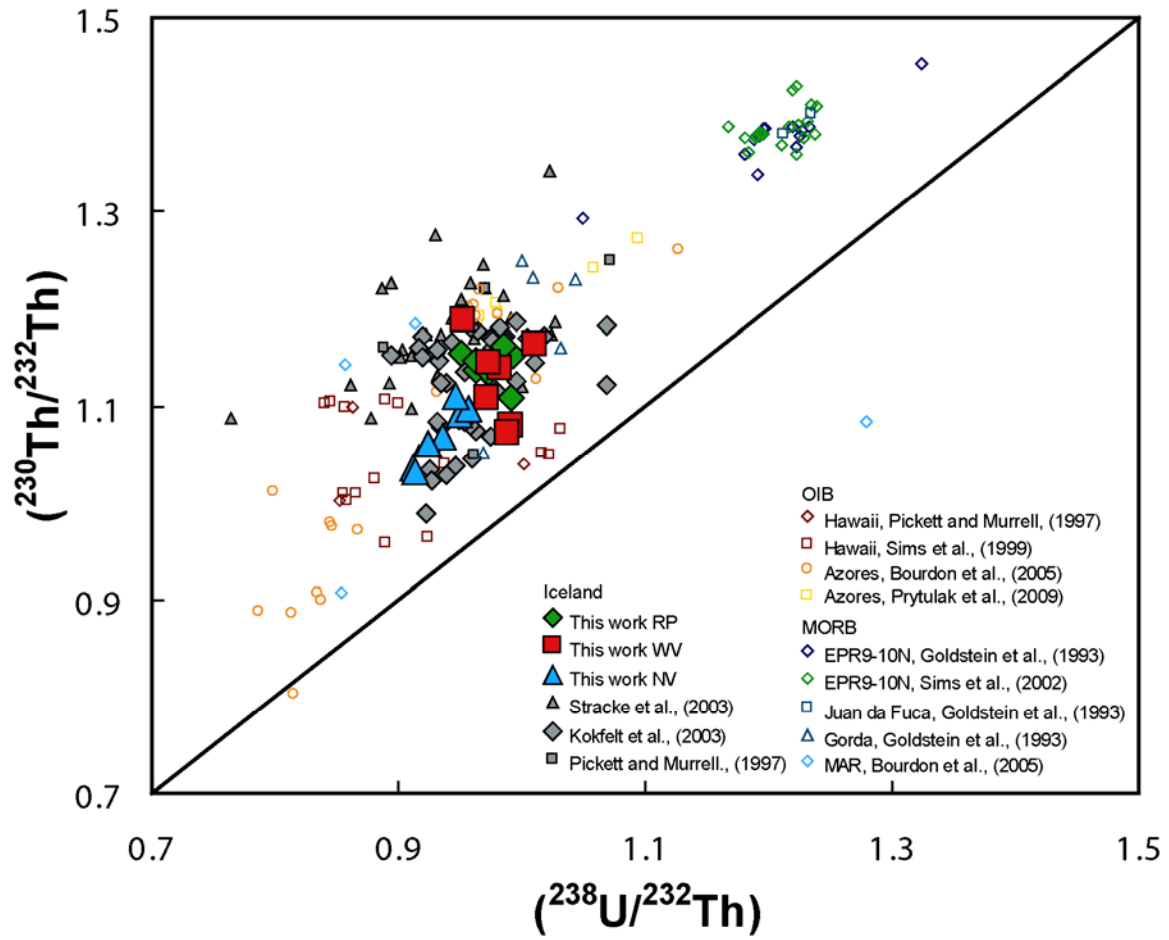


Figure 2. An equiline diagram showing Icelandic data from this work and from the literature. Data for other OIB and MORB samples are shown for comparison.

3.2 ^{231}Pa - ^{235}U disequilibria

Our new ^{231}Pa – ^{235}U disequilibria data show ^{231}Pa excesses for Iceland's main rift lavas with ($^{231}\text{Pa}/^{235}\text{U}$) between 1.333 and 1.925. In a diagram of ($^{230}\text{Th}/^{238}\text{U}$) versus ($^{231}\text{Pa}/^{235}\text{U}$) the data from a broad positive correlation (Fig. 3a). Some of the NV samples have low ($^{231}\text{Pa}/^{235}\text{U}$) = 1.33 -1.39 for a given ($^{230}\text{Th}/^{238}\text{U}$) = 1.14, and plot below the general correlation. The sample from Hallmundarhraun (WV31) has the highest ($^{231}\text{Pa}/^{235}\text{U}$) and ($^{230}\text{Th}/^{238}\text{U}$) ratios; two other WV samples (WV25 and WV21) have the lowest measured ($^{230}\text{Th}/^{238}\text{U}$) of 1.09 at ($^{231}\text{Pa}/^{235}\text{U}$) of 1.49 -1.55. The new Iceland data fall in between data for Hawaii (Sims et al., 1999) and data for MOR basalts, that in general have higher ^{231}Pa excesses at similar ^{230}Th excesses (Fig. 6). ($^{230}\text{Th}/^{238}\text{U}$) in Iceland are similar to those measured in lavas from the Azores (Bourdon et al., 2005; Prytulak and Elliott, 2009), but the ($^{231}\text{Pa}/^{235}\text{U}$) for Iceland are generally higher. In contrast to other OIB and MORB data ($^{231}\text{Pa}/^{235}\text{U}$) ratios for the Iceland main-rift samples (this work, Pickett and Murrell, 1997; Stracke et al., 2006; Stracke et al., 2003a) correlate well with ($^{230}\text{Th}/^{232}\text{Th}$) activity ratios (Fig.3b).

3.3 ^{226}Ra – ^{230}Th disequilibria

($^{226}\text{Ra}/^{230}\text{Th}$) ratios range between 0.801 to 1.218, but the majority of samples (21 out of 28) have ^{226}Ra excesses. In agreement with the Th and Pa disequilibria data, samples from the Western Volcanic Field show the largest variation almost covering the full measured range. The presence of ^{226}Ra excesses is in agreement with the ages of the samples being less than 8000 years (Table 1). Two of the WV samples as well as two of the Theistareykir samples have ^{226}Ra deficits. ^{226}Ra -deficits were also reported for OIB samples from the Azores and for the Pitcairn seamounts (Bourdon and Van Orman, 2009; Widom et al., 1992) and were ascribed to alteration, crystal fractionation or to melting in the presence of phlogopite. ^{226}Ra - ^{230}Th disequilibria do not correlate with U-Th or Pa-U disequilibria (Fig. 3c).

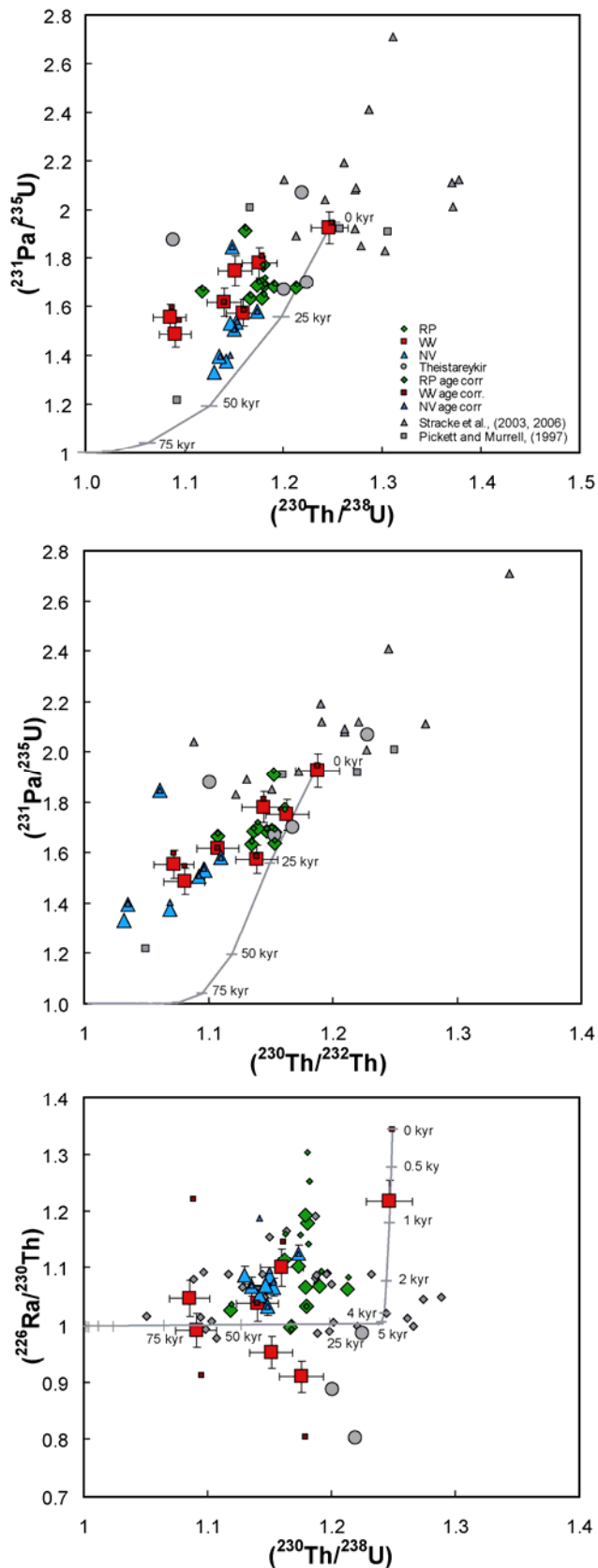


Figure 3. Diagrams of (a) $(^{230}\text{Th}/^{238}\text{U})$ versus $(^{231}\text{Pa}/^{235}\text{U})$, (b) $(^{230}\text{Th}/^{232}\text{Th})$ versus $(^{231}\text{Pa}/^{235}\text{U})$ and (c) $(^{226}\text{Ra}/^{230}\text{Th})$ versus $(^{231}\text{Pa}/^{235}\text{U})$ for samples from Iceland. Age corrected data (small symbols) is shown for samples with a known age. The effect of decay is shown by a theoretical decay trajectory calculated for sample WV31. Note the good correlation for Iceland data in diagram (b) as opposed to the less systematic variation in (a) and non systematic variability in (c). Error bars for WV samples represent 2σ standard deviations determined on multiple analyses of several rock standards digestions (Koornneef et al., 2010). For clarity these are only shown for WV samples.

Table 1. U-Th-Pa-Ra data on Icelandic postglacial main rift lavas

Sample	Flow	Long.	Lat.	Age ^a years	Distance ^b km	U μg/g	Th μg/g	Pa fg/g	Ra fg/g	(²³⁴ U/ ²³⁸ U) ^c	2SE 10 ⁻³	(²³⁸ U/ ²³² Th) ^c	2SE 10 ⁻³	(²³⁰ Th/ ²³² Th) ^c	2SE 10 ⁻³	(²³⁰ Th/ ²³⁸ U) ^c	2SE 10 ⁻³	(²³¹ Pa/ ²³⁵ U) ^c	2SE 10 ⁻³	(²²⁶ Ra/ ²³⁰ Th) ^c	2SE 10 ⁻³	(²³⁰ Th/ ²³⁸ U) _i ^d	(²³¹ Pa/ ²³⁵ U) _i	(²²⁶ Ra/ ²³⁰ Th) _i
RP1	Illahraun	21.991	64.054	784	226	0.163	0.515	90.8	78.1	1.003	3	0.962	7	1.136	9	1.181	10	1.686	19	1.180	11	1.182	1.697	1.252
RP2	Afstaparhraun	22.173	64.016	684	236	0.133	0.423	73.3	58.7	1.003	4	0.951	6	1.154	8	1.213	10	1.680	23	1.062	13	1.214	1.690	1.084
RP5	Stamparhraun	22.709	63.830	784	268	0.126	0.393	67.9	50.3	0.999	3	0.973	5	1.135	9	1.167	9	1.635	23	0.995	9	1.168	1.645	0.993
RP6	Eldvarpahraun	22.600	63.822	784	263	0.126	0.385	69.0	49.5	1.002	3	0.991	4	1.108	10	1.118	10	1.662	13				1.673	
RP9	Arnarsetur	22.426	63.890	784	253	0.175	0.534	110.0	77.7	1.004	1	0.992	8	1.153	11	1.162	12	1.911	37	1.026	8	1.119	1.679	1.036
RP10	Ögmundarhraun	22.233	63.854	784	246	0.133	0.419	73.8	58.1	1.002	0	0.963	7	1.147	9	1.191	10	1.684	19	1.067	13	1.192	1.696	1.094
RP11	Herdísarvík	21.786	63.870		225	0.117	0.361	68.4	49.0	1.001	4	0.985	5	1.162	9	1.180	9	1.773	17	1.032	10			
RP12	Grindaskörð	21.741	63.876	1049	223	0.165	0.512	89.0	79.8	1.003	1	0.978	8	1.154	12	1.179	13	1.636	12	1.193	14	1.181	1.650	1.304
RP15	Nesjahraun	21.445	63.956	1800	206	0.145	0.454	80.8	62.3	1.005	0	0.967	4	1.140	12	1.179	9	1.695	17	1.065	11	1.182	1.722	1.143
RP56	Ögmundarhraun	22.155	63.859	1009	242	0.132	0.409	73.5	59.2	1.002	2	0.981	8	1.151	11	1.174	12	1.687	19	1.102	13	1.175	1.702	1.158
WV16	Svinahraunsbruni	21.452	64.028	840	203	0.172	0.533	89.4	75.6	0.999	3	0.982	4	1.139	8	1.160	8	1.575	23	1.101	8	1.161	1.585	1.145
WV18	Skjaldbreiður I	20.920	64.437		165	0.068	0.205	39.4	25.7	1.002	4	1.010	5	1.163	8	1.152	9	1.750	23	0.952	10			
WV20	Skjaldbreiður II	20.783	64.444		159	0.142	0.445	75.8	57.8	0.994	3	0.971	7	1.108	9	1.140	11	1.618	18	1.038	12			
WV21	Sköflungur	20.650	64.447	5300	152	0.123	0.378	60.4	46.1	1.001	2	0.991	7	1.081	9	1.091	11	1.487	19	0.991	12	1.095	1.545	0.913
WV25	Thjófahraun	21.051	64.263	3600	176	0.192	0.590	98.4	74.7	1.003	4	0.985	8	1.070	10	1.087	12	1.558	12	1.044	10	1.089	1.602	1.210
						0.191	0.593	97.8	74.9	1.002	3	0.980	3	1.070	9	1.092	9	1.551	15	1.043	7	1.095	1.594	1.203
WV27	Nesjahraun	21.247	64.124	1800	190	0.142	0.443	83.3	52.2	0.999	3	0.973	4	1.144	7	1.176	7	1.781	20	0.909	8	1.179	1.811	0.803
WV31	Hallmundarhraun	20.842	64.745	1050	159	0.090	0.290	56.8		0.999	3	0.945	4	1.185	8	1.254	8	1.906	29			1.256	1.927	
						0.091	0.289	58.5	47.4	0.994	7	0.960	4	1.190	11	1.240	10	1.943	17	1.218	8	1.242	1.964	1.344
NV41	Prengslaborgir	16.948	65.575	3000	104	0.148	0.479	66.9	60.8	1.000	0	0.936	4	1.069	9	1.142	9	1.378	21	1.051	9	1.146	1.403	1.188
NV42	Elda	16.945	65.656	280	129	0.227	0.722	112.7	97.0	1.004	4	0.955	7	1.098	8	1.149	11	1.506	14	1.080	12	1.150	1.509	1.091
						0.227	0.728	116.9	94.8	1.001	4	0.946	3	1.094	10	1.156	10	1.565	15	1.052	7	1.157	1.568	1.059
NV45	Krafla	16.784	65.718	280	121	0.225	0.718	111.4	96.3	1.007	3	0.950	8	1.092	8	1.150	11	1.506	17	1.085	12	1.151	1.509	1.096
NV48	Daleldar	16.793	65.664		116	0.228	0.723	114.9	96.0	1.000	3	0.957	7	1.098	7	1.146	10	1.531	24	1.069	11			1.069
NV49	Krafla	16.841	65.795	25	129	0.164	0.526	85.2	74.5	1.001	0	0.946	7	1.110	9	1.174	10	1.580	17	1.125	13	1.174	1.580	1.126
NV50	Krafla	16.841	65.795	25	129	0.165	0.542	100.3	67.2	0.999	4	0.924	9	1.061	14	1.148	16	1.845	16	1.032	12	1.148	1.845	1.032
NV52	Askja	16.721	65.044	88	56	0.432		200.6	181.1	1.002	4							1.410	31				1.411	
						0.431	1.435	196.6	179.5	1.001	3	0.912	4	1.036	11	1.136	11	1.384	11	1.067	8	1.136	1.385	1.069
NV54	Frambruni	17.075	65.017		44	0.193	0.642	84.9	81.6	1.001	2	0.914	3	1.032	7	1.130	8	1.333	30	1.087	11			
9309	Theistareykir				132	0.028	0.084	19.1	9.4	1.039	4	1.007	3	1.228	11	1.220	9	2.068	37	0.801	6	1.220	2.068	0.801
9383	Theistareykir				141	0.059	0.188	33.1	24.5	1.006	4	0.953	3	1.168	10	1.225	9	1.701	43	0.985	7	1.225	1.701	0.985
9389	Theistareykir				141	0.030	0.094	16.3	10.9	1.035	4	0.960	3	1.153	11	1.201	10	1.670	24	0.887	6	1.201	1.670	0.887
9390	Theistareykir				142	0.006	0.017	3.5	0.0	1.099	8	1.012	2	1.101	13	1.089	12	1.877	13			1.089	1.877	

^a Ages are from Peate et al., (2008), Sinton et al., (2005) and K. Grönvold, personal communication^b Distance from the plume centre calculated using the sampling coordinates relative to coordinates 64.5°N, 17.3°W (Kokfelt et al., 2003)^c Activity ratios are calculated using: $\lambda_{234} = 2.8263 \times 10^6 \text{ y}^{-1}$, $\lambda_{235} = 9.8485 \times 10^{-10} \text{ y}^{-1}$, $\lambda_{238} = 1.5513 \times 10^{10} \text{ y}^{-1}$, $\lambda_{232} = 4.9475 \times 10^{11} \text{ y}^{-1}$, $\lambda_{230} = 9.1577 \times 10^6 \text{ y}^{-1}$, $\lambda_{231} = 2.1158 \times 10^8 \text{ y}^{-1}$, $\lambda_{226} = 4.3322 \times 10^4 \text{ y}^{-1}$ ^d Initial activity ratios corrected for post eruptive decay

3.4. Comparison of Theistareykir data with previous U-series data

The four samples from Theistareykir previously analysed by Stracke et al. (2003, 2006) have ($^{234}\text{U}/^{238}\text{U}$) higher than 1 (Table 1). Stracke et al., (2003) suspected that the high ($^{234}\text{U}/^{238}\text{U}$) obtained for the samples resulted partly from an analytical problem, however, we confirm here that the ($^{234}\text{U}/^{238}\text{U}$) are out of equilibrium, suggesting these samples were affected by water-rock interaction. The ($^{230}\text{Th}/^{238}\text{U}$) ratios measured previously by Stracke et al, (2003) are consistently lower than those reported here, owing to the lower U-concentrations compared to this study. The reason for this discrepancy is unclear, however, determination of U-concentrations on BCR-2 and W2a in this work confirm the accuracy of the techniques (Koornneef et al., 2010a; see Chapter 3). The Pa-excesses determined in this work are also generally lower than the ($^{231}\text{Pa}/^{235}\text{U}$) measured for Theistareykir (1.83-2.71) by Stracke et al., (2006). Two of the samples from Theistareykir that we re-analysed have significantly lower ($^{231}\text{Pa}/^{235}\text{U}$) (i.e. 10 and 22%) compared to that determined by Stracke et al, (2006) whereas the third sample is identical within analytical uncertainty. The higher Pa-excesses measured by Stracke et al., (2003, 2006) result from both lower U concentration determinations and higher Pa concentrations compared to those measured here. Note that Stracke et al., (2003, 2006) determined the U and Pa concentrations on separate sample aliquots in different laboratories, possibly contributing to the observed discrepancy (see discussion in Koornneef et al., 2010a). Furthermore, it is possible that the water-rock interaction indicated by the ($^{234}\text{U}/^{238}\text{U}$) resulted in cm-scale heterogeneity and/or redistribution of U and hence highly heterogeneous U-series composition. Measurements of BCR and W2a in the analytical session in which we re-analysed the Theistareykir samples yield ($^{231}\text{Pa}/^{235}\text{U}$) in equilibrium, confirming the accuracy of the data reported here.

4. Discussion

In the context of Iceland where source heterogeneities have clearly been documented, it is critical to establish the role of melting processes relative to the effect of variable source composition. Kokfelt et al., (2003) suggested that the U-series systematics in lavas from across Iceland primarily reflect differences in mantle upwelling velocity, a conclusion re-emphasized by Bourdon et al. (2006). A radial variation in the upwelling velocity beneath Iceland was inferred based on a systematic increase in ^{230}Th excesses with distance from the plume centre. The upwelling velocities were estimated to range from 1-4 cm/yr at the margins of Iceland to 5-20 cm/yr in the centre of the plume. In this framework, the ^{231}Pa excesses are expected to show a more pronounced relationship owing to the shorter half-life (~ 32 ka) of this daughter nuclide compared to the ^{230}Th (~ 75 ka).

In Figure 4, ($^{230}\text{Th}/^{238}\text{U}$), ($^{231}\text{Pa}/^{235}\text{U}$) and ($^{238}\text{U}/^{232}\text{Th}$) activity ratios are plotted against distance from the inferred plume centre, showing that the ^{230}Th and ^{231}Pa excesses broadly correlate with distance from the plume. This observation is consistent with the data of Kokfelt et al. (2003), although we found larger variability at a local scale. Samples from the Northern Volcanic zone closest to the plume centre have the lowest ^{230}Th - and ^{231}Pa excesses. Note, however, that these samples also have lower ($^{238}\text{U}/^{232}\text{Th}$) activity ratios (Fig 4c). In the equiline diagram (Fig. 2), the NV samples (and some Reykjanes Peninsula samples) define a trend sub-parallel to the equiline suggesting that mixing of melts from different sources may be important (e.g., Lundstrom et al., 1995). Samples from the Western Volcanic Zone and the Reykjanes Peninsula show more scatter in the ($^{230}\text{Th}/^{232}\text{Th}$) and ($^{238}\text{U}/^{232}\text{Th}$) data but form a broad perpendicular relation to the trend defined by NV samples (Fig 2).

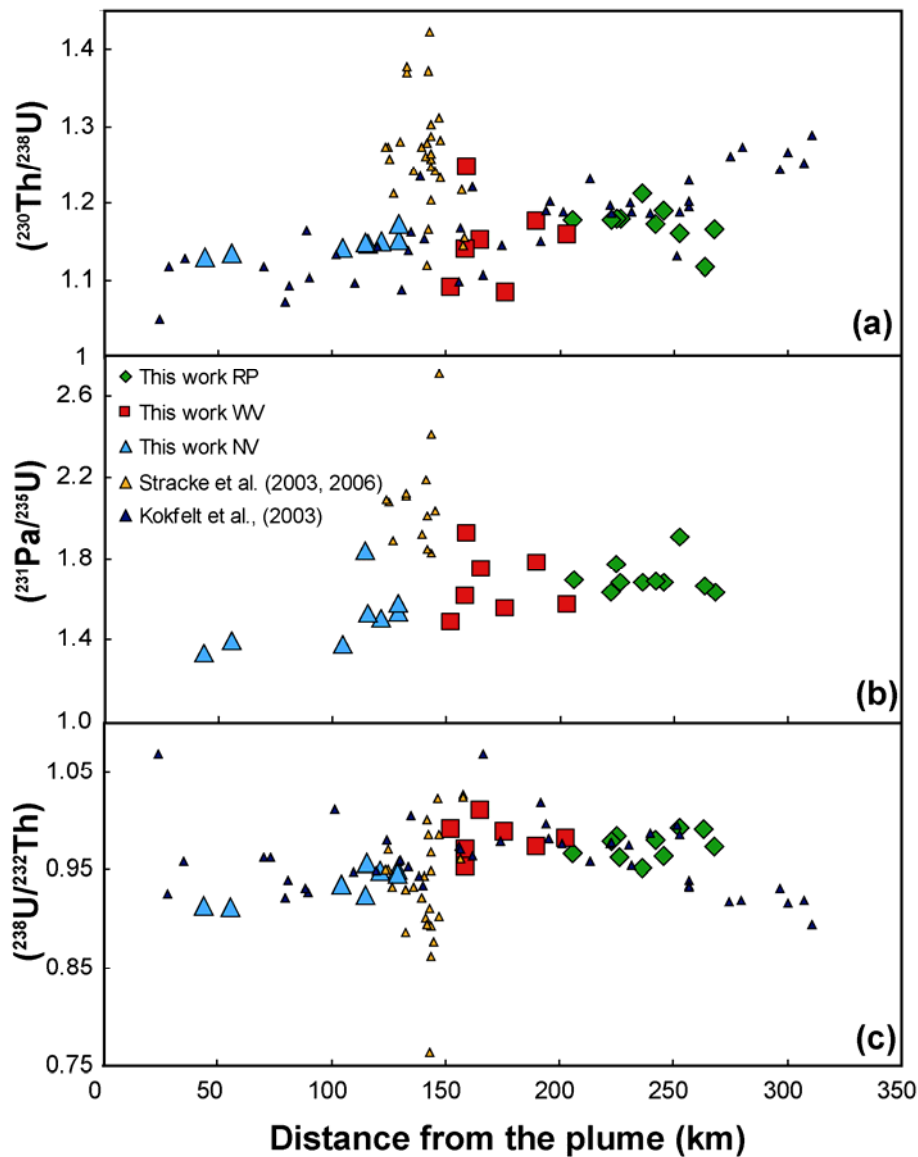


Figure 4. U-series disequilibria for Iceland versus distance from the inferred plume centre. Even though some of the NV samples that were collected closest to the inferred plume centre have the lowest ^{231}Pa excesses and relatively low ^{230}Th excess consistent with faster mantle upwelling, these samples also have lower $(^{238}\text{U}/^{232}\text{Th})$ activity ratios suggesting the lower excesses may result from mixing of melts from different sources. Furthermore, WV samples and samples from Theistareykir show considerable variability in $(^{230}\text{Th}/^{238}\text{U})$, $(^{231}\text{Pa}/^{235}\text{U})$ even though these samples are collected from relatively small areas at similar distances from the plume centre. This suggests that mantle upwelling rate is not the primary controlling factor in creating the disequilibria and that lithological heterogeneities having variable melt productivities may be more important instead.

In a diagram of ($^{230}\text{Th}/^{238}\text{U}$) versus ($^{231}\text{Pa}/^{235}\text{U}$) (Fig 6), the Icelandic main rift data show considerable variability compared to the Hawaiian samples which were also inferred to be controlled by regional variation in upwelling velocity across a hot buoyant plume (Bourdon et al., 2006; Sims et al., 1999). Samples from the Western Volcanic Zone have a large range in ($^{230}\text{Th}/^{238}\text{U}$) and ($^{231}\text{Pa}/^{235}\text{U}$) although these samples were collected from a relatively small area, a few square kilometres, implying a similar distance from the plume centre. This large local-scale variability in ^{230}Th and ^{231}Pa excesses suggests that these samples are produced with variable melting rates. This observation indicates either that the mantle upwelling velocity is variable at a local scale or that the melting behaviour of the source is variable in the melting region.

An interesting observation for the Icelandic data is that there is a good correlation between ^{231}Pa excesses and ($^{230}\text{Th}/^{232}\text{Th}$) activity ratios. This correlation suggests that the ($^{230}\text{Th}/^{232}\text{Th}$) and ($^{231}\text{Pa}/^{235}\text{U}$) are controlled by similar parameters. Compared with other OIB localities, Iceland is the only ocean island that displays such a good correlation between ($^{230}\text{Th}/^{232}\text{Th}$) and ($^{231}\text{Pa}/^{235}\text{U}$) indicating that the processes that results in this relation are indigenous to Iceland, rather than being a general feature of upper mantle melting.

4.1 A role for crustal level processes?

The primary U-series disequilibria are potentially affected by secondary processes such as (1) crystallisation of phases that fractionate the parent and daughter isotopes, (2) radioactive decay during long term magma storage, and (3) assimilation of (hydrothermally altered) wall rocks.

U, Th, Pa and Ra are all highly incompatible in olivine, clinopyroxene and plagioclase (Blundy and Wood, 2003; Fabbrizio et al., 2009) that crystallize in the tholeiitic basalts analysed here (Koornneef et al., 2011), and so their activity ratios are not significantly affected by fractional crystallisation.

Long-term magma storage could lead to decay of the melting-induced disequilibria and thereby lowering the ^{230}Th , ^{231}Pa and ^{226}Ra excesses. This effect is most significant for ^{226}Ra because of its short half life (~1.6 kyr) compared to ^{230}Th (~75 kyr) and ^{231}Pa (~32 kyr). Although samples from the Northern Volcanic Zone define a trend on a ($^{230}\text{Th}/^{238}\text{U}$) versus ($^{231}\text{Pa}/^{235}\text{U}$) diagram that could reflect radioactive decay over a few 10 kyr (Fig. 3), the presence of ^{226}Ra excesses (Table 1) shows that the magma storage

times are less than 8 kyr. NV samples that have the lowest ^{230}Th - and ^{231}Pa - excesses generally have slightly higher SiO_2 contents and lower MgO (4.7 – 7.8) indicative of more extensive crystal fractionation compared to the WV and RP samples. However, there is no clear relation between the indices of magma differentiation (e.g. MgO , $\text{CaO}/\text{Al}_2\text{O}_3$, SiO_2) and ($^{230}\text{Th}/^{238}\text{U}$), ($^{231}\text{Pa}/^{235}\text{U}$) and or ($^{226}\text{Ra}/^{230}\text{Th}$) (Fig. 5).

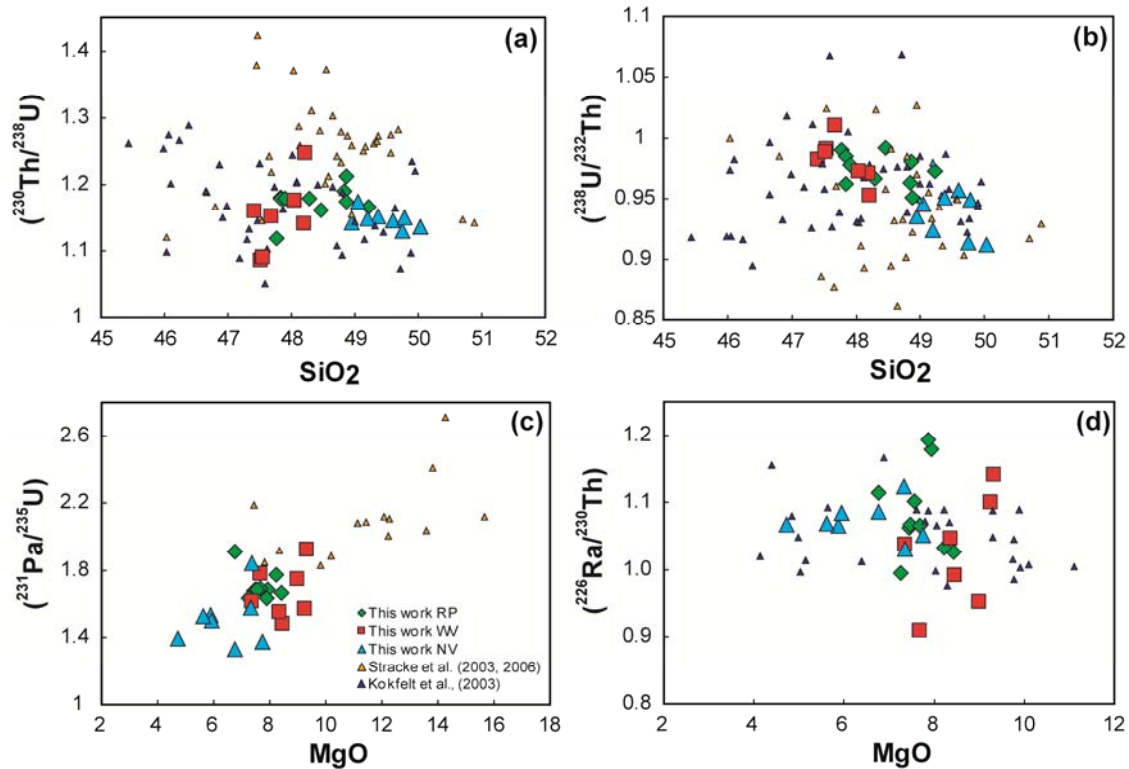


Figure 5. U-series disequilibria data versus indices of magma differentiation. NV samples that have the lowest ^{230}Th - and ^{231}Pa -excesses generally have slightly higher SiO_2 contents and lower MgO . However, lack of clear correlations suggests that magma storage is not a primary controlling factor to the U-series disequilibria.

Assimilation of crustal rocks, or of melts from these rocks, that are old and in secular equilibrium could also lower the U-series disequilibria that originally resulted from mantle melting. As pointed out above, NV (and RP) samples define a trend sub-parallel to the equiline suggesting mixing between a source with low U/Th and a source with high U/Th (Fig 2). Similar relationships for Icelandic basalts in the equiline diagram have previously been ascribed to assimilation by rhyolitic or dacitic crustal rocks or melts produced during shallow-level magma evolution, especially at central volcanoes

where bimodal volcanism is observed (Chekol et al., 2010; Kokfelt et al., 2003; Pietruszka et al., 2009; Sigmarsson et al., 1992; Sigmarsson et al., 1991). The combination of low ($^{231}\text{Pa}/^{235}\text{U}$), ($^{230}\text{Th}/^{232}\text{Th}$) and ($^{238}\text{U}/^{232}\text{Th}$) and the more evolved nature of the NV samples from the large central volcanoes Krafla and Askja could result from the effect of crustal assimilation. In the ($^{230}\text{Th}/^{238}\text{U}$) versus ($^{231}\text{Pa}/^{235}\text{U}$) diagram, the NV samples form a fairly steep positive trend directed towards ($^{230}\text{Th}/^{238}\text{U}$) \sim 1.08 and ($^{231}\text{Pa}/^{235}\text{U}$) = 1. If the relation reflects assimilation, this would require that the assimilant had an age between about 160 and 375 kyr (5 times the half life of ^{231}Pa and ^{230}Th , respectively) to explain the ^{230}Th excess of 8% with the ($^{231}\text{Pa}/^{235}\text{U}$) in equilibrium.

In contrast with the relation between ^{231}Pa - and ^{230}Th excesses, ^{226}Ra excesses (3 - 13%) observed for the NV samples are inconsistent with bulk mixing with a rhyolitic assimilant expected to be in Ra-Th equilibrium. However, Van Orman et al., (2006) and Saal et al., (2004) showed that diffusive interaction of the mantle melts with enriched wall rocks during prolonged magma residence time could result in substantial ^{226}Ra excess in the melts. The ^{226}Ra excesses are predicted to result from faster diffusion of divalent ^{226}Ra compared to its tetravalent parent ^{230}Th . The NV samples do not show relationships between the ^{226}Ra excesses and other divalent cations (e.g. Ba, Sr, Ni, Zn and Cu) to confirm such a process.

Binary mixing between a depleted initial melt (e.g. NV49, Table 1) and an evolved rock/melt would have a relatively large effect onto the incompatible element budget of the lava. Bulk assimilation of a rhyolite, for example, (Rhyolite SP40 collected from the Snaefellsness Peninsula) that has Th = 8.3 ppm and U/Th = 0.29, ($^{231}\text{Pa}/^{235}\text{U}$) in equilibrium and ($^{230}\text{Th}/^{238}\text{U}$) of 1.08 can reproduce the observed trends for the ($^{230}\text{Th}/^{232}\text{Th}$), ($^{230}\text{Th}/^{238}\text{U}$), ($^{231}\text{Pa}/^{235}\text{U}$) and ($^{238}\text{U}/^{232}\text{Th}$) data with 5% of assimilation.

Assimilation of a rhyolitic rock or melt could also explain the slightly higher SiO_2 , higher incompatible trace element concentrations and the flatter HREE patterns observed in NV samples (e.g. NV52, Koornneef et al., 2011) compared to other main rift lavas. It should be pointed out that the evidence for assimilation of NV samples is only revealed in combination with the U-series disequilibria. Based on major and trace elements alone it cannot be resolved as the required assimilant has similar highly incompatible trace element ratios as the inferred depleted mantle end member. Note that only samples from the more evolved large central volcanoes show evidence for

crystallisation, decay and assimilation; for samples away from these large volcanic centres crustal processes do not have a major role.

4.2 Interpreting U series data using dynamic melting

As standard batch melting models failed to explain U-series data in basalts, a range of melting models based on the difference in residence time between the parent and daughter nuclides in the melting column have been proposed. The difference in residence time allows an in-growth of the daughter nuclide while the parent nuclide is retained preferentially. As the Iceland lavas show evidence for compositional variations that are generated in the melting column (see Koornneef et al. 2011, correlations between isotopes, trace elements and major elements), we consider a dynamic melting model whereby melts do not re-equilibrate with its surrounding matrix as it rises to be appropriate to interpret the U-series data (see also, Bourdon et al., 2006; Bourdon et al., 2005; Claude-Ivanaj et al., 1998; Kokfelt et al., 2003; Prytulak and Elliott, 2009; Stracke et al., 2006; Stracke et al., 2003a).

The dynamic melting model, initially developed by (McKenzie, 1985), assumes that melts produced in the upwelling mantle escape the solid residue at a critical threshold porosity, after which there is no interaction between the solid and the melt. Since U, Th and Pa are highly incompatible elements, the U-series disequilibria are mostly formed at the onset of melting and thus reflect the conditions at the bottom of the melting region (see reviews by (Bourdon and Sims, 2003b; Elliott et al., 2003; Stracke et al., 2006). In-growth of daughter nuclides during melting in the dynamic melting model is directly dependent on the melting rate, which is a function of melt productivity and mantle upwelling velocity as described by the following equation:

$$\Gamma = \rho_s^2 g W \left(\frac{dF}{dP} \right)$$

where Γ is the melting rate in $\text{kg/m}^3/\text{s}$, ρ_s is the density of the solid in kg/m^3 , g is the gravitational acceleration in m/s^2 , W is the mantle upwelling velocity in m/s and (dF/dP) is the melt productivity in % of melt/GPa.

The melting model applied here is an incremental solution to dynamic melting as described in Stracke et al. (2003, 2006). U-series disequilibria in instantaneous melts are calculated in a one-dimensional melting column assuming that the source is homogeneous and initially in secular equilibrium (i.e. the source has been undisturbed

for > 350 ka). Mineral-melt partition coefficients, source mineralogy and melt productivity in the model are a function of pressure (Stracke et al., 2003a). In contrast to the analytical solution of McKenzie (1985), which assumes infinite melt extraction velocity, varying melt extraction velocity (v) is possible, thereby accounting for decay during melt transport.

4.3 U-series nuclide partitioning

In the context of dynamic melting, the U-series disequilibria are primarily a function of the relative fractionation between the nuclides which is controlled by their bulk partition coefficients and the time available for ingrowth of daughter nuclides during the melting process, i.e. the melting rate (McKenzie, 1985; Williams and Gill, 1989).

All U-series nuclides are known to be highly incompatible (Blundy and Wood, 2003) during peridotite melting and are therefore exhausted from the mantle residue after 2 - 5% of melting. Hence, the ^{230}Th , ^{231}Pa and ^{226}Ra excesses are mainly controlled by the bulk partition coefficients of the parent nuclides (i.e. D_U , D_{Th}) and any significant fractionation can only take place during the first 5% of melting. Garnet plays a key role for the fractionation between the U-series nuclides upon melting as U is more compatible compared to Th, Pa and Ra (Beattie, 1993b; Hauri et al., 1994; LaTourrette et al., 1993; Salters and Longhi, 1999). For clinopyroxene (cpx), the distribution coefficients were found to vary with the pressure-dependent mineral composition. Low Ca, aluminous cpx typically present in high pressure assemblages has higher D_U/D_{Th} compared to the low pressure high Ca cpx and is therefore capable of fractionating U from Th and Pa (Beattie, 1993a; Hauri et al., 1994; LaTourrette and Burnett, 1992; Salters et al., 2002; Wood et al., 1999). Olivine and orthopyroxene do not significantly fractionate U-series nuclides (Blundy and Wood, 2003). Based on dynamic melting calculations ^{230}Th excesses are larger for garnet-bearing assemblages that have large D_U/D_{Th} , while it is smaller for garnet free peridotite. However, the absolute D_U and D_{Th} can be relatively large owing to the high D values in high Ca cpx (McDade et al., 2003; Salters et al., 2002; Wood et al., 1999) resulting in substantial ^{231}Pa and ^{226}Ra excesses for small ^{230}Th excesses.

Experimentally determined mineral melt partition coefficients for garnet and cpx in mafic lithologies such as pyroxenite or eclogite show considerable overlap with partition coefficients determined for peridotite melting (Elkins et al., 2008; Klemme et

al., 2002; Pertermann and Hirschmann, 2002; Pertermann et al., 2004). The mineral-melt partition coefficients for pyroxenite depend on pressure and temperature and on mineral composition. Calculated bulk D_U/D_{Th} 's for pyroxenite range from being smaller to being larger than those in garnet-peridotite (Elkins et al., 2008; Pertermann et al., 2004; Prytulak and Elliott, 2009; Stracke et al., 2006). The magnitude of the U-Th fractionation and the difference in bulk partitioning behaviour of pyroxenite compared to peridotite therefore remains poorly constrained.

4.4 Melt productivity

Melt productivity (dF/dP), as defined in Equation 1 has an important control on the melting rate. Melt productivity is largely controlled by the residual mineralogy but also by the coexisting liquid (e.g., Asimow et al., 1997). Theoretical and experimental studies show that melt productivity of a peridotitic mantle increases with decreasing pressure and increasing melt fraction during progressive melting (Asimow et al., 1997; Asimow et al., 2001; Hirschmann et al., 1999; Hirschmann et al., 1998; Stolper and Asimow, 2007). For U-series disequilibria, as explained above, the near-solidus melt is particularly relevant. For peridotite the near solidus dF/dP is estimated to be between 1 and 5 %/GPa.

In MORB-like pyroxenitic lithologies, melt productivity at the onset of melting is substantially higher, ~13%/GPa (Pertermann and Hirschmann, 2003). Additionally, pyroxenite is expected to start melting at similar or higher pressures compared to peridotite owing to lower melting temperatures (Kogiso et al., 2004; McKenzie and Bickle, 1988; Pertermann and Hirschmann, 2003). Pertermann and Hirschmann, (2003) showed, before the onset of peridotite melting, the melt productivity of pyroxenite G2 increased up to 70%/GPa, partly due to heating of the pyroxenite by the enclosing peridotite. These characteristics potentially result in disproportionate contribution of pyroxenite veins or layers relative to their abundance (Hirschmann and Stolper, 1996; Pertermann and Hirschmann, 2003; Stracke et al., 1999).

4.5 Mantle upwelling velocity

The mantle upwelling velocity beneath Iceland depends on the complex interplay between the passive component of upwelling linked to the mid-Atlantic ridge and the

active component related to the excess mantle temperature of the Iceland plume. (e.g., Ito et al., 1996; Olson et al., 1993; Ribe et al., 1995).

Dynamic melting of a homogeneous garnet-bearing peridotitic source at variable upwelling velocities predicts positive correlations in diagrams of ($^{230}\text{Th}/^{238}\text{U}$) versus ($^{231}\text{Pa}/^{235}\text{U}$) (Fig. 6). Slow upwelling corresponding to low melting rates yields high ^{230}Th and ^{231}Pa excesses and fast upwelling corresponding to high melting rates yields low ^{230}Th and ^{231}Pa -excesses. Using various sets of partition coefficients, modal mineralogy, depth of melt initiation, or melt extraction rate results in changes in the slope in this diagram, but the trends always remain positive (Fig. 6). An exception to these positive slopes are predicted for melting in the spinel stability field applying the K_{DS} determined by McDade et al., (2003).

The Icelandic main rift data define a broad positive array in the ^{231}Pa versus ^{230}Th excess diagram, which could result from variable mantle upwelling rates across Iceland. The apparent steep positive relationship between the Northern Volcanic Zone (NV) and some of the Reykjanes Peninsula (RP) samples can, however, not solely be explained by varying mantle upwelling velocity, while keeping other parameters constant.

Comparison of the data with the dynamic model for a garnet peridotite in Figure 6 implies that the relatively low ^{231}Pa and ^{230}Th excess for NV samples may result from radioactive decay during melt extraction at a rate of ~ 1 m/yr (Fig 6). Alternatively, the radioactive decay could be concomitant with assimilation as discussed in section 4.1.

If one assumes that the mean ($^{230}\text{Th}/^{238}\text{U}$) ratios of Icelandic samples (see Fig. 7) result from melting an average homogeneous source at variable mantle upwelling velocity the mantle upwelling velocity (W) as a function of distance from the plume centre can be obtained. The estimated upwelling velocities range from 8.9 cm/yr at the plume centre to 2.3 cm/y at 300 km distance from the plume centre. This latter value compares favourably with the MAR spreading rate, which gives an order of magnitude for the passive upwelling rate (Iwamori, 1993).

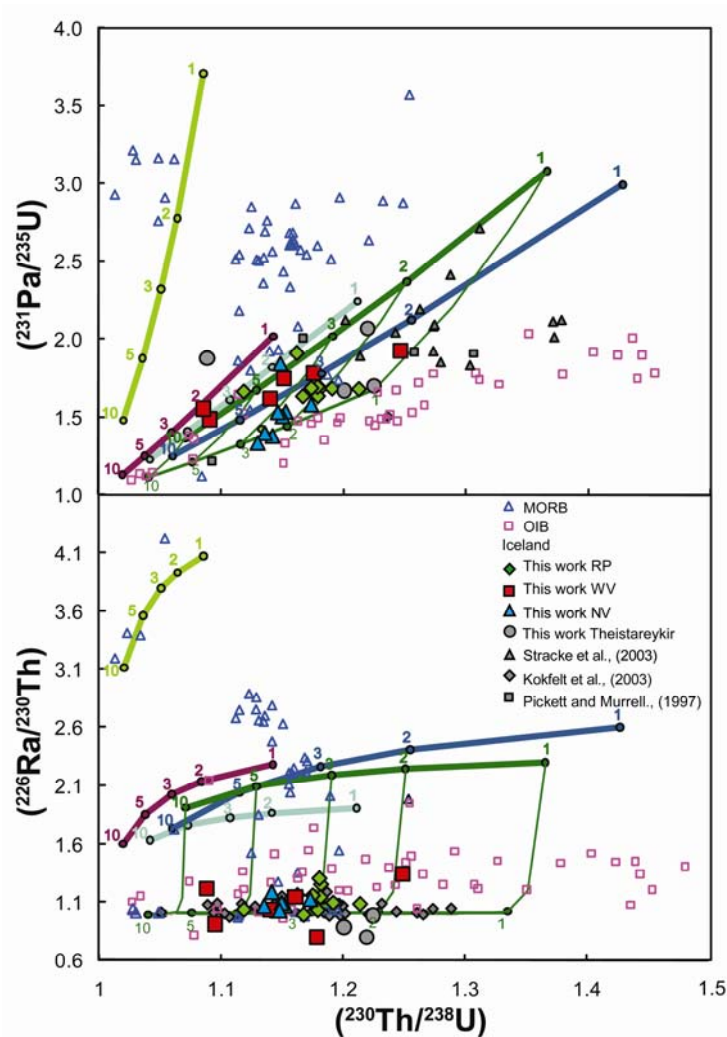


Figure 6. Diagram of $(^{230}\text{Th}/^{238}\text{U})$ versus $(^{231}\text{Pa}/^{235}\text{U})$ and $(^{226}\text{Ra}/^{230}\text{Th})$ showing Iceland data and OIB and MORB literature data. Model curves for dynamic melting of homogeneous pyroxenite and peridotite sources are also displayed. The calculated variations in ^{230}Th and ^{231}Pa excesses are a function of mantle upwelling velocity indicated by coloured numbers (cm/yr). The green curves represent calculations for a Spinel peridotite (light grey-green) and garnet peridotite (dark green) and are calculated using K_D s as in Table 2, the steep bright green curve is for a spinel peridotite calculated using partition coefficients for olivine and orthopyroxene from McDade et al., (2003) and clinopyroxene from Wood et al., (1999); the purple and blue curves are calculated for a pyroxenite with low (purple) and high D_U/D_{Th} (blue) respectively (Table 2). The effect of decay during melt transport is shown for the garnet peridotite (thin green curves) at various upwelling velocities and for a melt velocity of 1 m/yr (lower green curve). OIB data from: (Bourdon et al., 1998; Bourdon et al., 2005; Pickett and Murrell, 1997; Prytulak and Elliott, 2009; Sims et al., 1999); MORB data from: (Bourdon et al., 2005; Goldstein et al., 1993; Lundstrom et al., 1999; Lundstrom et al., 1998; Sims et al., 1995; Sims et al., 2002; Sturm et al., 2000)

In the estimation it is assumed that the samples were not significantly affected by decay during melt transport (i.e. melt transport time is short relative to the half life of the daughter nuclides). However, the relatively low measured mean ^{231}Pa and ^{226}Ra excesses with distance from the plume centre compared to the predicted trend for infinite melt extraction (Fig. 7c, d) suggest melt velocity not to be infinite, but to vary between 3 m/yr and 50 m/yr.

It should be noted that WV samples collected from closely spaced eruptive centres in the Western Rift Zone (~20 square km) show considerable variability in ^{230}Th excess and ^{231}Pa excesses (Fig. 7). The preservation of ^{226}Ra excesses in the WV sample with the lowest ($^{230}\text{Th}/^{238}\text{U}$) and ($^{231}\text{Pa}/^{235}\text{U}$) argues against slow melt extraction velocity as the dominant controlling process. The variation in U-series disequilibria could in principle result from: (1) local variability in mantle upwelling velocity reflected by spatial sampling from the large plume/ridge structure or (2) from temporal variability in mantle upwelling velocity as recorded by samples with different eruption ages (a few ky).

Extraction of melts from different parts in the melting regime beneath the MAR that is characterised by a combination of active and passive mantle upwelling could potentially result in a variability in upwelling recorded by lavas that erupt at a local scale (Ito et al., 1996; Ribe et al., 1995). To explain the largest and smallest ^{230}Th excesses within the WV group assuming melting of a garnet peridotite source and infinite melt velocity requires a variation in local mantle upwelling velocity to be significant (~2 to ~8 cm/yr, Fig. 6). ‘Vertical’ variation in upwelling velocity as proposed by Kokfelt et al., 2003, could produce some variability in ^{230}Th and ^{231}Pa excesses at a local scale. Large variability in trace element ratios that are sensitive to the degree of melting, i.e. La/Sm, La/Yb, indicate that melts are extracted from variable depths in the melting region. The lack of correlation between La/Sm and ($^{230}\text{Th}/^{238}\text{U}$) or ($^{231}\text{Pa}/^{235}\text{U}$) suggests, however, that the U-series disequilibria are not a function of depth of extraction and confirms that the U-series disequilibria are controlled by the initial stages of melting only. This indicates that vertical variation in upwelling velocity does not significantly influence the local variability in U-series disequilibria.

In contrast with a vertical variation in upwelling velocity, a lateral variation in upwelling velocity in the three dimensional melting regime may be expected with

varying distance from the spreading axis. Melts erupted at a given locality may have been sampled from the mantle flow regime farthest away from the spreading axis and plume centre will record slow melting rates, whereas melts extracted from the on-axis regime or even closer to the plume centre ~160 km to the east of the Western Volcanic Zone, should record faster melting rates. The two WV samples that have the lowest ^{231}Pa and ^{230}Th excesses have relatively high Sm/Yb (e.g. WV25 has Sm/YbN = 1.66), Lu/Hf and Tb/Yb compared to the other WV samples, which is consistent with deeper melt initiation. Note, however, that the combined ^{230}Th excess and ^{231}Pa excess for these samples plot outside the model grid for a garnet peridotite (Fig. 6). The low ($^{230}\text{Th}/^{238}\text{U}$) of 1.09 at ($^{231}\text{Pa}/^{235}\text{U}$) of 1.55 of WV25 requires melting at low $D_{\text{U}}/D_{\text{Th}}$ suggesting melting in the spinel stability field or, alternatively, melting of a mafic lithology that has low $D_{\text{U}}/D_{\text{Th}}$ (see section 4.3 and 4.6). Additionally, melts extracted from the far edges of the 3-D melting regime must travel a long distance before erupting at the rift. Melt transport with a significant horizontal component is expected to be 1 to 2 orders of magnitude slower compared to buoyancy-driven vertical melt transport (Ruedas et al., 2004). The slow melt transport would allow for radioactive decay of the initially high U-series excesses. WV31, the sample with the largest ^{231}Pa and ^{230}Th excesses also has high ^{226}Ra excesses, which argues against a long melt transport time.

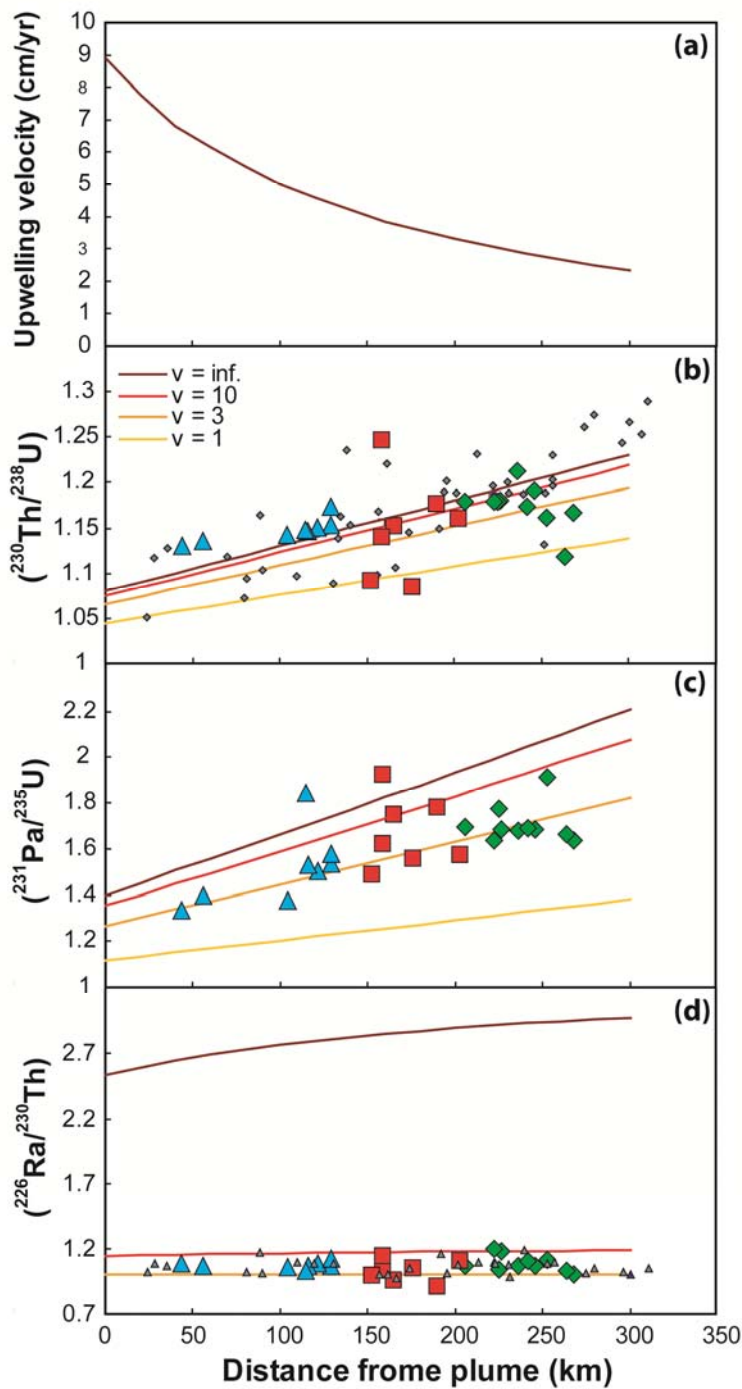


Figure 7. (a, b) Estimated upwelling velocity with distance from the Iceland plume centre based on the linear regression through $(^{230}\text{Th}/^{238}\text{U})$ in Icelandic basalts measured by Kokfelt et al., 2003 and this study. Data from Stracke et al, 2006, are not included due to suspected inaccuracy as discussed in section 3.4. The effect of decay during melt transport is shown for melt velocities of $v=10$ m/y, 3 m/y and 1 m/y. In this model the threshold porosity is set to 0.1%. (c, d) $(^{231}\text{Pa}/^{235}\text{U})$ and $(^{226}\text{Ra}/^{230}\text{Th})$ model predictions with distance from the plume for different melt velocities using the mean regression through $(^{230}\text{Th}/^{238}\text{U})$ as a reference. Based on the ^{226}Ra excess we can conclude that samples must have had melt velocities in between 3 and 10 m/yr.

Alternatively, temporal variations in mantle upwelling could influence the WV data. The oldest samples (WV21 and WV25) do have the lowest ($^{230}\text{Th}/^{238}\text{U}$) disequilibria that could reflect faster mantle upwelling (Table 1). Note, however, that these samples with low ^{230}Th -excesses do not have significantly lower ^{231}Pa excesses compared to other WV samples, which would be expected in case of faster upwelling. Thus, we consider local or temporal variability in mantle upwelling velocity not to be a primary controlling parameter. Instead, samples that have lower or higher ^{230}Th excesses compared to the mean trend in Fig. 7 can be explained by melting a lithology with different melting behaviour (see section 4.7).

4.6 Mantle porosity The escape porosity or threshold porosity of the mantle is an important parameter in the dynamic melting model as it controls the time available for ingrowth before a melt is stripped from the residue. In the calculations presented above we have assumed the porosity to be small and constant (0.1%) which allowed us to extract information on the melt velocity. Instead, one could assume negligible transport time and yield information on the escape porosity (Sims et al., 1999). Model curves for varying porosity and upwelling velocity at infinite melt extraction velocity are displayed in Fig. 8). The model predicts relatively low ^{226}Ra - excesses at a small range of ^{230}Th excess for large threshold porosities (at variable w) and relatively high ^{226}Ra - excesses at a large range of ^{230}Th excess for small threshold porosities (at variable w). The predicted ^{226}Ra excesses in the model using porosities up to 1% are larger than those observed for Icelandic samples, which suggests that decay during melt transport has indeed an important effect on the ^{226}Ra - ^{230}Th disequilibria. The significant range of ^{230}Th at low ^{226}Ra excesses are especially not compatible with large porosity assuming negligible transport time (Fig. 8). The variability in ^{226}Ra - ^{230}Th disequilibria for Iceland shown in Figure 8 can be explained with porosities ranging between 0.1 and 1% at a melt transport time of 10 m/yr. Note, however, that the variability could similarly be explained by variations in melt velocities at a certain threshold porosity (section 4.5) and that it is difficult to distinguish the relative effects of these two parameters.

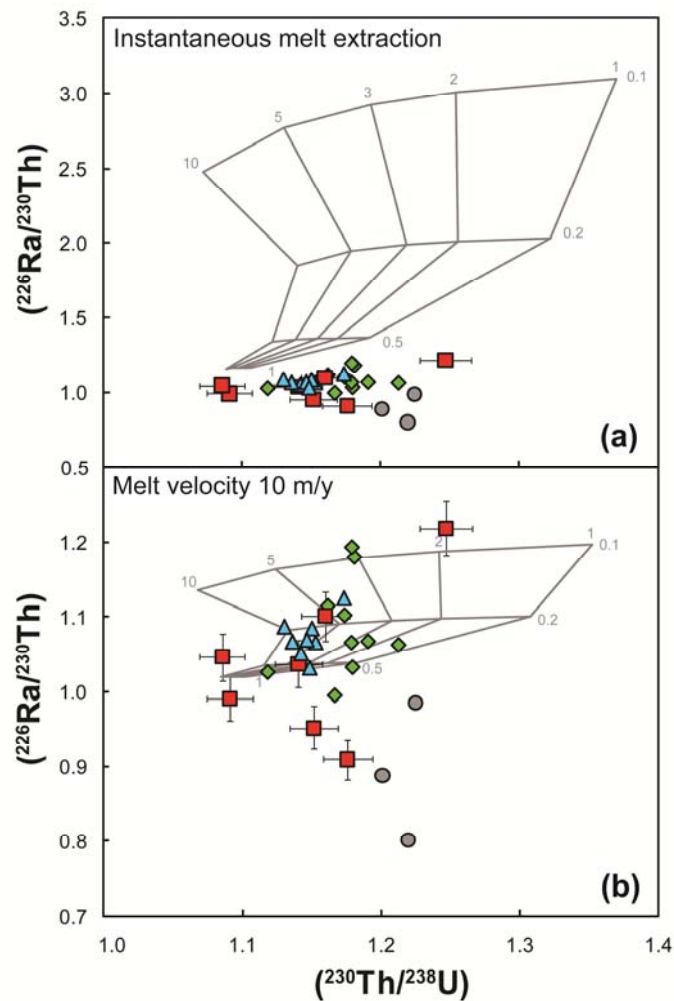


Figure 8. Dynamic melting model for variable upwelling velocities using different threshold porosities but assuming instantaneous melt extraction (a) and melt extraction of 10 m/y (b). Horizontal curves represent predicted disequilibria for variable upwelling velocities at a fixed porosity, whereas vertical, kinked curves are calculated for variable porosity at a fixed upwelling velocity. The combined ^{226}Ra - ^{230}Th excesses measured for Iceland can be explained with porosities ranging between 0.1 and 1% at a melt transport time of 10 m/yr.

4.7 The influence of source heterogeneity

The presence of mafic source heterogeneities could have a significant effect on the U-series disequilibria recorded by Icelandic basalts because larger melt productivity predicted for enriched mafic source lithologies results in higher melting rates (e.g., Hirschmann and Stolper, 1996; Pertermann and Hirschmann, 2003; Prytulak and Elliott, 2009; Stracke et al., 1999) (section 4.3). The mantle source beneath Iceland was shown to contain small-scale heterogeneities, which have been inferred to represent recycled oceanic crust (Chauvel and Hémond, 2000; Hanan et al., 2000; Kokfelt et al., 2006;

Skovgaard et al., 2001; Stracke and Bourdon, 2009; Stracke et al., 2003b). Strong depletion in Rb, Ba, U and Th and enrichment in Nb and Ta compared to La observed in the most enriched Icelandic samples suggest that the recycled component represents an E-MORB crust (Koornneef et al., 2011; McKenzie et al., 2004). Variable enrichments shown by high Nb/La and Nb/U and radiogenic Pb isotopic compositions for main rift lavas suggest that the proportion of the recycled enriched component is variable beneath the different main rift areas or that the enriched component is intrinsically heterogeneous in highly incompatible elements (Koornneef et al., 2011). In the Northern Volcanic Zone, including Theistareykir, limited enrichments indicate that the abundance of this component is small, whereas beneath the Western Volcanic Zone and the Reykjanes Peninsula, larger and highly variable enrichments suggest that the enriched component is more abundant and heterogeneously distributed. The local variability in U-series disequilibria as discussed in section 4.5 could result from melting a heterogeneous source with variable amounts of an enriched component. For example, samples with highest ($^{230}\text{Th}/^{238}\text{U}$) ratios on a local scale could represent melting the peridotite end-member characterised by low melt productivity whereas samples with the lowest ($^{230}\text{Th}/^{238}\text{U}$) could represent melting with more of an enriched end member with high melt productivity. In this scenario correlations between the U-series and incompatible trace elements and long-lived isotopes may be expected.

4.7.1 Evidence for variable melting behaviour?

As noted in section 4.5, the relatively low ^{230}Th -excesses at moderate ^{231}Pa -excess of WV25 and WV21 require a low bulk $D_{\text{U}}/D_{\text{Th}}$. These low $D_{\text{U}}/D_{\text{Th}}$ could either result from shallow melting in the spinel stability field or from melting a garnet pyroxenite with low $D_{\text{U}}/D_{\text{Th}}$. Low bulk $D_{\text{U}}/D_{\text{Th}}$ were determined experimentally for eclogite (run A343, Pertermann et al., (2004), Fig.6), and for a silica deficient pyroxenite by Elkins et al., (2008). Relatively fractionated Sm/Yb, Tb/Yb and Lu/Hf ratios for the WV samples with low ^{230}Th excess support the presence of garnet in their source (Fig. 10a). Furthermore, broad negative correlations between the ^{230}Th and ^{231}Pa excesses and U/Th, Nb/La and Nb/U ratios for WV samples and RP samples (Fig. 10) suggest a higher melting rate for samples that are more enriched. The combined low ^{231}Pa and ^{230}Th excesses and enriched highly incompatible element ratios therefore can be taken

as evidence for the influence of a mafic component with low D_U/D_{Th} and high melt productivity rather than melting a shallow spinel peridotite.

The combined U-series and highly incompatible trace element systematics of NV samples are opposite to those of the WV samples (Fig 9a, 10c), and thus the U-series variability for NV samples cannot be explained by mixing between a depleted peridotite and a recycled E-MORB, as the depleted component with low Th/U should have the largest ^{231}Pa excesses, which is not observed (Fig. 10c).

The well defined correlation between ($^{231}Pa/^{235}U$) and ($^{230}Th/^{232}Th$) for Icelandic samples (Fig 9b) can be used to extract information on the melting behaviour of the source, because these two ratios are controlled by different parameters: Although the ($^{231}Pa/^{235}U$) and ($^{230}Th/^{232}Th$) activity ratios are both a function of (1) the time available for ingrowth and/or decay of the daughter products and (2) the partition coefficients of U and the D_U/D_{Th} , the ($^{230}Th/^{232}Th$) ratio is also controlled by the U/Th concentration ratio of the source.

The fact that NV samples with a very different U/Th ratio compared to WV samples plot close to the WV samples in Fig. 9b suggests that they must result from melting a source with different melting behaviour. Note that the NV samples with low ($^{231}Pa/^{235}U$) are affected by mixing with melts/rocks that have low U/Th (see also section 4.1) whereas for the WV samples (WV25 and WV21) low ($^{231}Pa/^{235}U$) result from mixing with melts that have high U/Th (Fig 10c). Based on the low ($^{230}Th/^{238}U$) of WV samples, it can be inferred that the source with high U/Th has a low bulk D_U/D_{Th} . In contrast, NV samples with similarly low ($^{230}Th/^{232}Th$) and ($^{231}Pa/^{235}U$) as WV25 and WV21 but low U/Th must result from initial mantle melting at relatively high D_U/D_{Th} . The depleted WV31 and Theistareykir samples that have the highest ^{231}Pa excesses and high ($^{230}Th/^{232}Th$) also require melting a source at high bulk D_U/D_{Th} but with low to moderately U/Th ratio (Fig 9b, c).

The offset of the NV samples in the ($^{230}Th/^{238}U$) versus ($^{231}Pa/^{235}U$) diagram from the general positive correlation (Fig 3a, 6) may therefore result from melting at a relatively high bulk D_U/D_{Th} (at similar D_U) causing a horizontal shift in these diagrams, rather than resulting from assimilation and decay as discussed in section 4.1, which would result in an almost vertical shift. Melting at relatively high D_U/D_{Th} for NV samples can

also explain the high ($^{230}\text{Th}/^{238}\text{U}$) compared to the predicted values from the linear regression with distance from the plume (Fig. 7, section 4.4).

The relatively high melting rate predicted from the low ^{231}Pa excesses for NV samples could either result from higher melt productivity or from faster upwelling experienced by these samples. As the melt productivity for a depleted peridotite source is not predicted to vary by a large amount (section 4.3) the latter option is more likely.

In summary, it is inferred that NV samples that erupted close to the inferred plume centre result from melting a relatively depleted source with high $D_{\text{U}}/D_{\text{Th}}$ at a high upwelling velocity. Sample WV31 and the Theistareykir samples can be inferred to result from melting an even more depleted source with a relatively low melt productivity but high $D_{\text{U}}/D_{\text{Th}}$. Whereas WV samples with low ($^{230}\text{Th}/^{238}\text{U}$) and ($^{231}\text{Pa}/^{235}\text{U}$) result from melting an enriched source with low $D_{\text{U}}/D_{\text{Th}}$ at a high melt productivity. The required low bulk $D_{\text{U}}/D_{\text{Th}}$ for the source of WV samples is consistent with experimental melting of eclogite or Si-deficient pyroxenite (Elkins et al., 2008; Pertermann and Hirschmann, 2003).

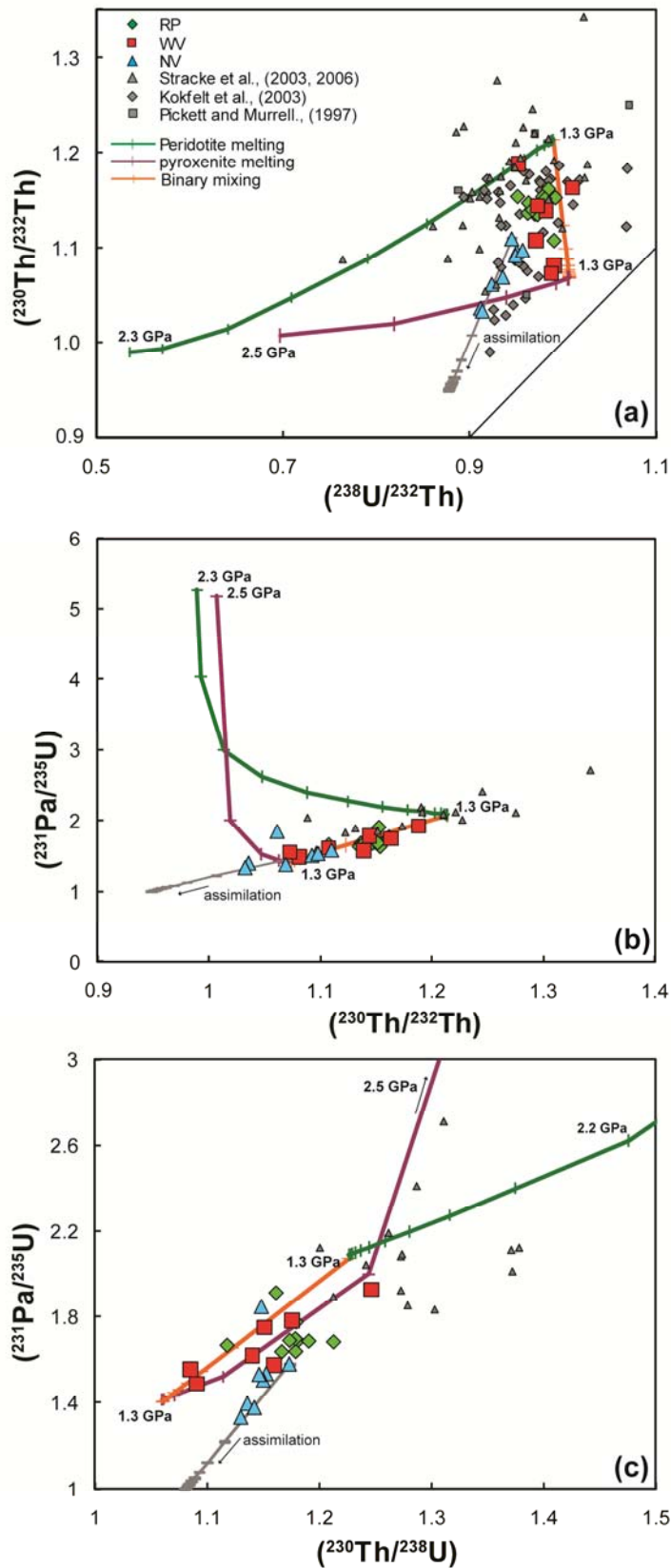


Figure 9. Diagrams of (a) $(^{230}\text{Th}/^{238}\text{U})$ versus $(^{231}\text{Pa}/^{235}\text{U})$, (b) $(^{230}\text{Th}/^{232}\text{Th})$ versus $(^{231}\text{Pa}/^{235}\text{U})$ and (c) $(^{226}\text{Ra}/^{230}\text{Th})$ versus $(^{231}\text{Pa}/^{235}\text{U})$ showing melting curves for a garnet peridotite (green) and a pyroxenite (purple) with low $D_{\text{U}}/D_{\text{Th}}$ that exhibits a high melt productivity. Binary mixing between the final accumulated melts is shown in orange. Tick marks on binary mixing curves represent 10% increments. Grey trends represent assimilation of sample NV48 by bulk rhyolite ($\text{Th} = 10$ ppm and Th/U of 3.6) assumed to be in secular equilibrium for $(^{231}\text{Pa}/^{235}\text{U})$ and have $(^{230}\text{Th}/^{238}\text{U})$ of 1.08.

4.7.2 Relationships between U-series and Hf and Nd isotopes

The positive correlation between ($^{231}\text{Pa}/^{235}\text{U}$) and Hf isotopic composition for WV and RP samples support melting and mixing of melts from two source components (Fig 10g). However, the relationships between ($^{230}\text{Th}/^{238}\text{U}$) and Hf and Nd isotopes are more ambiguous. Although the highly depleted WV31 and the Theistareykir samples with higher ^{231}Pa and ^{230}Th -excesses in general have higher Nd isotope composition compared to the other samples (Fig 10e-f), U-series data for RP and NV samples do not correlate with $^{143}\text{Nd}/^{144}\text{Nd}$.

Good correlations between Hf and Nd isotope compositions and trace element ratios that are sensitive to the degree of melting indicates that (at least) two source components present in the mantle beneath Iceland are sampled systematically as a function of the degree and pressure (Koornneef et al. 2011). In contrast to moderately incompatible elements and thus also Hf and Nd isotope ratios, highly incompatible element ratios and U-series disequilibria do not change significantly during progressive melting and mixing, which results in a decoupling of the long-lived Hf and Nd isotopes and U-series disequilibria. Thus, whereas the variability in Hf and Nd isotopic compositions is controlled by mixing during progressive melting and the depth of extraction of the mixed melts, the U-series variability is controlled by the melting behaviour at the onset of melting.

4.7.3 Mixing melts from a two-component source

Mixing between melts from a pyroxenite component and melts from the surrounding peridotite is a possible mechanism to create the large variability in ^{230}Th and ^{231}Pa excesses observed on a local scale in the Western volcanic zone and the Reykjanes peninsula. This hypothesis can be tested using a mixing model combined with the dynamic melting model for two source components that have different modal mineralogy, partitioning characteristics and melting behaviour (Table 2). The model applied here (section 4.3, Table 2) calculates compositions of instantaneous melts from two sources (depleted mantle and pyroxenite 1 in Table 2) separately and mixes the melts according to their relative mass proportions. For the sake of simplicity we assume here that the disequilibria for WV samples result from melting at a constant mantle upwelling velocity of 3 cm/yr.

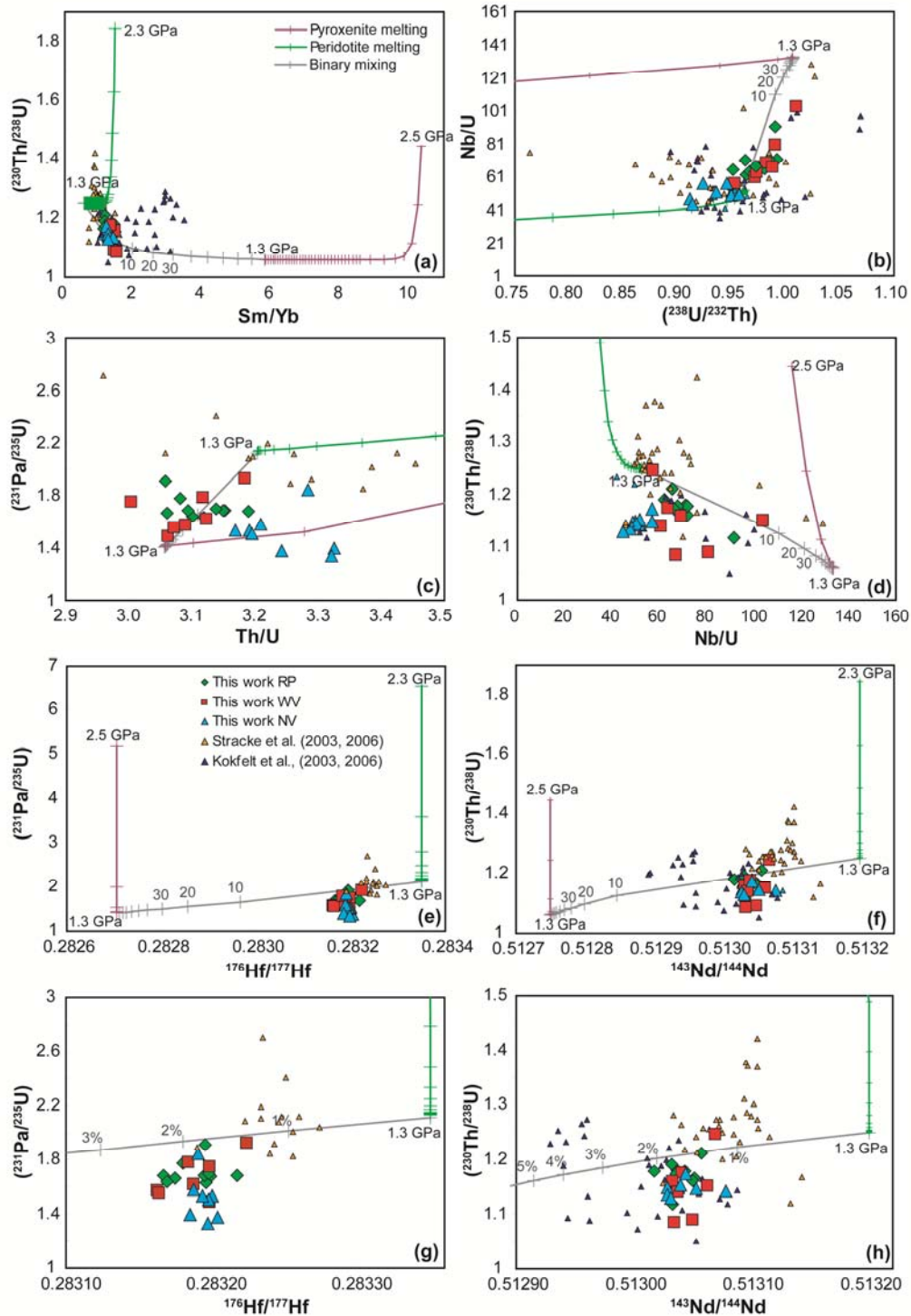


Figure 10. Combined trace element and Hf and Nd isotope ratios against $(^{230}\text{Th}/^{238}\text{U})$ and $(^{231}\text{Pa}/^{235}\text{U})$ with melting curves for a garnet peridotite and a pyroxenite (Table 2) and binary mixing curves where tick marks represent 10% increments of mixing between the peridotite and pyroxenite melts.

Koornneef et al. (2011) have established the importance of mixing of melts during melt extraction using a polybaric melting and mixing model that reproduced combined trace element and long-lived isotope data for Iceland. The model mixed the accumulated melts from the depleted mantle and a recycled E-MORB crust at every depth in the melting region. Due to the highly incompatible nature of the U-series nuclides the disequilibria for pure peridotitic or pyroxenitic sources calculated using dynamic melting only change significantly during the initial stages of melting (Fig. 9 and 10). Consequently, the effect of melting and mixing of a pyroxenite and a peridotite component and extraction of the mixed melts from various depths on the U-series disequilibria is small. As a result, the U-series disequilibria and highly incompatible trace element ratios of for Icelandic lavas can be approximated by binary mixing between the final accumulated melts from a peridotite and a recycled E-MORB (Fig 9 and 10).

The Nb/U, Nb/La and La/U ratios in Iceland main rift lavas correlate well with Th/U ratios suggesting that the enriched component is characterised by high Nb/U and Nb/La and a low Th/U ratio, whilst the depleted component has a high Th/U (Fig. 10b). Note that this is opposite to what is seen for other spreading ridges (e.g. EPR, Goldstein et al., 1993; Lundstrom et al., 1999) where the Th/U ratio of depleted samples is typically lower compared to enriched samples. Even though the variability in Th/U for Iceland's main rift lavas is small (3.004 to 3.325) the correlation with tracers for enrichment (Fig. 10b) is robust. WV Samples with lower Th/U but high Nb/U or Nb/La have relatively low ($^{231}\text{Pa}/^{235}\text{U}$) and ($^{230}\text{Th}/^{238}\text{U}$) (Fig. 9) whereas WV31 and Theistareykir samples have relatively low Nb/U but high Th/U have the highest ^{231}Pa and ^{230}Th excesses.

Mixing the depleted peridotite and enriched E-MORB component characterised by high melt productivity, but low $D_{\text{U}}/D_{\text{Th}}$ in variable proportions fits the variability of U-series disequilibria within the WV (and RP) group remarkably well (Fig 9). To explain the variability in U/Th by mixing with melts from a recycled E-MORB requires that the E-MORB end member has a Th concentration of ~ 0.135 ppm and a $\text{Th}/\text{U} \leq 3$.

In addition, the combined trace element and U-series data for Theistareykir, WV and RP samples is matched by mixing melts from the two components, supporting evidence for variable abundances of the enriched source component in the mantle beneath this part of Iceland (Fig. 10).

Table 2. Model input parameters

	Depleted mantle		50-50 E-MORB crust		
U (ppm)	0.0030		0.0448		
Th (ppm)	0.0092		0.1350		
Depth of melt initiation (km)	78		82		
Residual porosity (%)	0.10		0.10		
Productivity	onset	0.20%	>78 km	0.5-2.3%	
	final	2%	<78 km	0.55%	
Final degree of melting (%)	15		25		
Upwelling rate (cm/yr)	3		3		
Melt extraction velocity	infinite		infinite		

Mineral modes peridotite					
	ol	opx	cpx	gt	sp
Gt peridotite	0.53	0.08	0.34	0.05	0
Sp peridotite	0.53	0.26	0.18	0	0.03

KDs peridotite						
	ol	opx	hi Ca cpx	lo Ca cpx	gt	sp
U	0.00038	0.002	0.0113	0.0094	0.028	0
Th	0.00005	0.002	0.0057	0.0059	0.009	0

Bulk KD's peridotite			
	U	Th	U/Th
Gt peridotite	0.0056034	0.0025745	2.18
Sp peridotite	0.0024134	0.0016085	1.50

Mineral modes	Pyroxenite 1			Pyroxenite2		
	Pertermann et al., 2004			Pertermann et al., 2004		
	Run A343			Preferred		
	cpx	gt		cpx	gt	
	75	25		75	25	
KDs pyroxenite						
U	0.0041	0.0045		0.0041	0.02405	
Th	0.0032	0.0008		0.0032	0.00415	
Bulk KD						
	U	Th	U/Th	U	Th	U/Th
	0.420	0.260	1.62	0.909	0.344	2.64

4.7.4 Incomplete random mixing

As an alternative to complete mixing using variable abundances of the enriched component it was shown by Koornneef et al. (2011) that incomplete mixing and extraction of the incomplete mixtures from variable depths using a fixed source ratio could also reproduce combined trace element and long-lived isotope data for Iceland.

In this model the instantaneous melts of the peridotite and pyroxenite component are accumulated over 1 km depth intervals (= 0.03 GPa) and mixed according to their relative proportions at that depth (see Chapter 2). A constant peridotite- pyroxenite ratio of 97 : 3 is assumed according to the ratio that was found to be consistent with the data in Chapter 2. The pre-mixed melt batches are randomly and incompletely mixed over various pressure ranges to simulate extraction of the incompletely aggregated melts from various depths in the melt region. The probability (p) of mixing for each melt batch is assumed to be 0.8, i.e. the chance that the pre-mixed melt batches mix is 80%.

The model predicts considerable scatter for the incomplete random mixtures from a source containing 3% of pyroxenite (Fig. 11). For the highly incompatible elements, the extent of mixing with the initial deep melts is especially important in determining the final composition. Comparison of the model with the data indicates that: (1) Pure pyroxenite melts from the deepest parts of the melting column always mix with melts from the peridotite that form at lower pressures (2) Excluding the initial peridotite melt batch from mixing can be a mechanism to create melts with relatively low ^{230}Th and ^{231}Pa excesses but high Nb/U or U/Th such as the WV21 and WV25 samples. Furthermore these melts are also predicted to have high ($^{230}\text{Th}/^{232}\text{Th}$), which is opposite to what is seen for the WV samples. As was discussed earlier, to explain the combination of low ($^{230}\text{Th}/^{238}\text{U}$), ^{231}Pa -excess and low ($^{230}\text{Th}/^{232}\text{Th}$) ratios for WV21 and WV25 requires that these samples result from melting with a low $D_{\text{U}}/D_{\text{Th}}$. Mixing with larger abundances of melts from the pyroxenitic source with high Nb/U, U/Th, low $D_{\text{U}}/D_{\text{Th}}$ and high melt productivity is therefore the more likely scenario, rather than incomplete mixing of melts from a source with a fixed abundance ratio.

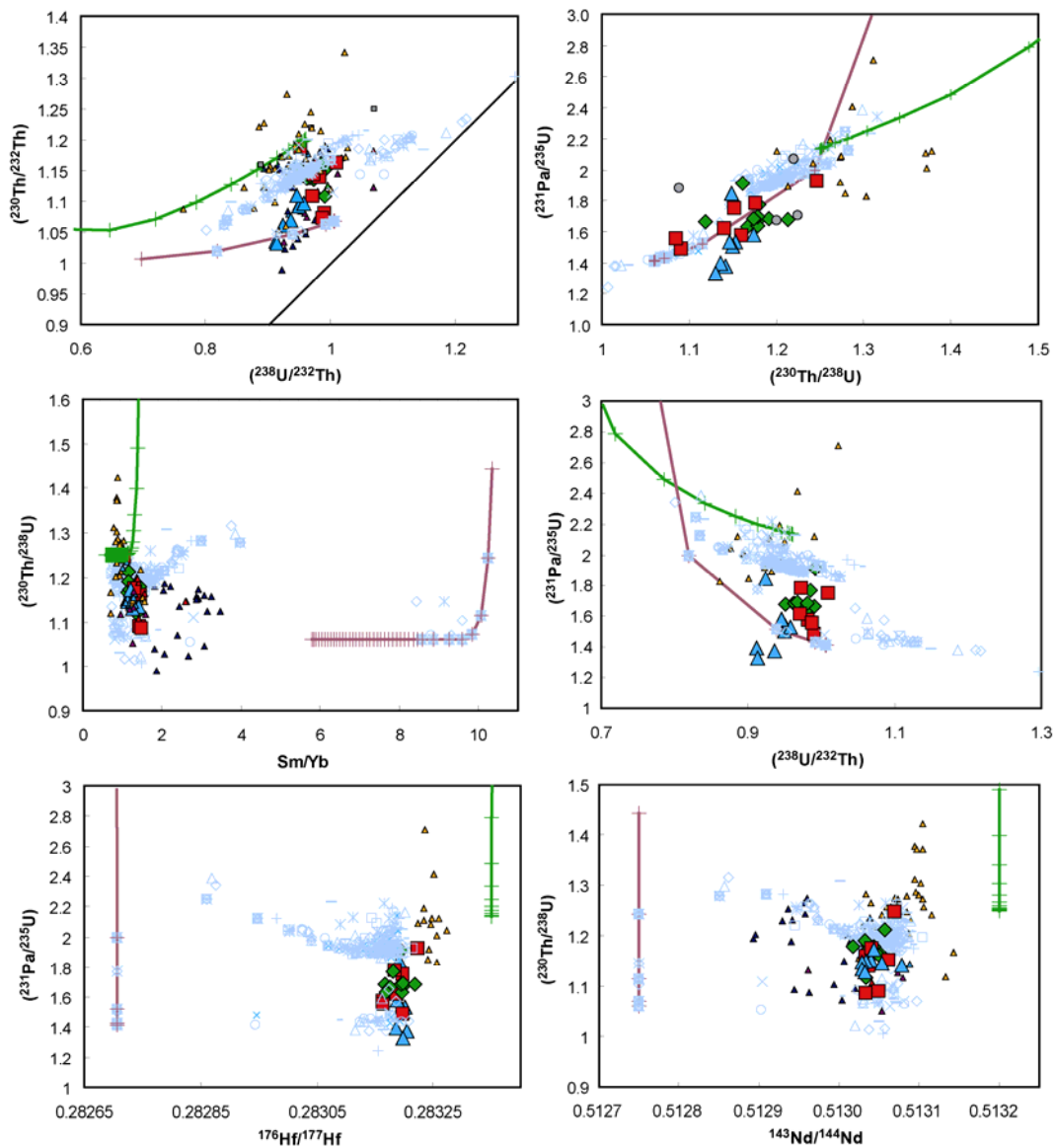


Figure 11. Diagrams for combined trace element and Hf and Nd isotope ratios against $(^{230}\text{Th}/^{238}\text{U})$ and $(^{231}\text{Pa}/^{235}\text{U})$ showing model calculations for incomplete and random mixing and extraction of these mixtures from variable depths. 10 random calculations are shown by different blue symbols for an initial peridotite-pyroxenite proportion of 97:3. Note that mixtures that do not include the initial peridotite melt batch have distinctly different compositions to the rest of the mixtures with relatively low ^{230}Th and ^{231}Pa excesses but high Nb/U or U/Th. Note, however, that these melts are also predicted to have high $(^{230}\text{Th}/^{232}\text{Th})$ which is opposite to what is seen for the WV samples.

In contrast, Prytulak and Elliott, (2008) who investigated the relation between melt productivity and the presence of pyroxenite in the melt source beneath the Azores based on combined ^{230}Th - ^{238}U and ^{231}Pa - ^{235}U disequilibria found no relation between

source composition and the U-series disequilibria. The limited variability in ^{230}Th and ^{231}Pa excesses were suggested to reflect melting of a peridotitic source alone and so a ‘distillation’ melting process that masks the effect of the mafic lithology was required. For Iceland, the relationship between highly incompatible trace element ratios and ^{231}Pa and ^{230}Th excesses indicates that the pyroxenitic melting behaviour is preserved in the melt mixtures and that a melt rock reaction as inferred by Prytulak et al., (2008) for the Azores is less likely beneath Iceland.

5. Conclusions

In agreement with previous U-series data for post-glacial tholeiites from Iceland’s main rift zones, it is found here that ^{230}Th and ^{231}Pa excesses correlate with distance from the plume centre. However, in addition to this overall positive relation we find significant variability on a local scale. The mean variation with distance from the plume centre can be explained by mantle upwelling velocities of ~ 9 cm/yr at the plume axis to ~ 2 cm/yr at the plume periphery. Variability from the mean regression at a local scale may partly be explained by decay during magma storage or slow melt transport, by variations in the threshold porosity and/or by variations in mantle upwelling velocity in the melting region at a local scale.

Based on the highly incompatible trace element, data there is, however, compelling evidence that the ($^{230}\text{Th}/^{238}\text{U}$) and ($^{231}\text{Pa}/^{235}\text{U}$) variability expressed by samples from the Western Volcanic Zone results from melting and mixing of melts from an enriched component that has a high melt productivity. This is consistent with the hypothesis that the most enriched samples in the Western Rift Zone of Iceland result from melting higher abundances of a recycled E-MORB component in the source. Low $^{230}\text{Th}/^{238}\text{U}$ activity ratios in the most enriched samples demonstrate that the enriched recycled component must have a low bulk $D_{\text{U}}/D_{\text{Th}}$, which is consistent with experimental melting of pyroxenite.

The majority of combined U-series and trace element data for Theistareykir, Western Rift Zone and Reykjanes Rift Zone samples are reproduced by binary mixing between melts from a garnet peridotite and a pyroxenite with high melt productivity. The combined low ($^{230}\text{Th}/^{232}\text{Th}$), ($^{230}\text{Th}/^{238}\text{U}$) and ($^{231}\text{Pa}/^{235}\text{U}$) at high U/Th for WV25 and WV21 samples necessitate larger amounts of pyroxenite in their source. Our results

exemplify therefore that important information on variability in regional mantle upwelling can be extracted from U-series disequilibria, but that lithological heterogeneities potentially affect the melting behaviour in MOR and OIB settings on a local scale.

References

- Asimow, P.D., Hirschmann, M.M. and Stolper, E.M., 1997. An analysis of variations in isentropic melt productivity. *Philosophical Transactions of the Royal Society a-Mathematical Physical and Engineering Sciences*, 355, 255-281.
- Asimow, P.D., Hirschmann, M.M. and Stolper, E.M., 2001. Calculation of peridotite partial melting from thermodynamic models of minerals and melts, IV. Adiabatic decompression and the composition and mean properties of mid-ocean ridge basalts. *Journal of Petrology*, 42, 963-998.
- Beattie, P., 1993a. The Generation of Uranium Series Disequilibria by Partial Melting of Spinel Peridotite - Constraints from Partitioning Studies. *Earth and Planetary Science Letters*, 117, 379-391.
- Beattie, P., 1993b. Uranium Thorium Disequilibria and Partitioning on Melting of Garnet Peridotite. *Nature*, 363, 63-65.
- Bijwaard, H. and Spakman, W., 1999. Tomographic evidence for a narrow whole mantle plume below Iceland. *Earth and Planetary Science Letters*, 166, 121-126.
- Blundy, J. and Wood, B., 2003. Mineral-melt partitioning of uranium, thorium and their daughters. *Rev Mineral Geochem* 52, 59-123.
- Bourdon, B., Joron, J.-L., Claude-Ivanaj, C. and Allegre, C.J., 1998. U-Th-Pa-Ra systematics for the Grande Comore volcanics: melting processes in an upwelling plume. *Earth and Planetary Science Letters*, 164, 119-133.
- Bourdon, B., Langmuir, C.H. and Zindler, A., 1996. Ridge-hotspot interaction along the Mid-Atlantic Ridge between 37[degree sign]30' and 40[degree sign]30'N: the U-Th disequilibrium evidence. *Earth and Planetary Science Letters*, 142, 175-189.
- Bourdon, B., Ribe, N.M., Stracke, A., Saal, A.E. and Turner, S.P., 2006. Insights into the dynamics of mantle plumes from uranium-series geochemistry. *Nature*, 444, 713-717.
- Bourdon, B. and Sims, K.W.W., 2003a. U-series constraints on intraplate basaltic magmatism. *Uranium-Series Geochemistry, Reviews in Mineralogy and Geochemistry* 52., 52, 215-254 pp.

- Bourdon, B. and Sims, K.W.W., 2003b. U-series constraints on intraplate basaltic magmatism. *Uranium-Series Geochemistry*, 52, 215-254.
- Bourdon, B., Turner, S.P. and Ribe, N.M., 2005. Partial melting and upwelling rates beneath the Azores from a U-series isotope perspective. *Earth and Planetary Science Letters*, 239, 42-56.
- Bourdon, B. and Van Orman, J.A., 2009. Melting of enriched mantle beneath Pitcairn seamounts: Unusual U-Th-Ra systematics provide insights into melt extraction processes. *Earth and Planetary Science Letters*, 277, 474-481.
- Chabaux, F., Othman, D.B. and Birck, J.L., 1994. A new Ra-Ba chromatographic separation and its application to Ra mass-spectrometric measurement in volcanic rocks. *Chemical Geology*, 114, 191-197.
- Chauvel, C. and Hémond, C., 2000. Melting of a complete section of recycled oceanic crust: Trace element and Pb isotopic evidence from Iceland. *Geochem. Geophys. Geosyst.*, 1, doi:10.1029/1999GC000002.
- Chekol, T.A., Kobayashi, K., Yokoyama, T., Sakaguchi, C. and Nakamura, E., 2010. Timescales of magma differentiation from basalt to andesite beneath Hekla Volcano, Iceland: Constraints from U-series disequilibria in lavas from the last quarter-millennium flows. *Geochimica et Cosmochimica Acta*, In Press, Accepted Manuscript.
- Claude-Ivanaj, C., Bourdon, B. and Allègre, C.J., 1998. Ra-Th-Sr isotope systematics in Grande Comore Island: a case study of plume-lithosphere interaction. *Earth and Planetary Science Letters*, 164, 99-117.
- Cohen, A. and O'Nions, S.R.K., 1993. Melting rates beneath Hawaii: Evidence from uranium series isotopes in recent lavas. *Earth and Planetary Science Letters*, 120, 169-175.
- Condomines, M., Morand, P., Allegre, C.J. and Sigvaldason, G., 1981. ^{230}Th - ^{238}U disequilibria in historical lavas from Iceland. *Earth and Planetary Science Letters*, 55, 393-406.
- Elkins, L.J., Gaetani, G.A. and Sims, K.W.W., 2008. Partitioning of U and Th during garnet pyroxenite partial melting: Constraints on the source of alkaline ocean island basalts. *Earth and Planetary Science Letters*, 265, 270-286.
- Elliott, T., Spiegelman, M., Heinrich, D.H. and Karl, K.T., 2003. Melt Migration in Oceanic Crustal Production: A U-series Perspective. In: *Treatise on Geochemistry*. Pergamon, Oxford, pp. 465-510.
- Elliott, T.R., Hawkesworth, C.J. and Gronvold, K., 1991. Dynamic Melting of the Iceland Plume. *Nature*, 351, 201-206.
- Fabbrizio, A., Schmidt, M.W., Gunther, D. and Eikenberg, J., 2009. Experimental determination of Ra mineral/melt partitioning for feldspars and Ra-226-disequilibrium crystallization ages of plagioclase and alkali-feldspar. *Earth and Planetary Science Letters*, 280, 137-148.

- Goldstein, S.J., Murrell, M.T. and Williams, R.W., 1993. ^{231}Pa and ^{230}Th chronology of mid-ocean ridge basalts. *Earth and Planetary Science Letters*, 115, 151-159.
- Hanan, B.B., Blichert-Toft, J., Kingsley, R. and Schilling, J.G., 2000. Depleted Iceland mantle plume geochemical signature: Artifact of multicomponent mixing? *Geochem. Geophys. Geosyst.*, 1, 1003, doi:10.1029/1999GC000009. .
- Hanan, B.B. and Schilling, J.G., 1997. The dynamic evolution of the Iceland mantle plume: the lead isotope perspective. *Earth and Planetary Science Letters*, 151, 43-60.
- Hauri, E.H., Wagner, T.P. and Grove, T.L., 1994. Experimental and Natural Partitioning of Th, U, Pb and Other Trace-Elements between Garnet, Clinopyroxene and Basaltic Melts. *Chemical Geology*, 117, 149-166.
- Hémond, C. et al., 1993. The Heterogeneous Iceland Plume - Nd-Sr-O Isotopes and Trace-Element Constraints. *Journal of Geophysical Research-Solid Earth*, 98, 15833-15850.
- Hirschmann, M.M., Asimow, P.D., Ghiorso, M.S. and Stolper, E.M., 1999. Calculation of peridotite partial melting from thermodynamic models of minerals and melts. III. Controls on isobaric melt production and the effect of water on melt production. *Journal of Petrology*, 40, 831-851.
- Hirschmann, M.M., Ghiorso, M.S., Wasylenki, L.E., Asimow, P.D. and Stolper, E.M., 1998. Calculation of peridotite partial melting from thermodynamic models of minerals and melts. I. Review of methods and comparison with experiments. *Journal of Petrology*, 39, 1091-1115.
- Hirschmann, M.M. and Stolper, E.M., 1996. A possible role for garnet pyroxenite in the origin of the "garnet signature" in MORB. *Contributions to Mineralogy and Petrology*, 124, 185-208.
- Ito, G., Lin, J. and Gable, C.W., 1996. Dynamics of mantle flow and melting at a ridge-centered hotspot: Iceland and the Mid-Atlantic Ridge. *Earth and Planetary Science Letters*, 144, 53-74.
- Iwamori, H., 1993. A model for disequilibrium mantle melting incorporating melt transport by porous and channel flows. *Nature*, 366, 734-737.
- Jull, M., Kelemen, P. and Sims, K.W.W., 2002. Consequences of diffuse and channelled porous melt migration on uranium series disequilibria. *Geochimica et Cosmochimica Acta*, 66, 4133-4148.
- Klemme, S., Blundy, J.D. and Wood, B.J., 2002. Experimental constraints on major and trace element partitioning during partial melting of eclogite. *Geochimica Et Cosmochimica Acta*, 66, 3109-3123.
- Kogiso, T., Hirschmann, M.M. and Pertermann, M., 2004. High-pressure partial melting of mafic lithologies in the mantle. *Journal of Petrology*, 45, 2407-2422.

- Kokfelt, T.F., Hoernle, K. and Hauff, F., 2003. Upwelling and melting of the Iceland plume from radial variation of ^{238}U - ^{230}Th disequilibria in postglacial volcanic rocks. *Earth and Planetary Science Letters*, 214, 167-186.
- Kokfelt, T.F. et al., 2006. Combined traced element and Pb-Nd-Sr-O isotope evidence for recycled oceanic crust (upper and lower) in the Iceland mantle plume. *Journal of Petrology*, 47, 1705-1749.
- Koornneef, J.M., Stracke, A., Aciego, S., Reubi, O. and Bourdon, B., 2010. A new method for U-Th-Pa-Ra separation and accurate measurement of ^{234}U - ^{230}Th - ^{231}Pa - ^{226}Ra disequilibria in volcanic rocks by MC-ICPMS. *Chemical Geology*, 277, 30-41.
- Koornneef, J.M. et al., 2011. Melting of a two-component source beneath Iceland. Submitted to *Journal of Petrology*.
- LaTourrette, T.Z. and Burnett, D.S., 1992. Experimental-Determination of U-Partitioning and Th-Partitioning between Clinopyroxene and Natural and Synthetic Basaltic Liquid. *Earth and Planetary Science Letters*, 110, 227-244.
- LaTourrette, T.Z., Kennedy, A.K. and Wasserburg, G.J., 1993. Thorium-Uranium Fractionation by Garnet - Evidence for a Deep Source and Rapid Rise of Oceanic Basalts. *Science*, 261, 739-742.
- Lundstrom, C., 2001. Models of U-series disequilibria generation in MORB: the effects of two scales of melt porosity. *Physics of the Earth and Planetary Interiors*, 121, 189-204.
- Lundstrom, C.C., Gill, J. and Williams, Q., 2000. A geochemically consistent hypothesis for MORB generation. *Chemical Geology*, 162, 105-126.
- Lundstrom, C.C., Gill, J., Williams, Q. and Perfit, M.R., 1995. Mantle Melting and Basalt Extraction by Equilibrium Porous Flow. *Science*, 270, 1958-1961.
- Lundstrom, C.C., Hoernle, K. and Gill, J., 2003. U-series disequilibria in volcanic rocks from the Canary Islands: Plume versus lithospheric melting. *Geochimica Et Cosmochimica Acta*, 67, 4153-4177.
- Lundstrom, C.C., Sampson, D.E., Perfit, M.R., Gill, J. and Williams, Q., 1999. Insights into mid-ocean ridge basalt petrogenesis: U-series disequilibria from the Siqueiros Transform, Lamont Seamounts, and East Pacific Rise. *Journal of Geophysical Research-Solid Earth*, 104, 13035-13048.
- Lundstrom, C.C., Williams, Q. and Gill, J.B., 1998. Investigating solid mantle upwelling rates beneath mid-ocean ridges using U-series disequilibria, 1: a global approach. *Earth and Planetary Science Letters*, 157, 151-165.
- MacLennan, J., 2008. Concurrent Mixing and Cooling of Melts under Iceland. *Journal of Petrology*, 49, 1931-1953.

- Maclennan, J. et al., 2003a. Melt mixing and crystallization under Theistareykir, northeast Iceland. *Geochemistry Geophysics Geosystems*, 4, 8624, doi:10.1029/2003gc000558.
- Maclennan, J., McKenzie, D., Hilton, F., Gronvold, K. and Shimizu, N., 2003b. Geochemical variability in a single flow from northern Iceland. *Journal of Geophysical Research-Solid Earth*, 108.
- McDade, P., Blundy, J.D. and Wood, B.J., 2003. Trace element partitioning on the Tinaquillo Lherzolite solidus at 1.5 GPa. *Physics of the Earth and Planetary Interiors*, 139, 129-147.
- McKenzie, D., 1985. ^{230}Th - ^{238}U disequilibrium and the melting processes beneath ridge axes. *Earth and Planetary Science Letters*, 72, 149-157.
- McKenzie, D. and Bickle, M.J., 1988. The Volume and Composition of Melt Generated by Extension of the Lithosphere, pp. 625-679.
- McKenzie, D. et al., 2004. Source enrichment processes responsible for isotopic anomalies in oceanic island basalts. *Geochimica Et Cosmochimica Acta*, 68, 2699-2724.
- Montelli, R., Nolet, G., Masters, G., Dahlen, F.A. and Hung, S.H., 2004. Global P and PP traveltimes tomography: rays versus waves. *Geophysical Journal International*, 158, 637-654.
- Olson, P., Schubert, G. and Anderson, C., 1993. Structure of Axisymmetrical Mantle Plumes. *Journal of Geophysical Research-Solid Earth*, 98, 6829-6844.
- Peate, D. et al., 2009. Historic magmatism on the Reykjanes Peninsula, Iceland: a snap-shot of melt generation at a ridge segment. *Contributions to Mineralogy and Petrology*, 157, 359-382.
- Peate, D.W., Hawkesworth, C.J., van Calsteren, P.W., Taylor, R.N. and Murton, B.J., 2001. ^{238}U - ^{230}Th constraints on mantle upwelling and plume-ridge interaction along the Reykjanes Ridge. *Earth and Planetary Science Letters*, 187, 259-272.
- Pertermann, M. and Hirschmann, M.M., 2002. Trace-element partitioning between vacancy-rich eclogitic clinopyroxene and silicate melt. *American Mineralogist*, 87, 1365-1376.
- Pertermann, M. and Hirschmann, M.M., 2003. Partial melting experiments on a MORB-like pyroxenite between 2 and 3 GPa: Constraints on the presence of pyroxenite in basalt source regions from solidus location and melting rate. *Journal of Geophysical Research-Solid Earth*, 108.
- Pertermann, M., Hirschmann, M.M., Hametner, K., Gunther, D. and Schmidt, M.W., 2004. Experimental determination of trace element partitioning between garnet and silica-rich liquid during anhydrous partial melting of MORB-like eclogite. *Geochemistry Geophysics Geosystems*, 5, Q05A01, doi:10.1029/2003gc000638.
- Pickett, D.A. and Murrell, M.T., 1997. Observations of $^{231}\text{Pa}/^{235}\text{U}$ disequilibrium in volcanic rocks. *Earth and Planetary Science Letters*, 148, 259-271.

- Pietruszka, A.J., Hauri, E.H. and Blichert-Toft, J., 2009. Crustal Contamination of Mantle-derived Magmas within Piton de la Fournaise Volcano, Reunion Island. *Journal of Petrology*, 50, 661-684.
- Prytulak, J. and Elliott, T., 2009. Determining melt productivity of mantle sources from ^{238}U - ^{230}Th - and ^{235}U - ^{231}Pa disequilibria; an example from Pico Island, Azores. *Geochimica Et Cosmochimica Acta*, 73, 2103-2122.
- Ribe, N.M., Christensen, U.R. and Theissing, J., 1995. The Dynamics of Plume-Ridge Interaction .1. Ridge-Centered Plumes. *Earth and Planetary Science Letters*, 134, 155-168.
- Ruedas, T., Schmeling, H., Marquart, G., Kreutzmann, A. and Junge, A., 2004. Temperature and melting of a ridge-centred plume with application to Iceland. Part I: Dynamics and crust production. *Geophysical Journal International*, 158, 729-743.
- Russo, C.J., Rubin, K.H. and Graham, D.W., 2009. Mantle melting and magma supply to the Southeast Indian Ridge: The roles of lithology and melting conditions from U-series disequilibria. *Earth and Planetary Science Letters*, 278, 55-66.
- Salters, V.J.M. and Longhi, J., 1999. Trace element partitioning during the initial stages of melting beneath mid-ocean ridges. *Earth and Planetary Science Letters*, 166, 15-30.
- Salters, V.J.M., Longhi, J.E. and Bizimis, M., 2002. Near mantle solidus trace element partitioning at pressures up to 3.4 GPa. *Geochemistry Geophysics Geosystems*, 3, 1038, doi:10.1029/2001gc000148.
- Schilling, J., 1973. Iceland Mantle Plume - Geochemical Study of Reykjanes Ridge. *Nature*, 242, 565-571.
- Shen, Y., Solomon, S.C., Bjarnason, I.T. and Wolfe, C.J., 1998. Seismic evidence for a lower-mantle origin of the Iceland plume. *Nature*, 395, 62-65.
- Sigmarsson, O., Condomines, M. and Fourcade, S., 1992. Mantle and crustal contribution in the genesis of Recent basalts from off-rift zones in Iceland: Constraints from Th, Sr and O isotopes. *Earth and Planetary Science Letters*, 110, 149-162.
- Sigmarsson, O., Hemond, C., Condomines, M., Fourcade, S. and Oskarsson, N., 1991. Origin of Silicic Magma in Iceland Revealed by Th Isotopes. *Geology*, 19, 621-624.
- Sims et al., (K.W.W.S., Donald J. DePaolo 2, Michael T. Murrell 3, W. Scott Baldrige 3, Steven J. Goldstein 3, and David A. Clague) 1995. Mechanisms of Magma Generation Beneath Hawaii and Mid-Ocean Ridges: Uranium/Thorium and Samarium/Neodymium Isotopic Evidence. *Science*, 267.
- Sims, K.W.W. et al., 1999. Porosity of the melting zone and variations in the solid mantle upwelling rate beneath Hawaii: inferences from ^{238}U - ^{230}Th - ^{226}Ra and ^{235}U - ^{231}Pa disequilibria. *Geochimica et Cosmochimica Acta*, 63, 4119-4138.

- Sims, K.W.W. et al., 2002. Chemical and isotopic constraints on the generation and transport of magma beneath the East Pacific Rise. *Geochimica et Cosmochimica Acta*, 66, 3481-3504.
- Sinton, J., K. Grönvold, and K. Sæmundsson, 2005. Postglacial eruptive history of the Western Volcanic Zone, Iceland. *Geochem. Geophys. Geosyst.*, 6, Q12009, doi:10.1029/2005GC001021.
- Skovgaard, A.C., Storey, M., Baker, J., Blusztajn, J. and Hart, S.R., 2001. Osmium-oxygen isotopic evidence for a recycled and strongly depleted component in the Iceland mantle plume. *Earth and Planetary Science Letters*, 194, 259-275.
- Slater, L., McKenzie, D.A.N., Grönvold, K. and Shimizu, N., 2001. Melt Generation and Movement beneath Theistareykir, NE Iceland, pp. 321-354.
- Spiegelman, M. and Elliott, T., 1993. Consequences of melt transport for uranium series disequilibrium in young lavas. *Earth and Planetary Science Letters*, 118, 1-20.
- Stolper, E. and Asimow, P., 2007. Insights into mantle melting from graphical analysis of one-component systems. *American Journal of Science*, 307, 1051-1139.
- Stracke, A. and Bourdon, B., 2009. The importance of melt extraction for tracing mantle heterogeneity. *Geochimica Et Cosmochimica Acta*, 73, 218-238.
- Stracke, A., Bourdon, B. and McKenzie, D., 2006. Melt extraction in the Earth's mantle: Constraints from U-Th-Pa-Ra studies in oceanic basalts. *Earth and Planetary Science Letters*, 244, 97-112.
- Stracke, A., Salters, V.J.M. and Sims, K.W.W., 1999. Assessing the presence of garnet-pyroxenite in the mantle sources of basalts through combined hafnium-neodymium-thorium isotope systematics. *Geochem. Geophys. Geosyst.*, 1, 1006, doi. 10.1029/1999GC000013.
- Stracke, A., Zindler, A., Salters, V.J.M., McKenzie, D. and Grönvold, K., 2003a. The dynamics of melting beneath Theistareykir, northern Iceland. *Geochem. Geophys. Geosyst.*, 4, 8513, doi: 10.1029/2002GC000347.
- Stracke, A. et al., 2003b. Theistareykir revisited. *Geochemistry Geophysics Geosystems*, 4, 8507, doi: 10.1029/2001GC000201.
- Sturm, M.E., Goldstein, S.J., Klein, E.M., Karson, J.A. and Murrell, M.T., 2000. Uranium-series age constraints on lavas from the axial valley of the Mid-Atlantic Ridge, MARK area. *Earth and Planetary Science Letters*, 181, 61-70.
- Turner, S., Hawkesworth, C., Rogers, N. and King, P., 1997. U-Th isotope disequilibria and ocean island basalt generation in the Azores. *Chemical Geology*, 139, 145-164.
- Widom, E., Schmincke, H.U. and Gill, J.B., 1992. Processes and timescales in the evolution of a chemically zoned trachyte - Fogo-a, Sao-Miguel, Azores. *Contributions to Mineralogy and Petrology*, 111, 311-328.

-
- Wolfe, C.J., Bjanason, I.Th., Vandecar, C.J., Solomon, S.C., 1997. Seismic structure of the Iceland mantle plume. *Nature*, 385, 245-247.
- Wood, B.J., Blundy, J.D. and Robinson, J.A.C., 1999. The role of clinopyroxene in generating U-series disequilibrium during mantle melting. *Geochimica Et Cosmochimica Acta*, 63, 1613-1620.
- Wood, D.A., 1981. Partial Melting Models for the Petrogenesis of Reykjanes Peninsula Basalts, Iceland - Implications for the Use of Trace-Elements and Strontium and Neodymium Isotope Ratios to Record Inhomogeneities in the Upper Mantle. *Earth and Planetary Science Letters*, 52, 183-190.
- Zindler, A., Hart, S.R., Frey, F.A. and Jakobsson, S.P., 1979. Nd and Sr Isotope Ratios and Rare-Earth Element Abundances in Reykjanes Peninsula Basalts - Evidence for Mantle Heterogeneity beneath Iceland. *Earth and Planetary Science Letters*, 45, 249-262.

Chapter 5

In situ analysis of U-Th disequilibria in titanite by femto second laser- ablation multi-collector ICP-MS

An application to Laacher See Volcano, East Eifel,
Germany, to derive time-scales of crystal growth

1. Introduction

1.1 U-series constraints on time scales of magma differentiation of Laacher See

U-series can, apart from their use as tracers to constrain timing of primary mantle melting processes discussed in Chapter 4, also be used to determine the time scales of magma evolution in crustal reservoirs. The fractionation between parent and daughter nuclides during fractional crystallization by U and Th enriched phenocrysts (e.g. zircon, titanite and apatite), can result in ($^{230}\text{Th}/^{238}\text{U}$) disequilibria. Analysis of different mineral phases present in the erupted lavas reflect the crystallization age provided that the minerals crystallized in a short time interval, initially had the same ($^{230}\text{Th}/^{232}\text{Th}$) and that the system remained closed after crystallization (Condomines et al., 2003).

Bourdon et al., (1994) (Bourdon et al., 1994) applied this technique to pumices and cumulate nodules from Laacher See Volcano, in East Eifel, Germany, to constrain the timing of differentiation from mafic to evolved magmas. The Laacher See Volcanic deposits (12.9 kyr BP) are unique in that they represent the eruption products of a mineralogically and chemically zoned phonolitic magma chamber that erupted consecutively from the top to the bottom of the reservoir (Wörner et al., 1983; Wörner, 1987; Worner et al., 1985; Worner and Wright, 1984). Bourdon et al., (1994), measured Th and U concentrations and isotopic compositions of purified mineral separates (feldspar, hauyne, amphibole, titanite, apatite and magnetite) and glass separates by SIMS and TIMS. The minerals from pumices recorded ages indistinguishable from the eruption age. The cumulate nodules yielded more imprecise ages that are 10-20 kyr older than the eruption age, which was thought to reflect the timescale of crystallisation.

These time scales are in accordance with estimates by Tait et al., (1989), who suggested that the zonation formed by convective fractionation and by (Wolff et al., 1990) who estimated the duration of fractionation for alkaline systems such as Laacher See of $10^3 - 10^4$ yrs. Recently, Schmidt et al., (2010) (Schmitt et al.) obtained refined U-Th isochron ages using zircons from Laacher See carbonatites that also support magmatic longevity of 10-20 kyr prior to eruption. The large range of estimated ages for the mafic cumulates found by Bourdon et al., (1994) was suggested to reflect residence of the crystallizing phases in a cooling boundary layer with temperatures between the liquidus and the solidus for longer periods of time. The crystals in this mushy boundary layer therefore possibly record a large age range as they grow over longer time spans.

Bulk analysis of these crystal separates therefore likely yield mean crystallization ages for the zoned phenocrysts.

To further investigate these crystallization ages, in-situ laser ablation (LA) MC-ICPMS analyses of individual titanite (sphene) and apatite cumulate crystals were performed in cooperation with the Laboratory of Inorganic Chemistry, at ETH Zürich. We aimed at identifying variability in the U-Th disequilibria of various U and Th rich crystals within a single cumulate sample and potentially also the spatial variability within the individual grains (i.e. core to rim).

1.2 In-situ analyses of U-series disequilibria

Previous in-situ measurements of U-series disequilibria have been conducted in various ways: (1) by micro sampling using a micro drill or saw combined with conventional sample dissolution, chemical separation, and analysis by TIMS or MC-ICPMS (Hoffmann et al., 2009; Neymark and Paces, 2000; Paces et al., 1998), (2) by in situ analysis by secondary ionization mass spectrometry (SIMS) (Bacon et al., 2000; Lowenstern et al., 2000; Paces et al., 2004; Reid et al., 1997; Schmitt, 2006; Schmitt et al.) and (3) by laser ablation (LA) MC-ICPMS (Bernal et al., 2005; Eggins et al., 2005; Potter et al., 2005; Stirling et al., 2000). The great benefit of LA analyses is that the technique is less labor intensive and time consuming and therefore permits larger sample throughput than micro-drilling followed by mass spectrometry. Compared to SIMS, a technique that allows excellent spatial resolution, LA-MC-ICPMS analyses are less limited by isobaric interferences, which are negligible at the high mass range using dry plasma conditions (Stirling et al., 2000). LA-MC-ICPMS data were previously reported for carbonates, Fe-hydroxides and teeth (Bernal et al., 2006; Eggins et al., 2005; Hoffmann et al., 2009; Potter et al., 2005) and for silicate glass, opal and zircon (Bernal et al., 2005; Stirling et al., 2000). However, the total number of studies and the types of materials analysed, remains to date relatively limited.

Analyses of silicate samples by LA-MC-ICPMS are especially challenging owing to the extreme isotope ratios (e.g. $^{232}\text{Th}/^{230}\text{Th} \sim 1 \times 10^4 - 10^5$ or $^{238}\text{U}/^{234}\text{U} \sim 1.8 \times 10^4$) requiring the use of an ion counting system in conjunction with Faraday cups. Additionally, the efficiency of sample transfer and ionization of U and Th from the aerosol in the plasma is limited to a few permils, which necessitates application of the technique to samples that contain high concentrations of U (and Th).

The other major challenge for obtaining the high level of accuracy needed to spatially resolve the variations in ($^{230}\text{Th}/^{238}\text{U}$) by La-MC-ICPMS is to effectively correct for elemental fractionation between U and Th in the ablation process and in the ICP source. Elemental fractionation in LA-(MC)-ICPMS is controlled by (1) evaporation and redistribution processes at the ablation site (e.g. Eggins et al., 1998; Le Harzic et al., 2002; Mank and Mason, 1999; Poitrasson et al., 2003) (2) differences in ionization efficiencies between elements in the plasma, and (3) the ablation aerosol particle size distribution and therefore plasma mass load (e.g. Guillong and Gunther, 2002; Koch and Gunther, 2007). More efficient sample transport and vaporization at the ablation site was demonstrated for short pulse femto second (fs) laser ablation which produces relatively finer aerosols (Koch et al., 2008). In this chapter I describe the techniques that we developed to accurately and precisely measure U-Th disequilibria in titanite and apatite by fs-LA-MC-ICPMS.

2. Analytical methods

2.1 System set-up

2.1.1 Mass spectrometry

The measurements were carried out using a Nu Plasma MC-ICPMS (Nu Plasma HR, Nu Instruments) at the Laboratory of Inorganic Chemistry, ETH Zürich. The instrument is equipped with 12 Faraday cups and three discrete dynode secondary electron multipliers (SEM) operating in pulse counting mode (IC0, IC1 and IC2). IC0 is equipped with an energy filter that improves abundance sensitivity. A membrane desolvation system (DSN-100, Nu Instruments) was operated with a PFA nebuliser (uptake rate of 20 $\mu\text{l}/\text{min}$) and was connected as the Ar mix gas to introduce solution standards for interspersed determinations of relative Faraday-ion counter gain and abundance sensitivity. The laser sample carrier gas is mixed with the Ar flow from the DSN prior to introduction into the plasma. An overview of operating conditions is given in Table 1. The instrument was allowed to stabilize at least two hours before measurement initiation. Tuning of the instrument and gas flows was done at the start of each analytical session to gain optimal sensitivity at stable plasma conditions (Fontaine et al., 2009).

Table 1. MC-ICPMS operating parameters

RF power	1300 W
Ar cooling gas flow rate	13 L/min
Ar sample gas flow rate	0.75 L/min
Ar nebuliser gas pressure	28.0 - 30.3 psi
Membrane sweep gas	2.7 - 3.4 l/min, ~120 °C
Spray chamber gas	0.25 L/min, ~110 °C
Interface cones	Nickel
Ion-lens settings	Regularly optimized for signal intensity and stability
Mass analyzer pressure	$3 \times 10^{-9} - 3 \times 10^{-8}$ mbar
Resolution mode	Low (400)
Detection system	Faraday cups (9), IC0, IC1, IC2
Signal analysis set-up	5 sec integration, 1 block, 20 cycles
Backgrounds	30s by ESA deflection
Nebulizer and uptake rate	Aridus microcentric PFA, 20 μ l/min
Typical sensitivity on ^{238}U mass	~0.5 V per ppb in 0.2% HCl: 0.2%HF

2.1.2 Laser ablation

The femto second laser at the Laboratory of Inorganic Chemistry, ETH, Zürich, is a chirped pulse amplification (CPA)-type Ti-sapphire-based laser system (Legend, Coherent Inc., Santa Clara, CA, USA) operated at a near infra red (NIR) centre wavelength of 800 nm producing pulses of < 150 fs duration at variable repetition rates and output energies of 2-3 mJ. The NIR wavelength can be converted to its third harmonic to obtain a UV wavelength of 265nm. The frequency doubling of the fundamental wavelength and mixing with the 2nd harmonic is done in a converting crystal (for details see, Koch et al., 2006). The laser radiation was focused onto the surface of the target sample positioned inside a cylindrical ablation cell ($V = 20 \text{ cm}^3$) (Fig. 1). In this study depth profile analyses with crater diameters of ~100 μm are employed as the aim was to sample and analyze specific growth zones in the Laacher See titanites and apatites. The cell was mounted on a stage that can be moved by computer control in the x, y and z directions. A CCD camera equipped with variable magnification was used for sample observation. Ablation aerosols were produced under helium atmosphere and transported to the mass spectrometer using a flow rate of ~0.9 L/min. The He sample flow was mixed with the Ar mix gas from the DSN (0.75 L/min) in a laminar flow adapter.

Table 2. Femto second laser ablation operating parameters

Centre NIR wavelength	800 nm
Converted UV wavelength	265 nm
Pit size	~100 μm
Energy at NIR	2800 μJ , Fluence ~36 J/cm^2
Energy at UV	170-230 μJ , Fluence 2.2 - 2.9 J/cm^2
Pulse rate	5-15 Hz
Carrier gas	Helium
He sample gas flow rate	0.8-0.9 L/min

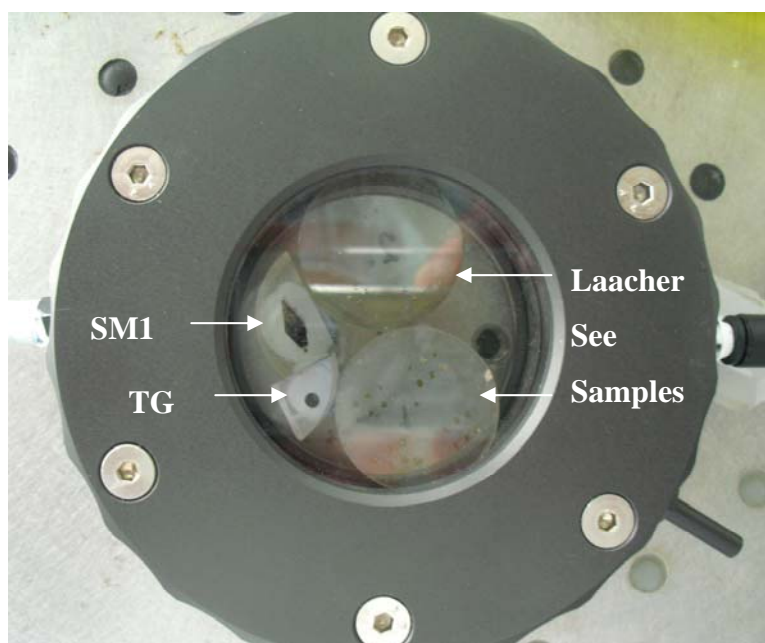


Fig. 1. The laser ablation cell loaded with standard materials SM1 (Large dark mineral), TG (small round glass) and Laacher See sample rings 1 (bottom right) and 2 (top right).

2.2 Reference materials and samples

2.2.1 LA reference materials

Existing micro analytical standard reference materials NIST611 and 613 are depleted in ^{235}U and ^{234}U relative to ^{238}U and have no detectable ^{230}Th , making them inappropriate as standards in the analyses of ($^{230}\text{Th}/^{238}\text{U}$) ratios (Bernal et al., 2005; Stirling et al., 2000). Furthermore, it was shown that matrix-matched standards are required for successful correction of elemental fractionation in LA-ICPMS analyses (e.g. Eggins et al., 1998; Guenther et al., 1997; Hirata and Nesbitt, 1995; Jeffries et al., 1996; Mank and Mason, 1999). We therefore aimed at obtaining homogeneous titanite and apatite standard minerals in U-series equilibrium (i.e. older than 350 kyr). Ideally, the standards should have similar concentrations to our target samples from the Laacher See Volcano.

Multiple natural apatite and titanite minerals obtained from the ETH mineral collection were checked for homogeneity by LA-ICPMS. This yielded a suitable apatite standard (AP1). However, all titanite minerals were found to be heterogeneous in their U and Th compositions. Even though the $^{230}\text{Th}/^{238}\text{U}$ in these heterogeneous minerals is still expected to be constant, fluctuations in the U/Th ratios would preclude use of the larger ^{232}Th and ^{235}U beams and the $^{232}\text{Th}/^{235}\text{U}$ ratio as a direct monitor for elemental

fractionation. Three of the titanite minerals were nevertheless used as standard materials in our tests: a dark titanite from Arendal, Norway (SM), a large brown titanite with unknown origin (SM2), and yellow/brown titanite from the Adamello granodiorite (SAD, dated to be 40.2 Ma). Preparation of the standards involved mounting in epoxy and polishing to acquire a flat surface.

Klemme et al., (2008) (Klemme et al., 2008) produced homogeneous synthesized titanite and apatite glasses (see also, Odegard et al., 2005) that were proposed to be suitable reference materials for U-series analyses by LA-MC-ICPMS. Analyses of these glasses (TNT150, TNT1500, STDP3 and STDP5) at ETH Zürich by solution mode MC-ICPMS showed, however, that the synthetic glasses contained no detectable ^{230}Th , making them unsuitable as standards for ($^{230}\text{Th}/^{238}\text{U}$) activity measurements.

Hence, in-house reference glasses were produced by fusion of powders from natural titanite (and apatite) minerals in secular equilibrium. In a first effort, 36 mg of titanite powder from SM2 was loaded in a Pt crucible, heated in a muffle furnace to 1520 °C for three hours and quenched rapidly in water (cooling rates of 500-1000 °C/s). Tests by LA-ICPMS demonstrated that this procedure yielded a homogeneous titanite glass indicating that 3 hours was sufficient to erase all chemical gradients by diffusion in the liquid. The first analyses by LA-MC-ICPMS revealed, however, that significant amounts of Pt from the capsule had diffused into the glass, forming micro nodules that gave rise to Pt Argide interferences onto the U isotope masses (^{234}U ($^{194}\text{Pt} + ^{40}\text{Ar}$), ^{235}U ($^{195}\text{Pt} + ^{40}\text{Ar}$), ^{236}U ($^{196}\text{Pt} + ^{40}\text{Ar}$) and ^{238}U ($^{198}\text{Pt} + ^{40}\text{Ar}$); Fig. 2).

In a second fusion experiment an aliquot of 25 mg SM2 powder was loaded in a graphite container (4 mm OD, 2.5mm ID and 5mm length) placed in a MgO cylinder inside a talc – Pyrex-glass – graphite - MgO piston cylinder assembly. The fusion experiment was run in a 14mm bore end-loaded piston cylinder apparatus at 6 kbar pressure. Temperature was increased with 80°C/min to the desired run temperature of 1580°C (1600°C at the sample location) and kept constant for 63 minutes. Pressure was stable within ± 100 bars and temperature within $\pm 2^\circ\text{C}$. The experiment was terminated by shutting off the heating power resulting in a quenching rate of 200-300°C/second. The recovered charge consisted of a transparent crystal-free glass. Homogeneity for the U and Th concentrations was tested by LA-ICPMS at the Laboratory of Inorganic Chemistry, ETH, Zürich. The U and Th concentrations and isotopic compositions of the

mineral and glass standard materials were determined by solution MC-ICPMS at the Institute of Geochemistry and Petrology, ETH, Zürich and are reported in Table 3.

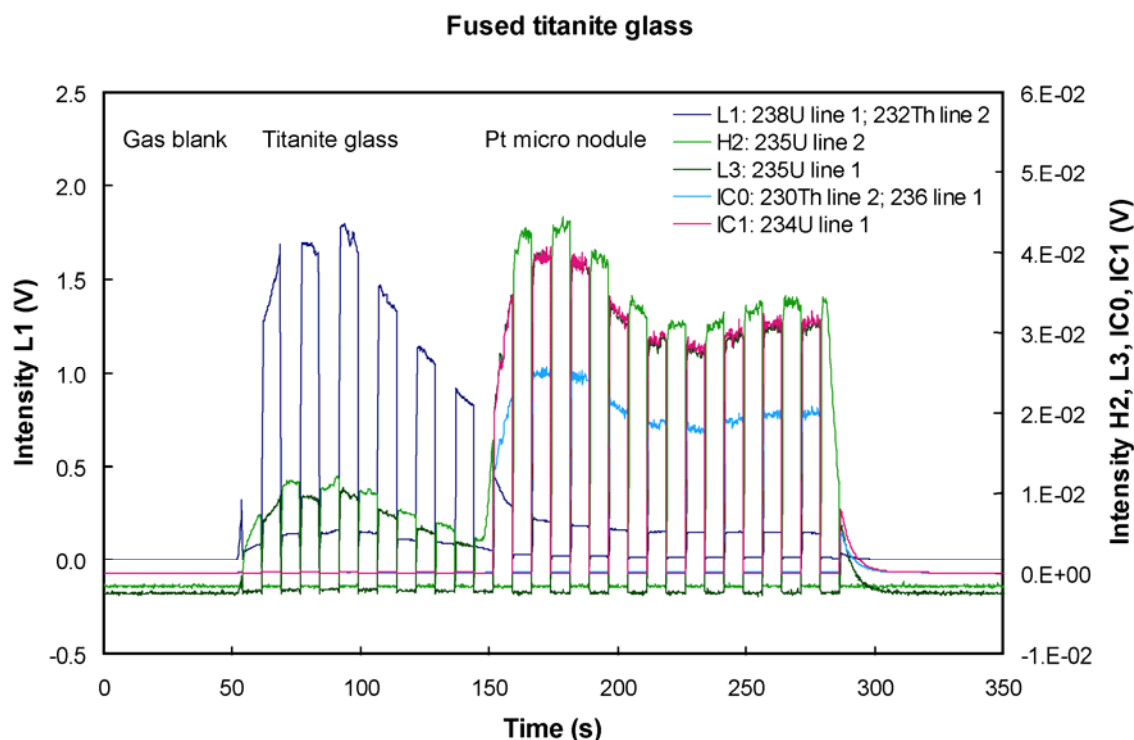


Fig. 2. Chart recording of a depth profile analysis of our in-house fused glass made in a Pt-crucible using a muffle oven. After about 100 seconds a Pt micro-nodule is sampled by the laser resulting in substantial interferences of Pt-argides on the ^{234}U , ^{235}U and ^{236}U masses.

Table 3. U -Th Composition of standard and sample minerals determined by solution mode MC-ICPMS

Sample	U (ppm)	2SE	Th (ppm)	2SE	$(^{234}\text{U}/^{238}\text{U})$	2SE	$(^{230}\text{Th}/^{232}\text{Th})$	2SE	$(^{238}\text{U}/^{232}\text{Th})$	2SE	$(^{230}\text{Th}/^{238}\text{U})$	2SE
This work												
SM1	213.2	5.8	268.6	7.397	1.025	0.002	2.451	0.022	2.425	0.005	1.011	0.010
SM2	54.67	0.7	13.48	0.176	1.002	0.002	12.20	0.120	12.30	0.005	0.992	0.011
SAD	207.7	3.9	627.6	0.031	1.025	0.001	1.020	0.016	1.012	0.002	1.008	0.008
TG	53.90	0.8	13.49	0.218	1.001	0.002	12.18	0.080	12.13	0.007	1.004	0.010
1075KA	13.16	0.2	116.7	2.080	1.004	0.002	0.750	0.007	0.342	0.006	2.191	0.026
Bourdon et al., (1994)												
1075KA	14.50		118.0		0.990	0.003	0.760	0.007	0.371	0.003	2.049	0.16
GT828	25.9		157		---		0.766	0.005	0.504	0.014	1.520	0.101

2.2.2 Solution mode reference standards

In order to monitor and correct for mass bias, relative Faraday-IC gains and ^{232}Th tailing we analysed pure U and Th solution standards that we interspersed with the laser ablation analyses on an hourly basis. Uranium reference solution SRM960 (also known as NBL-112a, New Brunswick Laboratory, Chicago, USA) was used to determine a

mass bias factor and the relative IC-Faraday gains for IC0 and IC1. Th standard IRMM-35 (Institute for Reference Materials and Measurements, Geel, Belgium) was used to determine the abundance sensitivity used to correct for tailing of large ^{232}Th beams onto the minor ^{230}Th mass. The solutions were introduced in a mixture of 0.2% HCl and 0.02% HF to avoid accumulation of U and Th in the DSN.

2.2.3 Laacher See samples

Titanites and apatites from 5 Laacher see mafic and felsic cumulates that belong to the Upper Laacher See Tephra (ULST) deposit were selected for U-Th analyses: 1075KA, GT828, 1097-1, 1099-1 and 1069. Most of these samples were previously analysed for whole rock and/or mineral major element compositions (Tait, 1988; Wörner, 1984). Two of the samples were analysed by Bourdon et al., (1994) for U-series disequilibria (1075KA and GT828). 1075KA is a coarse grained sanidine-rich felsic cumulate; GT828 is a coarse grained felsic cumulate containing 10% of interstitial glass; 1097-1 and 1099-1 are mixed lavas or so called 'hybrids' from the highest level of the ULST deposit whereas 1069, a mafic phonolite, was sampled from the lower parts of the ULST deposit.

Approximately six titanite and apatite minerals per sample were mounted in epoxy and polished to expose the minerals from core to rim. The polished samples were carbon coated and imaged using back scattered electron (BSE) and cathode luminescence (CL) imaging to reveal mineral zoning (Fig. 3). On BSE images titanite (and apatite) minerals display complex zoning patterns that are a combination of concentric growth zoning and sector zoning likely controlled by diffusion. Based on the BSE images and microscope inspection typically three locations per mineral were chosen for laser ablation analyses. Two sample mounts R1 and R2, containing large mineral fractions (1-4 mm) from samples 1075KA, GT828 and 1097-1 and smaller mineral fractions (0.5-2 mm) from 1075KA, GT828, 1097-1, 1099-1 and 1069, respectively were used for this study.

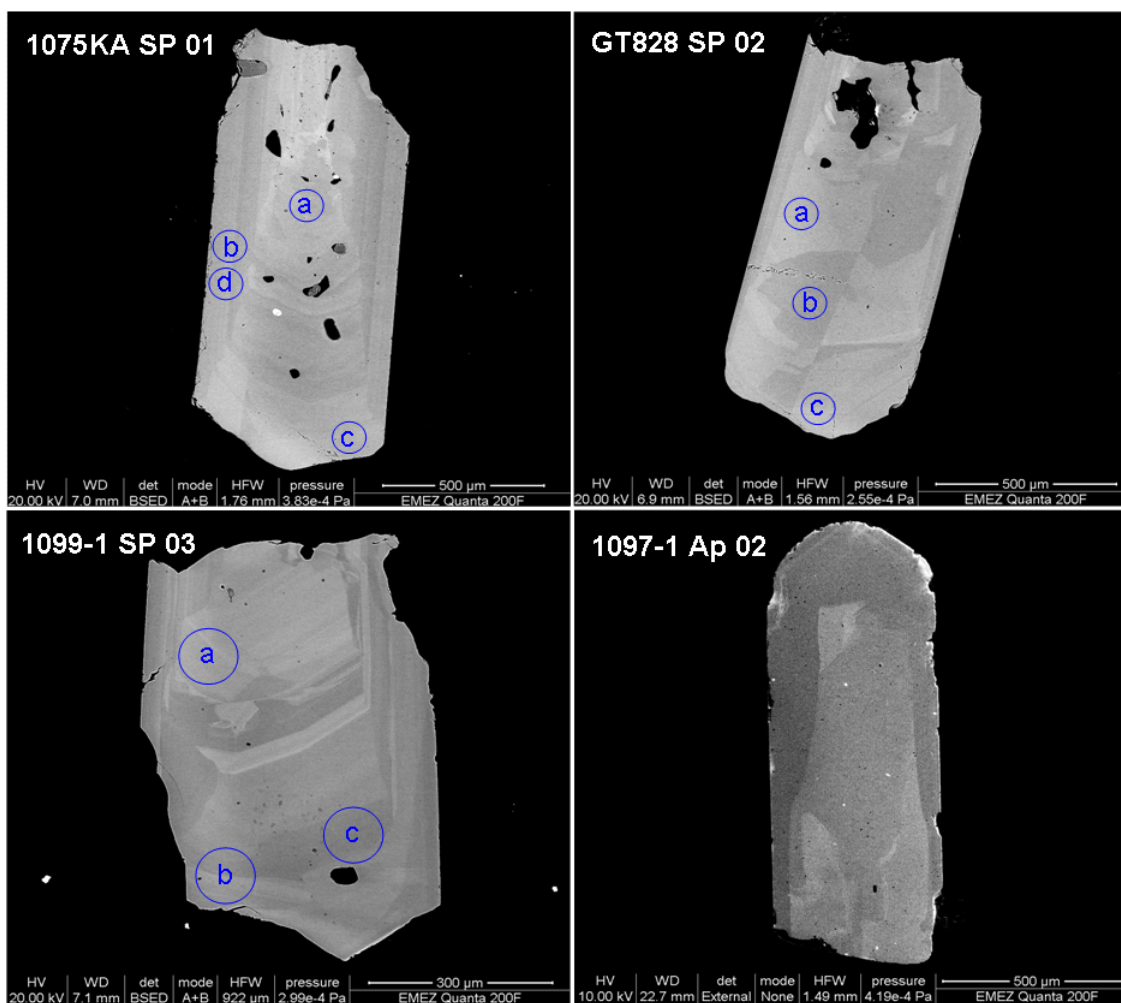


Fig. 3. BSE images of three Laacher See titanites (a, b, c) and a CL image of one Laacher See apatite (d). Titanite show complex zoning that is a combination of concentric growth zoning and patchy sector zoning. Blue circles define spots that we assigned for laser ablation analyses. The apatite shows patch zonation, analyses of apatite yielded too low signal intensities to obtain precise disequilibria data.

2.3 Analytical methods and data reduction

2.3.1 Analyses routines

Three analytical routines were adopted for (1) solution analyses of SRM960, (2) solution analysis of IRMM-35 and for (3) laser ablation analyses, respectively (Table 4).

(1) For the solution analyses of SRM960, determination of the mass bias and relative Faraday-IC gains required a dynamic measurement in two ‘lines’ corresponding to two magnetic field settings. In the first line the ^{234}U beam is collected in IC1, whereas in the second line it is collected in IC0 (Table 4). The mass bias factor and gains were

calculated using the widely adopted natural $^{238}\text{U}/^{235}\text{U}$ equal to 137.88 and the secular equilibrium $^{234}\text{U}/^{238}\text{U}$ ratio of (Cheng et al., 2000). The measurement routine involved an automatic peak centering followed by a baseline measurement of 30s done by ESA deflection. Data was collected in one block of 20 cycles with an integration time of 5s. (2) For the solution analysis of IRMM-35, the abundance sensitivity is determined in a routine where the ^{232}Th and ^{230}Th is measured on-peak for 5 s in the first line and where zero's at 0.7 and 0.5 mass units below and above the 230 mass are measured for 15 s in 4 additional lines (Table 4). Measurement of 4 zeros allows for a precise characterisation of the ^{232}Th tail in the ^{230}Th mass range (Hoffmann et al., 2007; Hubert et al., 2006). A thorough wash out procedure was performed between and after the analyses of the U and Th solution standards (2 x 5 min). During laser ablation analyses an ultra pure solution of 0.2%HCl and 0.02%HF was aspirated.

Table 4. Cup configurations for solution and laser ablation MC-ICPMS analyses

Line	Cup	H5	H4	H3	H2	H1	Ax	L1	L2	IC0	L3	IC1	L4	IC2	L5
Routine 1. Solution analysis on SRM 960 to determine mass bias and relative Faraday - Ion Counter gain															
1								238			235	234			
2						238			235	234					
Routine 2. Solution analysis on IRMM-35 to determine the Abundance sensitivity on IC0															
1								232		230					
2										229.3					
3										229.5					
4										230.5					
5										230.7					
Routine 3. Time-resolved fs-Laser ablation analysis															
1								238		236	235	234			
2					235			232		230					

(3) The laser ablation analyses require measurements in two lines as the collector block set-up of the MC-ICPMS instrument does not allow for simultaneous collection of ^{230}Th and ^{234}U in ion counters while the ^{232}Th , and ^{235}U and ^{238}U are collected in Faraday cups (see Table 4). The ^{230}Th beam is measured in IC0 as this SEM is equipped with an energy filter designed to improve abundance sensitivity, thereby reducing the tailing correction for ^{232}Th . Unfortunately, the ^{238}U cannot be measured in line 2 owing to the double mass spacing between H4 and H5. The intensity of ^{238}U in line two is therefore calculated from the measured $^{238}\text{U}/^{235}\text{U}$ ratio in line 1 and the intensity of the ^{235}U beam in line 2. Data is collected using the time-resolved Nu-instruments software, which allows the acquisition of an on peak gas blank analysis (30s) prior to the laser

ablation. Data acquisition and sample ablation were started simultaneously. The data was generally collected in 10 - 20 cycles with 5s integration times during the NIR mode analyses and in 16 cycles of 3s integrations time during the UV mode analyses, yielding total analyses times of 48 to 100 s. Taking into account the required time to stabilize the instrument, the solution analyses, the washout times, and laser ablation analyses it was possible to carry out 40 - 50 laser ablation analyses in a typical analytical session (~9 hrs).

2.3.2 Data reduction

On average, 15 laser ablation analyses (i.e. 8 bracketing standards and 7 'unknowns') were performed over the course of one hour which were bracketed by solution-mode analyses. The gains, mass bias factors and abundance sensitivity determined from the solution standards measured before and after the laser ablation analyses were linearly interpolated and used to correct the isotope ratios measured in the laser ablation analyses.

The first two cycles of data collected during laser ablation (6 - 10 s after start of ablation) were excluded from the data reduction. First, all beams were corrected for the background by subtraction of the gas blank measured before starting the laser. The data collected in line 1 and line 2 was integrated over 21 to 40 s depending on the U and Th concentrations in the ablated material and therefore the time that the signals lasted. The data for samples and bracketing standards were always integrated over the exact same amount of time. The background corrected averaged $^{234}\text{U}/^{238}\text{U}$ was corrected for mass bias and IC1 gain. The background corrected ^{230}Th signal was corrected for the tail contribution using the externally determined abundance sensitivity (routine 2, see above) and the background corrected ^{232}Th . The ^{238}U signal in line 2 was calculated using the $^{238}\text{U}/^{235}\text{U}$ measured in line one and the ^{235}U signal measured in line 2. The tail corrected ^{230}Th was then used to calculate the $^{230}\text{Th}/^{232}\text{Th}$ and $^{230}\text{Th}/^{238}\text{U}$ which were subsequently corrected for mass bias and IC0 gain. Activity ratios were calculated using: $\lambda_{234} = 2.8263 \times 10^{-6} \text{ y}^{-1}$, $\lambda_{238} = 1.5513 \times 10^{-10} \text{ y}^{-1}$, $\lambda_{232} = 4.9475 \times 10^{-11} \text{ y}^{-1}$, $\lambda_{230} = 9.1577 \times 10^{-6} \text{ y}^{-1}$. The ($^{230}\text{Th}/^{238}\text{U}$) of unknowns were finally corrected for elemental fractionation by sample-standard bracketing using the determined equilibrium value for the bracketing standard (SM in NIR mode analyses and TG in UV mode analyses). The

($^{238}\text{U}/^{232}\text{Th}$) was calculated by multiplying the ($^{230}\text{Th}/^{238}\text{U}$)⁻¹ and ($^{230}\text{Th}/^{232}\text{Th}$) activity ratios.

3. Results and discussion

The data presented in this chapter were collected in two separate analytical sessions carried out from 25th of Jan to the 4th of Feb 2010 and from the 26th to the 29th of April 2010. An initial session in November 2007 was performed to check for feasibility in terms of sensitivity and for preliminary set-up of analyses routines. During these initial tests it was found that ablation of apatite yielded relatively low signal intensities that decayed quickly compared to titanite likely owing to the physical properties of apatite (e.g. reduced hardness of apatite compared to titanite). The analytical development was hence as a first step concentrated on titanite, hoping to improve sensitivity for further application to apatite.

In the first analytical session in 2010 the analyses routines were set-up and tested during solution mode analyses using mixed U-Th solution standards. The last three days of the session were used for laser ablation analyses of standards and samples. The laser was operated at the centre NIR wavelength (800 nm) as this wavelength yielded the highest U and Th signal intensities that lasted over longer time spans. In the second analytical sequence the wavelength was converted to UV (265 nm) to test whether this would reduce observed time-dependent elemental fractionation when using NIR LA. The data for standards and samples collected per analytical sequence is presented in Tables 5, 6, 7 and 8, respectively.

3.1 NIR mode analyses

3.1.1 Standard data by NIR-fs-MC-ICPMS

During the NIR analytical sequence (800 nm wavelength), the natural sphene mineral SM was used as the bracketing standard. Ablation of SM yielded, on average, ^{238}U intensities of ~ 4 V and ^{232}Th intensities of ~1.5 V.

The accuracy and reproducibility of the U isotope analyses by laser ablation can be derived from repeated analyses of the bracketing standard ($^{234}\text{U}/^{238}\text{U}$), which gave 1.028 ± 0.032 (2SD, n=40) in perfect agreement with the value determined by solution analyses (Table3). Internal errors (2RSE) for the $^{234}\text{U}/^{238}\text{U}$ analyses were typically 1%,

which is relatively large compared to solution analyses (2 RSE of 0.3%) measured at similar ^{238}U and ^{234}U intensities.

The Th isotope composition for this standard cannot be used as a monitor for accuracy and/or reproducibility as the standard was determined to be heterogeneous in its U and Th composition. Measured ($^{230}\text{Th}/^{238}\text{U}$) activity ratios for SM yielded 0.386 ± 0.032 (2SD, n=40), which indicates that substantial elemental fractionation between U and Th occurs. The fractionation is relatively large ($^{230}\text{Th}/^{238}\text{U}$ should be ~ 1) compared to previous studies that report fractionation factors of 40 % to 0% (Bernal et al., 2005; Potter et al., 2005; Stirling et al., 2000). The relatively small 2SD indicates, however, that the amount of fractionation is stable over the two days of analyses (Fig 4a). Although the absolute amount of fractionation could be reduced by decreasing gas flows and increasing the distance between the torch and HV1 to create hotter plasma conditions (see also Bernal et al., 2005), we chose to run at ‘normal’ plasma conditions as these were shown to result in much more stable mass bias (Fontaine et al., 2009).

Table 5. NIR-mode standard reproducibility

	SM, n=40	SM2, n=5	SAD, n=2
$(^{234}\text{U}/^{238}\text{U})$	1.028	0.995	1.014
2SD	0.032	0.006	0.006
2RSD	3.1%	0.6%	0.6%
$(^{230}\text{Th}/^{232}\text{Th})$	2.758	14.65	1.505
2SD	0.643	5.217	0.963
2RSD	23.3%	35.6%	64.0%
$(^{230}\text{Th}/^{238}\text{U})_{\text{uncorr}}$	0.386	0.351	0.383
2SD	0.032	0.033	0.013
2RSD	8.3%	9.3%	3.4%
$(^{238}\text{U}/^{232}\text{Th})_{\text{uncorr}}$	2.381	13.71	1.291
2SD	0.508	3.689	0.714
2RSD	21.3%	26.9%	55.3%
$(^{230}\text{Th}/^{238}\text{U})_{\text{corr}}$		0.941	0.962
2SD		0.085	0.006
2RSD		9.0%	0.7%
$(^{238}\text{U}/^{232}\text{Th})_{\text{corr}}$		15.51	1.564
2SD		4.278	1.011
2RSD		27.6%	64.6%

Reproducibility and accuracy of the ($^{230}\text{Th}/^{238}\text{U}$) can be derived from analyses of calibrated equilibrium standard minerals SM2 and SAD bracketed by the SM standard mineral (Table 5). SM2 yielded ($^{230}\text{Th}/^{238}\text{U}$) of 0.941 ± 0.085 (n=5) which is low compared to the value determined by solution analyses (Table 3., 0.992 ± 0.011) but within the relatively large 2 sigma standard deviation (Fig 4a). 2SE of individual

analyses were approximately 5%, which is larger than the ~1% reported by Stirling et al., (2000) and Bernal et al., (2005), but similar to the errors reported by Potter et al., (2005). Two analyses of SAD yielded ($^{230}\text{Th}/^{238}\text{U}$) of 0.962 ± 0.006 , which is also low compared to the equilibrium value determined by solution mode analyses (1.008 ± 0.008). The ($^{234}\text{U}/^{238}\text{U}$) determined for SM2 gave 0.995 ± 0.006 (n=5) in excellent agreement with the determined equilibrium value (Table 5), whereas the ($^{234}\text{U}/^{238}\text{U}$) for SAD was 1.014 ± 0.006 , and therefore lower than that determined in solution analyses (1.025 ± 0.001). Relatively large 2 RSD's for ($^{230}\text{Th}/^{232}\text{Th}$) and ($^{238}\text{U}/^{232}\text{Th}$) analyses of SM2 and SAD (36 – 64%) are likely related to U and Th heterogeneity in these minerals.

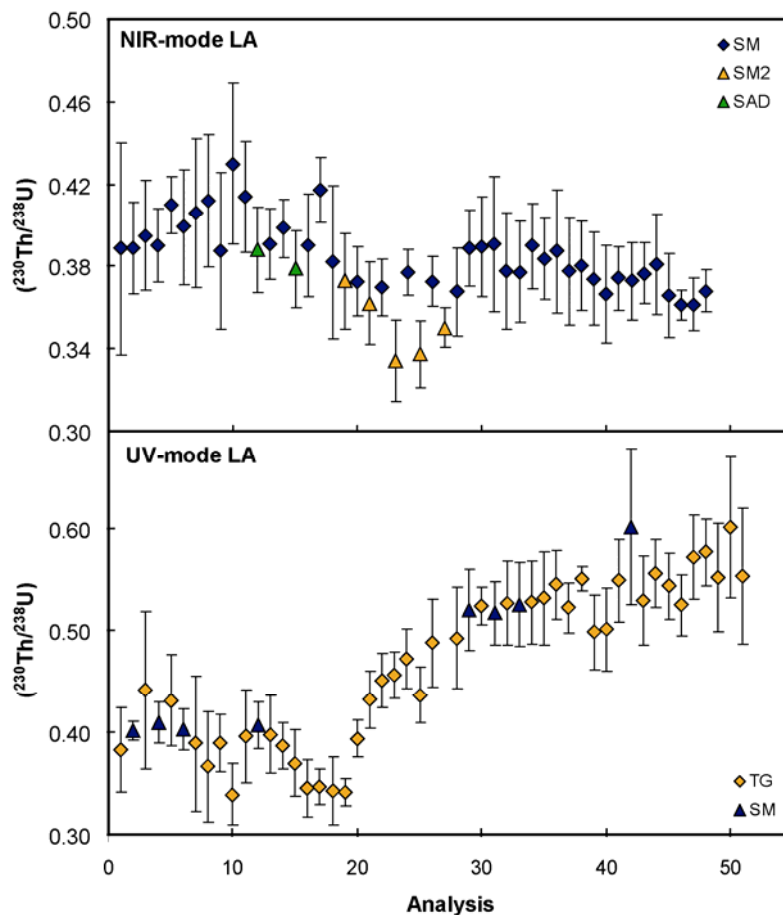


Figure 4. ($^{230}\text{Th}/^{238}\text{U}$) activity ratios for in-house standards SM, SM2, SAD and TG in NIR mode (a) and UV-mode (b). Note that there is substantial fractionation between U and Th, with Th loss of up to 65%. During the NIR-mode session the fractionation was relatively constant, but fractionations for SM2 and SAD were larger compared to SM. During the UV mode session there was substantial drift in the fractionation over the course of the session but the absolute fractionation for TG and SM was similar. Note that tuning remained constant.

3.1.2 Samples by NIR-fs-MC-ICPMS

We analysed 3 minerals from sample 1075KA, 2 minerals from sample GT828 and 1 mineral from sample 1097-1 for core to rim compositions and calculated the U-Th activity ratios using SM as the bracketing standard (see Fig 5). Sample analyses typically yielded average intensities of 0.3 V for ^{238}U and of 0.8 V for ^{232}Th . There are three main observations that hint toward problems with the analytical method: (1) The ($^{234}\text{U}/^{238}\text{U}$) activity ratios determined for the Laacher See samples are consistently 10 to 20% higher compared to the equilibrium values determined for the minerals by solution mode MC-ICPMS by Bourdon et al., (1994) and in this study for 1075KA. (2) The 2RSE internal measurement errors on the ($^{230}\text{Th}/^{238}\text{U}$) are large ranging from 4% up to 46% and (3) The ($^{230}\text{Th}/^{238}\text{U}$) of 1075KA are on average 22% higher compared to the Bourdon et al., (1994) value and 16% higher compared to that determined here at ETH Zürich. For GT828 the off-set with the Bourdon et al., (1994) value is even larger (32%). Note that the ($^{230}\text{Th}/^{232}\text{Th}$) activity ratios determined for 1075KA (and GT828) are in good agreement with those reported in Bourdon et al., (1994) and in excellent agreement with the solution measurements carried out at ETH.

The ($^{234}\text{U}/^{238}\text{U}$) ratios that are consistently too high for samples from Laacher see suggest an analytical artefact during analyses of samples compared to standard minerals. Even though the ($^{234}\text{U}/^{238}\text{U}$) data is not required to extract time-information on magma differentiation it is important to determine the cause of the analytical discrepancy as it possibly also affects other measured ratios. Two possibilities are considered: (1) interference of molecular species onto the ^{234}U mass that only occur during ablation of Laacher See samples, (2) tailing of ^{232}Th on the ^{234}U mass which is more pronounced during analyses of Laacher See samples.

Isobaric interferences are generally not found to be a major problem in the U and Th high mass range, although they could potentially be problematic on the small beams of ^{230}Th and ^{234}U . Interfering species at these high masses can only represent molecules consisting of multiple components that are abundant either in the ICP source or in the mineral matrix (e.g. ^{40}Ar , ^{40}Ca , ^{28}Si , ^{48}Ti , ^{16}O , ^1H). A possible interference onto the ^{234}U mass could be a double hydride + ^{232}Th , although the amount of H present in the plasma is negligible when using a membrane desolvator such as the DSN 100. The simplest interferences requires the presence of isotopes not to be expected in the titanite matrix (e.g. ^{194}Pt , ^{186}Os) and are therefore unlikely to be formed. An exception to this

could be a combination of ^{28}Si and ^{206}Pb , although the abundance of Pb in Laacher See titanite is not expected to be large (<5 ppm, determined on titanite in Laacher See carbonatites by F.Wetzel, personal communication). Moreover, a larger abundance of the $^{207}\text{Pb} + ^{28}\text{Si}$ interference on the 236 amu mass that is monitored during the analyses in IC0 is not observed.

The other possibility is that the excess ^{234}U measured during the analyses of samples is due to tailing of the relatively large ^{232}Th beam 2 mass units below. In contrast to the tail correction of the ^{232}Th on the ^{230}Th mass in IC0, a correction for tailing onto the ^{234}U mass was not applied. Note that IC1 is not equipped with an energy filter to improve abundance sensitivity so that this effect potentially is significant. The tailing on the high mass side of large beams is, however, less pronounced compared to that on the low mass side, which results from an asymmetry in the tail. This is due the fact that ions that lost energy owing to collisions in the region before the magnet are deflected stronger in the magnetic field. These ions therefore end up at the low mass side of the beam rather than at the high mass side.

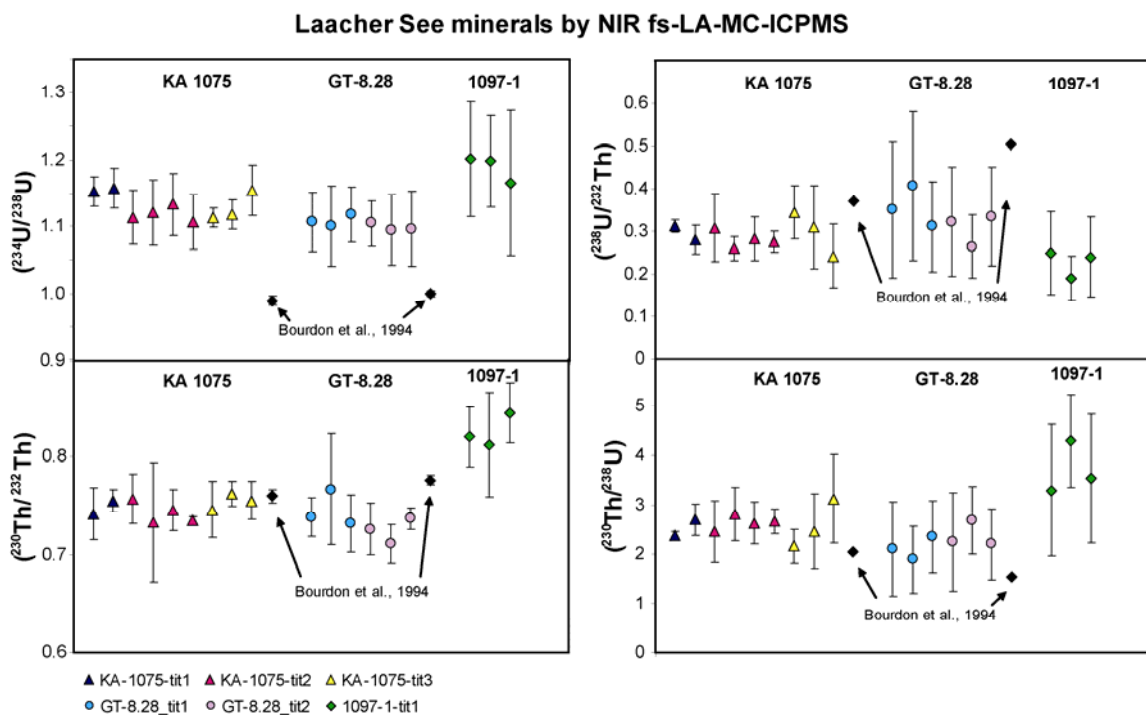


Figure 5. U and Th activity data for Laacher See titanite obtained by NIR fs-LA-MC-ICPMS. Triangles represent data for three minerals from 1075KA, circles for two minerals from GT828 and diamonds for one mineral from 1097-1. The black symbols are data obtained by Bourdon et al., (1994) by solution mode analyses for 1075KA and GT828 respectively.

A positive relation between the ($^{234}\text{U}/^{238}\text{U}$) and raw $^{232}\text{Th}/^{238}\text{U}$ ratios for samples and standards measured during the NIR session (Fig 6a) indeed suggests that samples with larger Th/U are more affected by the analytical artefact. Assuming that the ($^{234}\text{U}/^{238}\text{U}$) of samples is 1 the relation can be used to derive the 2 amu abundance sensitivity for the high mass tail of ^{232}Th on the ^{234}U in IC1 during the NIR session to be ~ 1.9 ppm. A determination of the high mass side 2 amu abundance sensitivity on IC1 is required to confirm the validity of this estimate.

Inspection of the $^{230}\text{Th}/^{238}\text{U}$ ratios collected during the ~ 30 s sample analyses revealed a drift in the raw ratios to higher values (Fig. 7b). The drift is observed for every sample analysis. The accuracy of the ($^{230}\text{Th}/^{232}\text{Th}$) data suggests that the applied tail and mass bias correction is effective and that therefore the drift results from variations in the U and/or Th beams. The effect is observed for both core and rim analyses suggesting that it does not reflect real variations in Th and U related to growth zoning. Rather, it indicates variability in elemental fractionation as ablation proceeds. The increasing $^{230}\text{Th}/^{238}\text{U}$ suggests that the fractionation between U and Th is reduced during ongoing ablation. A similar drift towards higher raw $^{230}\text{Th}/^{238}\text{U}$ ratios is observed for the bracketing analyses of SM that yielded relatively large 2RSE of 5%; however, the magnitude of the drift over the same time is significantly less (Fig.7a). This suggests that the observed time-dependent fractionation is different for the standard and the samples. The offset between the ($^{230}\text{Th}/^{238}\text{U}$) data obtained here and that acquired in solution mode analyses by Bourdon et al., (1994) and in this study therefore most likely results from inappropriate correction for the elemental fractionation. The observed ^{230}Th -excesses that are too large suggest that on average less fractionation occurs during sample analysis compared to during standard analysis. In contrast, our standard analyses on SM2 and SAD yielded 6 and 4 % lower ($^{230}\text{Th}/^{238}\text{U}$) than the calibrated equilibrium value suggesting an under-correction for the absolute elemental fractionation.

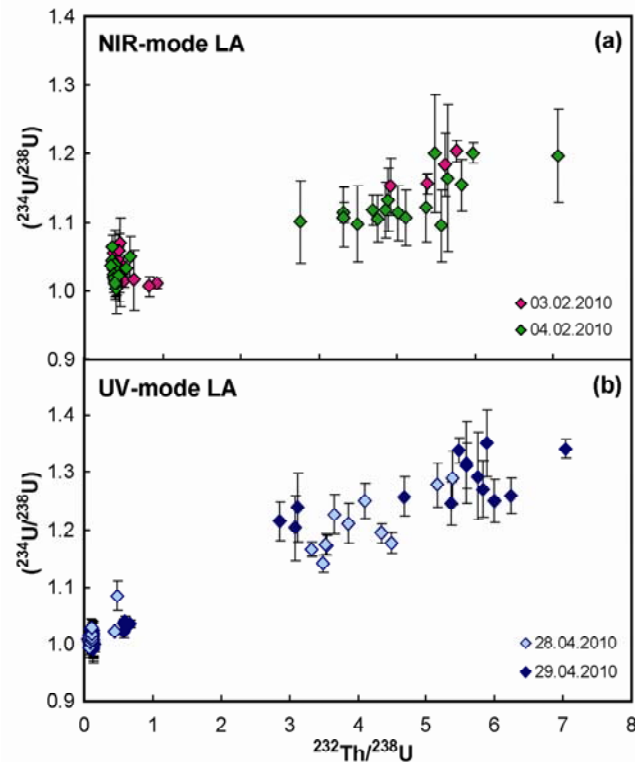


Figure 6. Observed relations between measured ($^{234}\text{U}/^{238}\text{U}$) and the raw measured Th/U ratio for all NIR-mode analyses (a) and UV-mode analyses (b). The positive correlation suggests that the too high ($^{234}\text{U}/^{238}\text{U}$) determined for Laacher See samples results from tailing of the relatively large Th beams onto the small ^{234}U beams measured in IC1.

Time dependent fractionation in depth profile analyses is commonly reported in studies applying nano-second (ns) laser ablation and was explained by (1) variable deposition and evaporation processes at the ablation site with increasing crater depth owing to heat penetration and thermal diffusion as well as energy dissipation in the expanding material (Eggins et al., 1998; Mank and Mason, 1999; Niemax, 2001); (2) the changing particle size distribution with ablation time resulting in variable ICP mass loads and changes in vaporization and ionization efficiency (e.g. (Guillong and Gunther, 2002; Kuhn and Gunther, 2003). For femto second laser ablation fractionation at the ablation site is thought much less important compared to ns laser ablation as the pulse duration is shorter than the solid thermal-relaxation time resulting in little heat transfer to the sample (e.g. (Russo et al., 2002). However, formation of cone-shaped craters owing to decrease of the fluence during the ablation process could still lead to preferential elemental evaporation (Koch et al., 2006). The particle size distribution of the aerosol in nano second laser ablation was shown to be dependent on the wavelength

of the laser, with larger wave lengths producing relatively larger sized particles (Guillong and Gunther, 2002; Russo et al., 2000). Comparison of particle size distribution of brass produced by NIR femto second laser ablation with NIR nano second laser ablation (Koch et al., 2004) showed that much finer aerosols resulted from fs LA compared to ns LA (nm versus μm). A more recent study of aerosols produced by UV fs-LA at ~ 265 nm and ~ 200 nm of silicate glass also demonstrated that the shorter wavelength produced smaller percentages of larger particles compared to the longer wavelength. Thus, use of shorter laser wavelengths may, effectively, decrease elemental fractionation. Horn and von Blanckenburg, (2007) (Horn and von Blanckenburg, 2007) demonstrated that time-dependent fractionation between Pb and U did not occur during spot ablation of NIST 610 using deep UV (~ 193 nm) fs-MC-ICPMS.

It is possible that our analyses in which we observed time-dependent fractionation suffer from the formation of cone-shaped craters owing to decrease of the fluence during ongoing ablation and/or from changing particle size distributions and therefore ICP mass load during the analyses using the relatively long NIR 800 nm wavelength. Interestingly, the degree of fractionation between the standard titanite mineral and the samples was also different, suggesting a possible effect of subtle differences in matrix compositions. Microprobe analyses of SM and Laacher See 1075KA demonstrate that the matrix is very similar for major elements such as TiO_2 , SiO_2 , CaO , and FeO . Only for Al_2O_3 , a minor element in titanite, are there significant differences between SM and 1075KA (1.2 wt.% versus 1.5 wt. %).

Table 6. Laacher See sample data measured by NIR fs-LA-MC-ICPMS

	^{238}U Int (V)	^{232}Th Int (V)	$(^{234}\text{U}/^{238}\text{U})$ 2SE	$(^{230}\text{Th}/^{232}\text{Th})$	2SE	$(^{230}\text{Th}/^{238}\text{U})$	2SE	$(^{238}\text{U}/^{232}\text{Th})$	2SE	
KA1075 sphene										
13-R1-I-05b	0.229	0.860	1.152	0.022	0.742	0.027	2.377	0.091	0.312	0.014
17-R1-I-05-5d	0.309	1.142	1.157	0.030	0.755	0.012	2.699	0.317	0.280	0.034
15-R1-I-01a	0.306	0.991	1.114	0.040	0.757	0.025	2.457	0.634	0.308	0.079
17-R1-I-01b	0.179	0.555	1.121	0.049	0.733	0.061	2.818	0.546	0.260	0.027
19-R1-I-01c	0.271	0.998	1.133	0.046	0.746	0.021	2.635	0.430	0.283	0.051
21-R1-I-01d	0.205	0.617	1.106	0.041	0.735	0.004	2.664	0.254	0.276	0.025
23-R1-I-03a	0.178	0.781	1.201	0.015	0.741	0.012	3.234	0.215	0.229	0.012
25-R1-I-03b	0.279	0.833	1.113	0.015	0.746	0.029	2.164	0.341	0.345	0.062
27-R1-I-03c	0.326	1.009	1.118	0.022	0.763	0.013	2.462	0.763	0.310	0.098
29-R1-I-03d	0.221	0.938	1.154	0.038	0.756	0.019	3.122	0.902	0.242	0.075
GT-8.28 sphene										
32-R1-III-01a	0.368	0.949	1.107	0.044	0.739	0.020	2.109	0.963	0.350	0.160
34-R1-III-01b	0.400	0.867	1.101	0.060	0.767	0.057	1.886	0.683	0.407	0.175
36-R1-III-01c	0.350	1.003	1.117	0.041	0.732	0.029	2.351	0.735	0.311	0.106
38-R1-III-05a	0.290	0.724	1.105	0.034	0.726	0.027	2.251	0.990	0.323	0.128
40-R1-III-05b	0.251	0.680	1.095	0.052	0.711	0.020	2.688	0.680	0.265	0.075
42-R1-III-05c	0.354	0.916	1.097	0.055	0.737	0.011	2.199	0.724	0.335	0.115
1097-1 sphene										
44-R1-IV-01a	0.181	0.649	1.200	0.086	0.820	0.030	3.292	1.332	0.249	0.098
46-R1-IV-01b	0.128	0.551	1.197	0.069	0.812	0.053	4.291	0.941	0.189	0.051
48-R1-IV-01c	0.140	0.546	1.165	0.108	0.845	0.031	3.533	1.297	0.239	0.094

It is possible, however, that the trace element contents, which were not determined, are significantly different for SM and samples resulting in different behaviour of the aerosols in the plasma. The distinction in colour between the standard mineral and Laacher See minerals supports a difference in minor or trace elemental composition. Note that for ns LA it was shown that the transparency of the ablated material also had an influence on the ablation process and therefore on the extent of fractionation (Russo et al., 2000). Opaque materials were shown to result in a more stable ablation rate compared to transparent material. This potentially leads to formation of less deep craters and reduced re-deposition at the ablation site when ablating opaque material. Also the particle size distribution may be different. The variable elemental fractionation between the dark brown standard titanite mineral and the light yellow Laacher See titanite thus possibly results from a transparency difference rather than from a compositional effect.

To investigate if we could eliminate the time-dependent fractionation and possibly also the different elemental fractionation behaviour between samples and standards, a second set of experiments were performed, using a converted UV wavelength of ~265 nm.

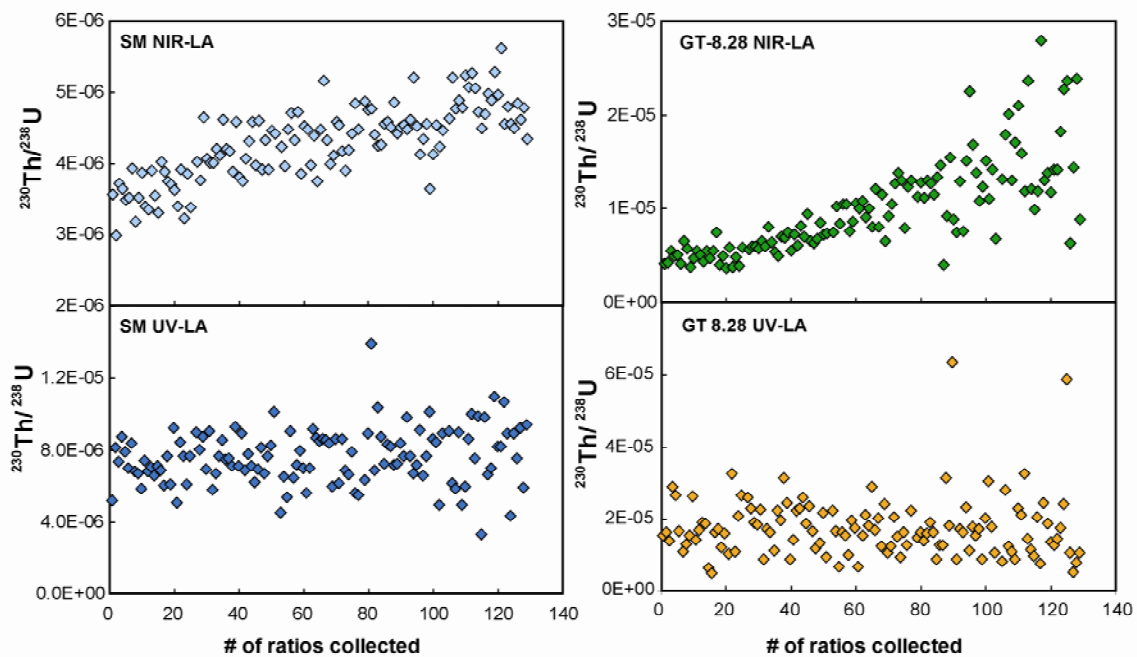


Fig.7. $^{230}\text{Th}/^{238}\text{U}$ collected during depth profile analyses of SM (a, c) and GT828 (b, d). Note that during NIR analyses (a, b) the $^{230}\text{Th}/^{238}\text{U}$ drifts towards higher values indicating time-dependent elemental fractionation. The fractionation is more pronounced for GT828 compared to SM. In the UV-mode analyses (c, d) the ratios remain constant although the scatter is larger owing to lower signal intensities.

3.2 UV-mode analyses

3.2.1 Standard data for UV-fs-MC-ICPMS

Compared to NIR, UV-mode laser ablation results in smaller beam intensities that decay over a shorter time spans using similar ablation crater size and repetition rates. This is a direct result from restricted energy conversion efficiency leading to lower average fluence (Table 2) and therefore lower ablation rates for UV LA compared to NIR LA (Koch et al., 2006). Increasing repetition rates to compensate for loss of sensitivity resulted in highly transient signals that lasted too short for precise analyses. On average, the sensitivity in UV-mode ablation was 3 to 4 times smaller than in NIR-mode.

Table 7. UV-mode standard reproducibility

	TG, n = 42	SM, n = 8
$(^{234}\text{U}/^{238}\text{U})$	1.007	1.029
2SD	0.021	0.014
2RSD	2.1%	1.4%
$(^{230}\text{Th}/^{232}\text{Th})$	12.41	2.688
2SD	0.969	0.166
2RSD	7.8%	6.2%
$(^{230}\text{Th}/^{238}\text{U})_{\text{uncorr}}$	0.466	0.473
2SD	0.159	0.155
2RSD	34.1%	32.8%
$(^{238}\text{U}/^{232}\text{Th})_{\text{uncorr}}$	9.096	1.904
2SD	3.410	0.610
2RSD	37.5%	32.1%
$(^{230}\text{Th}/^{238}\text{U})_{\text{corr}}$		1.005
2SD		0.106
2RSD		10.5%
$(^{238}\text{U}/^{232}\text{Th})_{\text{corr}}$		2.680
2SD		0.293
2RSD		10.9%

During the UV analytical session the homogeneous in-house titanite glass TG was used as the bracketing standard. Average ^{238}U beam intensities were 0.2 V for this standard that contains 54 ppm U. Forty-two analyses of TG yield an average $(^{234}\text{U}/^{238}\text{U})$ of 1.007 ± 0.021 consistent with the calibrated value (Table 7). Note that even though the internal measurement errors on the $^{234}\text{U}/^{238}\text{U}$ are larger compared to NIR mode analyses (2RSE of ~2.5% instead of ~1%), the external reproducibility is better in UV mode (2RSD 2.1% instead of 3.1%). The $(^{230}\text{Th}/^{232}\text{Th})$ measured on TG are slightly higher (1.8%) compared to those determined in solution mode, but are equal within the relatively large external error (2RSD = 7.8%, n=42). In principle, the variability of $^{230}\text{Th}/^{232}\text{Th}$ could result from variability in abundance sensitivity that was only determined on an hourly basis. The abundance sensitivity typically increased over the course of a day, which was related to a decrease in the mass spectrometers analyzer pressure. However, the small ^{232}Th beams in the measurements of TG result in the tail contribution on the ^{230}Th to be negligible (0.4%) precluding a drift in abundance sensitivity to be important.

The $^{230}\text{Th}/^{238}\text{U}$ for TG yielded on average 0.466 ± 0.159 (2SD, n=42), indicating that the absolute amount of elemental fraction during the UV mode session is smaller

compared to the NIR mode analyses. Note, however, that the $^{230}\text{Th}/^{238}\text{U}$ significantly drifted over the course of the UV-mode session even though the gas flows and other tuning parameters remained constant (Fig 4b). During a single spot analysis of TG there is no drift in the U/Th ratio, suggesting the absence of time-dependent fractionation during depth profiling in UV mode. Mineral SM was used as a secondary standard and was measured three times at the beginning of each analytical session and, afterwards, once every hour. Eight analyses gave ($^{230}\text{Th}/^{238}\text{U}$) of 1.005 ± 0.106 in excellent agreement with the equilibrium value. This implies that in UV LA the fractionation during ablation of SM is adequately corrected for using the measured ($^{230}\text{Th}/^{238}\text{U}$) in TG. The ($^{230}\text{Th}/^{232}\text{Th}$) in SM is 8.8% higher than determined in solution mode analyses, but this could arise from the U-Th heterogeneity in this mineral.

3.2.2 Samples by UV-fs-MC-ICPMS

In UV-mode we measured 10 titanite minerals from 5 Laacher See cumulates; 1075KA, GT828, 1099-1, 1097-1 and 1096. TG was used as the bracketing standard to correct for elemental fractionation. Sample analyses yielded average intensities, collected and integrated over 21 s, for ^{238}U between 45 and 150 mV and for ^{232}Th between 150 and 600 mV. The recording of a representative sample analysis is shown in Fig. 8. The data is shown in Table 8 and Figure 9.

Similarly to the NIR mode analyses the ($^{234}\text{U}/^{238}\text{U}$) analyses are affected by tailing of ^{232}Th on the ^{234}U mass. Comparatively larger offsets from the equilibrium value measured during the UV session suggest that the abundance sensitivity was higher (~ 2.4 ppm, which resulted in $\sim 25\%$ deviation in the $^{234}\text{U}/^{238}\text{U}$ ratio). Analyses of ($^{230}\text{Th}/^{232}\text{Th}$) in 1075KA and GT828 minerals do not reveal inter-mineral variability and are in good agreement with the solution mode data. However, as for NIR analyses, ($^{230}\text{Th}/^{238}\text{U}$) measured here are systematically higher than the values reported by Bourdon et al., (1994) or obtained by solution analyses at ETH Zürich (Table 3). In contrast to NIR mode analyses we do not observe drift in the $^{230}\text{Th}/^{238}\text{U}$ ratios during UV-mode analyses of Laacher See samples (fig 7d) suggesting that also for samples there is no time-dependent elemental fractionation. Note, that the internal errors on individual analyses are relatively large in UV mode analyses (2RSE of 3 – 20%) owing to limitations by counting statistics. Count rates on ^{230}Th of ~ 40 to 125 cps are the main limitation, but low signals of ^{235}U (0.5 -1.2 mV) in Faraday cups L3 and H2 further

limit the measurement precision as these transpose to the calculated ^{238}U intensity in line 2.

Even though for SM we obtain accurate Th-excess data in the UV session, for Laacher See samples the off-sets are similar as for the NIR mode analyses, suggesting that the analyses still suffer from an analytical bias. The accuracy of the ($^{230}\text{Th}/^{232}\text{Th}$) data suggests that the tail correction that is applied on IC0 is appropriate and that the bias does not result from an interfering species onto the small ^{230}Th beam.

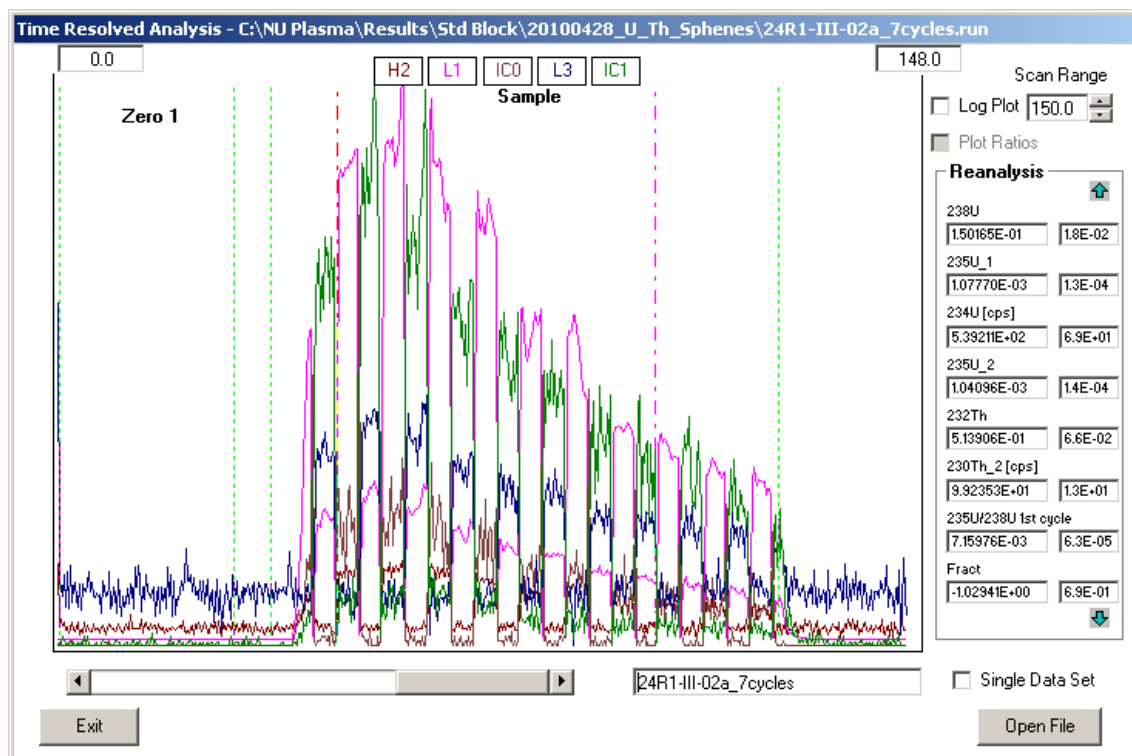


Figure 8. Chart recording generated by the time-resolved NU-instruments software during the analysis of GT828 in UV mode laser ablation. The data for samples and bracketing standards is integrated over 14 cycles (7 in each line) (see vertical pink lines), yielding data for each line collected in 21 seconds.

Note that the absence of time-dependent fractionation in the UV mode analyses could result from two different aspects. Either, the aerosol particles produced in UV mode are on average smaller resulting in more efficient evaporation and ionization in the ICP. Or, the reduced fluence and therefore ablation rate in UV mode compared to in IR mode results in formation of shallower ablation craters and therefore reduced deposition and fractionation at the ablation site. Possibly, both aspects play a role.

The higher ($^{230}\text{Th}/^{238}\text{U}$) obtained by LA-MC-ICPMS compared to solution TIMS and MC-ICPMS for samples GT828 and 1075KA (Table 3) likely result from improper correction for elemental fractionation during LA-MC-ICPMS. The too high values imply that elemental fractionation is overall less pronounced during ablation of the titanite Laacher See samples compared to the standard titanite glass. Even though the time-dependent elemental fractionation is eliminated using UV rather than NIR LA, there are still variations in absolute elemental fractionations between the standards and the sample titanite.

Table 8. Laacher See sample data measured by UV fs-LA-MC-ICPMS

	^{238}U Int (V)	^{232}Th Int (V)	$(^{234}\text{U}/^{238}\text{U})$	2SE ($^{230}\text{Th}/^{232}\text{Th}$)	2SE ($^{230}\text{Th}/^{238}\text{U}$)	2SE ($^{238}\text{U}/^{232}\text{Th}$)	2SE
1075KA sphene							
08R1-I-02a	0.062	0.235	1.236	0.156	0.750	0.067	2.725 0.414 0.275 0.020
10R1-I-02b	0.065	0.254	1.208	0.074	0.739	0.031	2.799 0.279 0.264 0.020
12R1-I-02c	0.068	0.259	1.193	0.064	0.721	0.033	2.751 0.099 0.262 0.007
17R1-I-04a	0.070	0.264	1.210	0.069	0.784	0.046	2.648 0.200 0.296 0.016
20R1-I-04b	0.063	0.221	1.226	0.067	0.753	0.025	2.470 0.136 0.305 0.018
22R1-I-04c	0.056	0.213	1.250	0.061	0.780	0.071	3.030 0.253 0.257 0.013
GT828 sphene							
24R1-III-02a	0.150	0.514	1.173	0.035	0.705	0.018	2.458 0.070 0.287 0.007
26R1-III-02b	0.171	0.544	1.166	0.026	0.753	0.050	2.462 0.183 0.306 0.014
28R1-III-02c	0.161	0.534	1.174	0.036	0.762	0.034	2.675 0.236 0.285 0.019
33R1-III-04a	0.127	0.415	1.141	0.030	0.733	0.077	1.964 0.216 0.373 0.026
35R1-III-04b	0.124	0.503	1.194	0.033	0.724	0.074	2.355 0.134 0.307 0.017
37R1-III-04c	0.144	0.630	1.177	0.036	0.734	0.022	2.416 0.174 0.304 0.019
1097-1 sphene							
39R1-IV-03a	0.061	0.303	1.278	0.076	0.820	0.032	3.188 0.186 0.257 0.015
41R1-IV-03b	0.062	0.306	1.290	0.093	0.798	0.023	3.148 0.281 0.253 0.022
08R1-IV-05a	0.057	0.162	1.203	0.113	0.833	0.064	1.713 0.257 0.487 0.051
10R1-IV-05b	0.067	0.198	1.215	0.067	0.868	0.049	1.682 0.238 0.516 0.071
12R1-IV-05c	0.053	0.154	1.238	0.119	0.847	0.055	1.682 0.194 0.504 0.050
1099-1 sphene							
14R2-IV-02a	0.055	0.263	1.292	0.153	0.836	0.094	2.986 0.606 0.280 0.039
16R2-IV-02b	0.090	0.371	1.257	0.069	0.796	0.058	2.379 0.141 0.334 0.023
18R2-IV-02c	0.059	0.357	1.341	0.034	0.778	0.035	3.702 0.133 0.210 0.003
23R2-IV-03a	0.099	0.467	1.246	0.077	0.626	0.022	2.053 0.101 0.305 0.019
25R2-IV-03b	0.082	0.453	1.271	0.100	0.682	0.029	2.456 0.141 0.278 0.013
27R2-IV-03c	0.074	0.370	1.313	0.080	0.684	0.038	2.358 0.215 0.290 0.025
1069 sphene							
29R2-VI-03a	0.044	0.217	1.351	0.116	0.792	0.058	2.782 0.282 0.285 0.029
31R2-VI-03b	0.047	0.248	1.317	0.143	0.755	0.073	2.540 0.441 0.297 0.021
33R2-VI-03c	0.048	0.245	1.339	0.045	0.723	0.016	2.373 0.063 0.305 0.014
35R2-VI-06a	0.053	0.231	1.259	0.062	0.808	0.017	2.723 1.091 0.297 0.115
37R2-VI-06b	0.058	0.247	1.249	0.076	0.743	0.031	2.561 0.240 0.290 0.038

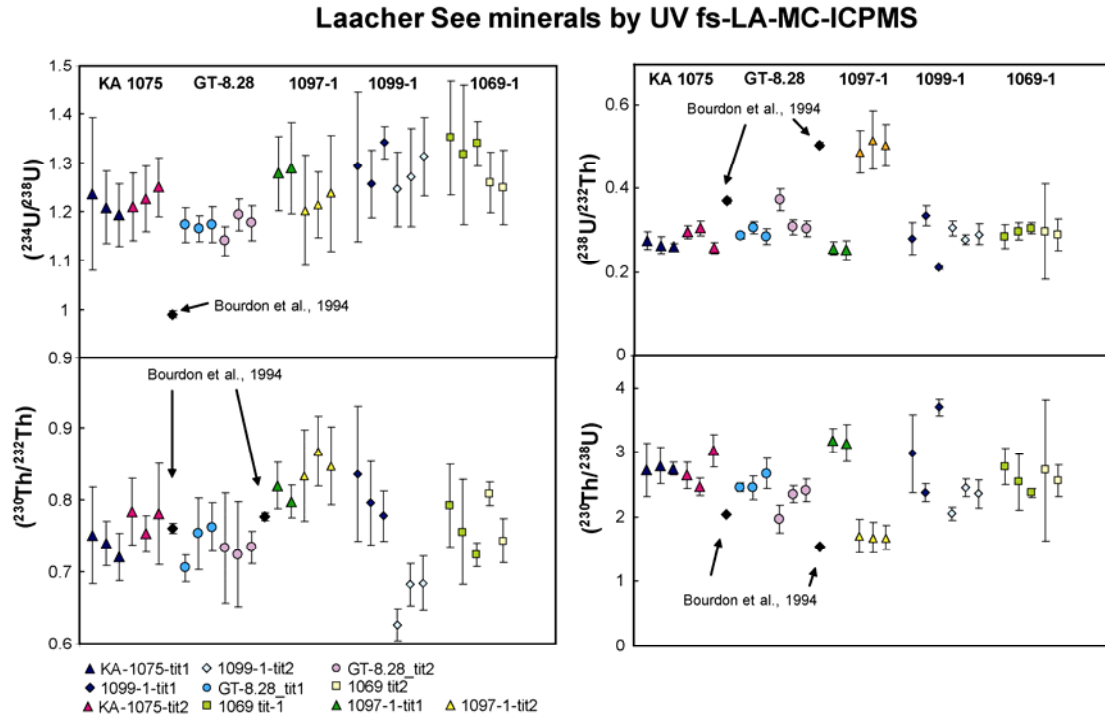


Figure 9. U and Th activity data for Laacher See titanite obtained by UV fs-LA-MC-ICPMS. Blue and pink triangles represent data for two minerals from 1075KA, circles for two minerals from GT828, green and yellow triangles for two minerals from 1097-1, diamonds for two mineral from 1099-1 and squares for two minerals from 1069. The black symbols are data obtained by Bourdon et al., (1994) by solution mode analyses for 1075KA and GT828.

The accurate data obtained for SM bracketed by TG suggest that the fractionation behaviour in UV-mode analyses is similar for the glass and the SM despite possible differences in matrix composition and physical and/or optical properties. The major and trace element composition of TG was not determined and therefore a matrix difference between TG and Laacher See samples is not confirmed. The other possible cause for the different behaviour between the Laacher See samples and TG and SM, as discussed above, may be the difference in transparency between the Laacher See minerals and TG. Possibly, ablation of the darker titanite glass (TG) results in formation of shallower craters and/or in aerosols having a different particle size distribution. Reduced fractionation for Laacher See samples suggested by the measured ($^{230}\text{Th}/^{238}\text{U}$) that are too high suggest that with larger crater depths the ablation of the lighter and more transparent samples results in a on average finer ablation aerosol or that with an increasing depth to diameter ratio the fractionation of U increases relative to Th. Note

that the effect onto the elemental fractionation must be relatively large to explain the offsets of 20-36 %

4. Conclusions

Accurate data collected by UV fs-LA-MC-ICPMS for our in-house standard titanite mineral (SM) bracketed by our in-house titanite glass (TG) are promising and show the great potential of this relatively fast analysis technique. Two aspects are, however, found to limit the accuracy and precision of data for Laacher See titanite minerals: (1) Variable elemental fractionation and (2) Low signal intensities.

The elemental fractionation between uranium and thorium during laser ablation analyses was found to be substantial with average ‘losses’ of Th relative to U between 40 and 60%. We demonstrated in this study that the wavelength of the fs laser has an influence onto time dependent fractionation observed during depth profile analyses of titanite minerals. In NIR laser ablation the elemental fractionation was shown to decrease over the course of an analysis, which either reflects changing particle size distribution during ongoing ablation or formation of cone-shaped craters owing to decrease of the fluence while the depth to diameter ratio increases. The time-dependent fractionation was not observed during the UV-mode analyses. This indicates that using this wavelength the aerosol consists of on average smaller particles or, alternatively, that due to the lower ablation rate and shallower ablation craters the fractionation at the ablation site is less pronounced. Note that using the shorter wavelength the difference in fractionation behaviour between the in-house standard glass and minerals and Laacher See titanite was still observed. This resulted in the measured ^{230}Th -excesses for Laacher See titanite 1075KA and GT828 to be too large (20 – 36 %) compared to values obtained from solution mode analyses.

The other major limitation is the low sensitivity that, especially during UV-mode analyses, resulted in large internal measurement errors (up to 20%) due to poor counting statistics. Variability between and within minerals from Laacher See could therefore not be resolved. The possibility to carry out the laser analyses with a single-line routine would lead to improvement, although this would require changing the collector block set-up of the MC-ICPMS. Together, unfortunately, the observed limitations prevent using the collected data to infer timescales of crystal growth for the Laacher See

samples. In addition, the application of the technique to apatite was not successful owing to small signal intensities.

Further analytical developments, to be performed in near future experiments could improve both analytical precision and accuracy:

- Create ablation craters in titanite glass using both NIR and UV LA during the exact same amount of time to determine the difference in crater depths and morphologies of deposits at the ablation site.
- Investigate the hypothesis that the transparency of the ablated material influences the extent of U-Th fractionation in both NIR and UV mode fs LA by ablating titanites with different optical properties and checking the crater morphologies.
- Use a second titanite glass (to be produced) with higher U concentrations as the bracketing standard.
- Reduce the laser energy in NIR mode, to reduce the fluence and ablation rate, to check if we can eliminate the time dependent fractionation while keeping the sensitivity to a level where we maintain good counting statistics.
- In UV-mode, reduce the spot size to increase the fluence but apply raster mode analyses in order to attain a higher sensitivity over a longer time span to improve counting statistics.

References

- Bacon, C.R., Persing, H.M., Wooden, J.L. and Ireland, T.R., 2000. Late Pleistocene granodiorite beneath Crater Lake caldera, Oregon, dated by ion microprobe. *Geology*, 28, 467-470.
- Bernal, J.-P., Eggins, S.M. and McCulloch, M.T., 2005. Accurate in situ ^{238}U - ^{234}U - ^{232}Th - ^{230}Th analysis of silicate glasses and iron oxides by laser-ablation MC-ICP-MS, pp. 1240-1249.
- Bernal, J.P., Eggins, S.M., McCulloch, M.T., Grun, R. and Eggleton, R.A., 2006. Dating of chemical weathering processes by in situ measurement of U-series disequilibria in supergene Fe-oxy/hydroxides using LA-MC-ICPMS. *Chemical Geology*, 235, 76-94.
- Bourdon, B., Zindler, A. and Worner, G., 1994. Evolution of the Laacher See magma chamber: Evidence from SIMS and TIMS measurements of U-Th disequilibria in minerals and glasses. *Earth and Planetary Science Letters*, 126, 75-90.
- Cheng, H. et al., 2000. The half-lives of uranium-234 and thorium-230. *Chemical Geology*, 169, 17-33.
- Condomines, M., Gauthier, P.J. and Sigmarsson, G., 2003. Timescales of magma chamber processes and dating of young volcanic rocks. In: *Uranium-Series Geochemistry, Reviews in Mineralogy and Geochemistry* 52. B. Bourdon, G.M. Henderson, C.C. Lundstrom and S.P. Turner (Editors), pp. 125-174.
- Eggins, S.M. et al., 2005. In situ U-series dating by laser-ablation multi-collector ICPMS: new prospects for Quaternary geochronology. *Quaternary Science Reviews*, 24, 2523-2538.
- Eggins, S.M., Kinsley, L.P.J. and Shelley, J.M.G., 1998. Deposition and element fractionation processes during atmospheric pressure laser sampling for analysis by ICP-MS. *Applied Surface Science*, 127, 278-286.
- Fontaine, G.H., Hattendorf, B., Bourdon, B. and Gunther, D., 2009. Effects of operating conditions and matrix on mass bias in MC-ICPMS. *Journal of Analytical Atomic Spectrometry*, 24, 637-648.
- Gunther, D., Cousin, H., Magyar, B. and Leopold, I., 1997. Calibration studies on dried aerosols for laser ablation-inductively coupled plasma mass spectrometry. *Journal of Analytical Atomic Spectrometry*, 12, 165-170.
- Guillong, M. and Gunther, D., 2002. Effect of particle size distribution on ICP-induced elemental fractionation in laser ablation-inductively coupled plasma-mass spectrometry. *Journal of Analytical Atomic Spectrometry*, 17, 831-837.

- Hirata, T. and Nesbitt, R.W., 1995. U-Pb Isotope Geochronology of Zircon - Evaluation of the Laser Probe-Inductively Coupled Plasma-Mass Spectrometry Technique. *Geochimica Et Cosmochimica Acta*, 59, 2491-2500.
- Hoffmann, D.L. et al., 2007. Procedures for accurate U and Th isotope measurements by high precision MC-ICPMS. *International Journal of Mass Spectrometry*, 264, 97-109.
- Hoffmann, D.L., Spol, C. and Mangini, A., 2009. Micromill and in situ laser ablation sampling techniques for high spatial resolution MC-ICPMS U-Th dating of carbonates. *Chemical Geology*, 259, 253-261.
- Horn, I. and von Blanckenburg, F., 2007. Investigation on elemental and isotopic fractionation during 196 nm femtosecond laser ablation multiple collector inductively coupled plasma mass spectrometry. *Spectrochimica Acta Part B: Atomic Spectroscopy*, 62, 410-422.
- Hubert, A., Bourdon, B., Pili, E. and Meynadier, L., 2006. Transport of radionuclides in an unconfined chalk aquifer inferred from U-series disequilibria. *Geochimica et Cosmochimica Acta*, 70, 5437-5454.
- Jeffries, T.E., Pearce, N.J.G., Perkins, W.T. and Raith, A., 1996. Chemical fractionation during infrared and ultraviolet laser ablation inductively coupled plasma mass spectrometry - Implications for mineral microanalysis. *Analytical Communications*, 33, 35-39.
- Klemme, S. et al., 2008. Synthesis and preliminary characterisation of new silicate, phosphate and titanite reference glasses. *Geostandards and Geoanalytical Research*, 32, 39-54.
- Koch, J. and Gunther, D., 2007. Femtosecond laser ablation inductively coupled plasma mass spectrometry: achievements and remaining problems. *Analytical and Bioanalytical Chemistry*, 387, 149-153.
- Koch, J., von Bohlen, A., Hergenroder, R. and Niemax, K., 2004. Particle size distributions and compositions of aerosols produced by near-IR femto- and nanosecond laser ablation of brass. *Journal of Analytical Atomic Spectrometry*, 19, 267-272.
- Koch, J., Walle, M., Pisonero, J. and Gunther, D., 2006. Performance characteristics of ultra-violet femtosecond laser ablation inductively coupled plasma mass spectrometry at similar to 265 and similar to 200 nm. *Journal of Analytical Atomic Spectrometry*, 21, 932-940.
- Koch, J., We, M., Dietiker, R. and Gunther, D., 2008. Analysis of laser-produced aerosols by inductively coupled plasma mass spectrometry: Transport phenomena and elemental fractionation. *Analytical Chemistry*, 80, 915-921.
- Kuhn, H.R. and Gunther, D., 2003. Elemental fractionation studies in laser ablation inductively coupled plasma mass spectrometry on laser-induced brass aerosols. *Analytical Chemistry*, 75, 747-753.

- Le Harzic, R. et al., 2002. Comparison of heat-affected zones due to nanosecond and femtosecond laser pulses using transmission electronic microscopy. *Applied Physics Letters*, 80, 3886-3888.
- Lowenstern, J.B. et al., 2000. U-Th dating of single zircons from young granitoid xenoliths: new tools for understanding volcanic processes. *Earth and Planetary Science Letters*, 183, 291-302.
- Mank, A.J.G. and Mason, P.R.D., 1999. A critical assessment of laser ablation ICP-MS as an analytical tool for depth analysis in silica-based glass samples. *Journal of Analytical Atomic Spectrometry*, 14, 1143-1153.
- Neymark, L.A. and Paces, J.B., 2000. Consequences of slow growth for Th-230/U dating of Quaternary opals, Yucca Mountain, NV, USA. *Chemical Geology*, 164, 143-160.
- Niemax, K., 2001. Laser ablation – reflections on a very complex technique for solid sampling. *Fresenius' Journal of Analytical Chemistry*, 370, 332-340.
- Odegard, M., Skar, O., Schiellerup, H. and Pearson, N.J., 2005. Preparation of a synthetic titanite glass calibration material for in situ microanalysis by direct fusion in graphite electrodes: A preliminary characterisation by EPMA and LA-ICP-MS. *Geostandards and Geoanalytical Research*, 29, 197-209.
- Paces, J.B., Neymark, L.A., Marshall, B.D., Whelan, J.F. and Peterman, Z.E., 1998. Inferences for Yucca Mountain unsaturated-zone hydrology from secondary minerals. *High-Level Radioactive Waste Management. Proceedings of the Eighth International Conference|High-Level Radioactive Waste Management. Proceedings of the Eighth International Conference*, 36-9|xviii+864.
- Paces, J.B., Neymark, L.A., Wooden, J.L. and Persing, H.M., 2004. Improved spatial resolution for U-series dating of opal at Yucca Mountain, Nevada, USA, using ion-microprobe and microdigestion methods. *Geochimica et Cosmochimica Acta*, 68, 1591-1606.
- Poitrasson, F., Mao, X.L., Mao, S.S., Freydier, R. and Russo, R.E., 2003. Comparison of ultraviolet femtosecond and nanosecond laser ablation inductively coupled plasma mass spectrometry analysis in glass, monazite, and zircon. *Analytical Chemistry*, 75, 6184-6190.
- Potter, E.-K., Stirling, C.H., Wiechert, U.H., Halliday, A.N. and Spotl, C., 2005. Uranium-series dating of corals in situ using laser-ablation MC-ICPMS. *International Journal of Mass Spectrometry*, 240, 27-35.
- Reid, M.R., Coath, C.D., Mark Harrison, T. and McKeegan, K.D., 1997. Prolonged residence times for the youngest rhyolites associated with Long Valley Caldera: ^{230}Th --- ^{238}U ion microprobe dating of young zircons. *Earth and Planetary Science Letters*, 150, 27-39.
- Russo, R.E., Mao, X., Gonzalez, J.J. and Mao, S.S., 2002. Femtosecond laser ablation ICP-MS. *Journal of Analytical Atomic Spectrometry*, 17, 1072-1075.

- Russo, R.E., Mao, X.L., Borisov, O.V. and Liu, H., 2000. Influence of wavelength on fractionation in laser ablation ICP-MS. *Journal of Analytical Atomic Spectrometry*, 15, 1115-1120.
- Schmitt, A.K., 2006. Laacher See revisited: High-spatial-resolution zircon dating indicates rapid formation of a zoned magma chamber. *Geology*, 34, 597-600.
- Schmitt, A.K., Wetzel, F., Cooper, K.M., Zou, H. and Worner, G., Magmatic Longevity of Laacher See Volcano (Eifel, Germany) Indicated by U-Th Dating of Intrusive Carbonatites. *Journal of Petrology*, 51, 1053-1085.
- Stirling, C.H., Lee, D.C., Christensen, J.N. and Halliday, A.N., 2000. High-precision in situ ^{238}U - ^{234}U - ^{230}Th isotopic analysis using laser ablation multiple-collector ICPMS. *Geochimica et Cosmochimica Acta*, 64, 3737-3750.
- Tait, S.R., 1988. Samples from the crystallising boundary layer of a zoned magma chamber. *Contributions to Mineralogy and Petrology*, 470-483.
- Wolff, J.A., Worner, G. and Blake, S., 1990. Gradients in physical parameters in zoned felsic magma bodies: Implications for evolution and eruptive withdrawal. *Journal of Volcanology and Geothermal Research*, 43, 37-55.
- Wörner, G., Beusen, J.M., Duchateau, N., Gijbels, R. and Schmincke, H.U., 1983. Trace element abundances and mineral/melt distribution coefficients in phonolites from the Laacher See volcano (Germany). *Contributions to Mineralogy and Petrology*, 84, 152-173.
- Wörner, G., Harmon, R. S. and Hoefs, J. , 1987. Stable isotope relations in an open magma system, Laacher See, Eifel (FRG). *Contributions to Mineralogy and Petrology*, Volume 95, 343-349.
- Worner, G., Staudigel, H. and Zindler, A., 1985. Isotopic constraints on open system evolution of the Laacher See magma chamber (Eifel, West Germany). *Earth and Planetary Science Letters*, 75, 37-49.
- Worner, G. and Wright, T.L., 1984. Evidence for magma mixing within the Laacher See magma chamber (East Eifel, Germany). *Journal of Volcanology and Geothermal Research*, 22, 301-327.
- Wörner, G.a.S., H.-U. , 1984. Mineralogical and Chemical Zonation of the Laacher See Tephra Sequence (East Eifel, W. Germany). *Journal of Petrology*, 25, 805-835.

Chapter 6

Conclusions and perspectives

Conclusions and perspectives

This thesis presented combined major- and trace element, long-lived isotope and U-series disequilibria data to unravel the relative importance of melting processes and source heterogeneity on the composition of Icelandic lavas.

Compared to other MORB or OIB settings, Icelandic lavas show unique correlations between tracers that are sensitive to the degree of melting and tracers of source heterogeneity. The correlations between La/Yb or La/Sm and Nd and Hf isotope compositions indicate a close and systematic relationship between the melting process and sampling of source heterogeneities. As a consequence, the final degree of melting affects both trace element ratios involving a moderately incompatible element and isotopic compositions. Local variability in the degree of melting is found to overwhelm the regional variation in the degree of melting as a function of distance from the plume centre. Thus based on the trace elements we cannot resolve the effect of excess temperature (ΔT) of the mantle plume. The local variability is interpreted to result from extraction of melts from variable depths in the melting region between separate eruptions.

Variable enrichments in highly incompatible trace element ratios such as Nb/U, Nb/La and U/La in different zones rift suggests that the enriched component, which has characteristics similar to a recycled E-MORB crust, is heterogeneously distributed in the mantle beneath Iceland, or is intrinsically heterogeneous.

The combined trace element and Nd-Hf-Sr-Pb isotope systematics in Icelandic basalts can be explained by mixing of melts from a two component source and extraction of the mixtures from variable depths in the melt region. Two mixing scenarios were evaluated: (1) complete mixing and (2) incomplete mixing. The mixing scenario that assumes complete accumulation of melts requires a higher abundance of the enriched component (up to 10%) beneath the Western Volcanic Zones to explain large enrichments in Nb/U and Pb isotopes. However, incomplete mixing of melts and extraction of these mixtures from variable depths also complies with the observed variability in the Icelandic lavas for a constant amount of the enriched component in the source.

In contrast to the trace elements and long-lived isotopes, the variability in U-series disequilibria reveals the influence of both ΔT and source heterogeneity. The melting

rates recorded by the U-series are controlled by the mantle upwelling and by melt source productivity. Because the disequilibria are produced during the initial stages of melting the depth of melt extraction does not affect them.

A general decrease in the ^{230}Th and ^{231}Pa excesses towards the centre of Iceland is consistent with increasing upwelling velocity and therefore with the presence of a buoyant thermal plume beneath Iceland. However, local variability in the ($^{230}\text{Th}/^{238}\text{U}$) and ($^{231}\text{Pa}/^{235}\text{U}$), especially for samples from the Western Rift Zone, which have variable Nb/U, Nb/La and U/Th, demonstrates the effect of source heterogeneity. The combination of low ^{230}Th and ^{231}Pa excesses and high Nb/U and U/Th suggests that increased abundances of the enriched component in the source results in higher melting rates on a local scale. This observation implies that the enriched source component is characterised by higher melt productivity, which is consistent with predictions from experimental studies. Low ($^{230}\text{Th}/^{238}\text{U}$) disequilibria in the most enriched samples furthermore demonstrate that the enriched recycled component must have a low bulk $D_{\text{U}}/D_{\text{Th}}$.

The relationships between highly incompatible elements and U-series disequilibria can be explained by mixing final melts from a pyroxenite and a peridotite in variable proportions. Incomplete mixing at a constant source ratio is inconsistent with the data for the most enriched samples, which confirms that larger abundances of the enriched component are required in the mantle beneath the South Western Rift Zone of Iceland. The applied mixing model indicates furthermore that melts formed in the deepest region are required to mix effectively with melts formed at higher levels in the melt region.

Note that these observations do not rule out that Icelandic lavas represent incomplete mixtures. The deep melts may mix with a higher probability relative to melts formed at shallower depths. The melt extraction mechanism remains poorly understood but is likely a complex system with melt focusing in multiple channels that converge at various levels within the mantle. Compared with the natural process the mixing model applied in this thesis is therefore highly simplified. The approach, however, demonstrates the large effect of incomplete mixing to final melt compositions and is therefore a step towards a better understanding. Evidently, further detailed sampling with more complex modelling is required to explore the full effects of incomplete mixing of melts from a three dimensional melt region.

Significant variability in ^{226}Ra - ^{230}Th disequilibria do not show relationships with tracers for magma differentiation, melting rate or source composition, which makes interpretation of the data difficult. The ^{226}Ra -deficits observed for four samples measured for this thesis are furthermore inconsistent with predictions from current melting models and suggest a process in which radium behaves more compatibly compared to Th. This unconstrained process may be responsible for the lack of relationships with other geochemical tracers.

In the last part of the thesis the potential of a new in-situ U-series analysis technique was evaluated to allow resolving spatial variation in ^{230}Th - ^{238}U disequilibria in zoned crystals. The accurate results obtained for the femto second LA-MC-ICPMS experiments on titanite standard materials reveal the potential of this relatively fast analysis technique. Further analytical tests are, however, required to investigate the effects of variable elemental fractionation between sample and standard materials and to improve the counting statistics during sample analysis. The required analytical developments will be performed in an extension of this project.

Acknowledgements

I am extremely thankful to all that made my ~3.7 years at ETH Zürich an enjoyable and successful experience, both scientifically and non-scientifically.

First of all I want to thank my direct supervisor Andreas Stracke who dedicated vast amounts of time to help me out on issues, have thorough discussions on the data and to improve my manuscripts. I very much enjoyed getting to know him in the field in Iceland where he showed his extreme dedication and enthusiasm, even at the cost of some of his fingers! I am very happy that he now has a well deserved professor position in Münster. Likewise, I want to thank my ‘doctor father’ Bernard Bourdon who also contributed a lot to the success of my thesis. We had several constructive discussions and his ideas helped to improve my work significantly.

I want to thank Max Schmidt for being my official internal supervisor after Bernard left for Lyon. I thank Tim Elliott and John MacLennan for their questions, comments and suggestions during the defence on the 26th of November 2010.

In addition to my supervisors there have been colleagues with whom I shared ideas on my work, either in the lab or at a later stage during writing. Especially Sarah Aciego who also trained me in maintaining NU1 was always very helpful in finding solutions to problems. The others that I want to thank are Sarah Bureau, Felix Oberli, Olivier Reubi, Ed Tipper, Colin Maden, and Gregory de Souza.

During the fieldwork in Iceland Karl Grönvold and John MacLennan were both fantastic field guides making sampling in the amazing landscape in North and Central Iceland even more enjoyable. I also thank Issy Sides, a student from Cambridge, for the good company during and after the fieldwork.

I would like to acknowledge Gerhard Wörner for providing samples from Laacher See Volcano, for my Laser Ablation study on sphene and apatite. At ETH Hönggerberg, I enjoyed working with Gisela Fontaine who was of great help during the LA-MC-ICPMS experiments. In addition Detlef Günther, Bodo Hattendorf and Joachim Koch provided useful ideas for refinement of the techniques. Peter Ulmer is thanked for his effort in producing homogeneous titanite and apatite standard glasses. From a technical point of view I would like to thank Donat Niederer, Urs Mennet and Andreas Süssli who maintained, adjusted and repaired the mass spectrometers. Heiri Bauer and Bruno Rüttsche are thanked for their IT support.

I would also like to thank Frowin Pirovino and Margrith Bischof for help with sample preparation and production of thin sections. Pierre Bouihol and Lydia Zehnder are thanked for their instructions on sample crushing and XRF analyses. Jessica Langlade was very patient and friendly in helping with the microprobe analyses.

At the Max Planck Institute, Mainz, Klaus-Peter Jochum and Brigitte Stoll were very kind in their support to analyse trace elements by LA-ICPMS. Also Men-Andrin Meijer a bachelor student at that time is thanked for his good company.

Apart from the afore mentioned people that were all involved in my work I am really grateful to all the people that, next to my work, made sure I had a brilliant time here in Zürich and in the weekends in Amsterdam.

Off course I start to thank Sander van Engelen who supported me in my work but nicely forced me to relax in the weekends we were together.

My flat mates Marion Louvel and Jessica Langlade have been the greatest girls to live with, always making life at home extremely easy. Furthermore, they were the force behind Friday Beer, our weekly pleasure after hard work. I want to thank my former and current office mates Mathieu Touboul, Jörg Rickli, Uli Hans, Gregory de Souza and Florian Wetzel for the many fun moments we shared. Other people that I had fun with and would like to thank are: Christoph Burkhardt, Antoine Roth, Ruth Hindshaw, Giuditta Felin, Caroline Fitoussi, Olivier Reubi, Colin Maden, Magali Pujol, Thomas Kruijjer, Peter Sprung, Pietro and Laura Sternai, Mathew and Caroline Fox, Teo Cassola, Jonas von Rütte, Barbara Tripoli, Steffi Luginbühl, Clemens Augenstein, Pinar Ozfirat, Rebecca Reverman, Daniela Hunziker, Achile Marsala, Ylona van Dinther, Remco Hin, Kees Weemstra, Hein van Heck, Alice Gabriel, Corinne Bachmann, Kerry Leith, Asha Kostylew, Alejandro Beltran, Julie Verbeke, Julia Schäfer, Michael Wagner, Olivier Cavalie, Joelle Nicoletti, Sabine Obrecht, Eli Wütrich, Pierre Bouilhol, Sabine Mehay, Maarten Aerts, Paola Ardia, Marion Campani, Simon Broggi, Kristina Kostan, Kasper Schaerrer and many more.

And last but not least I want to thank my family and friends in Amsterdam who supported me during my thesis and of which many came to visit Zürich: Marijn ten Holt, Dagmar, Jorren, Vincent, Filippien, Mattijs, Genevieve and Ruth Koornneef, Laura van der Waerden, Roos van Os, Anne Ridderikhoff, Rosa Groen, Rutger van Ree, Anoeska Titsing en Sander de Kivith, Ronnie Hendriks, Annelieke de Hoog, Eli van Es, Ramon van der Waerden, Corinna Kuchta, Kjell van Norel, Mark Jaspers, Ward

Venstra, Tessa de Reyck, Nienke Grimme, Rana van de Vegt, Michel Tol, Pauline Vos, Yemi Schneider, Ellen de Bruijn, Wouter Rhebergen and many more..

Curriculum Vitae

M.Sc. Janne Marij Koornneef

Herdernstrasse 16
8004 Zürich
Switzerland

Mobile: +41 77 4379179
E-mail: koornneef@erdw.ethz.ch

Javaplein 27C
1095CJ Amsterdam
The Netherlands

Phone: +31 20 8463357
Mobile: +31 6 41152227
E-mail: janne.koornneef@falw.vu.nl

Date of birth: 02/01/1979

Nationality: Dutch

Education

- 2007 – Nov 2010** **Ph.D. in Isotope Geochemistry. U-series constraints on melt generation and magma evolution, Institute of Geochemistry and Petrology, ETH Zürich.**
- 2004- 2007** **M.Sc. Earth Sciences: Lithosphere tectonics, petrology and isotope geochemistry, Vrije Universiteit Amsterdam.**
Cum laude
- 2001-2005** **B.Sc. Earth Sciences, Vrije Universiteit Amsterdam**
- 1991-1997** **Voorbereidend Wetenschappelijk Onderwijs (vwo), Fons Vitae Lyceum, Amsterdam.** Six year of high school education with a scientific background.

Work Experience

- 2006 – 2007** **Student assistant, Department of Petrology, Vrije Universiteit Amsterdam.** Technique development of in-situ Sr isotope analyses by LA-MC-ICPMS.

- 2003 – 2006** **Student assistant, Bureau of Education, Vrije Universiteit Amsterdam.** Assistant for? information and communication technology for the Faculty of Earth Sciences.
- 2005 – 2006** **Appointment Committee for Sedimentology, Vrije Universiteit Amsterdam.** Student member of the committee that advised the Faculty Board in the appointment of a new professor (head) for the Department of Sedimentology

Teaching Experience

Geological field course in the Alps, ETH Zürich. Student instructor during 1 week field course for first year B.Sc. Students, 2007 and 2008.

Crystals and Minerals, ETH Zürich. Student assistant in mineralogy practical. Active teaching in working groups of 6–8 students, 2007, 2008, 2009

Instrumental Experience

MC-ICPMS (Thermo Finnigan Neptune, VUA; Nu-Instruments, ETH Zürich): Analysis of Sr, Hf and U-series isotopes. I was responsible for the half-yearly maintenance on the Nu Instruments MC-ICPMS at ETH-Zürich, including the dismounting and cleaning of lens stacks and replacement of slits.

TIMS (Thermo Finnigan MAT-262, VUA; Triton, ETH Zürich): Analysis of Sr, Rb, Nd and Th isotopes

ICP-MS (Thermo Finnigan Element 2, Perkin-Elmer ELAN DRC-e): Trace element analysis.

Laser ablation (ArF excimer, Nd-YAG, fs laser): Whole rock trace element analyses, Sr isotope composition of plagioclase, U-Th isotopes in sphene and apatite

XRF: Major and trace element of whole rocks

Microprobe: Major element composition of minerals

Additional training

Workshop on Laser Ablation, 05/2006, VU, Amsterdam. Two days of seminars and two days of practical work (speakers: S. Eggins, P. Mason J. Kosler a.o.).

Workshop on Mass Spectrometry, 07/2007, ETH Zürich. Full week of seminars. (speakers: H. Baur, B. Hattendorf, F. Oberli, B. Bourdon, D. Günther)

Awards and Honors

- 2006** **Van Rijngelden Grant.** Grant for student-assistantship at the Department of Petrology, Vrije Universiteit Amsterdam.
- 2007** **W.P. de Roever Prize for best M.Sc. Thesis 2007.** Award (750 EUR) for M.Sc. thesis: Modification of the Tanzanian Lithospheric Mantle by Multi-stage Metasomatism: A Geochemical and Isotopic Study of Xenoliths from Labait Volcano, Northern Tanzania

Manuscripts and abstracts

Koornneef, J.M., Stracke, A., Bourdon, B., Grönvold, K., 2011. U–Th–Pa–Ra disequilibria in post-glacial tholeiites from Iceland; evidence for melting a heterogeneous source. To be submitted to *Geochimica and Cosmochimica Acta*.

Reubi, O., Bourdon, B., Dungan, M.A., **Koornneef, J.M.**, Sellés, D., Langmuir, C., Aciego, S., Stracke, A., 2010. Assimilation of the plutonic roots of the Andean arc controls variations in U–Th–Pa–Ra isotopes disequilibria at Volcan Llaima, Chile. *Earth and Planetary Science Letters*, in Press.

Koornneef, J.M., Stracke, A., Meier M.A., Bourdon, B., Jochum, K.P., Stoll, B., Grönvold, K., 2010 Melting and mixing of a two-component source beneath Iceland, *Journal of Petrology*, in review.

Koornneef, J.M., Stracke, A., Aciego, S, Reubi, Bourdon, B., 2010. A new method A new method for U–Th–Pa–Ra separation and accurate measurement of ^{234}U – ^{230}Th – ^{231}Pa and ^{226}Ra disequilibria in volcanic rocks by MC-ICPMS, *Chemical Geology* 277, 30-41.

Koornneef J.M., Stracke A, Meier M-A, Bourdon B, Grönvold K, Jochum K-P., Stoll B (2010). Plume-Influenced melting of a two-component source beneath Iceland. Goldschmidt Conference Abstract. *Geochimica et Cosmochimica Acta* 74, A530.

Koornneef, J.M., Stracke, A., Bourdon, B., Aciego, S., Gronvold, K., Stoll, B. & Jochum, K. P., 2009. Melting dynamics beneath Iceland from U–Th–Pa–Ra disequilibria in post-glacial tholeiites. Goldschmidt Conference Abstract. *Geochimica et Cosmochimica Acta* 73, A682.

Koornneef, J.M., Davies, G.R. Dopp, S.P., Vukmanovic, Z., Nikogosian, I. K., Mason, P.R.D., 2009. Nature and timing of multiple metasomatic events in the sub-cratonic lithosphere beneath Labait, Tanzania. *Lithos*, 112: 896-912.

Koornneef, J.M., Stracke, A., Meier M.A., Bourdon, B., Jochum, K.P., Stoll, B., Grönvold, K., 2008. Imaging the Icelandic plume by means of geochemistry. *Eos Trans. AGU*, 89(53), Fall Meet. Suppl., Abstract V51G-08

Vroon, P.Z., van der Wagt, B., **Koornneef, J.M.** and Davies, G.R., 2008. Problems in obtaining precise and accurate Sr isotope analysis from geological materials using laser ablation MC-ICPMS. *Analytical and Bioanalytical Chemistry*, 390(2): 465-476.

References

B. Bourdon, Institute of Geochemistry and Petrology, ETH Zurich, e-mail :
bourdon@erdw.ethz.ch, Now at : Ecole Normale Supérieure de Lyon, France. Phone :
0033 4 72 72 81 87

A. Stracke, Institute of Geochemistry and Petrology, ETH Zurich. Now at : Institut für
Mineralogie, Westfälische Wilhelms Universität, Münster, Germany. Email:
stracke.andreas@uni-munester.de, phone: 0049-251-8333487

G.R. Davies, Department of Petrology, Vrije Universiteit Amsterdam, e-mail:
gareth.davies@falw.vu.nl, Phone: 0031 20 598 7329